Department of Petroleum Engineering

CO_2 wettability of rock and implications for core-flooding

Ahmed Zarzor Hussien Yaseri

This thesis is presented for the Degree of

Doctor of Philosophy
of
Curtin University

October 2017

Declaration

To the best of my knowledge and belief this thesis contains no material previously published by any other person except where due acknowledgment has been made.

This thesis contains no material which has been accepted for the award of any other degree or diploma in any university.

Ahmed Zarzor Hussien Yaseri

Signature:

Date: 15/10/2017

Copyright

Ahmed Zarzor Hussien Yaseri

Signature:

Date: 15/10/2017

To my beloved family

Abstract

Increasing energy demands and associated global warming are unarguably two of the most pressing challenges the world currently faces. One of the ideas to reduce the carbon footprint while increasing the efficiency of energy extraction is 1) geo-storage (CCS) in high salinity sandstone formations and 2) enhanced oil or gas recovery schemes. However, to improve containment security in CCS and better reservoir-scale predictions of oil and gas, recovery projects need to understand and improve the knowledge of the wetting characteristics of CO_2 in rock. This is because the wettability of the rock matrix has a strong effect on capillary pressure, relative permeability, and the phases distribution within the pore space and thus on the entire displacement mechanism and storage capacity. Moreover, it is important to understand the nature of interactions between fluid and rock, because these affect the rock permeability and consequently the injectivity.

In this work, the CO_2 wettability was measured via contact angle measurements and the results show that rock became more CO_2 wet with increasing pressure, temperature and brine salinities and less CO_2 wet with increasing surface roughness. Moreover, we found here that caprock can be weakly water wet or intermediate wet at typical storage conditions. Consequently, a lower storage capacity can be inferred for structural trapping in such cases. We also demonstrate that gas densities correlate remarkably well with wettability. Finally, a physical model based on the diffusion double layer theory was developed to provide a theoretical framework for the observed behavior of the systems analyzed. The model correctly predicted the influence of the different variables (ion type, ionic concentration, temperature, and pressure) and can be used to describe the physical phenomena behind the results obtained in a qualitative framework. A quantitative analysis can also be performed with the proposed model to predict the contact angles if all parameters needed are available.

Furthermore, the permeability of sandstone samples has been evaluated because of the injection of brine, CO_2-saturated brine or supercritical CO_2 at reservoir conditions, and it was found that permeability was reduced, which was likely caused by fines release and subsequent pore throat plugging. We expect that this phenomenon can have a significant and detrimental influence on CO_2injectivity,

which would be reduced accordingly. Therefore, the plugging mechanisms and characteristics with a particular focus on the effect of wettability because of fines injection was investigated here using a combination of *ex-situ* (coreflooding measurements, SEM imaging) and *in-situ* (NMR, μCT) methods. Thus, we showed that the deposited fines were tightly packed, apparently because of strong adhesion forces.

Acknowledgements

I would like to thank my family, who continue to provide their support. To my supervisors (Prof. Stefan Iglauer, Prof. Maxim Lebedev, and Prof. Ahmed Barifcani) who provided me with the confidence, material, structure, and scope to complete this project to the best of our liking as a team.

The Iraqi Ministry of Higher Education and Scientific Research is thanked for providing financial support during my study. I also owe a debt to the Department of Petroleum Engineering at Curtin University for providing lab equipment and facilities.

Finally, I wish to thank all the respected academics whose works have been cited throughout this dissertation. None of this would have been possible without prior study and documentation.

List of Publications included as part of the thesis

Iglauer, S., Sarmadivaleh, M., **Al-Yaseri, A.** and Lebedev, M., 2014. Permeability evolution in sandstone due to injection of CO_2-saturated brine or supercritical CO_2 at reservoir conditions. Energy Procedia, 63, pp.3051-3059.

Al-Yaseri, A., Sarmadivaleh, M., Saeedi, A., Lebedev, M., Barifcani, A. and Iglauer, S., 2015. N_2+ CO_2+ NaCl brine interfacial tensions and contact angles on quartz at CO_2 storage site conditions in the Gippsland basin, Victoria/Australia. Journal of Petroleum Science and Engineering, 129, pp.58-62.

Sarmadivaleh, M., **Al-Yaseri, A.Z.** and Iglauer, S., 2015. Influence of temperature and pressure on quartz–water–CO_2 contact angle and CO_2–water interfacial tension. Journal of Colloid and Interface Science, 441, pp.59-64.

Al-Yaseri, A.Z., Lebedev, M., Vogt, S.J., Johns, M.L., Barifcani, A. and Iglauer, S., 2015. Pore-scale analysis of formation damage in Bentheimer sandstone with in-situ NMR and micro-computed tomography experiments. Journal of Petroleum Science and Engineering, 129, pp.48-57.

Iglauer, S., **Al-Yaseri, A.Z.**, Rezaee, R. and Lebedev, M., 2015. CO_2 wettability of caprocks: Implications for structural storage capacity and containment security. Geophysical Research Letters, 42(21), pp.9279-9284.

Al-Yaseri, A.Z., Lebedev, M., Barifcani, A. and Iglauer, S., 2016. Receding and advancing (CO_2+ brine+ quartz) contact angles as a function of pressure, temperature, surface roughness, salt type and salinity. The Journal of Chemical Thermodynamics, 93, pp.416-423.

Roshan, H., **Al-Yaseri, A.Z.**, Sarmadivaleh, M. and Iglauer, S., 2016.On wettability of shale rocks. Journal of Colloid and Interface Science, 475, pp.104-111.

Al-Yaseri, A.Z., Roshan, H., Lebedev, M., Barifcani, A. and Iglauer, S., 2016. Dependence of quartz wettability on fluid density. Geophysical Research Letters, 43(8), pp.3771-3776.

Al-Yaseri, A.Z., Hani A., Lebedev, Barifcani, A. and Iglauer, S., 2016.Impact of fines and rock wettability on Reservoir formation damage. Journal of Geophysical Prospecting, 64 (4), pp.860-874.

List of publications by the candidate relevant to the thesis but not forming part of it

Arif, M., **Al-Yaseri**, A.Z., Barifcani, A., Lebedev, M. and Iglauer, S., 2016. Impact of pressure and temperature on CO_2–brine–mica contact angles and CO_2–brine interfacial tension: Implications for carbon geo-sequestration. Journal of colloid and interface science, 462, pp.208-215.

Al-Yaseri, A.Z., Roshan, H., Zhang, Y., Rahman, T., Lebedev, M., Barifcani, A. and Iglauer, S., 2017. Effect of the Temperature on CO_2/Brine/Dolomite Wettability: Hydrophilic versus Hydrophobic Surfaces. Energy & Fuels, 31(6), pp.6329-6333.

H Roshan, H Masoumi, M Sarmadivaleh, Y Zhang, **AZ Al-Yaseri**, M Lebedev, S Iglauer. Microstructural alteration of gas shales: relative humidity versus liquid water. Journal of Geotechnical and Geoenvironmental Engineering, in press.

Al-Yaseri, A.Z., Zhang, Y., Ghasemiziarani, M., Sarmadivaleh, M. Lebedev, M., Roshan, H. and Iglauer, S., 2017. Permeability Evolution in Sandstone due to CO_2 Injection. Energy & Fuels, in press.

Al-Yaseri, A.Z., Roshan, H., Xiaomeng, X., Zhang, Y., Sarmadivaleh, M. Lebedev, M., Barifcani. A. and Iglauer, S., 2017. Coal Wettability after CO_2 Injection. Energy & Fuels, in press

Table of Contents

1 Introduction

CO_2 emissions have recently been recognized as a major cause of climate change [IPCC, 2005]; also the growing demand for power because of industrialization leads to increase in fossil fuel consumption and consequently the generation of CO_2 [International Energy Agency, 2010; IPCC, 2005].In order to simultaneously address climate change mitigation and improve economics of CO_2 sequestration, CO_2 enhanced oil recovery projects may be given an increased attention. CO_2 Enhanced Oil Recovery Projects may offer an added advantage in that the production of oil and gas is accompanied by sequestration of carbon dioxide in subterranean reservoirs. In recent years, the carbon geostorage(CGS) in deep sandstone saline aquifers has attracted a lot of attention [IPCC, 2005], but to safely store CO_2 in the ground, it is important to understand the nature of fluid-rock [Sayegh et al. 1990; Nightingale et al. 2009; Carroll et al., 2011; Iglauer et al., 2015a] and fluid-fluid interaction [Adamson, and Gast 1997; Georgiadis et al., 2010, Georgiadis 2011]. In addition, the injected CO_2 is partially miscible with the resident brine and reacts with the water to form an acidic environment [Sayegh et al. 1990]:

$$CO_2 + H_2O \leftrightarrow H_2CO_3 \quad (1)$$

$$H_2CO_3 \leftrightarrow HCO_3^- + H^+ \quad (2)$$

$$HCO_3^- \leftrightarrow CO_3^{2-} + H^+ \quad (3)$$

This carbonic acid [Nightingale et al. 2009, Carroll et al., 2011, Iglauer 2011] can react with rock minerals and lead to ionic dissolution-precipitation, as well as form secondary minerals [Worden and Smith, 2004]; especially given that the CO_2 can be trapped in the pore spaces of rock for several hundreds of years [Ballentine et al., 2001]. Fines released from acid-rock interaction could migrate toward pore throats and lead to permeability reduction, which has a significant and detrimental influence on CO_2 injectivity (reduced storage capacity).

Therefore, permeability changes were carefully evaluated along with the plugging mechanisms and characteristics, with a particular focus on the effect of wettability because of fines injection.

Furthermore, the CO_2wettability of the rock and CO_2-water interfacial tension have a dramatic impact on structural and residual trapping, and CO_2 movement through the rock [IPCC, 2005, Iglauer et al., 2017, Morrow1990, Spiteri et al., 2008, Iglauer et al., 2010, Iglauer et al., 2012a] because of the small capillary-like pores in the rock that form a complex network. In addition, relative permeability [McCaffery and Bennion, 1974] and capillary pressures [Morrow 1976; Anderson 1987] that determine reservoir-scale fluid flow are also dependent on the CO_2 wettability and interfacial tension. Therefore, CO_2-water-rock contact angle, which is essentially an expression of the rock wettability, was measured here, along with the influence of pressure, temperature, rock surface roughness, gas density, and brine salinities.

1.1 **Aims and objectives**

The main objective of this research is to establish a fundamental and solid understanding of the CO_2 wettability of rock by studying:

1. The effect of different solid surfaces (quartz and shale) on CO_2wettability.
2. The effect of surface roughness on contact angle values.
3. The effect of gas density on water-rock wettability.
4. The effect of increasing pressure on water-rock wettability.
5. The effect of increasing temperature on water-rock wettability.
6. The effect of water salinity on water-rock wettability.
7. The effect of CO_2 injection on rock permeability.
8. The effect of rock wettability on permeability reduction and fines migration.

2 Literature Review

2.1 CO_2-rock wettability and CO_2-water interfacial tension

Two parameters, which have received little attention but have a dramatic impact on structural and residual trapping because of the small capillary-like pores in the rock, are the CO_2-wettability of the rock [IPCC, 2005, Iglauer et al., 2017] and CO_2-water interfacial tension [Morrow1990, Spiteri et al., 2008,Iglauer et al., 2010, Iglauer et al., 2012b]. In addition, relative permeability [McCaffery and Bennion, 1974] and capillary pressures [Morrow 1976; Anderson 1987] that can determine reservoir-scale fluid flow are two key variables that also depend on CO_2 wettability and interfacial tension. Contact angle, which is an expression of the rock wettability, is a factor that is highly variable. However, published data of CO_2-water-rock contact angles have a large uncertainty even with the simplest systems: For instance, water contact angles for CO_2/quartz varied between 0 and 95 degrees, the main reasons being that receding and advancing angles were not distinguished and surface contamination led to artificially high contact angles [Dehghanpour et al., 2012]. Therefore, it is necessary to constrain this parameter to a reasonable level to enable reliable reservoir flow predictions. It is also necessary to understand the interfacial characteristics of the rock-fluid–fluid system in more depth to reduce project risk. Note that increasing the contact angle and interfacial tension values led to reduced structural and residual trapping capacities.

2.1.1 Effect of temperature on contact angle

It was reported that contact angle increases with temperature [Yang et al., 2008, Farokhpoor et al., 2013]; however, there are other works [De Ruijter et al., 1998, Saraji et al., 2014, Arif et al., 2016] showing that the contact angle decreases with temperature. Further, Roshan et al. [2016] observed theoretically (Eq.1) that contact angle is a function of temperature through several parameters, among which are the dielectric constant of the solution (D_f), the interfacial tension (γ_{lg}) between the fluids, the density difference between the phases ($\Delta\rho$) and temperature (T) itself. The effect of temperature on D_f [Floriano and Nascimento, 2004] is insignificant compared to its effect on the density difference and interfacial tension between fluids

[Jho et al., 1978] and temperature itself. Thus, three parameters compete against each other contact angle decreases with temperature and with increases in Δρ by temperature, but increases because of a decrease in γ_{lg} with temperature [Sarmadivaleh et al., 2015, Al-Yaseri et al., 2016a]; however, in one case, the contact angle increased with temperature, which shows the effect of temperature on γ_{lg} over-compensated for the effect of density difference and temperature and, thus, caused the contact angle to increase. A further change in contact angle can take place as a result of a microscopic change in the van der Waals potential caused by temperature. However, this effect is neglected herein, as these microscopic variations are not yet fully understood [Roshan et al., 2016].

$$\cos\theta = -1 + \frac{I\boldsymbol{\Delta\rho}}{\gamma_{lg}} - \frac{\varepsilon_0 \psi_S^2 D}{2\gamma_{lg}} \left(\frac{2e^2 \mathbf{n_{bulk}} \mathbf{z}^2}{N_a \varepsilon_0 K_B \mathbf{D_f T}} \right)^{1/2} \quad (1)$$

Where, $\Delta\rho$ is the density difference between gas phase and liquid-gas phase and $I = -\int_{z_{\min}}^{\infty} V(z)dz$ where V is the net preference of the adsorbate molecule for wetting the substrate instead of forming a droplet due to intermolecular forces. where D_f is the dielectric constant of the solution in the presence of charged surfaces, T is the temperature, z is the ionic valency, K_B is the Boltzmann constant (1.38×10^{-23} JK^{-1}), n_{bulk} is the ionic concentration of the solution (mol/m^3), N_a is the Avogadro constant (6.022×10^{23} mol^{-1}) and e is the electric charge (1.602×10^{-9} C). ψ is the electric potential of the solid surface , D is the dielectric constant of the medium and ε_0 is the permittivity of vacuum

2.1.2 Effect of ion concentration and type on contact angle

It was reported that the contact angle consistently increased with increasing ionic concentration (n) [Farokhpoor et al., 2013,Saraji et al., 2014, Arif et al., 2016, Mugele et al., 2016, Roshan et al., 2016]. This effect is primarily caused by two main parameters (Equation 1, above): the ionic concentration (n) itself and D_f. D_f decreases with increasing n. Thus, both effects result in a contact angle increase with

increasing n, consistent with literature data [Farokhpoor et al., 2013,Saraji et al., 2014, Arif et al., 2016, Mugele et al., 2016]. Further, it was found that $MgCl_2$ produced the highest contact angles, followed by $CaCl_2$, NaCl, and KCl, at any pressure, temperature, and ionic concentration [Saraji et al., 2013a, Mugele et al., 2015, Arif et al., 2016, Mugele et al., 2016]. This is also consistent with the theory (Eq. 1), predicting that an increase inion valency increases the contact angle [Roshan et al., 2016]. Moreover, if the same valency is considered, for instance, Na^+ and K^+, the variation in contact angle can be attributed to a change in solution dielectric constant (D_f), (Eq. 1). D_f of NaCl is lower than D_f of KCl, e.g., D_f of 1M NaCl is 63 while D_f of 1M KCl is 70 [Levy et al., 2012]. A lower D_f consequently increases the contact angle (Eq. 1) as seen from Figs 4-6 in Roshan et al. [2016]; however, it is also dependent on the ionic absorption potential of the minerals' surfaces. The bivalent ions (Ca^{2+} and Mg^{2+}), for instance, can be strongly absorbed on clay surfaces in shale and reduce the surface potential. This can, in turn, increase the contact angle, although such interactions are not yet fully understood [Roshan et al., 2016].

2.1.3 Effect of pressure on contact angle

Increasing pressure significantly reduces the density difference and causes the contact angle to increase [Al-Yaseri et al., 2016a].This is well supported by much literature data [Dicksonet al., 2006, Ameri et al., 2013, Saraji et al., 2013b, Arif et al., 2016] and molecular dynamics data [Jung and Wan 2012, Iglauer et al., 2012b, McCaughan et al., 2013, Sedghi et al., 2014, Chen et al., 2015]. Furthermore, pressure has a profound effect on contact angle, both on charged and neutral surfaces. When examining Eq. 1, clearly several parameters are a function of pressure. For instance, the increase in pressure slightly affects the interfacial tension between the fluids [Hjelmel and et al., 1986] along with the dielectric constant of the liquid phase (D_f) [Floriano and Nascimento 2004]; however, the main effect primarily occurs through the change in the density difference of the phases by pressure [Georgiadis et al., 2010].

2.1.4 Effect of pressure and temperature on interfacial tension

Increasing pressure significantly reduces the CO_2-water interfacial tension. This is well supported by much literature data [Chun and Wilkinson 1995, Park et al., 2005, Georgiad is et al., 2010, Nielsen et al., 2012, Sarmadivaleh et al., 2015, Arif et al., 2016] and molecular dynamics data [Iglauer et al., 2012b, Tsuji et al., 2013]. Furthermore, it was reported that CO_2-water interfacial tension increases with increasing temperature [Chun and Wilkinson 1995, Park et al., 2005, Georgiadis et al., 2010, Iglauer et al., 2012b, Tsuji et al., 2013, Sarmadivaleh et al., 2015, Arif et al., 2016]. However, little literature data have shown a constant relation of IFT with increasing temperature [Tsuji et al., 2013, Nielsen et al., 2012].

2.2 The influence of rock wettability on permeability reduction because of fines migration.

Fines migration and plugging of pores and pore throats by solid particles can be caused by drilling, completion, cementing, perforation, workover, stimulation, and injection of water and chemicals during enhanced oil recovery, with the potential consequence of a significant reduction in rock permeability [Civan 2007; Kalfayan 2008]. Such plugging may also result from proppant crushing at high fracture closure pressure during hydraulic fracturing [Kalfayan 2008]. Furthermore, fines are mobilized if the critical flow velocity (i.e., the critical value of viscous forces) for a particular rock is reached and particles detach from the matrix [Civan 2007]. Krueger [1988], Economides and Nolte [1987], and Amaerule et al. [1988] indicated that migration of formation fines is the major factor for permeability damage, and it is well established the induced permeability impairment strongly depends on particle and pore space geometry [e.g. Muecke 1979,Civan 2007]. Generally, this damage is a problem in various fields, ranging from water production [McDowell-Boyer et al.,1986,Torkzaban et al., 2007,Bradford et al., 2011], geothermal energy efficiency [Mahmoudi et al., 2010, Rosenbrand et al., 2014, Rosenbrand et al., 2015], hydrocarbon recovery [Ahmed and McKinney 2005; Iglauer et al., 2010] to carbon geo-storage [Iglauer et al., 2017].

Furthermore, wettability is another factor influencing fines migration. In two-phase flow experiments, Muecke [1979] found that calcium carbonate particles (2 to 15 μm size) migrated faster through quartz sand packs if the phase that wets them is moving. Sarkar and Sharma [1990] investigated fines migration in single-phase and two-phase flow through Berea sandstone, and they found that formation damage was significantly lower in two-phase flow (permeability ratio reduced from 1 to 0.04 compared with a reduction from 1 to 0.0016 in single phase flow). However, there is a lack of analysis in terms of how combinations of rock-fines wettability affect formation damage, and particularly a lack of *in-situ* experiments. Considering that wettability of petroleum reservoirs can vary widely [Cuiec 1984, Buckley et al., 1997, Buckley and Monsterleet 1998], and that wettability at the wellbore can be altered by drilling, completion and flooding fluids [Cuiec 1984, Sharma and Wunderlich 1987, Kalfayan 2008], this factor requires further attention.

2.3 **Permeability reduction because of CO_2 injection**

It is important to understand the nature of the interaction between fluid and rock in order to safely store CO_2 in the ground [Sayegh et al., 1990, Nightingale et al., 2009, Carroll et al., 2011]. Such interactions, on the other hand, affect the aquifer permeability and consequently the injectivity [Wiese et al., 2010]. Therefore, permeability and permeability alteration should be carefully evaluated to properly design CO_2 injection projects, because injected CO_2 dissolves in reservoir in-situ water to produce a weak carbonic acid [Nightingale et al. 2009, Carroll et al., 2011, Iglauer 2011]. This acid reacts with rock minerals leading to ionic dissolution-precipitation as well as forming secondary minerals [Worden and Smith, 2004]. Therefore, sandstone formations are considered to be the best candidates for CO_2 sequestration [IPCC 2005]. However, sandstone typically contains components (cements, clays) other than quartz [Delle et al., 2013], and these impurities usually have a substantially higher reactivity in an acidic environment than quartz [Fischer et al., 2010; Carroll et al., 2011], especially in the carbonate brine (live brine) at reservoir condition, which has low pH (about 3 to 4) [Schaeff and McGrail, 2004, Sigfusson et al., 2015]. Also, CO_2 can be trapped in the pore spaces of rock for several hundreds of years [Ballentine et al., 2001].

The main reactions that occur during the dissolution of CO_2 in water are:

$$CO_2 + H_2O \leftrightarrow H_2CO_3 \quad (1)$$

$$H_2CO_3 \leftrightarrow HCO_3^- + H^+ \quad (2)$$

$$HCO_3^- \leftrightarrow CO_3^{2-} + H^+ \quad (3)$$

Among initial attempts to map such variability, Sayegh et al. 1990 tested five sandstone reservoir samples from the Cardium formation in the Pembina Oil Field area of Western Canada (average permeability = 0.04md, average porosity = 0.13, where the XRD analysis showed quartz (~ 50%), chert, siderite and calcite as dominant minerals) at a pressure of 13.8MPa, temperature of 318K and a flow rate of 0.3 cm^3/min for carbonated brine (5wt% NaCl+ CO_2). Sayegh et al. [1990] reported that the permeabilities of the tested samples dropped toward a minimum value of93%; however, the permeabilities increased again after 25 to 50 hours of the flooding time (approaching the original value). Furthermore, the calcium ion content (150 ppm and 250 ppm) slightly increased in the collected effluent while the level of sodium ions stayed unchanged during the test. (No significant amount of magnesium ions was observed.) Moreover, one more sample was flooded by noncarbonated-brine (without CO_2) and no calcium or magnesium ions were noticed in the XRD analysis.

Sayegh et al. [1990] concluded that the initial permeability reduction occurred by fines migration through pore throat blocking mechanisms that were later dissolved and led to an increase in the permeability. Ochi and Vernoux [1998] observed permeability decline by more than 50% because of injection of synthetic (no CO_2) brines (0.01 to 0.5M NaCl) into Berea sandstone plugs (from Ohio, USA with average permeability~ 380md) at reservoir conditions (pressure 22 MPa and temperature 363K). They also reported higher permeability reduction with increasing injection rates ($\geq$ 3.6 cc/sec). They interpreted that permeability reduction as being linked to the fines migration and resultant plugging that was initiated by the chemical reaction between the injected fluid and the rock. It was in fact shown that a critical flow rate exists above which the permeability decreases as a consequence of the hydrodynamic release of particles. This critical flow rate was found to be higher than those observed in the literature. The filtering or size exclusion appears to be the

principal cause of permeability decrease at high injection flow rates. They concluded that the hydrodynamic effect can reduce the permeability by more than 50%, but is less severe than the chemical effect. Wellman et al. [2003] also found that dissolution was relatively uniform and the surface reaction rate was quite slow during CO_2 injection into sandstone rocks. Interestingly, a significant reduction in well injectivity (from 10 to 100%) was reported in the reservoir because of CO_2 injection [Grigg et al., 2003, Zeng et al., 2005]. In addition, Raistrick et al. [2009] recorded an increase in Ca^{2+}, Mg^{2+}, K+, SO_4^{2-}, HCO_3^-, and CO_2 concentrations in produced brines after CO_2 injection (for EOR purpose) into a sandstone reservoir (Weyburn oil field in Canada) towing to the dissolution of calcite, dolomite and K-feldspars. Nightingale et al. [2009] tested different sandstone samples from the Cardium formation in the Pembina field (Alberta, Canada) and found residual clays and feldspar grains in the rock samples after CO_2 injection. Mohamed et al. [2012] tested Berea samples (XRD that showed 79.61wt% quartz, 7.21wt% kaolinite, and 4.11wt% illite) at constant pressure (8.96MPa) and flow rate (5.0 cm^3/min) while the temperature ranged from 294 Kto 394 K. Significant reductions in cores permeabilities were observed (35 to 55% loss) by reason of CO_2 injection (WAG cycles of CO_2 and brine, or continuous CO_2 injections). In their experiments, the calcium ions concentration slightly increased (from 5.023 to 7.393 wt%) in the effluent brine while the concentration of the sodium and magnesium ions did not vary significantly. Furthermore, for longer WAG injection (less brine volume injected per cycle and low temperature) less permeability reduction was noted. The damage in permeability was explained by precipitation of the reaction products and/or because of the migration of clay particles. Pini et al. [2012] did not observe any change in the permeability (no change in pressure drop across the core) of Berea samples (280 md) towing to CO_2-saturated brine injection. Their experiments were carried out at reservoir conditions (9 MPa pore pressure, 12 MPa confining pressure, 298 K and 323 K temperatures, from 1 to 50 ml/min flow rates).However, their Berea sandstone samples were heated to 973 K for two hours to stabilize swelling clay minerals. Ma and Morrow [1994] clarified that no clay minerals were observed in Berea after heat treatment (≥973K). Therefore, the permeability was supposed to stay unchanged in the Pini et al. [2012] study [Sayegh et al., 1990,Worden and Smith, 2004]. However, it has been reported that the reaction kinetic rate between the clay minerals and acid is very slow [Knauss and Wolery 1989, Nagy 1995, Blum and Stillings 1995, Xu et al., 2004, Xu et al.,

2007, Luquot et al., 2012] and the effect of the acidic environment on clay particle detachment remains uncertain.

3 Conclusions

The wettability of rock with respect to CO_2 and water is of vital importance in CO_2 geo-storage as it strongly affects residual and structural trapping by reason of the small capillary-like pores in the rock [IPCC, 2005, Iglauer et al., 2017]. Therefore, the contact angle was measured here because it is an expression of the rock wettability; however, there is much uncertainty associated with the published data [Iglauer et al. 2014a]. Thus was reported inhere the experimental (brine + CO_2) advancing and receding contact angles on quartz/shale surfaces; specifically, the impact of pressure, salinity, gas density, salt type, surface roughness and temperature conditions.

In this work, it was observed that a higher surface roughness resulted in lower advancing (θ_a) and receding (θ_r) contact angles (Al-Yaseri et al., 2016b). Further, values of θ_a and θ_r increased as pressure and temperature increased (Sarmadivaleh et al., 2016, Al-Yaseri et al., 2016b, Al-Yaseri et al., 2016a, Roshan et al., 2016, Iglauer et al., 2015b). In addition, it was shown that gas densities can be used to predict water contact angles on quartz for a specific temperature and brine composition, and thus rock wettability (Al-Yaseri et al., 2016a). Effectively, the impact of pressure and gas type can be correlated by gas density, which represents a remarkable simplification of a complex phenomenon (Al-Yaseri et al., 2016a). Thus, these findings enable more rapid and simplified determination of θ. Associated with that, there is more reliable pore scale and reservoir scale predictions as gas densities can be swiftly and reliably calculated. Moreover, a physical model was developed based on the diffusion double layer theory to provide a framework for the observed experimental data (Roshan et al., 2016).

It was found that the permeability did not significantly change in clean sandstone consisting of pure quartz (Fonteinemebleau) towing to live or dead brine injection, although permeability changed because of $scCO_2$ injection by ~23% (Iglauer et al., 2014b). The permeability in the Berea sandstone, however, changed because of live or dead brine injection, by up to 35% (Iglauer et al., 2014b). This permeability reduction in Berea sandstone was likely caused by fines release and subsequent pore throat plugging as the damage was more significant at higher injection rates (Iglauer et al., 2014b, Sayegh et al., 1990). Therefore, plugging mechanisms and

characteristics with a combination of ex situ (i.e., coreflooding measurements and scanning electron microscopy imaging) and in situ (i.e., nuclear magnetic resonance and μCT) methods, with a particular focus on the effect of wettability was investigated inhere (Al-Yaseri et al, 2015, Al-Yaseri et al, 2016c).The corefloods indicated that permeability drops rapidly when fines are injected; mechanistically thin pore throats are plugged first, followed by the filling of adjacent pore bodies with the fine material (Al-Yaseri et al, 2015). Furthermore, it was clearly shown that wettability played a major role: If fines and rock wettability are identical, plugging is significantly accelerated; wettability also controls the 3D distribution of the fines in the pore space (Al-Yaseri et al, 2015).Also, the deposited fines were tightly packed, apparently because of strong adhesion forces (Al-Yaseri et al, 2015, Al-Yaseri et al, 2016c).

4 Bibliography: list of all references cited in the introduction and overview

Adamson, A.W. and Gast, A.P., 1967. Physical chemistry of surfaces.

Ahmed T. and P.D. McKinney 2005. Advanced Reservoir Engineering. Gulf Publishing Burlington, MA 01803, USA, 1-401.

Al-Yaseri, A., Al Mukainah, H., Lebedev, M., Barifcani, A. and Iglauer, S., 2016c. Impact of fines and rock wettability on reservoir formation damage. Geophysical Prospecting, 64(4), pp.860-874.

Al-Yaseri, A.Z., Lebedev, M., Barifcani, A. and Iglauer, S., 2016b. Receding and advancing (CO2+brine+quartz) contact angles as a function of pressure, temperature, surface roughness, salt type and salinity. The Journal of Chemical Thermodynamics, 93, pp.416-423.

Al-Yaseri, A.Z., Lebedev, M., Vogt, S.J., Johns, M.L., Barifcani, A. and Iglauer, S., 2015. Pore-scale analysis of formation damage in Bentheimer sandstone with in-situ NMR and micro-computed tomography experiments. Journal of Petroleum Science and Engineering, 129, pp.48-57.

Al-Yaseri, A.Z., Roshan, H., Lebedev, M., Barifcani, A. and Iglauer, S., 2016a. Dependence of quartz wettability on fluid density. Geophysical Research Letters, 43(8), pp.3771-3776.

Amaerule J.O., Kersey D.G., Norman D.K., and Shannon P.M., 1988. Advances in formation damage assessment and control strategies. Petroleum Society of Canada 65.1-65.37.

Ameri, A., Kaveh, N.S., Rudolph, E.S.J., Wolf, K.H., Farajzadeh, R. and Bruining, J., 2013. Investigation on interfacial interactions among crude oil–brine–sandstone rock–CO_2 by contact angle measurements. Energy & Fuels, 27(2), pp.1015-1025.

Anderson, W.G., 1987. Wettability literature survey-part 4: Effects of wettability on capillary pressure. Journal of Petroleum Technology, 39(10), pp.1-283.

Arif, M., Al-Yaseri, A.Z., Barifcani, A., Lebedev, M. and Iglauer, S., 2016. Impact of pressure and temperature on CO_2–brine–mica contact angles and CO2–brine interfacial tension: Implications for carbon geo-sequestration. Journal of colloid and interface science, 462, pp.208-215.

Ballentine, C.J., Schoell, M., Coleman, D. and Cain, B.A., 2001. 300-Myr-old magmatic CO_2 in natural gas reservoirs of the west Texas Permian basin. Nature, 409(6818), pp.327-331.

Blum, A.E., Stillings, L.L., 1995. Feldspar dissolution kinetics, Chapter 7. In: White, A.F., Brantley, S.L. (Eds.), Chemical Weathering Rates of Silicate Minerals. Mineral Society of America 31, Washington DC, pp. 291–351.

Blunt, M., Fayers, F.J. and Orr, F.M., 1993. Carbon dioxide in enhanced oil recovery. Energy Conversion and Management, 34(9-11), pp.1197-1204.

Bradford S.A., Torkzaban S., and Simunek J. 2011. Modeling colloid transport and retention in saturated porous media under unfavorable attachment conditions.Water Resources Research 47, (10), W10503.

Buckley J. S., Liu Y., and Monsterleet S. 1998. Mechanisms of wetting alteration by crude oils. SPE J., 54–61.

Buckley J.S., Liu Y., Xie X., and Morrow N. 1997. Asphaltenes and crude oil wetting-The effect of oil composition. SPE J., 2, 107–119.

Carroll, S.A., McNab, W.W. and Torres, S.C., 2011. Experimental study of cement-sandstone/shale-brine-CO2interactions.Geochemical transactions, 12(1), pp.1-19.

Chen, C., Wan, J., Li, W. and Song, Y., 2015. Water contact angles on quartz surfaces under supercritical CO2 sequestration conditions: Experimental and molecular dynamics simulation studies. International Journal of Greenhouse Gas Control, 42, pp.655-665.

Chun, B.S. and Wilkinson, G.T., 1995. Interfacial tension in high-pressure carbon dioxide mixtures. Industrial & engineering chemistry research, 34(12), pp.4371-4377.

Civan, F., 2007.Reservoir Formation Damage Fundamentals, Modeling, Assessment and Mitigation, second edition. Houston, TX: GulfPublishing Company, 1114pp.

Cuiec L. 1984. Rock/crude-oil interactions and wettability: an attempt to understand their interrelations. Annual Technical Conference and Exhibition of the SPE, Houston, Texas, 16-19 September 1984.

De Ruijter, M., Kölsch, P., Voué, M., De Coninck, J. and Rabe, J.P., 1998. Effect of temperature on the dynamic contact angle. Colloids and Surfaces A: Physicochemical and Engineering Aspects, 144(1), pp.235-243.

Dehghanpour, H., Zubair, H.A., Chhabra, A. and Ullah, A., 2012. Liquid intake of organic shales. Energy & Fuels, 26(9), pp.5750-5758.

Delle Piane, C., Olierook, H.K.H., Timms, N.E., Saeedi, A., Esteban, L., Razaee, R., Mikhaltsevitch, V. and Lebedev, M., 2013. Facies-based rock properties distribution along the Harvey 1 stratigraphic well. Australian National Low Emissions Coal Research & Development CSIRO Report Number EP133710.

Dickson, J.L., Gupta, G., Horozov, T.S., Binks, B.P. and Johnston, K.P., 2006. Wetting phenomena at the CO2/water/glass interface. Langmuir, 22(5), pp.2161-2170.

Economides M.J., and Nolte K.G. 1987. Reservoir stimulation. Houston, TX: Schlumberger Educational Services.

Farokhpoor, R., Bjørkvik, B.J., Lindeberg, E. and Torsæter, O., 2013. Wettability behaviour of CO_2 at storage conditions. International Journal of Greenhouse Gas Control, 12, pp.18-25.

Fischer, S., Liebscher, A., Wandrey, M. and CO2 SINK Group, 2010. CO_2–brine–rock interaction—first results of long-term exposure experiments at in situ P–T conditions of the Ketzin CO_2 reservoir. Chemie der Erde-Geochemistry, 70, pp.155-164.

Floriano, W.B. and Nascimento, M.A.C., 2004. Dielectric constant and density of water as a function of pressure at constant temperature. Brazilian Journal of Physics, 34(1), pp.38-41.

Georgiadis, A., 2011. Interfacial tension of aqueous and hydrocarbon systems in the presence of carbon dioxide at elevated pressures and temperatures (Doctoral dissertation, Imperial College London).

Georgiadis, A., Maitland, G., Trusler, J.M. and Bismarck, A., 2010. Interfacial tension measurements of the (H_2O+ CO_2) system at elevated pressures and temperatures. Journal of Chemical & Engineering Data, 55(10), pp.4168-4175.

Grigg, R.B., McPherson, B.J. and Svec, R.K., 2003, May. Laboratory and model tests at reservoir conditions for CO_2-brine-carbonate rock systems interactions. In The Second Annual DOE Carbon Sequestration Conference.

Hjelmeland, O.S. and Larrondo, L.E., 1986. Experimental investigation of the effects of temperature, pressure, and crude oil composition on interfacial properties.SPE Reservoir Engineering, 1(04), pp.321-328.

Iglauer S., Favretto S., Spinelli G., Schena G., and Blunt M.J. 2010. X-ray tomography measurements of power-law cluster size distributions for the non-wetting phase in sandstones. Physical Review E 82, 05631.

Iglauer S., Sarmadivaleh M., Al-Yaseri A., and Lebedev M. 2014b. Permeability evolution in sandstone due to injection of CO_2-saturated brine or supercritical CO2 at reservoir conditions. Energy Procedia 63: 3051-3059.

Iglauer, S., 2011. Dissolution trapping of carbon dioxide in reservoir formation brine-a carbon storage mechanism. INTECH Open Access Publisher.

Iglauer, S., 2017. CO_2–Water–Rock Wettability: Variability, Influencing Factors, and Implications for CO2Geostorage. Accounts of Chemical Research, 50(5), pp.1134-1142.

Iglauer, S., Al-Yaseri, A.Z., Rezaee, R. and Lebedev, M., 2015b. CO_2 wettability of caprocks: Implications for structural storage capacity and containment security. Geophysical Research Letters, 42(21), pp.9279-9284.

Iglauer, S., Fernø, M.A., Shearing, P. and Blunt, M.J., 2012a. Comparison of residual oil cluster size distribution, morphology and saturation in oil-wet and water-wet sandstone. Journal of colloid and interface science, 375(1), pp.187-192.

Iglauer, S., Mathew, M.S. and Bresme, F., 2012b. Molecular dynamics computations of brine–CO_2 interfacial tensions and brine–CO_2–quartz contact angles and their effects on structural and residual trapping mechanisms in carbon geo-sequestration. Journal of colloid and interface science, 386(1), pp.405-414.

Iglauer, S., Paluszny, A. and Blunt, M.J., 2013. Simultaneous oil recovery and residual gas storage: A pore-level analysis using in situ X-ray micro-tomography. Fuel, 103, pp.905-914.

Iglauer, S., Pentland, C.H. and Busch, A., 2015a. CO_2 wettability of seal and reservoir rocks and the implications for carbon geo-sequestration. Water Resources Research, 51(1), pp.729-774.

Iglauer, S., Salamah, A., Sarmadivaleh, M., Liu, K. and Phan, C., 2014a. Contamination of silica surfaces: impact on water–CO_2–quartz and glass contact angle measurements. International Journal of Greenhouse Gas Control, 22, pp.325-328.

International Energy Agency, 2010. Key World Energy Statistics, Paris.

IPCC, 2005. Working Group III of the Intergovernmental Panel on Climate Change, pp. 1–443.

Jho, C., Nealon, D., Shogbola, S. and King, A.D., 1978. Effect of pressure on the surface tension of water: adsorption of hydrocarbon gases and carbon dioxide on water at temperatures between 0 and 50 C. Journal of Colloid and Interface Science, 65(1), pp.141-154.

Jung, J.W. and Wan, J., 2012. Supercritical CO_2 and ionic strength effects on wettability of silica surfaces: Equilibrium contact angle measurements. Energy & Fuels, 26(9), pp.6053-6059.

Kalfayan, L. 2008. Production enhancement with acid stimulation. Pennwell Books, 270 pages.

Knauss, K.G., Wolery, T.J., 1989. Muscovite dissolution kinetics as a function of pH and time at 70C. Geochim. Cosmochim. Acta 53, 1493–1501.

Krueger R.F. 1988. An overview of formation damage and well productivity in oilfield operations: An update. SPE California Regional Meeting, Long Beach, California 23-25 March, 1988.

Levy, A., Andelman, D. and Orland, H., 2012. Dielectric constant of ionic solutions: A field-theory approach. Physical review letters, 108(22), p.227801.

Luquot, L., Andreani, M., Gouze, P. and Camps, P., 2012. CO_2 percolation experiment through chlorite/zeolite-rich sandstone (Pretty Hill Formation–Otway Basin–Australia).Chemical geology, 294, pp.75-88.

Ma, S. and Morrow, N.R., 1994. Effect of firing on petrophysical properties of Berea sandstone. SPE Formation Evaluation, 9(03), pp.213-218.

Mahmoudi H., Spahis N., Goosen M.F., Ghaffour N., Drouiche N., and Ouagued A. 2010. Application of geothermal energy for heating and fresh water production in a brackish water greenhouse desalination unit: A case study from Algeria. Renewable and Sustainable Energy Reviews 14, (1), 512-517.

McCaffery, F.G. and Bennion, D.W., 1974. The Effect of Wettability On Two-Phase Relative Penneabilities. Journal of Canadian Petroleum Technology, 13(04).

McCaughan, J., Iglauer, S. and Bresme, F., 2013. Molecular dynamics simulation of water/CO_2-quartz interfacial properties: Application to subsurface gas injection. Energy Procedia, 37, pp.5387-5402.

McDowell-Boyer L.M., Hunt J.R., and Sitar N. 1986. Particle transport through porous media. Water Resources Research 22, (13), 1901-1921.

Mohamed, I.M., He, J. and Nasr-El-Din, H.A., 2012. Carbon Dioxide Sequestration in Sandstone Aquifers: How Does It Affect the Permeability?. In Carbon Management Technology Conference.

Morrow, N.R., 1976.Capillary pressure correlations for uniformly wetted porous media. Journal of Canadian Petroleum Technology, 15(04).

Morrow, N.R., 1990.Wettability and its effect on oil recovery. Journal of Petroleum Technology, 42(12), pp.1-476.

Muecke T.W. 1979. Formation fines and factors controlling their movement in porous media. Journal of Petroleum Technology 31,144-150.

Mugele, F., Bera, B., Cavalli, A., Siretanu, I., Maestro, A., Duits, M., Cohen-Stuart, M., van den Ende, D., Stocker, I. and Collins, I., 2015. Ion adsorption-induced wetting transition in oil-water-mineral systems. Scientific reports, 5.

Mugele, F., Siretanu, I., Kumar, N., Bera, B., Wang, L., de Ruiter, R., Maestro, A., Duits, M., van den Ende, D. and Collins, I., 2016. Insights From Ion Adsorption and Contact-Angle Alteration at Mineral Surfaces for Low-Salinity Waterflooding. SPE Journal.

Nagy, K.L., 1995. Dissolution and precipitation kinetics of sheet silicates. Reviews in Mineralogy and Geochemistry, 31(1), pp.173-233.

Nielsen, L.C., Bourg, I.C. and Sposito, G., 2012. Predicting CO_2–water interfacial tension under pressure and temperature conditions of geologic CO_2 storage. Geochimicaet Cosmochimica Acta, 81, pp.28-38.

Nightingale, M., Johnson, G., Shevalier, M., Hutcheon, I., Perkins, E. and Mayer, B., 2009. Impact of injected CO2 on reservoir mine ralogy during CO2-EOR.Energy Procedia, 1(1), pp.3399-3406.

Ochi, J. and Vernoux, J.F., 1998. Permeability decrease in sandstone reservoirs by fluid injection: hydrodynamic and chemical effects. Journal of Hydrology, 208(3), pp.237-248.

Park, J.Y., Lim, J.S., Yoon, C.H., Lee, C.H. and Park, K.P., 2005. Effect of a fluorinated sodium bis (2-ethylhexyl) sulfosuccinate (aerosol-OT, AOT) analogue surfactant on the interfacial tension of CO_2+ water and CO_2+ Ni-

plating solution in near-and supercritical CO_2. Journal of Chemical & Engineering Data, 50(2), pp.299-308.

Pini, R., Krevor, S.C. and Benson, S.M., 2012. Capillary pressure and heterogeneity for the CO_2/water system in sandstone rocks at reservoir conditions. Advances in Water Resources, 38, pp.48-59.

Rosenbrand E., Kjøller C., Riis J. F. Kets F., and Fabricius I. L. 2015. Different effects of temperature and salinity on permeability reduction by fines migration in Berea sandstone. Geothermics 53, (0), 225-235.

Rosenbrand E., Haugwitz C., Jacobsen P.S.M., Kjøller C., and Fabricius I.L. 2014.The effect of hot water injection on sandstone permeability. Geothermics 50, (0), 155-166.

Roshan, H., Al-Yaseri, A.Z., Sarmadivaleh, M. and Iglauer, S., 2016. On wettability of shale rocks. Journal of colloid and interface science, 475, pp.104-111.

Saraji, S., Goual, L. and Piri, M., 2013a. Dynamic adsorption of asphaltenes on quartz and calcite packs in the presence of brine films. Colloids and Surfaces A: Physicochemical and Engineering Aspects, 434, pp.260-267.

Saraji, S., Goual, L., Piri, M. and Plancher, H., 2013b. Wettability of supercritical carbon dioxide/water/quartz systems: Simultaneous measurement of contact angle and interfacial tension at reservoir conditions. Langmuir, 29(23), pp.6856-6866.

Saraji, S., Piri, M. and Goual, L., 2014.The effects of SO_2 contamination, brine salinity, pressure, and temperature on dynamic contact angles and interfacial tension of supercritical CO_2/brine/quartz systems. International Journal of Greenhouse Gas Control, 28, pp.147-155.

Sarkar A.K., and Sharma M.M. 1990. Fines migration in two-phase flow. Journal of Petroleum Technology, 42, (05), 646-652.

Sarmadivaleh, M., Al-Yaseri, A.Z. and Iglauer, S., 2015. Influence of temperature and pressure on quartz–water–CO 2 contact angle and CO_2–water interfacial tension. Journal of colloid and interface science, 441, pp.59-64.

Sayegh, S.G., Krause, F.F., Girard, M. and DeBree, C., 1990. Rock/fluid interactions of carbonated brines in a sandstone reservoir: Pembina Cardium, Alberta, Canada. SPE formation evaluation, 5(04), pp.399-405.

Schaeff, H.T. and McGrail, B.P., 2004. Direct measurements of pH in H_2O-CO_2 brine mixtures to supercritical conditions. In Proceedings of the 7th International Conference on Greenhouse Gas Control Technologies (GHGT-7).

Sedghi, M., Piri, M. and Goual, L., 2014. Molecular dynamics of wetting layer formation and forced water invasion in angular nanopores with mixed wettability. The Journal of chemical physics, 141(19), p.194703.

Sharma M.M., and Wunderlich R.W. 1987. The alteration of rock properties due to interactions with drilling-fluid components. Journal of Petroleum Science and Engineering 1, (2), 127-143.

Sigfusson, B., Gislason, S.R., Matter, J.M., Stute, M., Gunnlaugsson, E., Gunnarsson, I., Aradottir, E.S., Sigurdardottir, H., Mesfin, K., Alfredsson, H.A. and Wolff-Boenisch, D., 2015. Solving the carbon-dioxide buoyancy challenge: The design and field testing of a dissolved CO_2 injection system. International Journal of Greenhouse Gas Control, 37, pp.213-219.

Spiteri, E.J., Juanes, R., Blunt, M.J. and Orr, F.M., 2008. A new model of trapping and relative permeability hysteresis for all wettability characteristics. SPE Journal, 13(03), pp.277-288.

Torkzaban S., Bradford S.A., and Walker S.L. 2007. Resolving the Coupled Effects of Hydrodynamics and DLVO Forces on Colloid Attachment in Porous Media. Langmuir 23, (19), 9652-9660.

Tsuji, S., Liang, Y., Kunieda, M., Takahashi, S. and Matsuoka, T., 2013. Molecular dynamics simulations of the CO_2-water-silica interfacial systems. Energy Procedia, 37, pp.5435-5442.

Wellman, T.P., Grigg, R.B., McPherson, B.J., Svec, R.K. and Lichtner, P.C., 2003. Evaluation of CO_2-brine-reservoir rock interaction with laboratory flow tests and reactive transport modeling. In International symposium on oilfield chemistry. Society of Petroleum Engineers.

Wiese, B., Nimtz, M., Klatt, M. and Kühn, M., 2010. Sensitivities of injection rates for single well CO_2 injection into saline aquifers. Chemie der Erde-Geochemistry, 70, pp.165-172.

Worden, R.H. and Smith, L.K., 2004. Geological sequestration of CO_2 in the subsurface: lessons from CO_2 injection enhanced oil recovery projects in oilfields. Geological Society, London, Special Publications, 233(1), pp.211-224.

Xu, T., Apps, J.A. and Pruess, K., 2004. Numerical simulation of CO_2 disposal by mineral trapping in deep aquifers. Applied geochemistry, 19(6), pp.917-936.

Xu, T., Apps, J.A., Pruess, K. and Yamamoto, H., 2007. Numerical modeling of injection and mineral trapping of CO_2 with H2S and SO_2 in a sandstone formation. Chemical Geology, 242(3), pp.319-346.

Yang, D., Gu, Y. and Tontiwachwuthikul, P., 2008. Wettability determination of the crude oil− reservoir brine− reservoir rock system with dissolution of CO_2 at high pressures and elevated temperatures. Energy & Fuels, 22(4), pp.2362-2371.

Zeng, Z.W., Bai, B., Liu, Y. and West, P., 2005. Improving CO_2 efficiency for recovering oil in heterogeneous reservoirs. Report No. DE-FG26-01BC15364, New Mexico Petroleum Recovery Research Center, New Mexico Institute of Mining and Technology.

5 Publications Forming Part of Thesis

5.1 **Permeability evolution in sandstone due to injection of CO_2-saturated brine or supercritical CO_2 at reservoir conditions**

Iglauer, S., Sarmadivaleh, M., **Al-Yaseri, A.** and Lebedev, M., 2014. Permeability evolution in sandstone due to injection of CO_2-saturated brine or supercritical CO_2 at reservoir conditions. Energy Procedia, 63, pp.3051-3059.

Permeability evolution in sandstone due to injection of CO_2-saturated brine or supercritical CO_2 at reservoir conditions.

S. Iglauer[a]*, M. Sarmadivaleh[a], A. Al-Yaseri[a], M. Lebedev[b]

[a]Department of Petroleum Engineering, Curtin University, 26 Dick Perry Avenue, 6151 Kensington, Australia

[b]Department of Exploration Geophysics, Curtin University, 26 Dick Perry Avenue, 6151 Kensington, Australia

Abstract

We measured the change in permeability of two selected sandstones (Berea, Fonteinebleau) due to injection of CO_2-saturated ("live") brine, unsaturated ("dead") brine or supercritical (sc) CO_2 at reservoir conditions. We found that the permeability did not significantly change in a clean sandstone consisting of pure quartz (Fonteinemebleau) due to live or dead brine injection, although permeability changed due to scCO_2 injection by ~23%. The permeability in the Berea sandstone, however, changed due to live or dead brine injection, by up to 35%; this permeability reduction in Berea sandstone was likely caused by fines release and subsequent pore throat plugging as the damage was more significant at higher injection rates. We expect that this phenomenon – i.e. rock permeability reduction due to CO_2 injection into the formation – can have a significant and detrimental influence on CO_2 injectivity, which would be reduced accordingly.

Keywords

permeability reduction, sandstone, CO_2-saturated brine, live brine, supercritical CO_2, injectivity decrease.

1. Introduction

Injection of CO_2 deep into the subsurface is a recognized method to reduce anthropogenic greenhouse gas emissions [1]. During this process, CO_2 sweeps the target formation and is eventually immobilized by structural [2,3], residual [4-6], dissolution [7,8] or mineral [9.10] trapping mechanisms. The injected CO_2 is partially miscible with the resident brine (up to 0.01mol% of water can be dissolved in CO_2 at 323K and 20MPa, [11]; and up to 2.6mol% of CO_2 can dissolve in brine, [12]) and reacts with the water to form an acidic environment [8]:

$$CO_2(sc) + 3\,H_2O \leftrightarrow CO_2(aq) + 3\,H_2O \quad (a)$$

$$H_2O + CO_2(aq) \leftrightarrow H_2CO_3 \quad (b)$$

$$H_2CO_3 \leftrightarrow HCO_3^- + H^+ \quad (c)$$

$$HCO_3^- \leftrightarrow CO_3^{2-} + H^+ \quad (d)$$

Scheme 1: Formation and dissociation of carbonic acid.

When inspecting scheme 1 several conclusions can be reached:

a) as the partial CO_2 pressure is high at reservoir conditions, reaction (a) is shifted to the right, which causes.
b) increased formation of carbonic acid (reaction (b)) according to Le Chatelier's principle, which again.
c) significantly increases proton concentration (reaction (c)), thus significantly lowering the pH value.

Schaeff and McGrail [13] and Sigfusson et al. [14] report that the acidity created can reach significant levels (pH values 3-4 were measured at reservoir conditions for CO_2-saturated ("live") brine); and it is well established that such acidic environments can severely impact on the permeability and pore morphology of limestones: the acid "eats" into the carbonate forming large holes, so-called "wormholes" (e.g. [15-17]), which dramatically increase the permeability of the rock. This is a very significant effect, which, however, Gilfillan et al. [18] claim is a buffered reaction at reservoir scale (pH values increase to ~5.5).

Canal et al. [19] reported a similar effect in a Spanish sandstone, where live brine led to a four-fold increase of permeability. The sandstone Canal et al. [19] investigated contained 92.1vol% quartz, 5.0vol% kaolinite, 0.3vol% Mg-calcite, 0.5vol% K-feldspar, 0.1vol% muscovite, 0.9vol% goethite, 0.03vol% apatite and 0.1vol% rutile; based on chemical analysis of the effluents they concluded that mainly the Mg-calcite dissolved and was transported out of the plug. Indeed, sandstone typically contains considerable quantities of components (cements, clays) other than quartz (e.g. [20-23]), and these impurities usually have a substantially higher reactivity in an acidic environment than quartz [22,24]. Dissolution of such components is thus expected to increase permeability. However, sandstone is frequently considered to be pure quartz, and it is thus usually assumed that the permeability of sandstone reservoirs does not change due to CO_2 injection (e.g. [5,25,26]).

A phenomenon related to this, which received less attention, but which can also have a dramatic impact on reservoir permeability, is the decrease in permeability due to the injection of supercritical (sc) CO_2 and associated live brine flow. This effect has been observed by a number of researchers [27,28] who report permeability decreases up to 60% and hypothesize that it is caused by either mineral precipitation or fines migration.

From a carbon geo-storage project perspective this is a highly significant effect, because - as Wiese et al. [29] pointed out - aquifer permeability has a dominant effect on injectivities. Permeability and permeability changes thus need to be carefully assessed prior to CO_2 injection to avoid project failure.

In this work we flooded sandstone plugs with live brine and scCO_2 and measured the permeability evolution with time; we demonstrate that the permeability reduction can be significant and is caused by fines migration, and not by mineral precipitation.

2. Experimental Methodology

A Berea and a Fonteinebleau sandstone plug were selected for the experiments, their petrophysical and chemical properties are listed in Table 1. Porosity and nitrogen permeability were measured as a function of confining stress with an AP-608 Coretest instrument; Figure 1 shows that porosity and permeability only slightly depended on effective stress. The compositions of the plugs were measured via XRD with a Bruker-AXS D8 Advance Diffractometer on fragments obtained from the same blocks just adjacent to the drill holes.

Table 1: Petrophysical and chemical properties of the sandstone plugs used in the experiments (porosity and permeability values reported were measured at 10.69MPa effective stress).

sample	porosity [%]	Klinkenberg permeability [mD]	composition	length [mm]	diameter [mm]
Berea	20.6	490	95wt% quartz, 4wt% alumina, 0.1wt% ferric oxide, 0.55wt% ferrous oxide, 0.25wt% magnesium oxide, 0.1wt% calcium oxide	80.7	38.7
Fonteinebleau	7.9	78.8	100wt% quartz	84.1	38.2

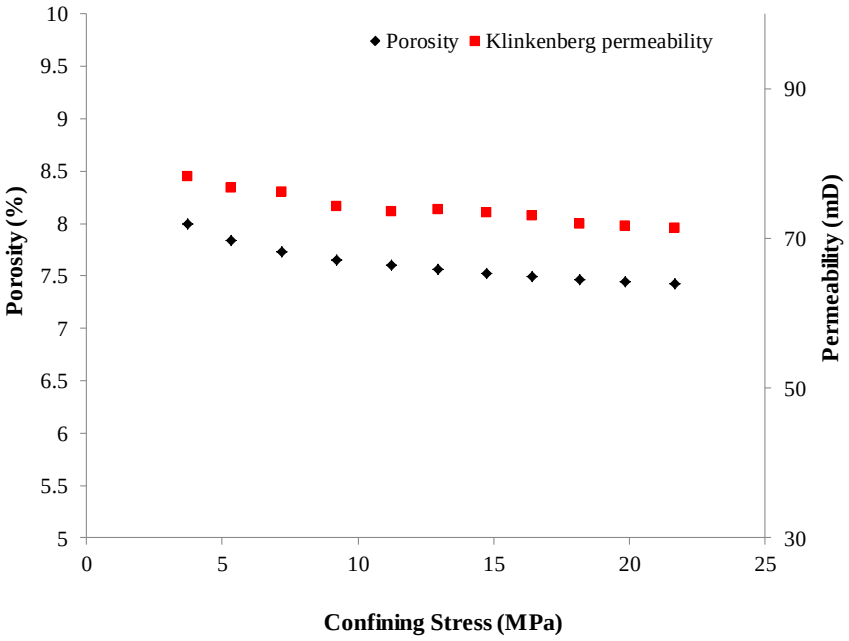

(a)

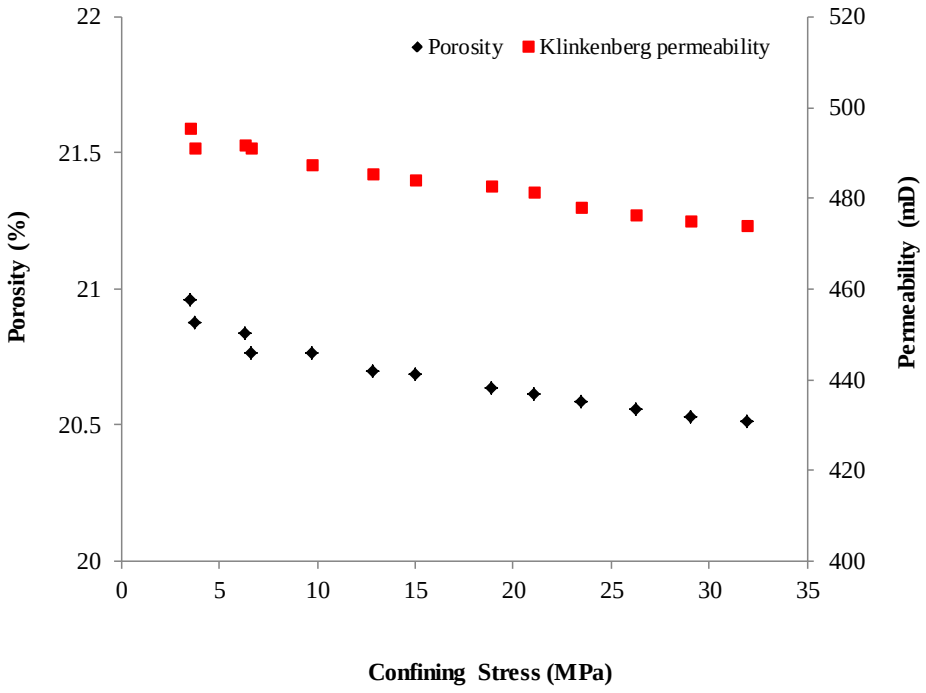

(b)

Fig. 1. Porosity and Klinkenberg permeability of (a) Berea, (b) Fonteinebleau sandstone as a function of effective stress.

After the porosity and permeability tests, each plug was wrapped in PTFE tape, Aluminum foil, and again PTFE tape. The specimen was then covered by a heat-shrinkable PTFE sleeve, which was cured with a heat gun, and finally placed in a rubber sleeve. For a flooding experiment, a plug was then housed in a high pressure elevated temperature core holder, which was initially vaccumed for more than 24 hours (to remove air), and then saturated with dead brine (5 wt% NaCl + 1 wt% KCl in deionized water). Subsequently the confining stress was increased to 10.69MPa, the rig heated to 323K (± 1K) and brine pore pressure was increased to 10MPa by a high precision syringe pump; these thermophysical conditions approximately correspond to a storage formation at 1000m depth. Finally dead brine was injected into the plug with a second high precision syringe pump at constant flow rates, which were stepwise increased (0.3, 1, 2, 3, 5, 10, 20, 50 mL/min); this flooding sequence was repeated with live brine; the live brine was prepared in a mixing reactor described earlier [30]. The pressure drop across the plug was continuously measured with high accuracy pressure sensors (Keller 33X, accuracy = ±1500Pa), and the associated dynamic permeability was calculated with Darcy's law. For the Fonteinebleau plug, three permeability tests with dead and live brine were performed, but between each test $scCO_2$ was injected, again at increasing flow rates up to capillary pressures of ~80kPa (the detailed procedure for this measurement is described elsewhere [31]).

3. Results and discussion

Figure 2 shows the pressure drop evolution with time measured for the Berea sample for the different flow rates used (left: dead brine; right: live brine). As expected a higher flow rate increased the pressure drop significantly; furthermore, it is clear that the pressure drop also continuously and significantly increased with time for constant flow rates. This effect was stronger for live brine injection, but it was also observed for dead brine. An increasing pressure gradient is equivalent to a decreasing brine permeability as illustrated in Figure 3.

The decrease in permeability Δk was related to the injection flow rate, a higher flow rate led to larger Δk, Table 2. This is an indication of fines transport, which should be more significant at higher flow rates as then the shear stresses which release the fines are higher [32]. Moreover, if one hypothesizes that reactive transport, the second

possible plugging mechanism, see above, is responsible for the Δk, then it would be expected that the Damköhler number (= ratio of reaction timescale to convective mass flow timescale) is reduced at higher flow rates thus more plugging should happen at lower flow rates. This is therefore indirect evidence that the formation damage is caused mainly due to fines migration. In addition, the permeability continuously and smoothly dropped with progressing time and we expect a further drop with further extended injection time. This is consistent with Sayegh et al.'s [27] results; we note that Sayegh et al. [27] observed an increase in permeability at significantly longer time scales.

The overall permeability decrease for live brine lied between 10% (1 mL/min flow rate) to 35% (50mL/min flow rate), which is consistent with data reported by Sayegh et al. [27] and Mohamed et al. [28]. This drop in permeability is highly significant and implies that injectivities will be detrimentally affected during live brine migration through a storage formation having similar geochemical characteristics as Berea sandstone. We note that live brine is present in all reservoir volumes swept by $scCO_2$, including the advancing brine front which has been loaded with CO_2 [33] and deeper areas into which live brine sinks due to gravitational instabilities [34].

The picture for Fonteinebleau sandstone was quite different though: essentially brine permeability was only marginally affected by live or dead brine, Figures 4-6 and Table 2. We explain this difference with the different chemical compositions of Fonteinebleau (Table 1), Fonteinebleau is pure quartz, and apparently does not easily release colloids or fines. However, injection of $scCO_2$ significantly decreased brine permeability (by ~23%) and a milky-coloured effluent was observed; cp. Figure 6: $scCO_2$ was injected after each test, the permeability was reduced substantially after the first CO_2 injection (change from test 1 to test 2), but not after the second CO_2 flood.

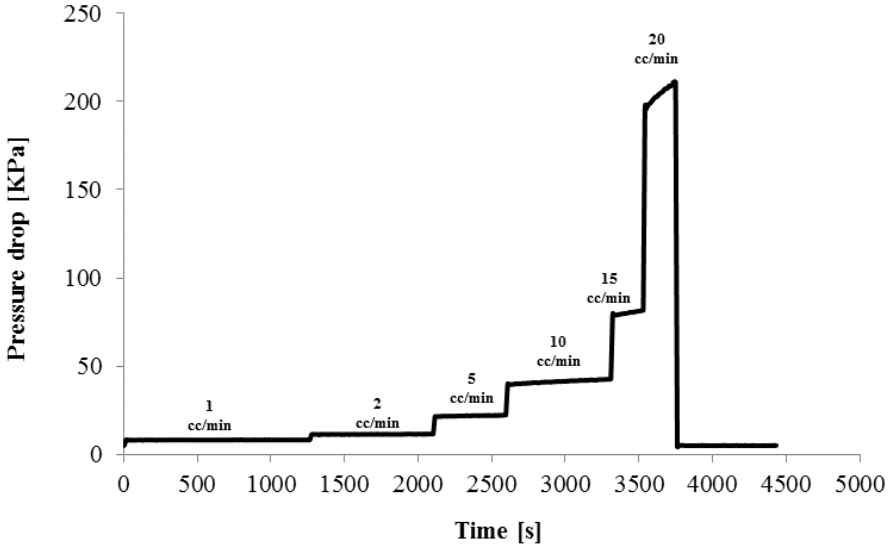

Fig. 2a. Change in pressure drop across the Berea sample as a function of dead brine injection time and injection rate.

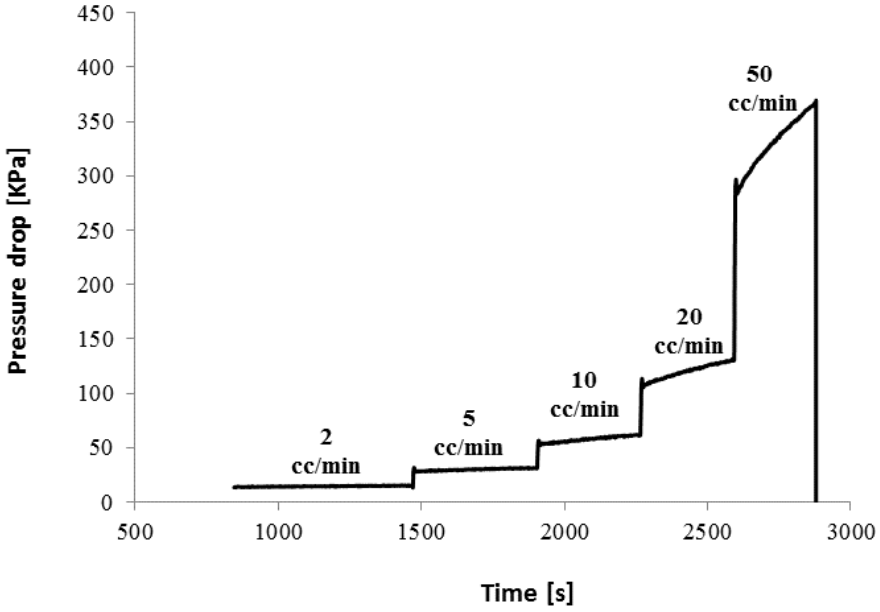

Fig. 2b. Change in pressure drop across the Berea sample as a function of live brine injection time and injection rate.

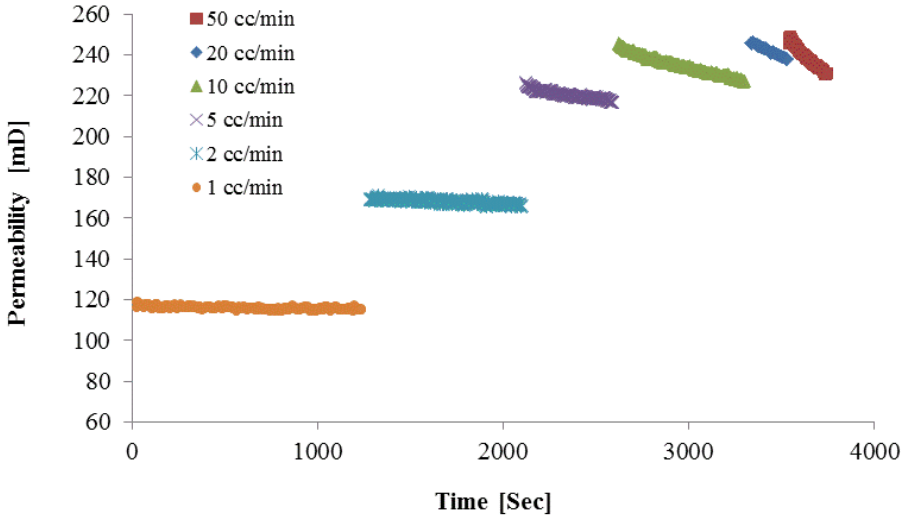

Fig. 3a. Change in permeability of the Berea sample as a function of dead brine injection time and injection rate.

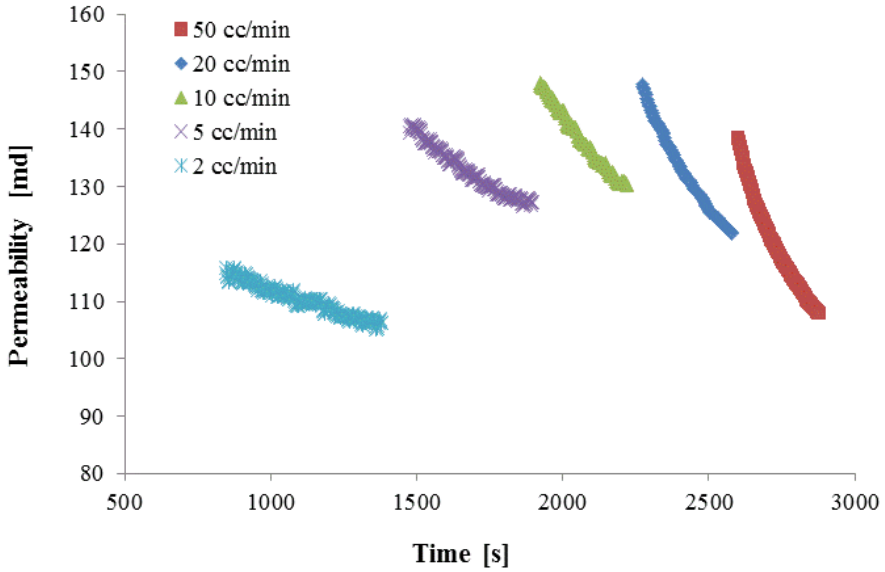

Fig. 3b. Change in permeability of the Berea sample as a function of live brine injection time and injection rate.

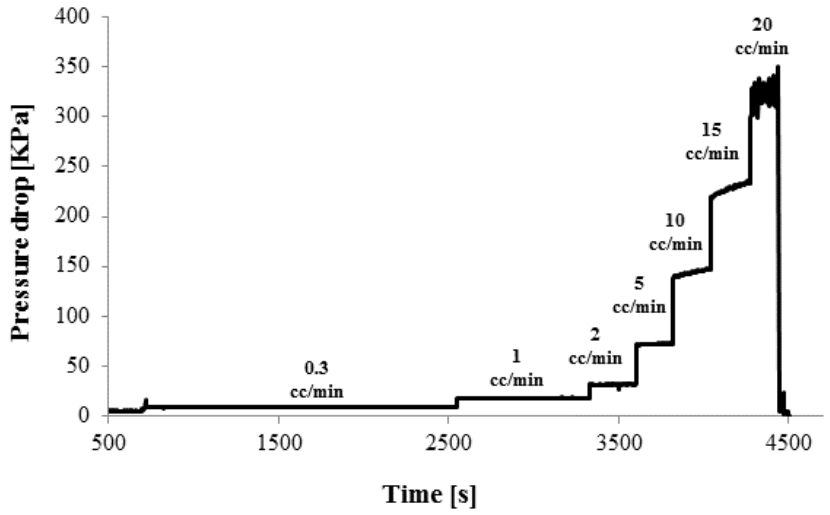

Fig. 4a. Fonteinebleau test 1: change in pressure drop across the sample as a function of dead brine injection time and injection rate.

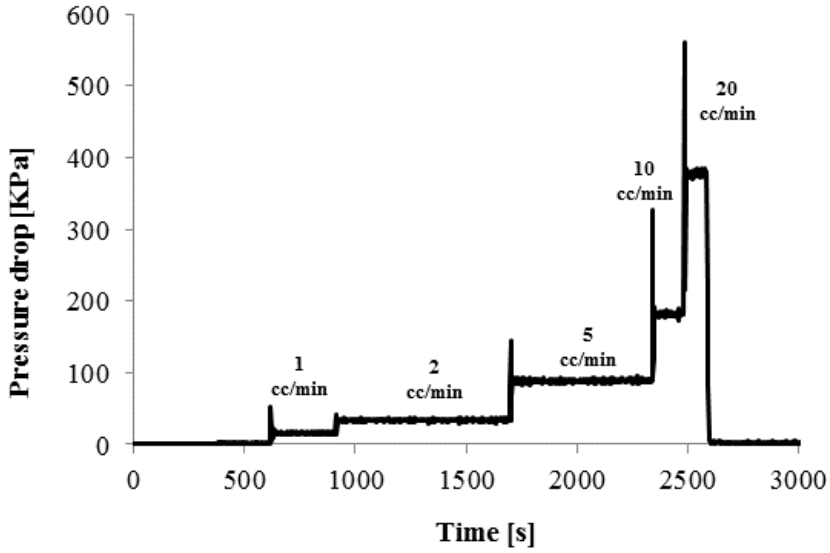

Fig. 4b. Fonteinebleau test 3: change in pressure drop across the sample as a function of dead brine injection time and injection rate

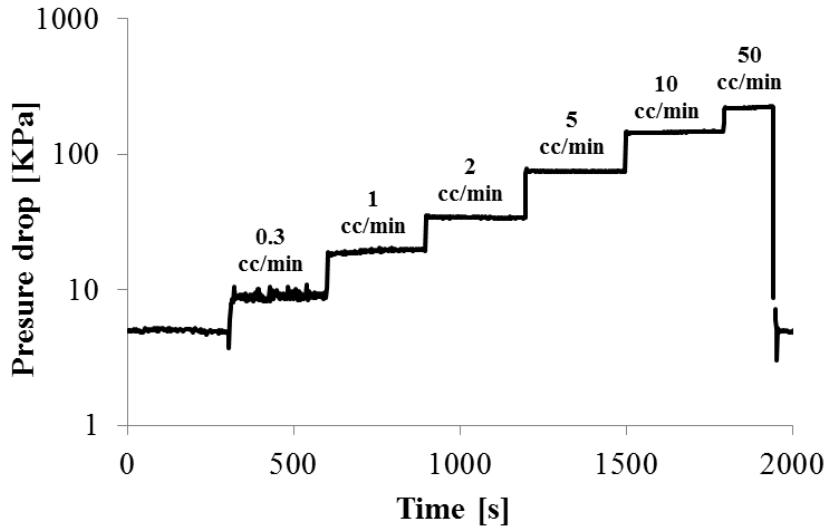

Fig. 5a. Fonteinebleau test 1: change in pressure drop across the sample as a function of live brine injection time and injection rate.

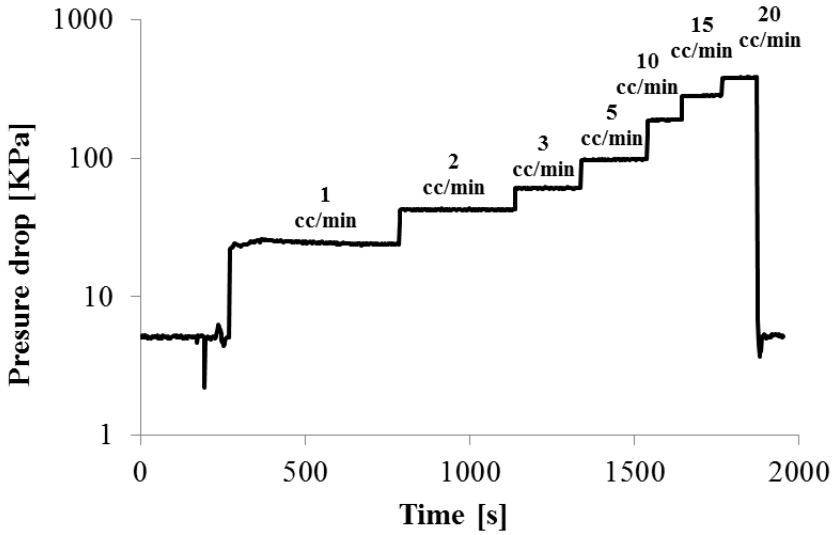

Fig. 5b. Fonteinebleau test 2: change in pressure drop across the sample as a function of live brine injection time and injection rate.

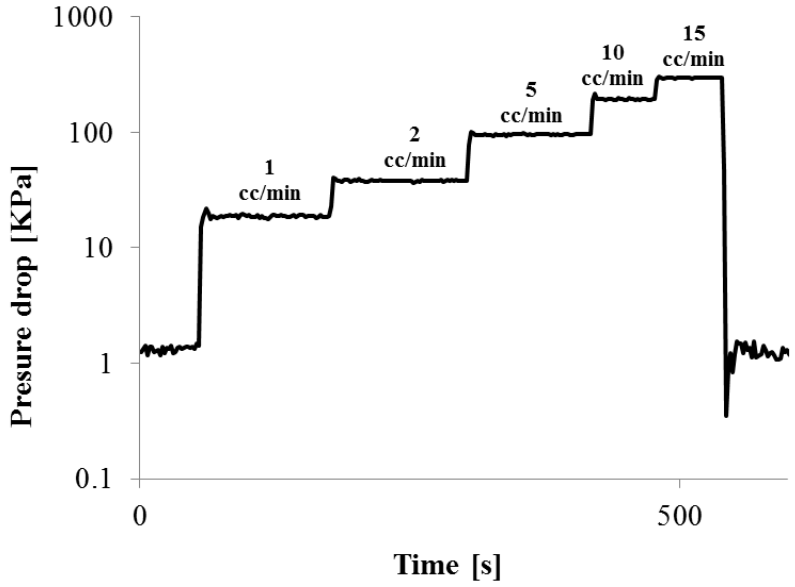

Fig.5c. Fonteinebleau test 3: change in pressure drop across the sample as a function of live brine injection time and injection rate.

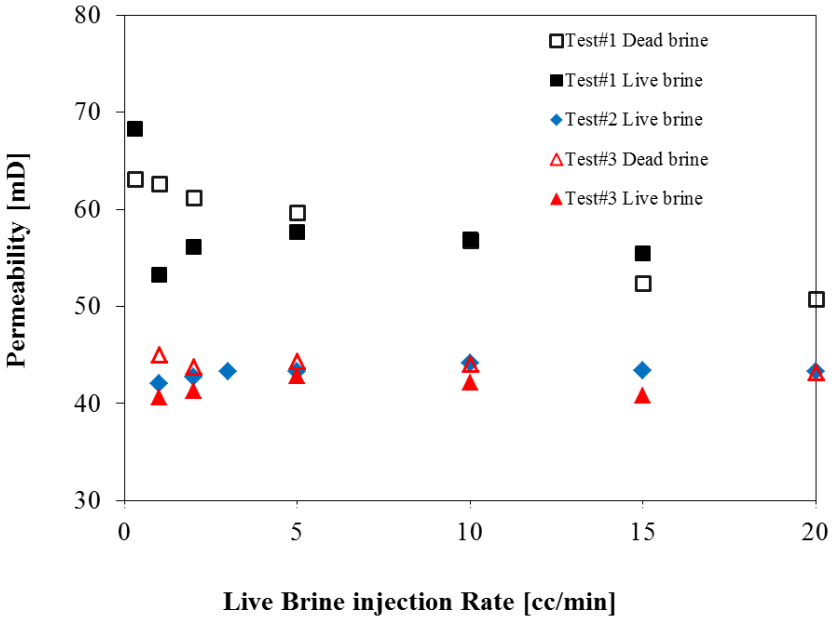

Fig. 6a. Changes in brine permeability of the Fonteinebleau sample as a function of live brine injection time and injection rate for the three tests conducted.

Table 2: Permeability changes in Berea and Fonteinebleau sandstone due to dead or live brine injection.

sample	Flow rate [mL/min]	Brine permeability before flooding [mD]	Brine permeability after flooding [mD]	Permeability change [%]
Berea - dead brine	1	116.5	116.0	0.5
	2	169.2	166.0	3.1
	5	226.3	216.8	9.5
	10	245.0	226.9	18.0
	20	245.6	237.7	7.9
	50	248.2	230.3	17.8
Berea - live brine	1	104.9	96.9	7.9
	2	138.9	122.3	16.5
	5	164.4	148.5	16.0
	10	169.3	150.9	18.4
	20	168.7	141.8	26.9
	50	161.1	125.6	35.5
Fonteinebleau – test 1 Dead brine				
	0.3	62.9	60.4	2.4
	1	62.1	61.6	0.5
	2	61.0	60.6	0.3
	5	56.4	56.0	0.4
	10	56.7	54.8	1.8
	15	52.7	48.1	4.6
	20	50.8	48.3	2.5
Fonteinebleau – test 1 live brine	0.3	68.3	62.6	5.7
	1	53.2	52.6	0.6
	2	56.5	56.3	0.2
	5	57.3	57.1	0.1
	10	57.0	56.8	0.1
	15	55.3	54.9	0.4
Fonteinebleau – test 3 dead brine	1	45.3	44.8	0.5
	2	44.1	42.9	1.1
	5	44.5	44.2	0.2
	10	44.6	44.4	0.1
	20	43.0	42.9	0.1

Fonteinebleau – test 3 live brine	1	40.5	40.1	0.4
	2	42.8	42.4	0.3
	5	42.6	42.5	0.1
	10	42.0	41.8	0.1
	15	41.0	40.8	0.1

Conclusions

We conclude that the permeability of sandstone storage rock can be significantly reduced by live brine or $scCO_2$ flow. The Berea sample was probably damaged by fines release, migration and pore throat plugging as higher permeability reductions were observed for higher flow rates (while mineral precipitation in a hypothesized reactive transport model should increase plugging with reduced flow rate). We measured a maximum drop in permeability of 35%; consistent with data reported by Sayegh et al. [27] (up to 60% drop reported), or Mohamed et al. [28] (up to 53% drop reported). We note, however, that after extended time (4-10 hours) Sayegh et al. (1990) measured an increase in permeability, but the permeability never reached again the original value and remained substantially reduced. It is thus likely that live brine movement through typical sandstone storage rock (which contains impurities such as cements and clays) damages the reservoir. We also note that dead brine, particularly at higher flow rates, can significantly reduce permeability. Furthermore we observed that live or dead brine injection did not significantly affect the permeability of a clean sandstone (Fonteinebleau); however, injection of $scCO_2$ substantially reduced the Fonteinebleau rock permeability (by ~ 23%). Considering that permeability is – apart from formation thickness - the dominant variable determining injectivities [29], these effects should be assessed in more detail and we recommend that these relationships should be evaluated for all storage rocks.

References

[1] Metz B, Davidson O, de Coninck H, Loos M, Meyer M (Eds.) Carbon Dioxide Capture and Storage, Special Report of the Intergovernmental Panel on Climate Change. Cambridge University Press. 2005. ISBN: 9780521685511

[2] Hesse MA., Orr FM., Tchelepi HA. Gravity currents with residual trapping, *Journal of Fluid Mechanics* 2008; 611:35-60.

[3] Iglauer S,Fernø MA, Shearing P, Blunt MJ. Comparison of residual oil cluster size distribution, morphology and saturation in oil-wet and

water-wet sandstone. *Journal of Colloid and Interface Science* 2012; 375:187-192.

[4] Juanes R, Spiteri EJ, Orr FM., Blunt MJ. Impact of relative permeability hysteresis on geological CO_2 storage. *Water Resources Research* 2006; 42:1-13.

[5] Pentland CH, El-Maghraby R, Iglauer S, Blunt MJ. Measurements of the capillary trapping of super-critical carbon dioxide in Berea Sandstone. *Geophys Res Lett*, 2011; 38:L06401.

[6] Iglauer S, Paluszny A, Pentland CH, Blunt MJ. Residual CO_2 imaged with x-ray micro-tomography. *Geophysical Research Letters* 2011; 38:L21403.

[7] Lindeberg E, Wessel-Berg D. Vertical convection in an aquifer column under a gas cap of CO_2. *Energy Conversion Management* 1997; 38:229-234.

[8] Iglauer S. Dissolution Trapping of Carbon Dioxide in Reservoir Formation Brine – A Carbon Storage Mechanism. In: Mass Transfer (ed.: Nakajima H), Rijeka: InTech 2011.

[9] Xu TF, Apps JA, Pruess K. Reactive geochemical transport simulation to study mineral trapping for CO_2 disposal in deep arenaceous formations. *J. Geophys. Res.* 2003; 108(B2):2071–2084

[10] Gaus I. Role and impact of CO_2-rock interactions during CO_2 storage in sedimentary rocks. *International Journal of Greenhouse*

Gas Control 2010; 4:73-89.

[11] Sabirzyanov AN, Il'in AP, Akhunov AR, Gumerov FM. Solubility of water in supercritical carbon dioxide, *High Temperature* 2002; 40:203-206.

[12] Bando S, Takemura F, Nishio M, Hihara E, Akai M. Solubility of CO_2 in aqueous solutions of NaCl at (30 to 60) ºC and (10 to

20) MPa. *Journal of Chemical & Engineering Data* 2003; 48:576-579.

[13] Schaeff HT, McGrail BP. Direct measurements of pH in H_2O-CO_2 brine mixtures to supercritical conditions, Proceedings of

the7th International Conference on Greenhouse Gas Control Technologies (GHGT-7), Vancouver, Canada, 2004.

[14] Sigfusson B, Gislason SR, Matter JM, Stute M, Gunnlaugsson E, Gunnarsson I, Aradottir ES, Sigurdardottir H, Mesfin K,

Alfredsson HA, Wolff-Boenisch D, Arnarson MT, Oelkers EH. Solving the carbon-dioxide buoyancy challenge: The design and field

testing of a dissolved CO_2 injection system. *International Journal of Greenhouse Gas Control Technologies*, in press.

[15] Luquot L, Gouze P. Experimental determination of porosity and permeability changes induced by injection of CO_2 into carbonate

rocks. *Chemical Geology* 2009; 265:148-159.

[16] Smith MM, Sholokhova Y, Hao Y, Carroll SA. CO_2-induced dissolution of low permability carbonates. Part I: characterisation and experiments. *Advances in Water Resources* 2013; 62:370–387.

[17] Luquot L, Rodriguez O, Gouze P. Experimental characterisation of porosity structure and transport property changes in limestone undergoing different dissolution regimes. *Transport in Porous Media* 2014; 101:507–532.

[18] Gilfillan SMV, Sherwood Lollar B, Holland G, Blagburn D, Stevens S, Schoell M, Cassidy M, Ding Z, Zhou Z, Lacrampe-Couloume G, Ballentine CJ. Solubility trapping in formation water as dominant CO_2 sink in natural gas fields, *Nature* 2009; 458:614-618.

[19] Canal J, Delgado J, Falcon I, Yang Q, Juncosa R, Barrientos V. Injection of CO_2-saturated water through a siliceous sandstone plug from the Hontomin test

site (Spain): experiment and modeling. *Environmental Science and Technology* 2013; 47:159–167.

[20] Liu L, Suto Y, Bignall G, Yamasaki N, Hashida T. CO_2 injection to granite and sandstone in experimental rock/hot water systems. *Energy Conversion Management* 2003; 44:1399-1410.

[21] Nightingale M, Johnson G, Shevalier M, Hutcheon I, Perkins E, Mayer B. Impact of injected CO_2 on reservoir mineralogy during CO_2-EOR, Energy Procedia 2009; 1:3399-3406.

[22] Fischer S, Liebscher A, Wandrey M. CO_2-brine-rock interactions – first results of long-term exposure experiments at in situ P-T

conditions of the Ketzin CO_2 reservoir. *Chemie der Erde* 2010; 70:155-164.

[23] Delle Piane C, Olierook HK, Timms NE, Saeedi A, Esteban L, Rezaee R, Mikhaltsevich V, Iglauer S, Lebedev M. Facies-based rock properties distribution along the Harvey 1 stratigraphic well. CSIRO report EP133710; 2013.

[24] Carroll SA, McNab WW, Torres SC. Experimental study of cement-sandstone/shale-brine-CO_2 interactions. *Geochemical Transactions* 2011; 12:9.

[25] Qi R, LaForce TC, Blunt MJ. Design of carbon dioxide storage in aquifer. *International Journal of Greenhouse Gas Control* 2009; 3:195-205.

[26] Krevor SCM., Pini R, Zuo L, Benson SM. Relative permeability and trapping of CO_2 and water in sandstone rocks at reservoir conditions. *Water Resources Research* 2012;48:W02532.

[27] Sayegh SG, Krause FF, Girard M, DeBree C. Rock/fluid interactions of carbonated brines in a sandstone reservoir: Pembina

Cardium, Alberta, Canada. *SPE Formation Evaluation* 1990;399-405.

[28] Mohamed IM, He J, Nasr-El-Din HA. Carbon dioxide sequestration in sandstone aquifers: how does it affect permeability? CMTC 149958, Proceedings of the Carbon Management Technology Conference, Orlando, Florida, USA, 7-9th February; 2012.

[29] Wiese B, Nimtz M, Klatt M, Kuehn M. Sensitivities of injection rates for single well CO2 injection into saline aquifers. *Chemie der Erde* 2010; 70:165-172.

[30] El-Maghraby R, Pentland CH, Iglauer S, Blunt MJ. A fast method to equilibrate carbon dioxide with brine at high pressure and elevated temperature including solubility measurements. *Journal of Supercritical Fluids* 2012; 62: 55-59.

[31] Sarmadivaleh M, Iglauer S. Capillary drainage pressure curve for the system Berea sandstone-CO_2-brine. Fourth EAGE Geological CO_2 Storage Workshop, Stavanger, Norway, 26-28th April; 2014

[32] Civan F. Reservoir Formation Damage Fundamentals, Modeling, Assessment and Mitigation. Gulf Publishing Company: Houston; 2007.

[33] Pentland CH, Iglauer S, El-Maghraby R, Tsuchiya Y, Okabe H, Blunt MJ. Measurement of carbon dioxide capillary trapping in core analysis, SPE 138476, Proceedings of the SPE International Conference on CO_2 Capture, Storage, and Utilization, New Orleans,

Lousiana, USA, 10-12 November; 2010.

[34] Riaz A, Hesse M, Tchelepi HA, Orr FM. Onset of convection in a gravitationally unstable diffusive boundary layer in porous media. *Journal of Fluid Mechanics* 2006; 548:87-111.

5.2 N_2+ CO_2+ NaCl Brine Interfacial Tensions and Contact Angles on Quartz at CO_2 Storage Site Conditions in the Gippsland Basin, Victoria/Australia

Al-Yaseri, A., Sarmadivaleh, M., Saeedi, A., Lebedev, M., Barifcani, A. and Iglauer, S., 2015. N_2+ CO_2+ NaCl brine interfacial tensions and contact angles on quartz at CO_2 storage site conditions in the Gippsland basin, Victoria/Australia. Journal of Petroleum Science and Engineering, 129, pp.58-62.

$N_2 + CO_2 + NaCl$ brine interfacial tensions and contact angles on quartz at CO_2 storage site conditions in the Gippsland Basin, Victoria /Australia

Ahmed Al-Yaseri[1], Mohammad Sarmadivaleh[1], Ali Saeedi[1], Maxim Lebedev[2], Ahmed Barifcani[3], and Stefan Iglauer[1]

[1]Curtin University, Department of Petroleum Engineering, 26 Dick Perry Avenue, 6151 Kensington, Australia

[2]Curtin University, Department of Exploration Geophysics, 26 Dick Perry Avenue, 6151 Kensington, Australia

[3]Curtin University, Department of Chemical Engineering, 26 Dick Perry Avenue, 6151 Kensington, Australia

Abstract

Carbon geo-sequestration (CGS) has been identified as an important method to reduce carbon dioxide (CO_2) emissions to the atmosphere thus mitigating global warming. In CGS, the CO_2 captured from large point source emitters is injected into hydrocarbon reservoirs for enhanced oil and gas recovery or into deep saline aquifers for storage. In this context the State of Victoria (southeast Australia) is reviewing the suitability of Victorian sedimentary basins as CO_2 sinks. The main focus is on the Gippsland basin, which has been positively evaluated from a geological point of view. Now it is necessary to assess the storage capacity of the formation and thus the intimately related fluid–fluid–rock properties. We therefore conducted interfacial tension and contact angle measurements at the prevailing storage conditions (13 MPa, 333 K); as a result, we show that CO_2 has a relatively high water contact angle (θ= 47°), while lower θ values were measured for N_2 (θ=40.6°) and for a 50 mol% CO_2 + 50 mol% N_2 mixture (θ=33.9°). Consequently all systems were weakly water-wet. This implies that residual and structural trapping capacities are reduced; however, both mechanisms should work adequately. Specifically, we predict that a CO_2 column height of ~698 m can be permanently immobilized beneath the caprock.

Keywords

carbon geo-sequestration, interfacial tension, contact angle, quartz, carbon dioxide, nitrogen.

1. Introduction

Understanding the interfacial characteristics of brine, CO_2, N_2 and flue gas in rock is of vital importance in carbon geo-storage (CGS), and petroleum engineering operations where these gases are injected deep into the subsurface for storage (IPCC, 2005; Iglauer, 2011; Kaveh et al., 2014) or for oil and gas recovery schemes (Blunt et al., 1993; Islam et al., 2009; Iglauer et al., 2013). Particularly, the quality of CGS containment security and oil and gas production optimization hinge on reducing the current uncertainty associated with these parameters (Morrow, 1990; Iglauer et al., 2012a; Iglauer et al., 2015). For instance, the contact angle (θ) between the rock, water and gas and the gas–water interfacial tension γ strongly affect residual trapping in CGS schemes (Iglauer et al., 2011; Chaudhary et al., 2013) and residual oil saturations in oil recovery operations (Morrow, 1990; Spiteri et al., 2008; Iglauer et al., 2012b). In addition, relative permeabilities (McCaffery and Bennion, 1974) and capillary pressures (Morrow,1976; Anderson, 1987) are two key variables which also depend on θ and γ, and which determine reservoir-scale fluid flow. Furthermore, θ and γ strongly influence structural trapping, the primary CO_2 trapping mechanism in CGS (Iglauer et al., 2012b). It is therefore essential that θ and γ are well constrained to make reliable reservoir predictions, and related economic and safety risk assessments.

In this context, several authors reported CO_2/brine contact angles on silica substrates and CO_2–water interfacial tensions at reservoir conditions (Massoudi and King, 1974; Jho et al., 1978; Byung-Soo et al., 1995; Wesch et al., 1997; Hebach et al., 2002; Park et al., 2005; Chiquet et al., 2007; Sutjiadi-Sia et al., 2008; Bachu and Bennion, 2009; Chalbaud et al., 2009; Georgiadis et al., 2010; Bikkina, 2011; Mills et al., 2011; Jung and Wan, 2012; Broseta et al., 2012; Li et al., 2012; Farokhpoor et al., 2013; Saraji et al., 2013; Iglauer et al., 2014; Sarmadivaleh et al., 2015). However, N_2 and flue gas systems were assessed to much lesser extent: Kaveh et al. (2014) found that water contact angles (θ) for CO_2-deionized water–Bentheimer sandstone systems are higher than those forflue gas (20 mol% CO_2 and 80 mol% N_2) at low to moderate pressures (up to 14 MPa) and 318 K. Kaveh et al.(2013,2014) also found that γ for N_2 is higher than for flue gas (20 mol% CO_2 and 80 mol% N_2) or CO_2 at 313 K and pressures below 15 MPa, consistent with previous results

(Wiegand and Franck, 1994; Yan et al., 2001). Mills et al. (2011) observed a small difference in θ between N_2 and CO_2 at 313K and 5.5 MPa or 13MPa pressure in a quartz-brine (35000ppm salt brine: 18200ppm Cl-, 11700 ppm Na+, 3180ppm SO_4^{2-}, 1170ppm Ca^{2+}, 326ppm Mg^{2+}, 123ppm K^{+}) system. However, there is only very scant information available in terms of such contact angles at higher temperatures and high pressures; these are, nevertheless, most relevant in industry.

In this study we focus on the thermophysical conditions prevailing at a proposed Australian CO_2 storage formation (Gippsland Basin), and present related experimental contact angle and interfacial tension data. The Gippsland Basin is one of the largest sedimentary basins in Victoria, Australia, comprising a total area of approximately of 56,000 km^2 (one third onshore and two thirds offshore), Gibson et al. (2006). Several research projects examined the geology of the basin in terms of CGS projects (Annetts et al., 2012; Gibson et al., 2006), and they conclude that it is an optimal CO_2 storage site with a suggested target injection depth of ~1600m, (Gibson et al., 2006). We now assess the structural trapping capacity of the formation, based on our θ and γ measurements.

Experimental methodology

The composition of a core recovered from the Gippsland Basin at the target storage depth (1602.03m; gas permeability 990.27mD and 25.58% porosity) was measured via XRD with a Bruker-AXS D9 Advance Diffractometer (Kaolinite 2.3 wt%, Quartz 82 wt%, Rutile 0.3wt%, Muscovite 1.8wt%, Barite 4wt%, and Amorophous 9wt%); this indicated that the formation is relatively clean and consists mainly of quartz. We thus conduct our contact angle measurements on a smooth alpha-quartz crystal surface (RMS roughness ~56 nm measured with atomic force microscopy (model AFM DSE 95-200), Figure 1).

The salinity of the brine in the Gippsland basin at a depth of 1600m was determined as ~5000ppm (Michael et al., 2011), and the temperature and pressure at 1600m depth were measured as 13MPa and 333K (Ozimic et al. 1987); we thus conducted the measurements at these thermophysical conditions using 5000ppm NaCl brine.

Contact angle measurements

The quartz substrate was first cleaned with acetone and then exposed to an air plasma apparatus for at least 15min. Plasma cleaning is of prime importance as surface contamination can have a dramatic impact on measured contact angle values (Mahadevan, 2012; Iglauer et al. 2014). The substrate was then placed in a high pressure cell, and the system was flooded for at least 10min with CO_2 (99.9mol%), N_2 (99.9mol%) or with CO_2-N_2 mixture of 50 mol% CO_2 + 50 mol% N_2 (note that the purity of the N_2-CO_2 mixture has an uncertainty of ±1mol%). Subsequently the gas pressure in the cell was increased to a pre-set value with a high precision syringe pump (Figure 2). A de-gassed (i.e. placed under vacuum for more than 10 hours) brine (5000ppm NaCl in deionized water) droplet (average volume of a single brine drop was ~7μL) was then dispensed onto the substrate's surface, followed by a second and a third drop, while a special high resolution video camera (Basler scA640-70fm and 35mm CCTV lens) recorded the dispensing process as a movie. The contact angle of the drop just before the three phase line jumped forward (due to adding more water) was set to the advancing θ. The water advancing contact angles θ were then measured from the images extracted from the movie files. Temperature and pressure were kept constant (13MPa and 333K), and each experiment was repeated three times for each type of gas; the associated standard deviation of these measurements was 3° based on replicate measurements. We note that the experiments were conducted with dry gases and under-saturated brine; however, we also investigated the effect of CO_2-brine equilibration time on θ: CO_2 and brine were equilibrated in a mixing reactor described earlier (El-Maghraby et al., 2012) and θ was measured for the equilibrated fluids and compared with the θ measured for fresh fluids as a function of time.

Interfacial tension measurements

For measuring the interfacial tension, the pendant drop method at high pressure and high temperature conditions was used (Adamson, and Gast, 1997; Georgiadis, 2011; Sarmadivaleh et al. 2015).

Experimentally, a pressure cell was heated (333K), and then CO_2 was injected into the cell with a high precision syringe pump (ISCO pump model 500D) until the prescribed pressure was obtained (13 MPa). Subsequently brine was introduced from the top of the cell through a needle which was connected to another syringe pump

(ISCO pump model 500D). This pump was set to a constant flow rate (0.35 ml/min) and pressure (13MPa); consequently, a drop of brine at the bottom of the needle was formed. The drop volume gradually increased until it fell down due to gravity forces. A high resolution video camera (Basler scA640-70fm) was used to record the whole process, and images were extracted from the movie files for the γ measurement (Georgiadis, 2011). Each γ measurement was repeated three times for each type of gas, and then arithmetic averages were calculated together with standard deviations, Figure 5. The standard deviation of these measurements was 3mN/m based on the replicate measurements. Note that for the computations, the density difference (Δρ) was taken from Georgiadis et al. (2010).

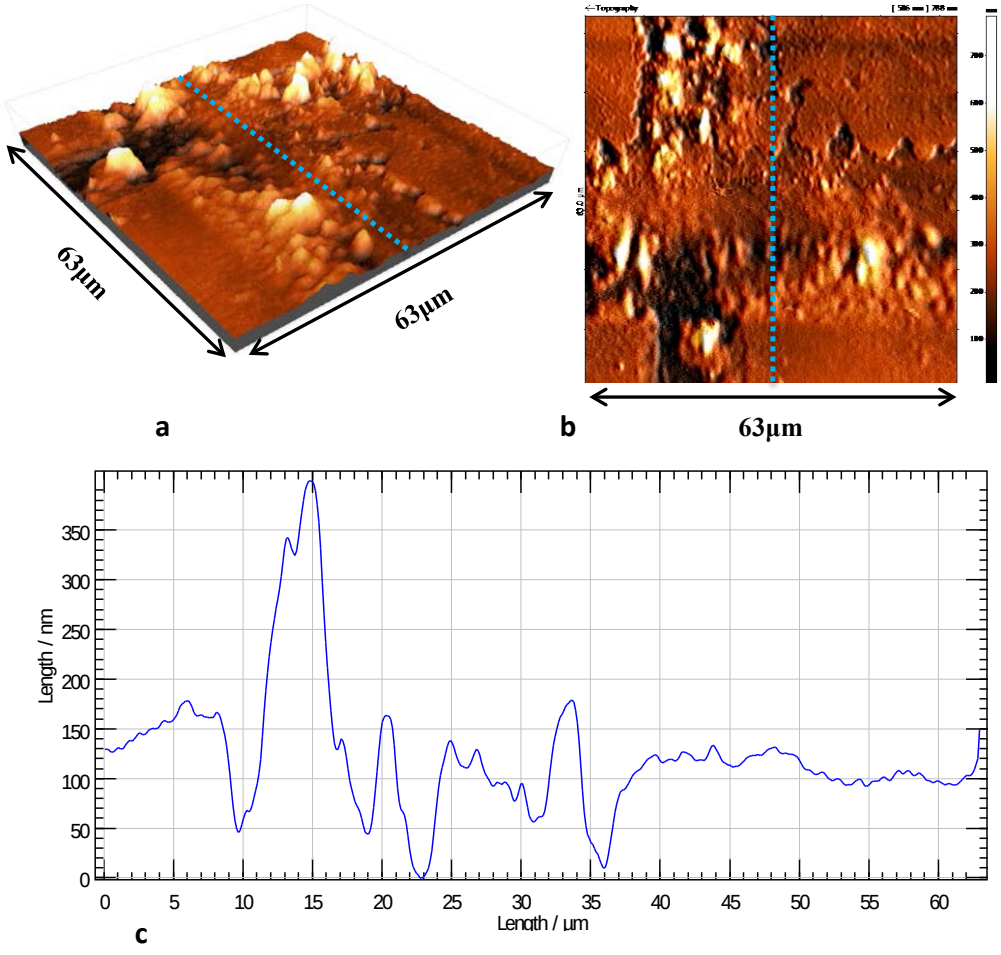

Figure. 1. Atomic Force Microscopy images of the quartz surface used in the experiments. (a) 3D topography of the substrate; (b) deflection signal, different heights are coloured (black is 0nm, white is 800nm); (c) surface profile (blue dotted line shown in Figures (a) and (b)).

Results and discussion

We measured CO_2/N_2-brine interfacial tensions and CO_2/N_2-brine-quartz contact angles at conditions prevailing at the CarbonNet storage site to provide structural trapping capacity predictions. Specifically, we will predict the maximum CO_2 column height, which can be permanently stored beneath the caprock.

Contact Angles

The data measured shows that CO_2 had a relatively high water advancing contact angle ($\theta = 47° \pm 3.4°$), which apparently was caused by the elevated temperature (Saraji et al., 2013; Sarmadivaleh et al., 2015) and pressure (Chiquet et al., 2007; Broseta et al., 2012; Iglauer et al., 2012a,2014; McCaughan et al., 2013; Sarmadivaleh et al., 2015), Figure 3. While the θ increase with pressure can be explained by increased intermolecular interactions between CO_2 and quartz (due to increased CO_2 density), Iglauer et al. (2012a), it is currently unclear why θ increases with temperature. N_2 ($40.6° \pm 3.9°$) and the CO_2/N_2 mixture ($33.9° \pm 6°$) also showed increased contact angles, although θ was higher for CO_2; note that the contact angles for air and CO_2 are ~0° at ambient conditions (Grate et al., 2012; Iglauer et al., 2014). Consequently all systems were weakly water-wet at the tested reservoir conditions, i.e. elevated pressure and temperature at moderate salinity (13 MPa, 333K, 5000ppm NaCl). As a comparison, Kaveh et al. (2014) measured a θ at 318K of ~3° at 2 MPa which increased to ~8° at 14 MPa on Bentheimer sandstone (which consisted of 96% quartz) for flue gas (20mol% CO_2 + 80mol% N_2). The difference between Kaveh et al. (2014), and our results is probably due to the composite (porous) character of the rock. Mills et al. (2011), measured a θ of ~33° for N_2 on quartz at 313K and 13 MPa which slightly decreased to ~30° at a lower pressure of 5.5 MPa. This is consistent with our results and our finding that increased temperature increases θ (Sarmadivaleh et al., 2015; Saraji et al. 2013). Figure 4 shows that there was no significant effect of CO_2-brine equilibration on rapid contact angle measurements (completed within a minute; note that our measurements took less than 30seconds); however, with extended time a significant effect developed, which is probably due to mass transfer (Wang et al., 2013). It is well known that

solubility of CO_2 in water is higher than that of N_2 (Kolev, 2012); we thus expect a less significant equilibration effect for N_2 or the N_2-CO_2 mixture.

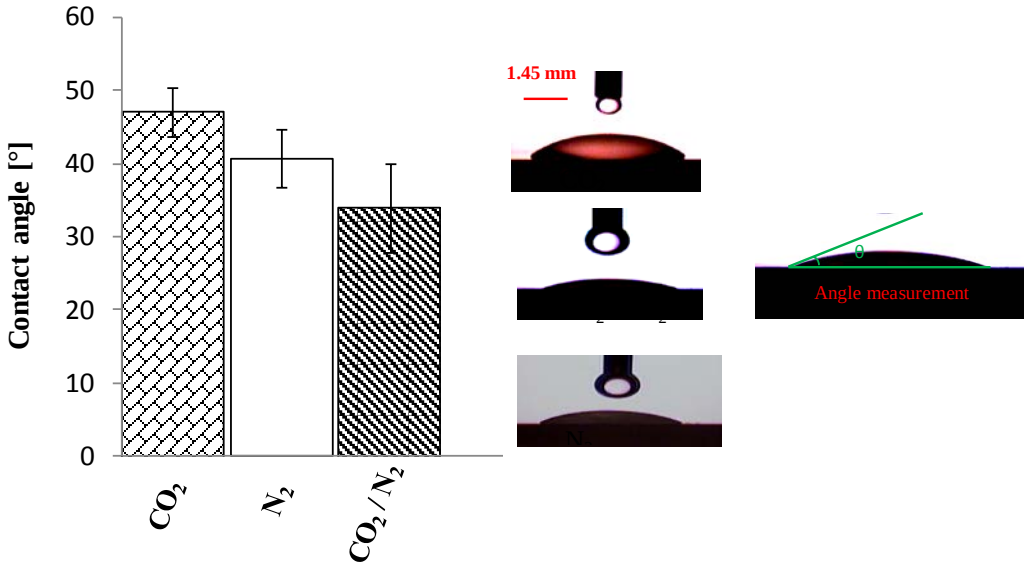

Figure 3. Arithmetic average of the measured advancing water contact angles on quartz for 50 mol%:50mol% CO_2/N_2 mixture, N_2, CO_2 - brine - quartz systems at (measured at 313K and 13 MPa). The error bars represent the standard deviations based on replicate measurements.

Interfacial Tension

A CO_2-brine interfacial tension of 38.7 mN/m ± 3.9 mN/m was measured, consistent with literature data (Massoudi and King 1974; Jho et al., 1978; Byung-Soo et al., 1995; Wesch et al., 1997; Hebach et al., 2002; Park et al., 2005; Bachu and Bennion, 2009; Chalbaud et al., 2009; Georgiadis et al., 2010; Li et al., 2012), while nitrogen had a higher interfacial tension (60.5mN/m ± 3.7 mN/m), as expected, and consistent with (Yan et al., 2001), who measured a γ of ~52mN/m and Wiegand and Franck (Wiegand and Franck, 1994) who measured ~62mN/m at the same thermophysical conditions (note: we interpolated their results for comparison purposes), Figure 5. The 50mol%:50mol% CO_2-N_2 mixture had a lower interfacial tension (40.6mN/m ± 3 mN/m), similar to the CO_2-brine γ, while Kaveh et al. 2013,2014), measured ~55mN/m for a 20mol% CO_2/80mol% N_2 mixture at 318K and 13 MPa, which is significantly higher than the values we measured for the gas mixture, probably because of the different chemical compositions.

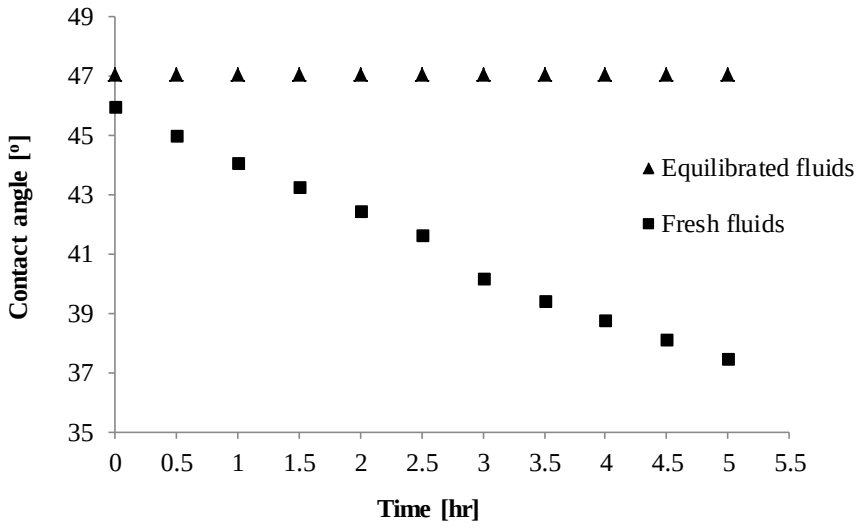

Figure 4. CO_2–brine-quartz water advancing contact angles at 13MPa and 333K for equilibrated and fresh CO_2-brine fluid systems.

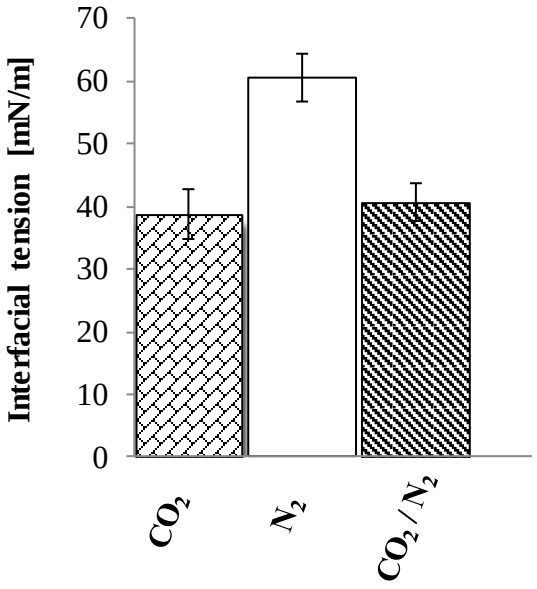

Figure 5. Arithmetic average of the measured interfacial tensions for CO_2, N_2, and 50mol%N_2:50mol% CO_2. The error bars represent the standard deviations based on replicate measurements.

Implications of measured data

We predict that a maximum CO_2 column height h of ~698m can be permanently immobilized beneath the Gippsland basin caprock using a capillary force-buoyancy force balance, equation 1 (Dake 1978); and the values measured for θ (=47°), γ (=39 mN/m), Δρ (≈518, Georgiadis et al., 2010), and pore radius *r* (≈0.015μm, Rezaee et al., 2013).

$$h = \frac{2\gamma cos\theta}{\Delta\rho g r} \quad (1)$$

Conclusions

We conclude that N_2, CO_2, and 50mol%:50mol% N_2/CO_2 – advancing water contact angles θ on clean quartz are elevated at storage conditions specific to the CarbonNet project in the Gippsland basin (333K, 13 MPa, 5000ppm NaCl). A significant increase in θ – up to ~50° for CO_2, ~40° for N_2, and ~35° for N_2/CO_2 - was measured (when compared to ambient conditions (Grate et al. 2012, Iglauer et al. 2014). We thus expect that residual and structural trapping capacities are significantly reduced (Naylor et al. 2011, Iglauer et al. 2011,2012a,b, Chaudhury et al. 2013), however, all systems studied were weakly water-wet, which implies that residual and structural trapping will work at the given thermophysical conditions. Relative permeabilities are also probably affected (McCaffery and Bennion 1974, Levine et al. 2014). Furthermore, we note that the N_2-brine interfacial tension measured was higher than the CO_2-brine or N_2/CO_2-brine interfacial tensions (which were similar), and this may influence residual gas saturations.

Acknowledgements

The authors wish to acknowledge financial assistance provided through Australian National Low Emissions Coal Research and Development (ANLEC R&D). ANLEC R&D is supported by Australian Coal Association Low Emissions Technology Limited and the Australian Government through the Clean Energy Initiative.

References

Adamson, A.W., and Gast, A.P., 1997. Physical chemistry of surfaces. New York: John Wiley and Sons.

Anderson, W.G., 1987. Wettability Literature Survey- Part 4: Effects of Wettability on Capillary Pressure. Journal of Petroleum Technology. 39(10), 1283–1300.

Annetts D., Hauser J., Gunning J., Gurevich B., Bona A., Pevzner R., Harris Brett ., Urosevic M., al Ajami M., Cant J., 2012. A deployment strategy for effective geophysical remote sensing of CO_2 sequestration. Technical Report EP125197, ANLEC R&D.

Bachu, S., and Bennion, D.B., 2009. Interfacial Tension between CO_2, Freshwater, and Brine in the Range of Pressure from (2 to 27) MPa, Temperature from (20 to 125) °C, and Water Salinity from (0 to 334000) mg·L-1. J. Chem. Eng. 54, 765–775.

Bikkina, P.K., 2011. Contact angle measurements of CO_2-water-quartz/calcite systems in the perspective of carbon sequestration. International Journal of Greenhouse Gas Control. 5, 1259-1271.

Blatt, H., and Schultz, D.J., 1976. Size distribution of quartz in mudrocks. Sedimentology. 23, 857-866.

Blunt, M., Fayers, F.J., and Orr, F.M., 1993. Carbon dioxide in enhanced oil recovery.
Energy Conversion and Management. 34 (9), 1197-1204.

Broseta, D., Tonnet, N., and Shah, V., 2012. Are rocks still water-wet in the presence of dense CO_2 or H2S? Geofluids. 12(4), 280-294.

Byung-Soo, C., Gordon, and Wilkinson, T., 1995. Interfacial Tension in High-pressure Carbon Dioxide Mixtures. Ind. Eng. Chem. Res.. 34, 4371-4377.

Chalbaud, R.M., Lombard, J.M, Martin, F., Egermann, P., Bertin, H., 2009. Interfacial Tension Measurements and Wettability Evaluation for Geological CO_2 Storage. Adv. Water Res. 32, 98–109.

Chaudhary, K., Bayani, C.M., Wolfe, W.W., Maisano, J.A., Ketcham, R.A., and Bennett, P.C., 2013. Pore-scale trapping of supercritical CO_2 and the role of grain wettability and shape, Geophysical Research Letters. 40, 1-5.

Chiquet, P., Broseta, D., Thibeau, S., 2007. Wettability alteration of caprock minerals by carbon dioxide. Geofluids. 7, 112–122.

Dake L.P., 1978. Fundamentals of Reservoir Engineering. Developments in Petroleum Science, 8. Elsevier, Amsterdam-London-New York-Tokyo.

El-Maghraby, R., Pentland, C., Iglauer, S., and Blunt, M., 2012. A fast method to equilibrate carbon dioxide with brine at high pressure and elevated temperature including solubility measurements. Journal of Supercritical Fluids. 62, 55-59.

Farokhpoor, R., Bjørkvik, B.J.A., Lindeberg, E., and Torsæter, O., 2013. Wettability behaviour of CO_2 at storage conditions. International Journal of Greenhouse Gas Control. 12, 18-25.

Georgiadis, A., 2011. Interfacial Tension of Aqueous and Hydrocarbon Systems in the Presence of Carbon Dioxide at Elevated Pressures and Temperatures. PhD thesis, Imperial College London.

Georgiadis, A., Geoffrey, M., Martin, J.P., and Alexander, B., 2010. Interfacial Tension Measurements of the (H_2O+CO_2) System at Elevated Pressures and Temperatures. J. Chem. Eng.55, 4168–4175.

Gibson P., C. M., S. Edwards, R. Langford, and B. Vakarelov, 2006. Review of geological storage opportunities for Carbon Capture and Storage (CCS) in Victoria.

Technical Report ICTPL–RPT06–0506, CRC for Greenhouse Gas Technologies, the University of Adelaide.

Grate, J.W., Dehoff, K.J., Warner, M.G., Pittman, J.W., Zhang, C., Oostrom, M., 2012. Correlation of oil-water and air-water contact angles of diverse silanized surfaces and relationship to fluid interfacial tensions. Langmuir. 28, 7182-7188.

Hebach, A., Oberhof, A., Dahmen, N., Ko¨gel, A., Ederer, H., Dinjus, E., 2002. Interfacial Tension at Elevated Pressures Measurements and Correlations in the Water + Carbon Dioxide System. J. Chem. Eng. 47, 1540–1546.

Iglauer, S., 2011. Dissolution Trapping of Carbon Dioxide in Reservoir Formation Brine A Carbon Storage Mechanism. In: Mass Transfer - Advanced Aspects, Hironori Nakajima (Ed.). ISBN: 978-953-307-636-2, InTech.

Iglauer, S., Fernø, M.A., Shearing, P., Blunt, M.J., 2012b. Comparison of residual oil cluster size distribution, morphology and saturation in oil-wet and water-wet sandstone. Journal of Colloid and Interface Science. 375, 187-192.

Iglauer S., Paluszny A., and Blunt M. J., 2013. Simultaneous oil recovery and residual gas storage: A pore-level analysis using in situ X-ray micro-tomography. Fuel, 103(0), 905-914.

Iglauer, S., Hassan, A., Sarmadivaleh, M., Liu, K., and Pham, C., 2014. Contamination of silica surfaces: impact on water-CO_2-quartz and glass contact angle measurements. International Journal of Greenhouse Gas Control. 22, 325-328.

Iglauer, S., Mathew, M., and Bresme, F., 2012a. Molecular dynamics computations of brine-CO_2 interfacial tensions and brine-CO_2-quartz contact angles and their effects on structural and residual trapping mechanisms in carbon geo-sequestration. J Colloid Int Sci. 386, 405-414.

IPCC, 2005. Carbon dioxide capture and storage. Working Group III of the Intergovernmental Panel on Climate Change. pp. 443.

Islam, Didarul, M.d., Alshehhi, M., Ohadi, M., 2009. Emerging applications in cryogenics--Nitrogen injection for reservoir Enhanced Oil Recovery. ASHRAE Transactions. 15(2), 959-966.

Jho, C., Nealon, D., Shogbola, S., and King, A.D., 1978. Effect of Pressure on Surface Tension of Water: Adsorption of Hydrocarbon Gases and Carbon Dioxide on Water at Temperatures Between 0 and 50 °C. J. Colloid Interface Sci. 65, 141–154.

Jung, J.W., Wan, J., 2012. Supercritical CO_2 and ionic strength effects on wettability of silica surfaces: equilibrium contact angle measurements. Energy and Fuels. 26, 6053–6059.

Levine, J.S., Goldberg, D.S., Lackner, K.S., Matter, J.M., Supp, M.G., and T.S. Ramakrishnan, 2014. Relative permeability experiments for carbon dioxide displacing brine and their implications for carbon sequestration. Environmental Science & Technology. 48, 811–818.

Michael K., Varma S., Bekele E., 2011. Challenges of modelling the impact of multi-purpose aquifer utilization on variable-density groundwater flow. International Conference on Flows and Mechanics in Natural Porous Media from Pore to Field Scale, 16-18 November 2011, France.

Naylor M., Wilkinson M., and Haszeldine R. S., 2011. Calculation of CO_2 column heights in depleted gas fields from known pre-production gas column heights. Marine and Petroleum Geology, 28(5), 1083-1093.

Kaveh, S.N., Rudolph, N., Rossen, E.S.J., van Hemert, WR., P. and Wolf, K.H., 2013. Interfacial tension and contact angle determination in water- sandstone systems with injection of flue gas and carbon dioxide. IOR 2013 - 17th European Symposium on Improved Oil Recovery. EAGE, St. Petersburg, Russia.

Kaveh, S.N., Rudolph, N., van Hemert, W.R., Rossen, E.S.J., and Wolf, K.H., 2014. Wettability evaluation of CO_2-water-Bentheimer sandstone system: contact angle, dissolution and bubble size. Energy and Fuels, 28(6), 4002-4020.

Kolev N., 2012. Solubility of O2, N2, H2 and CO2 in water Multiphase Flow Dynamics 4. Springer Berlin Heidelberg, pp. 209-239.

Li, X., Edo, B., Geoffrey, C.M., and Martin, J.P., 2012. Interfacial Tension of (Brines + CO_2): (0.864 NaCl + 0.136 KCl) at Temperatures between (298 and 448) K, Pressures between (2 and 50) MPa, and Total Molalities of (1 to 5) mol·kg^{-1}. Journal of Chemical & Engineering. 57, 1078−1088.

Mahadevan, J., 2012. Comments on the paper titled "Contact angle measurements of CO_2-water-quartz/calcite systems in the perspective of carbon sequestration: A case of contamination. International Journal of Greenhouse Control. 7, 261-262.

Massoudi R, and King A.D., 1974. Effect of Pressure on Surface Tension of Water Adsorption of Low Molecular Weight Gases on Water at 25 Degrees. J. Phys. Chem. 78, 2262–2266.

McCaffery, F.G., Bennion, D.W., 1974. The effect of wettability on two-phase relative permeabilities. Journal of Canadian Petroleum Technology. 13, 42-53.

McCaughan, J., Iglauer, S., and Bresme, F., 2013. Molecular dynamics simulation of water/CO_2-quartz interfacial properties: application to subsurface gas injection, Energy Procedia, 37, 5387-5402.

Mills, J., Riazi, M., Sohrabi, M., 2011. Wettability of common rock-forming minerals in a CO_2-brine system at reservoir conditions. In: Proceedings of the International Symposium of the Society of Core Analysts, SCA2011-06, Austin, Texas, USA,18–21 September 2011.

Morrow, N.R., 1976. Capillary Pressure Correlations for Uniformly Wetted Porous Media. Journal of Canadian Petroleum Technology. 15(4), 49–69.

Morrow, NR., 1990. Wettability and Its Effect on Oil Recovery. J. Pet. Tech., 42(12), 1476-1484.

Ozimic S., Nicholas E., Pain L., and Vuckovic V., 1987. Gippsland Basin, Victoria. Australian Petroleum Accumulations Report 3.

Park, J.Y., Lim, J.S., Yoon, C.H., Lee, C.H., Park, K.P., 2005. Effect of a Fluorinated Sodium Bis(2-Ethylhexyl) Sulfosuccinate (Aerosol-OT, AOT) Analogue Surfactant on the Interfacial Tension of CO_2 + Water and CO_2 + Ni-Plating Solution in Near- and Supercritical CO_2. J. Chem. Eng. 50, 299–308.

Rezaee R., Saeedi A., Iglauer S., and Brian Evans B., 2013.CarbonNet Dynamic Seal Capacity. ANLEC R&D internal report.

Saraji, S., Goual, L., Piri, M., and Plancher, H., 2013. Wettability of supercritical carbon dioxide/water/quartz systems: simultaneous measurement of contact angle and interfacial tension at reservoir conditions. Langmuir. 29, 6856-6866.

Sarmadivaleh, M., Al-Yaseri, A. Z., and Iglauer, S., 2015. Influence of temperature and pressure on quartz-water- CO_2 contact angle and CO_2-water interfacial tension. Journal of Colloid and Interface Science, 441(0), 59-64.

Spiteri, E., Juanes, R., Blunt, M., Orr, F., 2008. A new model of trapping and relative permeability hysteresis for all wettability characteristics. SPE Journal. 13, 277-288.

Sutjiadi-Sia, Y., Jaeger, P., Eggers, R., 2008. Interfacial phenomena of aqueous systems in dense carbon dioxide. Journal of Supercritical Fluids. 46, 272–279.

Wang, S., Edwards, I.M., and Clarens, A.F., 2013. Wettability phenomena at the CO_2-brine- mineral interface: implications for geologic carbon sequestration. Environmental Science and Technology. 47(1), 234-24.

Wesch, A., Dahmen, N., Ebert, K., and Schön, J., 1997. Grenzflächenspannungen, Tropfengrößen und Kontaktwinkel im Zweiphasensystem $H2O/CO_2$ bei Temperaturen von 298 bis 333 K und Drücken bis 30 MPa. Chemie Ingenieur Technik. 69(7), 942-946.

Wiegand, G., and Franck, E.U., 1994. Interfacial tension between water and non-polar fluids up to 473K and 2800bar. Ber. Bunsen-Ges. Phys. Chem. 98, 809-817.

Yan, W., Zhao, G.Y., Chen, G.J., Guo, T.M., 2001. Interfacial tension of (methane + nitrogen) + water and (carbon dioxide + nitrogen) + water systems. J. Chem. Eng. Data, 46, 1544-1548.

5.3 **Influence of Temperature and Pressure on Quartz–Water–CO_2 Contact Angle and CO_2–Water Interfacial Tension**

Sarmadivaleh, M., **Al-Yaseri, A.Z.** and Iglauer, S., 2015. Influence of temperature and pressure on quartz–water–CO_2 contact angle and CO_2–water interfacial tension. Journal of colloid and interface science, 441, pp.59-64.

Influence of temperature and pressure on quartz-water-CO_2 contact angle and CO_2-water interfacial tension

Mohammad Sarmadivaleh[1], Ahmed Al-Yaseri[1], Stefan Iglauer[1*]

[1]Curtin University, Department of Petroleum Engineering, 26 Dick Perry Avenue, 6151 Kensington, Australia.

Abstract

We measured water-CO_2 contact angles on a smooth quartz surface (RMS surface roughness ~40nm) as a function of pressure and temperature. The advancing water contact angle θ was 0° at 0.1MPa CO_2 pressure and all temperatures tested (296K-343K); θ increased significantly with increasing pressure and temperature (θ = 35° at 296K and θ = 56° at 343K at 20MPa). A larger θ implies less structural and residual trapping and thus lower CO_2 storage capacities at higher pressures and temperatures. Furthermore we did not identify any significant influence of CO_2-water equilibration on θ. Moreover, we measured the CO_2-water interfacial tension γ and found that γ strongly decreased with increasing pressure up to ~10MPa, and then decreased with a smaller slope with further increasing pressure. γ also increased with increasing temperature, but this effect was smaller than the effect of pressure.

Keywords

carbon geo-sequestration, residual trapping, structural trapping, interfacial tension, contact angle, quartz, carbon dioxide, temperature.

1. Introduction

Carbon geo-storage (CGS) has been recognized as a key technology to substantially reduce anthropogenic CO_2 emissions to the atmosphere and thus mitigate climate change [1]. In CGS, CO_2 is pressed into subsurface formations for storage, i.e. into deep saline aquifers or oil and gas reservoirs for enhanced hydrocarbon production [1-4]. However, CO_2 is buoyant because it has a lower density than the formation brine and consequently flows upwards. Four trapping mechanisms prevent the CO_2 from leaking to the surface: 1. Structural trapping [5], 2. Residual trapping [6,7], 3. Dissolution trapping [8] and 4. Mineral trapping [9]. In this context, the wettability of a rock-CO_2-water system plays a crucial role as it strongly impacts on the two most important trapping mechanisms, namely structural [10-12] and residual trapping [7,13,14], and thus also indirectly on dissolution and mineral trapping [12,15].

It is therefore necessary to understand the interfacial characteristics of the rock-fluid-fluid system in more depth to reduce project risk.

Specifically the contact angle between the rock, water and gas θ – which quantifies wettability of a mineral substrate [13,17] - and the gas-water interfacial tension γ strongly affect residual saturations [14,18-20], and the column height of CO_2 (i.e. volume) which can be permanently immobilized beneath a caprock [11,12]. Wettability also significantly influences relative permeabilities [21-23] and capillary pressures [8,13,24-26] and thus reservoir scale (hectometre scale) flow predictions. In fact relative permeabilities and capillary pressures are essential input parameters into reservoir simulators and the output computations are very sensitive to these parameters [27]; so it is important to precisely know these quantities.

In order to study the rock-CO_2-water wettability, several researchers measured water-CO_2 contact angles on silica substrates (as a representative of sandstone) and CO_2-water interfacial tensions at low to high pressure conditions [28-50]. It is clear that γ drops with increasing pressure, and there is evidence that γ increases with increasing temperature [32,36,45,46]; furthermore, it appears that θ increases with increasing pressure although the uncertainty associated with the θ measurements is high, cp. the

recent review published by Iglauer et al. [13]. This is also true for the influence of temperature on θ, no clear trend could be identified and less data is available, particularly there is a lack of systematic investigations.

In this context, Saraji et al. [45] and Farokhpoor et al. [47] measured an increase in θ with increasing pressure and temperature for deionized (DI) water ([45]: from ~12° at approximately 4 MPa and 308K to ~35° at 333K at 8-12 MPa; [47]: from ~10° at 309K to ~20° at 339K over a pressure range of 35MPa; Figure 3). In contrast, Saraji et al. [46] reported a slight decrease in θ (by up to ~5°) with increasing temperature (333K to 353K) at high pressures (~13.7-27 MPa) for 1M brine and Wang et al. [50] did not observe a significant increase in θ with pressure or temperature (from 7-20 MPa and 303-323K), cp. Figure 3. Molecular dynamics (MD) simulations – which provide a theoretical foundation for these relationships – also do not provide a clear picture; different groups report different results, cp. Table 1.

Table 1. Molecular dynamics predictions for the influence of pressure and temperature on the water-CO_2-quartz contact angle θ and CO_2-water interfacial tension γ. *Liu et al. [51] simulated a β-christobalite surface.

reference	influence of pressure	Influence of temperature
Liu et al. [51]*	θ increases	
Iglauer et al. [12]	θ increases; γ decreases	θ decreases; γ increases
McCaughan et al. [52]	θ increases	
Tsuji et al. [53]	constant θ; γ decreases	γ constant or decreases
Nielsen et al. [54]	γ decreases	γ ~constant

In order to reduce uncertainty in this area and to better constrain θ and γ, we conducted measurements at the relevant thermophysical conditions (i.e. high pressure, elevated temperature) and compared our results with the experimental literature data and MD model predictions.

We note that for reliable and reproducible contact angle measurements the surface roughness of the substrate needs to be quantified [55], and related to this the advancing and receding contact angles need to be distinguished; moreover, it is vital that the surfaces are cleaned with appropriate methods [48,56]. The fact that not all groups strictly applied these prescribed requirements may explain the uncertainty to some extent.

2. Experimental methodology

2.1 Contact angle measurements

A smooth alpha-quartz crystal surface (RMS surface roughness ~40nm and z-range ~290nm measured via Atomic Force Microscopy, Figure 1) was cleaned with acetone and then exposed to an air plasma for at least 15min. We note that oxygen plasma is one prescribed surface cleaning method; and it is vital that surfaces are cleaned properly as inappropriate cleaning and surface contamination, respectively, have a dramatic impact on measured contact angle values (typically increased water contact angles are measured, which is highly biased [48]). We note that oxygen plasma increases the number of hydroxyl groups on the quartz surface [57], which leads to lower θ [52]. However, on a subsurface quartz surface, which was exposed to formation brine for very long times, we expect that the surface silanol group concentration is at its maximum (4.6 silanol groups per nm^2, [58]), and this condition is again well represented by an O_2-plasma cleaned surface. We also note that oxygen plasma does not significantly affect the surface roughness of the substrate [59].

Quartz was used for this work because this material is the most common constituent of mudrocks and sandstone storage rocks [34,60,61]. Once cleaned, the substrate was placed into a high pressure cell, and the apparatus was flooded for at least 10min with CO_2 gas. Subsequently the gas pressure in the cell was increased to a pre-set value with a high precision syringe pump (Figure 2). A droplet of deionized water was then dispensed onto the substrate's surface, followed by a second and a third drop, while a video camera recorded the dispensing process as a movie. The contact angle of the drop just before the three phase line jumped forward (due to adding more water) was set to the advancing θ; the volume of the advancing drop was approximately 20μL. The time interval for one measurement (from initial drop

dispensation to the advancing three-phase line observation) amounted to less than 30seconds, which is sufficiently rapid to avoid mass transfer effects [62]. The advancing water contact angles θ were then measured on the images extracted from the movie files. An experimental matrix with different temperatures (296K, 323K and 343K) and pressures (0.1MPa, 5MPa, 10MPa, 15MPa, and 20MPa) was tested to systematically investigate the impact of pressure and temperature on θ. The reproducibility of the experiment was high with an average standard deviation of 3°.

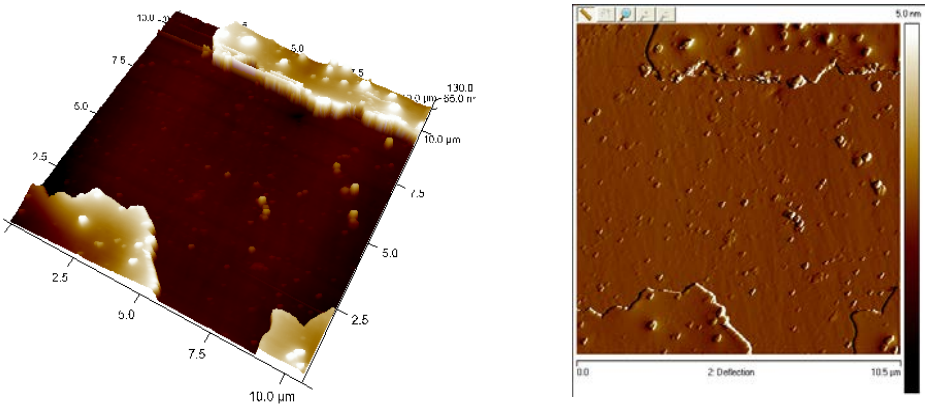

Fig. 1. Atomic Force Microscopy images of the quartz surface used in the experiments. Left: 3D topography of the substrate; right: deflection signal. Different heights are coloured differently (light yellow: 130nm height, dark brown: 0nm). The RMS surface roughness is approximately 40nm, which is very smooth. The area shown is ~10µm x 10µm.

Furthermore, we compared contact angles for equilibrated and non-equilibrated CO_2-water systems (note that CO_2-water is a partially miscible system, up to 2.6mol% of CO_2 can dissolve in water, Bando et al. [63]); equilibrated fluids are present deeper in the reservoir, when CO_2 had sufficient exposure to formation brine, while non-equilibrated fluids are located closer to the injection well [64]. In order to equilibrate CO_2 and water, we used a mixing reactor described earlier [65]; as un-equilibrated fluids dry gas and fresh de-gassed (i.e. vacuumed for more than 10 hours) water were used. The fluid densities used in the calculations were taken from Georgiadis et al. [38].

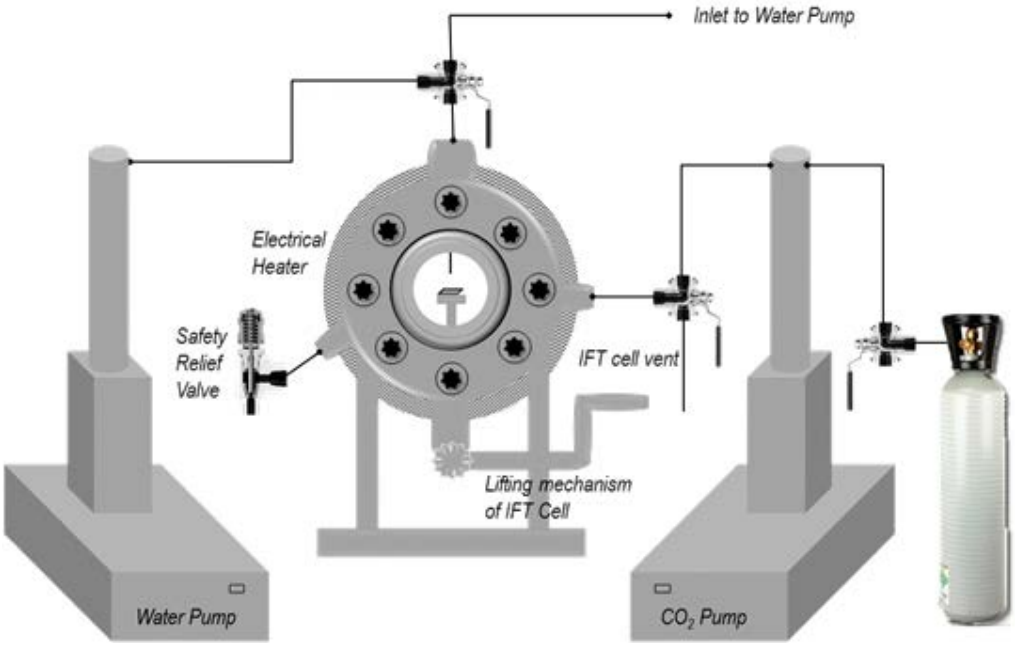

Fig. 2. Schematic diagram of the high temperature/high pressure contact angle measurement apparatus used for the interfacial tension and contact angle measurements.

2.2 Interfacial tension measurements

The pendant drop method was used for measuring the interfacial tension [65]. When a higher density liquid is dispensed into a lower density fluid environment through a needle, a drop is formed, which is called pendant drop. The curvature of the fluid-fluid interface of this drop is determined by the balance between interfacial (LaPlace equation 1) and gravitational forces (equation 2),

$$\Delta p_p = \gamma\left(\frac{1}{\mathrm{R}_1} + \frac{1}{R_2}\right) \tag{1}$$

$$\Delta \mathrm{p}_{\mathrm{apex}} - \Delta \mathrm{p}_{\mathrm{p}} = \mathrm{z}\Delta\rho\mathrm{g} \tag{2}$$

where γ is the interfacial tension, R_1 and R_2 are the curvature radii of two orthogonal curves through the same point on the drop's surface, $\Delta \mathrm{p}_{\mathrm{p}}$ is the pressure difference between water and CO_2 at a random point P on the fluid-fluid interface at height z, $\Delta \mathrm{p}_{\mathrm{apex}}$ is the pressure difference between water and CO_2 at the apex point of the

drop (z=0), Δρ is the density difference between CO_2 and water, and g is the local acceleration due to gravity.

When combining these equations and after some mathematical manipulations equation 3 is obtained with which γ can be computed:

$$\gamma = \frac{\Delta\rho g}{\left(\beta k_{apex}\right)^2} \quad (3)$$

where k_{apex} is the curvature at the apex point of the drop, and β is the shape parameter (dimensionless). Equation 3 implies that, if the acceleration due to gravity and the density difference between the fluids are known, γ can be calculated.

Experimentally, a high pressure cell was heated (to 296K, 323K or 343K) and flooded with CO_2 gas for at least 10min; subsequently gas pressure was increased (to 0.1MPa, 5MPa, 10MPa, 15MPa or 20MPa) with a syringe pump. Then a drop of fresh water was introduced into the cell through a needle with a second high precision syringe pump set to a constant flow rate. The water formed a drop at the bottom of the injection needle, and if a sufficient amount of water was added to the pendant drop, the drop separated from the needle and fell down. Two additional drops were produced in this way and the whole process was recorded with a video camera. From the drop images extracted from the movie files, the shape of the drop was measured and γ was calculated with equation 3. The standard deviation associated with these measurements was 3mN/m.

3. Results and discussion

3.1 Contact angle measurements

3.1.1 Influence of CO_2-water equilibration

The influence of thermodynamic CO_2-water equilibration on θ was tested for one thermo-physical condition (323K, 5 MPa), and we observed no significant difference during the measurement time (i.e. less than 30seconds, see above), Table 2. Note that for longer experimental times θ drops for un-equilibrated fluids due to mass transfer effects [50,66]. This measurement was highly reproducible (cp. Table 2). We

emphasise that in our experiments the drop volume and base radius were constant (20μL and 4.4mm). We conclude that the degree of mutual CO_2-H_2O dissolution (CO_2 into H_2O and H_2O into CO_2) has no significant effect on θ. This is contrary to Wang et al.'s [50] and Kaveh's [49] result; this discrepancy may be due to the shrinking drop size in Wang et al.'s and Kaveh et al.'s experiments (overlap with possible mass transfer kinetics and/or gravitational effects) or possible contamination effects which are expected to be increasingly likely to occur with experimental time [48,56]. Most importantly Wang et al. [50] and Kaveh et al. [49] did not clearly identify advancing (or receding) θ, and distinguish them from a random sessile drop θ (note: by adding more fluid to the drop θ will increase until the advancing θ is reached; and differences between advancing and receding θ typically range from 5-20°, but can be significantly higher, [55]). Finally Kaveh et al. [49] used sandstone as a substrate, not quartz, and the composite character of the rock (solid and pores) makes it difficult to directly compare these substrates. The remaining θ tests in our experimental matrix were conducted with fresh fluids (i.e. dry gas and fresh water).

Table 2. Advancing water contact angles on quartz in CO_2 atmosphere at 5MPa and 333K; right: equilibrated CO_2-water system; left: fresh CO_2-water system (i.e. dry gas, fresh water). The standard deviation for these measurements was estimated as ±1° based on replicate measurements.

Contact angle [°]	Equilibrated fluids	Fresh fluids
1st measurement	22	20
2nd measurement	23	19
3rd measurement	21	21
average	22±1	20±1

3.1.2 Influence of pressure and temperature on θ

θ at ambient conditions (296K, 0.1MPa CO_2 pressure) was 0°, consistent with literature results [48,67]. θ continuously increased with increasing pressure, and reached values of 35° (at 296K) to 56° (at 343K) at 20MPa, Figure 3. The observed increase in θ with pressure is consistent with literature data [31,34,35,42,44,45,48]

and molecular dynamics (MD) simulations [12,51,52], although Tsuji et al. [53] predicted a quasi constant value, Table 1; Iglauer et al. [12] explain the increase in θ with a higher CO_2 density, which leads to stronger CO_2-quartz intermolecular interactions, which again de-wet the substrate (= higher θ).

θ also increased with temperature: while θ at ambient conditions was 0° for all temperatures tested (296K, 323K, 343K), and the quartz remained completely water-wet, de-wetting was significant particularly at higher pressures and temperatures (at 343K: θ = 54° at 15MPa and = 56° at 20MPa). This is consistent with Saraji et al.'s [45] and Farokhpoor et al.'s [47], measurements, but not with Wang et al.'s [50] or Saraji et al.'s [46]. The different results Saraji et al. [46] reported may be due to the higher salt content in the water, however, an overall higher θ is expected for Saraji et al. [45,46] as they used an ultra-smooth glass surface (surface roughness = 0.5nm), which is expected to increase θ as higher surface roughness leads to lower θ [55]. The fact that they used glass, not quartz, may also explain this discrepancy. Farokhpoor et al. [47] and Wang et al. [50] did not report surface roughness, so the difference might be caused by a higher surface roughness of their substrates; moreover, they did not distinguish between receding and advancing θ, and a sessile drop θ is expected to a) be generally lower than the advancing θ [64], and b) can lie anywhere between the advancing and receding θ, so it is possible that they systematically measured a θ closer to the receding point which is expected to be substantially lower than the associated advancing θ. The factors responsible for this discrepancy need to be further analysed.

Theoretically, none of the MD simulations predicted the influence of temperature correctly, and this is probably due to the complex surface chemistry of the quartz in an aqueous and acidic environment [68], which was not fully appreciated in the MD models; we conclude that the MD models need to be improved.

We note that $\theta \leq 50°$ has no influence on the primary drainage capillary pressure curve [24], which determines the draining characteristics of a storage formation (change in water saturation with increasing CO_2 pressure). However, a $\theta > 0$ implies partial de-wetting of the sandstone surface, which a) is expected to reduce structural [11,12] and residual (c. Figure 2 in Spiteri et al. [14]) CO_2 trapping capacities, and b)

change the morphology of the CO_2 phase in the rock [20], which again is expected to have implications for dissolution and mineral trapping capacities (mainly through different CO_2-water interfacial areas). Finally a variation in θ has been shown to cause a change in the CO_2-water fluid dynamics in the rock [22], thus changing flow patterns and consequently injectivities, leakage risk and project economics.

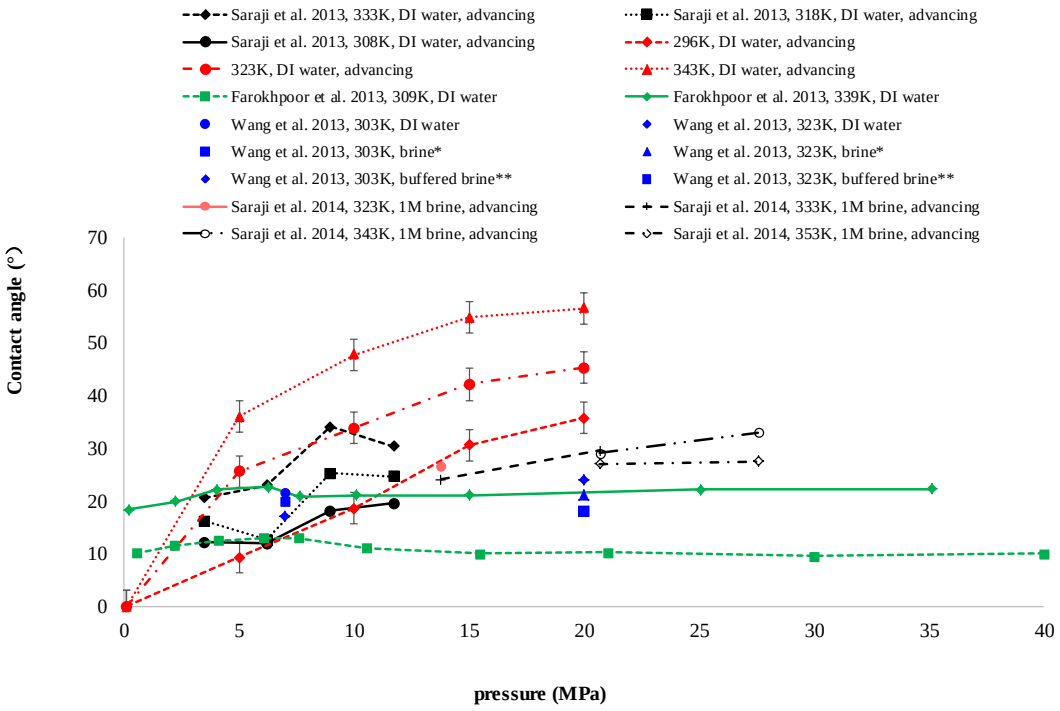

Fig. 3. Advancing water contact angles for CO_2/water/quartz systems as a function of pressure and temperature (the error bar represents the standard deviation of the measurements). Literature data is added for comparison [45,47,50]. *Ionic strength = 1.1-1.2 mol/L; contains: Na^+, Cl^-, Ca^{2+}, SO_4^{2-}, Mg^{2+}; pH = 3.0-5.0; pH = 7.8 at ambient conditions; **buffered brine: 0.74-0.75 mol/L; contains: Na^+, Cl^-, Ca^{2+}, SO_4^{2-}, Mg^{2+}, CO_3^{2-}, HCO_3^-, $B_4O_7^{2-}$; pH = 5.8-5.9; pH = 10.0 at ambient conditions.

3.2 Interfacial tensions

The CO_2-water interfacial tension was measured at different pressures (0.1MPa, 5MPa, 10MPa, 15MPa, and 20MPa) and temperatures (296K, 323K and 343K) for dry CO_2 and fresh deionized water. The results measured are consistent with literature data [28-33,36-38,43], Figure 4. The CO_2-water interfacial tension strongly

decreased with increasing pressure until a pressure of approximately 10MPa was reached. By further increasing the pressure, γ decreased further, but with a smaller slope. γ increased with an increase in temperature, but the effect was smaller than that caused by pressure change. This is again consistent with literature data [30,33,38]. We note that several MD models correctly predicted these relationships, Table 1.

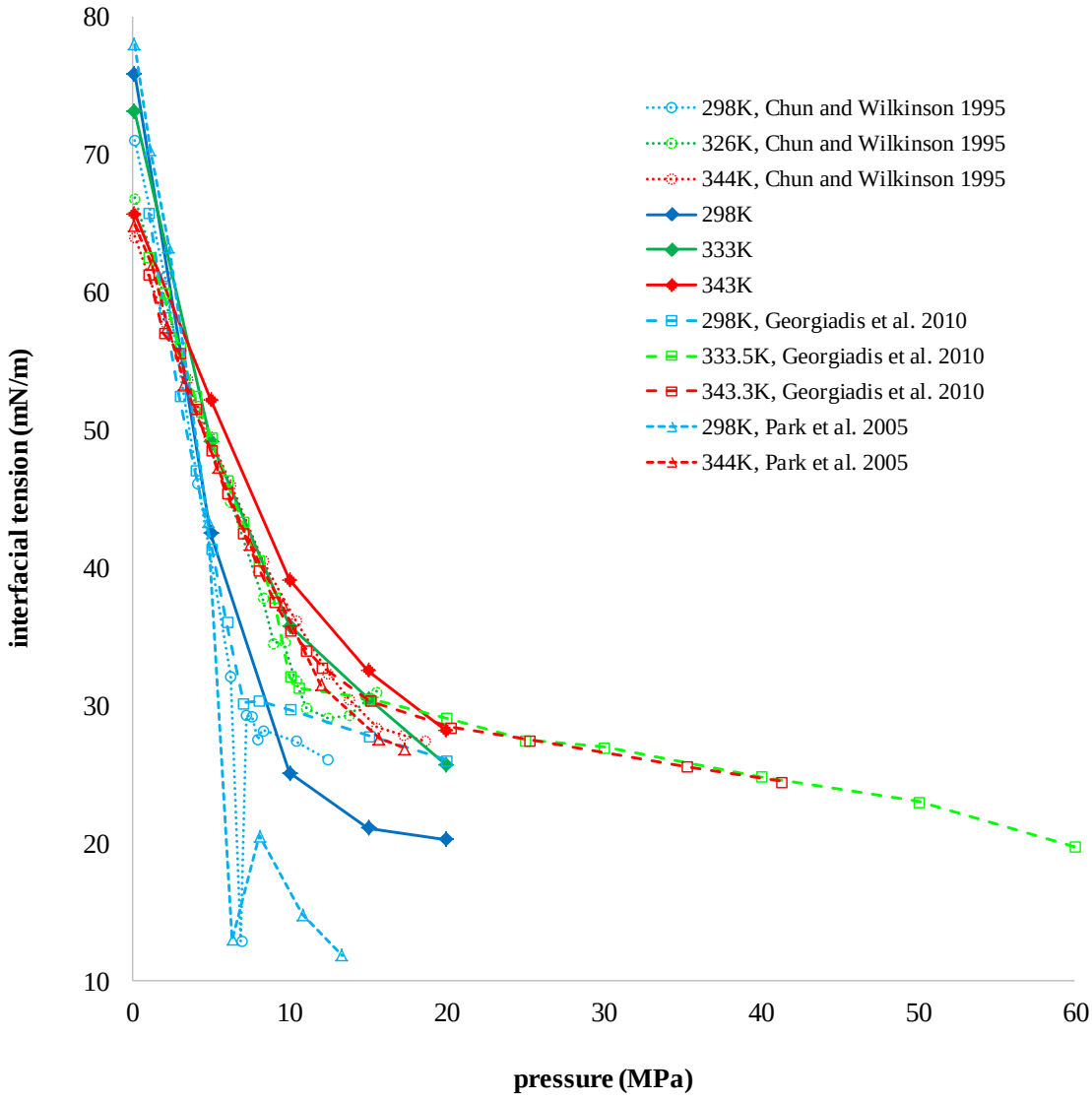

Fig. 4. CO_2-water interfacial tensions as a function of pressure and temperature. For comparison, literature data is also plotted (Chun and Wilkinson 1995 [30], Park et al. 2005 [33], Georgiadis et al., 2010 [38]).

Conclusions

CO_2-wettability is of key importance in CO_2 geo-storage schemes [11,12,14]; however, despite its importance, CO_2-wettability is still poorly understood and a large uncertainty is associated with the reported data [13]. We thus measured the advancing water contact angle θ on a smooth quartz surface (RMS surface roughness ~40nm) as a function of pressure and temperature. Furthermore we analysed the effect of CO_2-water equilibration (fresh fluids versus thermodynamically equilibrated fluids) on θ. We found that:

- θ was identical (within experimental error; note that the experiments were completed within 30seconds and mass transfer effects were thus negligible) for fresh and thermodynamically equilibrated fluids. This is consistent with Al-Yaseri et al. [62]; we note that Wang et al. [50] and Kaveh et al. [49] observed a changing θ for unequilibrated fluids with time, which was probably due to mass transfer effects at extended experimental times [62].
- θ increased with increasing pressure. This is consistent with most published experimental literature data [31,34,35,40-42,44,45,48,49], except [39,50]. Any discrepancies probably arose from surface contamination [40,48,56] or the fact that not all researchers distinguished between advancing, receding or sessile drops.
- θ increased with increasing temperature; which is consistent with some reported data [45], but not all [40,46,50]. Again discrepancies are probably caused by the above mentioned reasons.
- θ was still weakly water-wet at expected CO_2 storage conditions; however, an increased θ implies a reduction in structural and residual trapping capacities [11,12,14].

Moreover, we measured CO_2-water interfacial tensions γ as a function of pressure and temperature, and the results indicated that:

- γ decreased strongly with pressure up to a pressure of ~10MPa and then decreased further but with a smaller slope, which is consistent with literature data [28-50].

- γ increased with temperature, which is also consistent with literature data [32,36,45,46].

Acknowledgements

The authors wish to acknowledge financial assistance provided through Australian National Low Emissions Coal Research and Development (ANLEC R&D). ANLEC R&D is supported by Australian Coal Association Low Emissions Technology Limited and the Australian Government through the Clean Energy Initiative.

References

[1] B. Metz, O. Davidson, H. de Coninck, M. Loos, L. Meyer (Eds.), Intergovernmental Panel on Climate Change Special Report on Carbon Dioxide Capture and Storage, Cambridge University Press, 2005.

[2] M.J. Blunt, F.J. Fayers, F.M. Orr, Energy Conversion and Management 34 (1993) 1197.

[3] D.M. Islam, M. Alshehhi, M. Ohadi, ASHRAE Transactions 15(2009) 959.

[4] S. Iglauer, A. Paluszny, M.J. Blunt, Fuel 103 (2013) 905.

[5] M.A. Hesse, F.M. Orr, H.A. Tchelepi, J. Fluid Mech. 611 (2008) 35.

[6] R. Juanes, E.J. Spiteri, F.M. Orr, M.J. Blunt, Water Resour. Res. 42 (2006) W12418.

[7] S. Iglauer, A. Paluszny, C.H. Pentland, M.J. Blunt, Geophys. Res. Lett. 38 (2011) L21403.

[8] C.H. Pentland, R. El-Maghraby, S. Iglauer, M.J. Blunt, Geophys. Res. Lett. 38 (2011) L06401.

[9] S. Iglauer, in: H. Nakajima (Ed.), Mass Transfer, InTech, Rijeka, 2011, p. 233.

[10] I. Gaus, Int. J. Greenh. Gas Con. 4 (2010) 73.

[11] M. Naylor, M. Wilkinson, R.S. Hazeldine, Mar. Petrol. Geol. 28 (2011) 1083.

[12] S. Iglauer, M. Mathew, F. Bresme, J Colloid Int Sci. 386 (2012) 405.

[13] S. Iglauer, A. Busch, C.H. Pentland, Water Resour. Res. (submitted).

[14] E.J. Spiteri, R. Juanes, M.J. Blunt, F.M. Orr, SPE J. 13 (2008) 277.

[15] K. Chaudhary, M.B. Cardenas, W.W. Wolfe, J.A. Maisano, R.A. Ketcham, P.C. Bennett, Geophys. Res. Lett. 40 (2013) 1.

[16] C.H. Pentland, S. Iglauer, O. Gharbi, K. Okada, T. Suekane, SPE 158516, Proc. Asia Pacific Oil and Gas Conf. and Exhib. 2012.

[17] E.C. Donaldson, W. Alam, Wettability, Gulf Publishing Company, Houston, 2008.

[18] N.R. Morrow, J. Pet. Tech. 42 (1990) 1476.

[19] S. Iglauer, S. Favretto, G. Spinelli, G. Schena, M.J. Blunt, Phys. Rev. E 82 (2010) 056315.

[20] S. Iglauer, M. Fernø, P. Shearing, M.J. Blunt, J. Colloid Interface Sci. 375 (2012)187.

[21] W.W. Owens, D.L. Archer. J. Pet. Tech. 23 (1971) 873.

[22] F.G. McCaffery, D.W. Bennion, J. Can. Pet. Tech. 13 (1974) 42.

[23] J.S. Levine, D.S. Goldberg, K. S. Lackner, J.M. Matter, M.G. Supp, T.S. Ramakrishnan, Environ. Sci. Tech. 48 (2014) 811.

[24] N.R. Morrow, J. Can. Pet. Tech. 4 (1976) 49.

[25] W.G. Anderson, J. Pet. Tech. 39 (1987) 1283.

[26] M. Sarmadivaleh, S. Iglauer, Fourth EAGE Geol. CO_2 Work. 2014.

[27] L.P. Dake, Fundamentals of reservoir engineering. Elsevier: Oxford, 1978.

[28] R. Massoudi, A.D. King. J. Phys. Chem. 78 (1974) 2262.

[29] C. Jho, D. Nealon, S. Shogbola, A.D. King, J. Colloid Int Sci. 65 (1978) 141.

[30] B.S. Chun, G.T. Wilkinson, Ind. Eng. Chem. Res. 34 (1995) 4371.

[31] A. Wesch, N. Dahmen, K. Eber, J. Schön, Chem. Ing. Tech..69 (1997) 942.

[32] A. Hebach, A. Oberhof, N. Dahmen, A. Kogel, H. Ederer, E. Dinjus, J. Chem. Eng. 47 (2002) 1540.

[33] J.Y. Park, J.S. Lim, C.H. Yoon, C.H. Lee, K.P. Park, J. Chem. Eng 50 (2005) 299.

[34] P. Chiquet, D. Broseta, S. Thibeau, Geofluids 7 (2007) 112.

[35] Y. Sutjiadi-Sia, P. Jaeger, R. Eggers, J. Supercrit. Fluid 46 (2008) 272.

[36] C. Chalbaud, M. Robin, J.M. Lombard, F. Martin, P. Egermann, H. Bertin. Adv. Water Res. 32 (2009) 98.

[37] S. Bachu, D.B. Bennion, J. Chem. Eng. 54 (2009) 765.

[38] A. Georgiadis, G. Maitland, J.P.M. Trusler, A. Bismarck. J. Chem. Eng. 55 (2010) 4168.

[39] D.N. Espinoza, J.C. Santamarina, Water Resour. Res. 46 (2010) W0753.

[40] P.K. Bikkina, Int. J. Greenh. Gas Contr. 5 (2011) 1259.

[41] J. Mills, M. Riazi, M. Sohrabi, SCA2011-6, Proc. Int. Symp. Soc. Core Ana. 2011.

[42] D. Broseta, N. Tonnet, V. Shah. Geofluids 12 (2012) 280.

[43] X. Li, E. Boek, G.C. Maitland, J.P.M. Trusler, J. Chem. Eng. 57 (2012) 1078.

[44] J.W. Jung, J. Wan, Energ. Fuel 26 (2012) 6053.

[45] S. Saraji, L. Goual, M. Piri, H. Plancher, Langmuir 29 (2013) 6856.

[46] S. Saraji, M. Piri, L. Goual, Int. J. Greenh. Gas Control 28 (2014) 147.

[47] R. Farokhpoor, B.J.A. Bjørkvik, E. Lindeberg, O. Torsæter, Int. J. Greenh. Gas Control 12 (2013) 18.

[48] S. Iglauer, A. Hassan, M. Sarmadivaleh, K. Liu, C. Pham, Int. J. Greenh. Gas Control 22 (2014) 325.

[49] N.S. Kaveh, E.S.J. Rudolph, P. van Hemert, W.R. Rossen, K.H. Wolf, Energ Fuels 28 (2014) 4002.

[50] S. Wang, I.M. Edwards, A.F. Clarens, Environ. Sci. Tech. 47 (2013) 234.

[51] S.Y. Liu, X.N. Yang, Y. Qin Y, Chin Sci Bul 55 (2010) 2252.

[52] J. McCaughan, S. Iglauer, F. Bresme, Energ Proc 37 (2013) 5387.

[53] S. Tsuji, Y. Liang, M. Kunieda, S. Takahashi, T. Matsuoka, Energ Proc 37 (2013) 5435.

[54] L.C. Nielsen, I.C. Bourg, G. Sposito. Geochim Cos Act 81 (2012) 28.

[55] H.-J. Butt, K. Graf, M. Kappl, Physics and Chemistry of Interfaces, Wiley-VCH,Weinheim, 2006.

[56] J. Mahadevan, Int. J. Greenh. Gas Control 7 (2012) 261.

[57] A.U. Alam, M.M.R. Howlander, M.J. Deen, ECS J. Sol. Stat Sci Tech 2 (2013) P515.

[58] L.T. Zhuravlev, Colloids Surf A 173 (2000) 1.

[59] A.U. Alam, M.M.R. Howlander, M.J. Deen, J. Micromech. Microeng. 24 (2014) 035010.

[60] H. Blatt, D.J. Schultz, Sediment. 23 (1976) 857.

[61] D. Tiab, E.C. Donaldson, Petrophysics, Elsevier, Amsterdam, 2004.

[62] A. Al-Yaseri, M. Sarmadivaleh, A. Saeedi, A. Barifcani, S. Iglauer, J. Pet. Sci. Eng. (submitted).

[63] S. Bando, F. Takemura, M. Nishio, E. Hihara, M. Akai, *J ChemEng Data* 48 (2003) 576.

[64] C.H. Pentland, S. Iglauer, R. El-Maghraby, Y. Tsuchiya, H. Okabe, M.J. Blunt, SPE 138476, Proc. SPE Int. Conf. CO_2 Capt, Stor. Util., 2010.

[65] R. El-Maghraby, C.H. Pentland, S. Iglauer, M. J. Blunt, J. Supercrit Fluid 62 (2012) 55.

[66] A.W. Adamson, A.P. Gast, Physcial chemistry of surfaces, John Wiley and Sons: New York, 1997.

[67] J.W. Grate, K.J. Dehoff, M.G. Warner, J.W. Pittman, C. Zhang, M. Oostrom, Langmuir 28 (2012) 7182.

[68] E.F. Vansant, P. Van der Voort, K.C. Vrancken, Characterisation and chemical modification of the silica surface. Elsevier: Amsterdam, 1995.

5.4 Pore-Scale Analysis of Formation Damage in Bentheimer Sandstone With in-situ NMR and Micro-Computed Tomography Experiments

Al-Yaseri, A.Z., Lebedev, M., Vogt, S.J., Johns, M.L., Barifcani, A. and Iglauer, S., 2015. Pore-scale analysis of formation damage in Bentheimer sandstone with in-situ NMR and micro-computed tomography experiments. Journal of Petroleum Science and Engineering, 129, pp.48-57.

Pore-scale analysis of formation damage in Bentheimer sandstone with in-situ NMR and micro-computed tomography experiments

Ahmed Al-Yaseri[1], Maxim Lebedev[2], Sarah J. Vogt[3], Michael L. Johns[3], Ahmed Barifcani[4], and Stefan Iglauer[1]

[1]Curtin University, Department of Petroleum Engineering, 26 Dick Perry Avenue, 6151 Kensington, Australia

[2]Curtin University, Department of Exploration Geophysics, 26 Dick Perry Avenue, 6151 Kensington, Australia

[3]University of Western Australia, School of Mechanical and Chemical Engineering, 35 Stirling Highway, 6009, Crawley, Australia

[4]Curtin University, Department of Chemical Engineering, 26 Dick Perry Avenue, 6151 Kensington, Australia

Abstract

We investigated fines movement through sandstone in-situ at the micrometre pore scale and studied the associated pore-scale mechanisms leading to formation damage. We used two *in-situ* techniques to accomplish this, namely nuclear magnetic resonance T_2 relaxation time (NMR) measurements (of pore size distributions) and high resolution x-ray micro-computed tomography (μCT; at high resolutions of $(0.89\mu m)^3$ and $(3.4\mu m)^3$). The μCT images showed the precise 3D location of the fines particles in the plug and demonstrated that initially pore throats are plugged, followed by filling of adjacent pore bodies by solid particles. These measurements in combination with traditionally used (indirect) permeability and production curve measurements and ex-situ SEM imaging enabled us to propose a new mechanistic pore-scale plugging model; furthermore we demonstrated that the amount of fines trapped decayed rapidly with core depth. We conclude that it is feasible to analyse formation damage *in-situ* by a combination of NMR and μCT measurements.

Keywords

Formation damage, micro tomography, NMR, plugging mechanism, permeability reduction.

1. Introduction

Migration of colloids (≤ 5 μm) and dispersed small solid particles (< 100 μm) through a porous medium is a key problem in various fields as deposition of such particles can severely reduce permeability. Areas which face this problem include hydrology, where the focus is on water production [McDowell et al., 1986; Bradford et al., 2001; Torkzaban et al, 2007], geothermal engineering, where cold water is pumped through subsurface reservoirs to produce warm water [Mahmoudi et al., 2010; Rosenbrand et al., 2014; Rosenbrand et al., 2015], wellbore drilling [Byrne et al. 2007, Civan 2007] and petroleum recovery, where water is injected to maintain reservoir pressure and mobilize additional hydrocarbons by viscous forces [Ahmed and McKinney, 2005; and Iglauer et al. 2010].

Common to all these processes is that water added to a reservoir can cause the release of colloids and fine particles in the rock due to subtle changes in fluid composition [Ryan and Elimelech, 1996] or through shear forces [Tran et al., 2009]; furthermore, surface water - which freely percolates into the formation due to gravitational forces or may be injected by force in an industrial process - contains fine particles [McDowell et al., 1986, Bennion et al., 2011] as filtration is uneconomical [Bennion et al., 2011]. Consequently, in case of injected water, certain quality requirements need to be fulfilled, i.e. the water must not contain solid particles which are larger than a certain maximum size [Bennion 1998]. It is thus important to understand the particles' impact on fluid dynamics and associated pore-scale plugging mechanisms, which cause the formation damage [Nowark and Krueger, 1951; Krueger et al. 1967; McDowell et al., 1986; Ryan and Elimelech, 1996; Civan 2007; Rosenbrand et al., 2014 and 2015].

Traditionally, various techniques were used to investigate the characteristics of such formation damage. This usually included the measurement of the injection flow rate and pressure drop across the sample to determine dynamic permeability, and the measurement of produced fluid mass versus time [e.g. Krilov et al., 1991; Asghari et al., 1995; Tran et al., 2010]. Frequently these measurements were supported by x-ray diffraction (XRD) measurements [e.g. Krilov et al., 1991; Seright et al., 2006; Potter et al., 2011; Green et al., 2013] and petrographic thin section analysis [e.g. Gulati et al.,1975; Bowers et al., 1995; Hidajat, 2002; Green et al., 2013]. Furthermore scanning electron microscopy (SEM) was used to study fines deposition at the

nanometre to micrometre scale [e.g. Kandarpa and Joh 1981; Byrne et al., 2000; Green et al., 2013], and nuclear magnetic resonance (NMR) T_2 relaxation measurements were used to probe changes in the associated pore size distributions [Tran et al., 2010; Fischer et al., 2011]. More recently, medical x-ray computer tomography has been used to image the distribution of fines within the rock at low spatial resolution (1mm) [Tran et al., 2010; Green et al., 2013].

However, all these techniques have serious limitations: dynamic permeability measurements and fluid mass production curves are indirect observations, while thin section analysis, XRD and SEM only measure *ex-situ* data. NMR is a bulk measurement and does not provide information about spatial distributions. 3D medical x-ray tomography, however, can provide a 3D spatial map of the CT numbers (which is related to the x-ray attenuation of the different minerals [Okabe et al, 2013]), but here spatial resolution is low (0.5-1mm) and individual pores or fine particles can thus not be observed.

Recently, with the advent of micro-computed tomography (µCT), it has become possible to overcome these limitations [Blunt et al. 2013, Wildenschild and Sheppard 2013]. Green et al. [2013] for instance imaged representative core samples of varying permeabilities (8 to 7000 mD) at a µCT resolution of 10-15µm *in-situ* in order to investigate the damage caused by drilling mud invasion.

We are now paying attention to the detailed pore-scale plugging mechanisms via a combination of high resolution µCT imaging (0.9µm and 3.4µm resolution), standard coreflooding, SEM and NMR analysis. Using these methods we were able to visualize the precise 3D distribution of fines within the pore space of the plug, and were able to develop a new mechanistic plugging model; we discuss this new model in the context of established literature models.

2. Experimental Methodology

2.1 Materials

The experiments were performed on two homogeneous cylindrical Bentheimer sandstone plugs (diameter = 5.2mm, length = 32.5mm); these were sister plugs drilled from the same block, the drill holes were just adjacent to each other. Their

brine permeabilities were 559mD and 523mD, and their porosities were 21% and 23%, Table 1. The composition of the Bentheimer sandstone was measured via XRD with a Bruker-AXS D9 Advance Diffractometer (Kaolinite 0.7 wt%, Quartz 99.0 wt%, Rutile 0.3wt%) on a fragment obtained from the same block just adjacent to the drill holes; this indicated that the sandstone was quite clean and consisted mainly of quartz.

As a representative for the fines in the subsurface, we selected a fine barite powder [Krilov et al., 1991; Tran et al, 2010]. The barite particles had a broad particle size distribution, which ranged from 0.4-80μm and peaked at 25μm, Figure 1 (measured with a Mastersizer Malvern Hydro 2000S). The barite particles were suspended in brine (5wt% NaCl + 1 wt% KCl in deionized water) by constant agitation with a magnetic stirrer.

Table 1. Bentheimer sandstone porosities and permeabilities before and after fines injection. *The initial porosity was set to the μCT porosity, see left column.

	Porosity measured by μCT	Porosity measured by NMR	Brine permeability (Darcy)
Sample #1 before damage	0.21	0.21*	0.559
Sample #2 before damage	0.23	0.23*	0.523
Sample #1 damage by 10g/L barite	0.15	0.176	0.11
Sample #2 damage by 20g/L barite	0.10	0.121	0.048

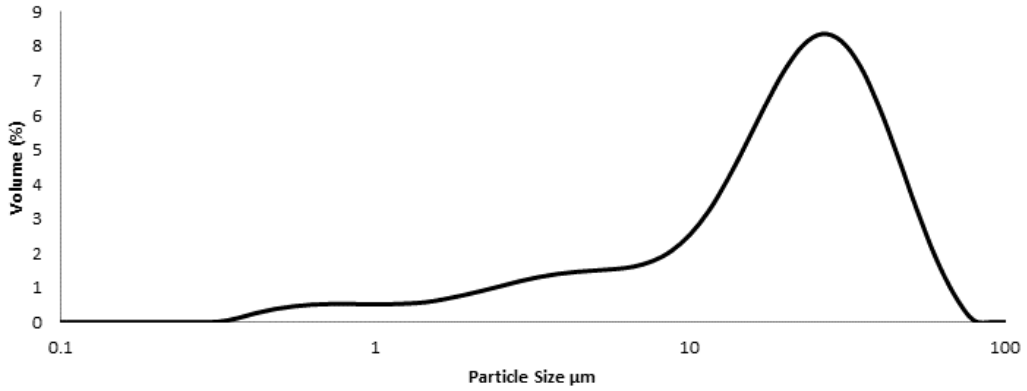

Figure 1. Particle size distribution of barite powder used in the experiments.

2.2 Simulation of fines migration in the subsurface

In order to mimic fines flow in the subsurface, the Bentheimer plugs were sealed with a PTFE heat shrink sleeve, which was cured at 653K for ~20min, vacuumed for 40 minutes, and then saturated with brine. Subsequently the brine permeability of each plug was measured by injecting water at a constant flow rate with a peristaltic pump (Masterflex model 7518-10), while the pressure drop across the plug was measured; brine permeability was then calculated using Darcy's law. This permeability measurement was continued during fines injection, see below. The samples were then imaged with a µCT scanner (Xradia Versa XRM-500T) at a resolution of $(3.4\mu m)^3$, and NMR T_2 response curves were measured for each specimen on a (^{1}H resonance) 20 MHz Bruker Minispec benchtop NMR instrument. The NMR T_2 response time correlates with the pore size distribution in the core [Talabi et al. 2009, Fridjonsson et al. 2013], and it thus constitutes an independent measurement.

The samples were then flooded with the barite suspension (two different barite concentrations were tested: 10 g/L and 20 g/L), and simultaneously the mass of produced fluid was measured with a balance (Phoenix, BTA/BTB series, accuracy = 0.001g) as a function of time. All experiments were conducted at ambient conditions, i.e. 130000 Pa (±20000Pa) pressure and (296K ±2K) temperature.

Once the plug samples were highly damaged by the fines injection process (permeability reduced by ~90%), the plugs were µCT imaged again at two different

but high resolutions $(3.4\ \mu m)^3$ and $(0.89\mu m)^3$. All μCT images were filtered with a non-local means filter [Buades 2005] and segmented according to Otsu's algorithm [Otsu 1979]. On the segmented images porosities, pore volumes, and pore radius distributions were measured; we note that these parameters are affected by fines migration [Civan 2007]. Furthermore, the precise 3D location of the barite particles was observed, this is discussed further below.

After μCT scanning the plugs were subjected to another NMR T_2 response measurement to measure any changes in the pore size distributions.

3. Result and discussion

The evolution of the permeability with time during fines suspension injection is shown in Figure 2. The permeability (k) continuously and smoothly decreased with time (t) following a power law $k=3.94t^{-0.343}$, Pearson coefficient R^2=0.996, (sample#1); $k=2.701t^{-0.403}$, R^2=0.978 (Sample#2), and the permeability reduction was more significant for the higher barite concentration as expected, consistent with trends reported in the literature [Krilov et al., 1991, Asghari et al., 1995]; moreover, Nguyen and Civan [2005] and Tran et al. [2009 and 2010] observed an exponential correlation for the dynamic permeability as a function of time with exponents and coefficients depending on several variables including α (cement exclusion parameter, dimensionless), σ (particle volume fraction, fraction), and β (pore-to-particle diameter, dimensionless), which is approximately consistent with our results. Specifically, we measured a permeability reduction from 559mD to 110mD for 10 g/L barite concentration and from 523mD to 48mD for 20 g/L barite concentration. The plugging time (note that plugging occurs at the discontinuity in the production curve [Tran et al., 2009 and 2010], Figure 3) was faster when the particles' concentration increased. Plugging time was 1.38hr for the 20 g/L suspension, while it was 4.47hr for the 10 g/L suspension, Figure 3.

Note that plugging time for Krilov et al.'s [1991] study was ≈30min, they flooded outcrop sandstone (permeabilities 144, 1549, 71, 40 mD and porosities 13.3, 21.2, 22.7 and 21.2 respectively) with barite suspensions (particle sizes varied from 2 to 60 μm); Asghari et al. [1995] reported plugging times ≈200min after injecting filtered

sea water (filtration through a 10μ filter) through carbonate rock (core plugs from Siri oil field in Iran with an average permeability of 7.9 mD and average porosity 20%); and Tran et al. [2010] reported a plugging time ≈2.5hr after injecting drilling mud (bentonite and barite with 5wt% barite concentration and 1.2 to 12μm barite particles size range) through Berea samples sandstone (permeabilities 1240, 265 mD and porosity 20.6%, 17.5% respectively).

Figures 4 and 5 show the NMR T_2 response curves for the undamaged and damaged samples for both fines concentrations, respectively. The T_2 NMR measurement is related to the surface S to volume V ratio of the pore structure by the equation $1/T_2 = \rho S/V$, where ρ is the surface relaxivity, a parameter dependent on the composition of the rock [Kleinberg, 1994], which we assume to be constant between the two Bentheimer samples tested in this work. Therefore, a shorter T_2 relaxation time corresponds to a larger surface to volume ratio and thus smaller pores. Initially the NMR signal indicated a primarily homogeneous pore space, with approximately 10-20% of the signal originating from secondary (smaller) pores, consistent with previous measurements for similar sandstone [Liaw et al., 1996]. The integral of the NMR T_2 signal, which corresponds to the amount of water in the pore space, was substantially reduced for the damaged samples, which corresponds to a substantially reduced porosity [Allen et al., 1997], Table 1. This was measured for both fines concentrations, although the 20g/L suspension was more effective in terms of porosity reduction. Furthermore, the bimodal character of the pore space changed into a multimodal system indicating that the homogeneous larger pores were segmented into heterogeneous smaller pores after damage [Liaw et al., 1996]. Moreover, the average T_2 times for the samples calculated from the distributions in Figures 4 and 5 decreased after the samples were damaged with barite indicating smaller pores sizes. The average T_2 time of the sample injected with 10 g/L barite suspension decreased from 0.72s before damage to 0.31s after damage, a reduction of 57%. For the sample injected with 20 g/L barite suspension, the average T_2 time decreased from 0.86s to 0.25s, a reduction of 71%. This clear shift in the NMR T_2 response towards smaller relaxation times indicates shrinking pore sizes [Talabi et al., 2009] with the effect more pronounced for the suspension which contained the higher barite concentration.

In addition to a shift of the average T_2 time to shorter times, the T_2 signal distributions shown in Figures 4 and 5 also clearly show that the longest T_2 peak (associated with the larger pores) decreased after damage for both samples, with a larger decrease in the long peak for the sample damaged with 20 g/L barite suspension. This indicates that the larger pores in the structure have been plugged and split into smaller pores which is consistent with literature results [Tran et al. 2010]; however, Tran et al.'s [2010] NMR results showed smaller changes in porosity (20.6% to 17.6% for their first Berea sample (rock permeability 1240mD) and 17.5% to 16.9% for their second Berea sample (rock permeability 265mD), which was probably caused by the different rock pore morphology and mineralogy and the different particles injected (they used a bentonite/barite mixture, which simulated drilling mud; barite concentration was 5wt% with 1.2 to 12μm barite particles sizes).

Consistent with the NMR data, the μCT results showed that particularly large pore sizes (pore diameter >85μm for sample#1 and >136μm for sample#2) have been damaged, Figures 6 and 7. Specifically, pores with diameters less than 51μm (sample#1) and less than 102 μm (sample#2) showed a significantly higher frequency after damage. As mentioned above, the barite particle size distribution comprised sizes from 0.4-80μm and peaked at 25μm (Figure 1); while the sandstone pore sizes ranged from ~1-340μm (Figures 6 and 7). Consequently these distributions overlapped and the fines caused plugging, consistent with predictions based on the aspect ratio β, see discussion below (Civan 2007, Tran et al. 2009, 2010).

Figures 8 and 9 show that the amount of barite *y* (porosity fraction) trapped in the core a) increased with barite concentration in the suspension, consistent with literature results [Tran et al., 2009 and 2010] and b) decreased with depth d following a polynomial $k=0.0202d^2-0.1152d+0.2067$, $R^2=0.81$, (sample#1); $k=0.0345d^2-0.1642d+0.237$, $R^2=0.82$ (sample#2); this is approximately consistent with Nguyen's and Civan's [2005] and Tran et al.'s [2010] results, which showed an exponential reduction. Note that the 10g barite/L data can also be fitted well with a linear least square fit ($k=-0.046d+0.1558$, $R^2=0.754$); however, a linear fit through the 20g barite/L data is poor ($k=-0.0256d+0.1958$, $R^2=0.374$).

The reason for this behaviour is visualized in Figures 10 and 11: the fines flow frequently penetrated into the pore space until a thin pore throat was reached (note that conceptually in pore network models, which quantify the complex pore morphology, pore throats are the smallest pores connecting the larger pore bodies [Dong and Blunt 2009; Ebrahimi et al. 2013]). We conclude that at these points the fines flow was stopped, i.e. the fines were deposited here first (cp. for instance Figures 11c, 11f, and 11i), and subsequently the larger adjacent pore bodies were filled with barite; this was essentially a jamming process [Civan, 2007]. In addition, the fines clustering in Figure 11c is more localized than in Figure 11i as a pore throat was just adjacent to the main body of fines agglomerate (left side of cube).

The high resolution images (Figure 12) provide evidence in terms of the exact plugging mechanism; the water-wet barite particles adhered to the water-wet rock surface, and the barite particles also agglomerated into rather compact conglomerates [Israelachvili 2011, and Torkzaban et al, 2007], which, however, were not loosely packed as previously suggested [Gulati et al.,1975; Civan, 2007; and Elsaeh, 2014].

The SEM images shown in Figures 13c and 13d also demonstrate that adhesion forces between barite particles and quartz surface were acting; and an analogue situation is illustrated in Figures 13e and 13f for the barite-barite particle interactions. Moreover, the SEM images clearly show the arrangement of the particles at the pore-scale. Note that in the SEM images published by Kandarpa et al. [1981]; Byrne et al. [2000]; Tran et al. [2010]; and Green et al. [2013], these details were not visible because of low image resolution.

Based on the results discussed above we postulate a new formation damage model which we hypothesize will hold for water-wet fines and water-wet rock (and very likely oil-wet fines and oil-wet rock):

A combination of intermolecular forces and pore geometry leads to the build-up of solid particles in the smallest pore throats. As the pore throats determine permeability [Tiab and Donaldson 2004] a substantial decrease in permeability is the consequence.

While the impact of pore geometry can be predicted in a straightforward way by using an aspect ratio (β = pore throat to particle diameter length ratio) correlation: if

$\beta < 7$, then bridging can occur [Civan, 2007], a prediction of the impact of intermolecular forces is more involved. For the specific system we are considering (i.e. sandstone and barite) we hypothesize that the silanol groups on the quartz (sandstone) surface [Zhuravlev 2000, McCaughan et al. 2013] strongly attract the hydroxyl groups on the barite surface [Fenter et al. 2001; note that Fenter et al. observed adsorbed water on the barite surface, but could not identify the exact molecular species as the experimental technique they used did not allow them to observe protons], certainly leading to strong Debye and Keesom forces [Israelachvili 2011], probably hydrogen bridges and possibly condensation reactions (Figure 14). This scenario would explain the fact that the barite particles were packed tightly as shown in Figures 12 and 13.

We thus conclude that a) fines damaging a reservoir might be more difficult to remove than expected based on earlier models, however, b) chemicals may be found which can break the strong intermolecular bonds and release the fines again. Furthermore we hypothesize that wettability plays a primary role in plugging.

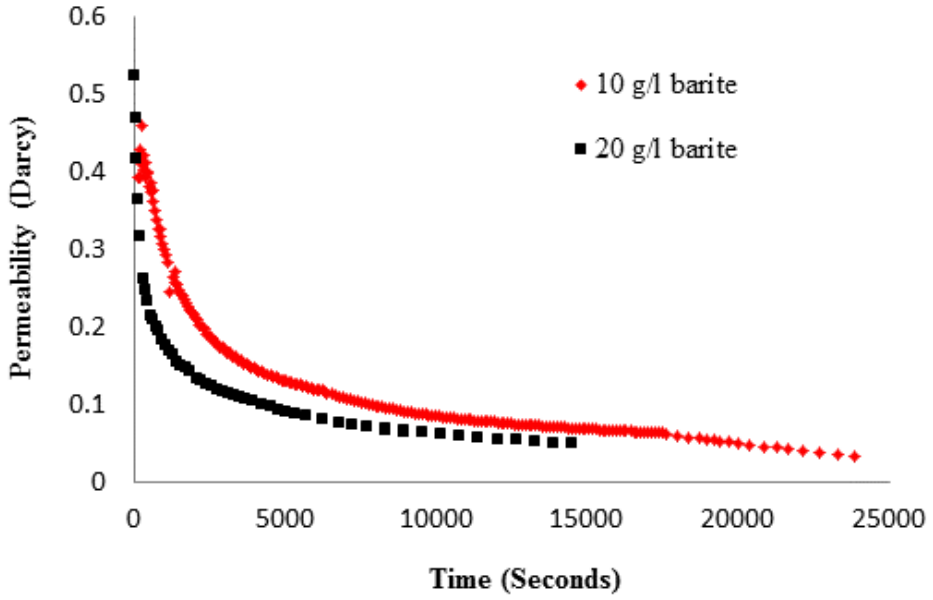

Figure 2. Permeability measured versus time for different barite concentrations (10 g/L and 20 g/L), The permeability (k) continuously and smoothly decreased with time (t) following a power law, $k=3.94t^{-0.343}$, $R^2=0.996$ for 10 g/L); and $k=2.701t^{-0.403}$, $R^2=0.978$ for 20 g/L.

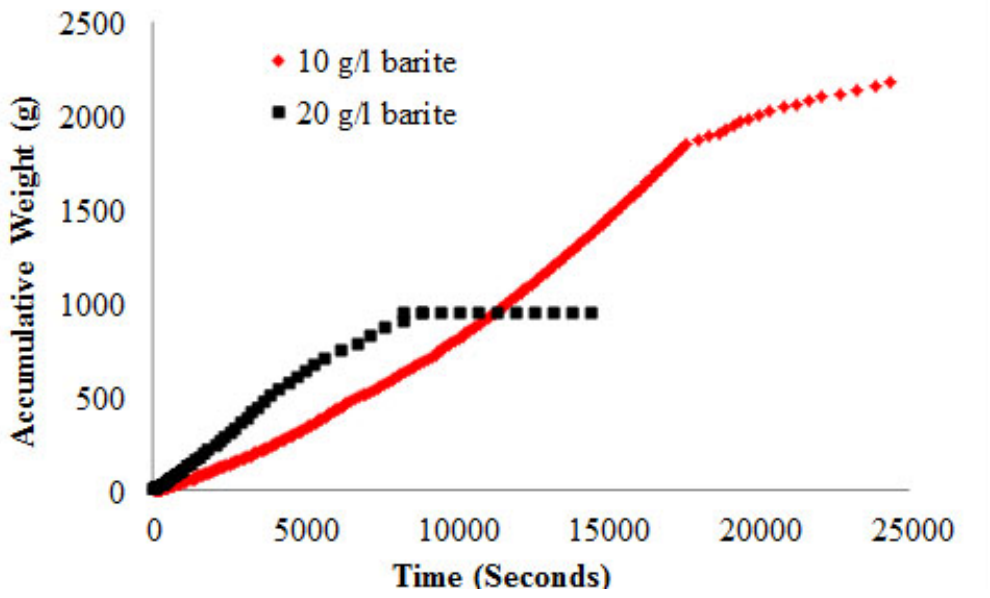

Figure 3. Accumulative weight of produced fluid versus time for different barite concentrations (10 g/L and 20 g/L).

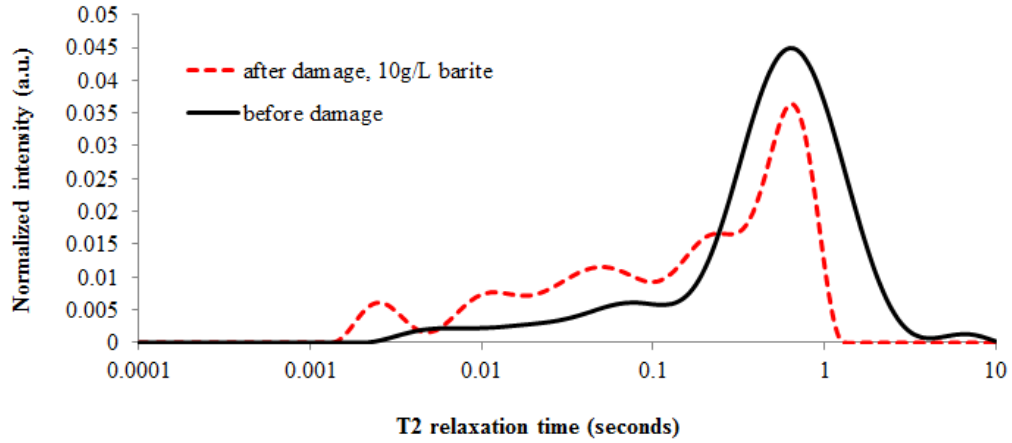

Figure 4. NMR T_2 response curves before and after injection of 10 g/L barite suspension. Porosity was reduced from 21% to 17.6%.

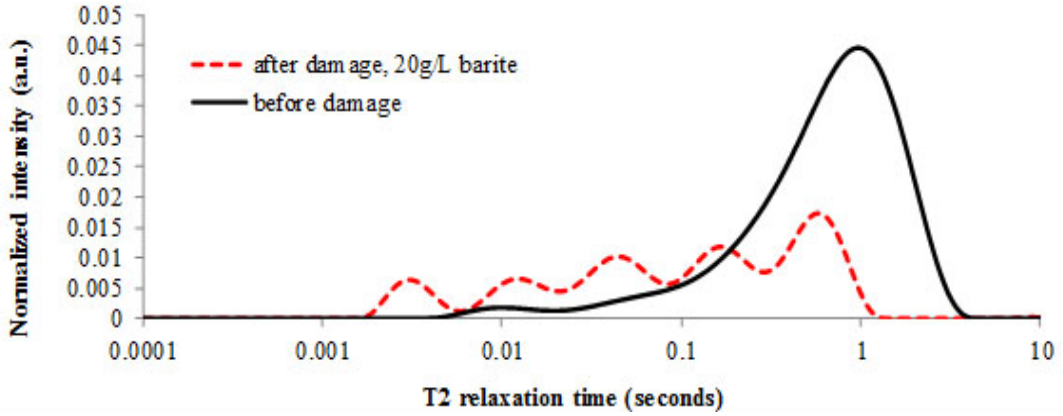

Figure 5. NMR T_2 response curves before and after injection of 20 g/L barite suspension. Porosity was reduced from 23% to 12.1%.

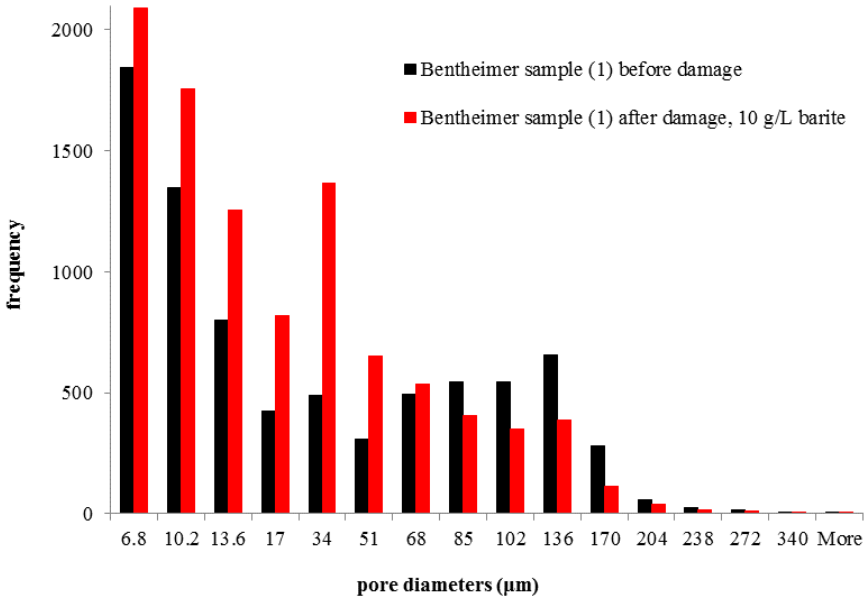

Figure 6. Bentheimer #1 pore diameters before and after damaged caused by fines injection (10 g/L barite) measured with µCT.

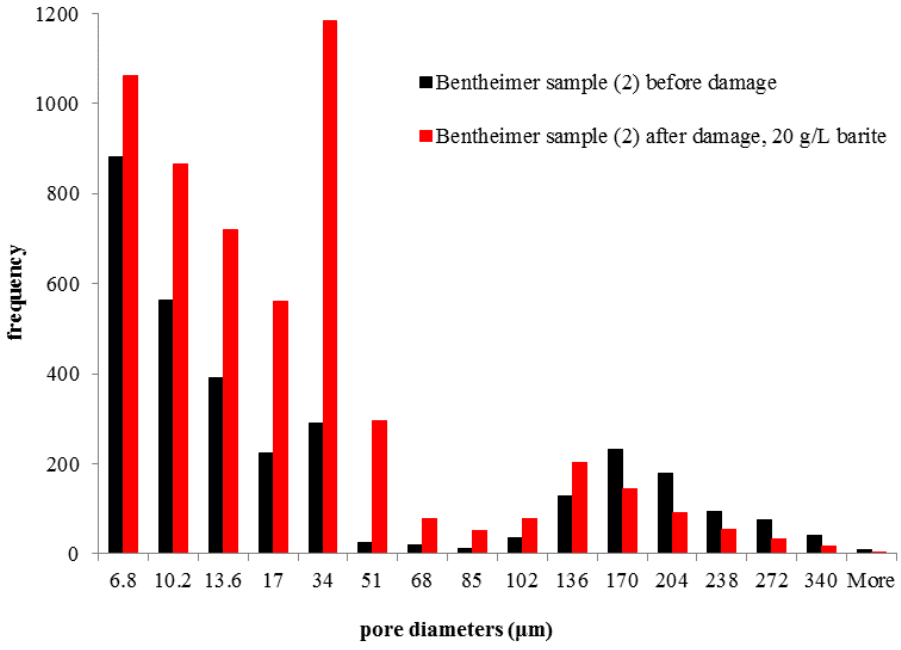

Figure 7. Bentheimer #2 pore diameters before and after damaged caused by fines injection (20 g/L barite) measured with µCT.

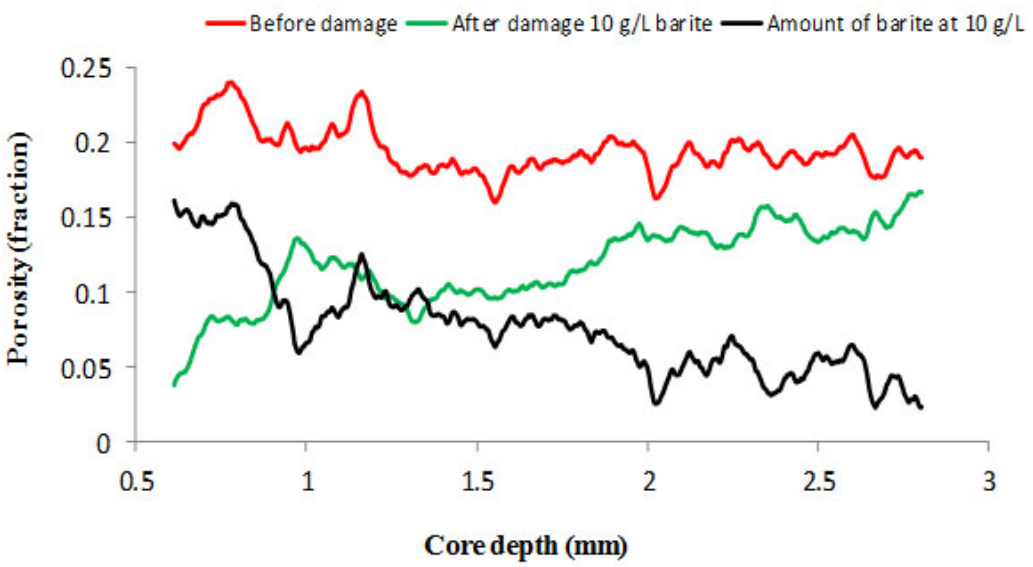

Figure 8. Porosity versus core length before (red) and after (green) damage and amount of barite trapped (black) versus core depth (10 g/L barite).

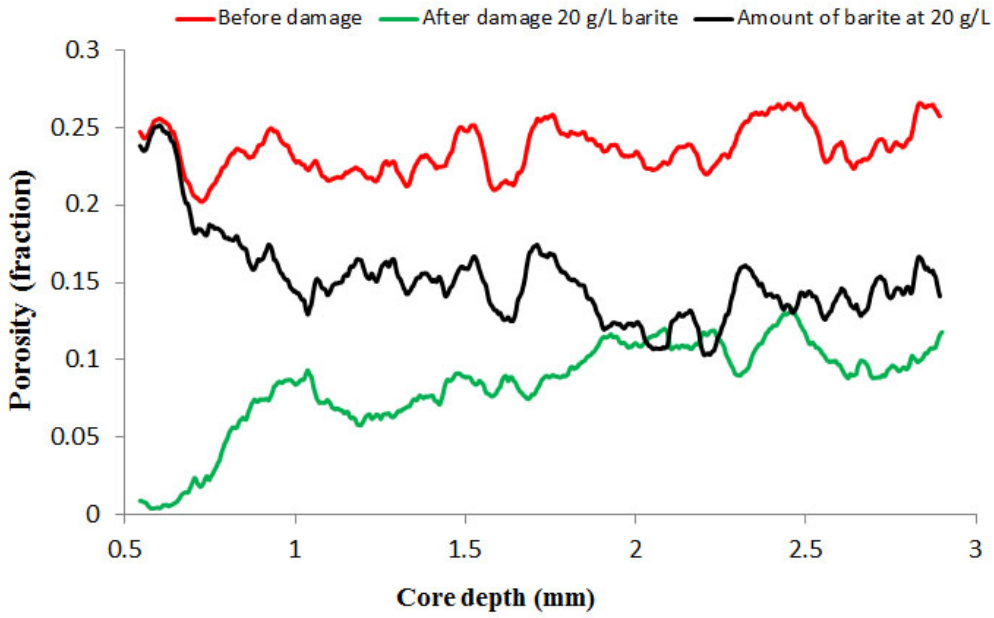

Figure 9. Porosity versus core length before (red) and after (green) damage and amount of barite trapped (black) versus core depth (20 g/L barite).

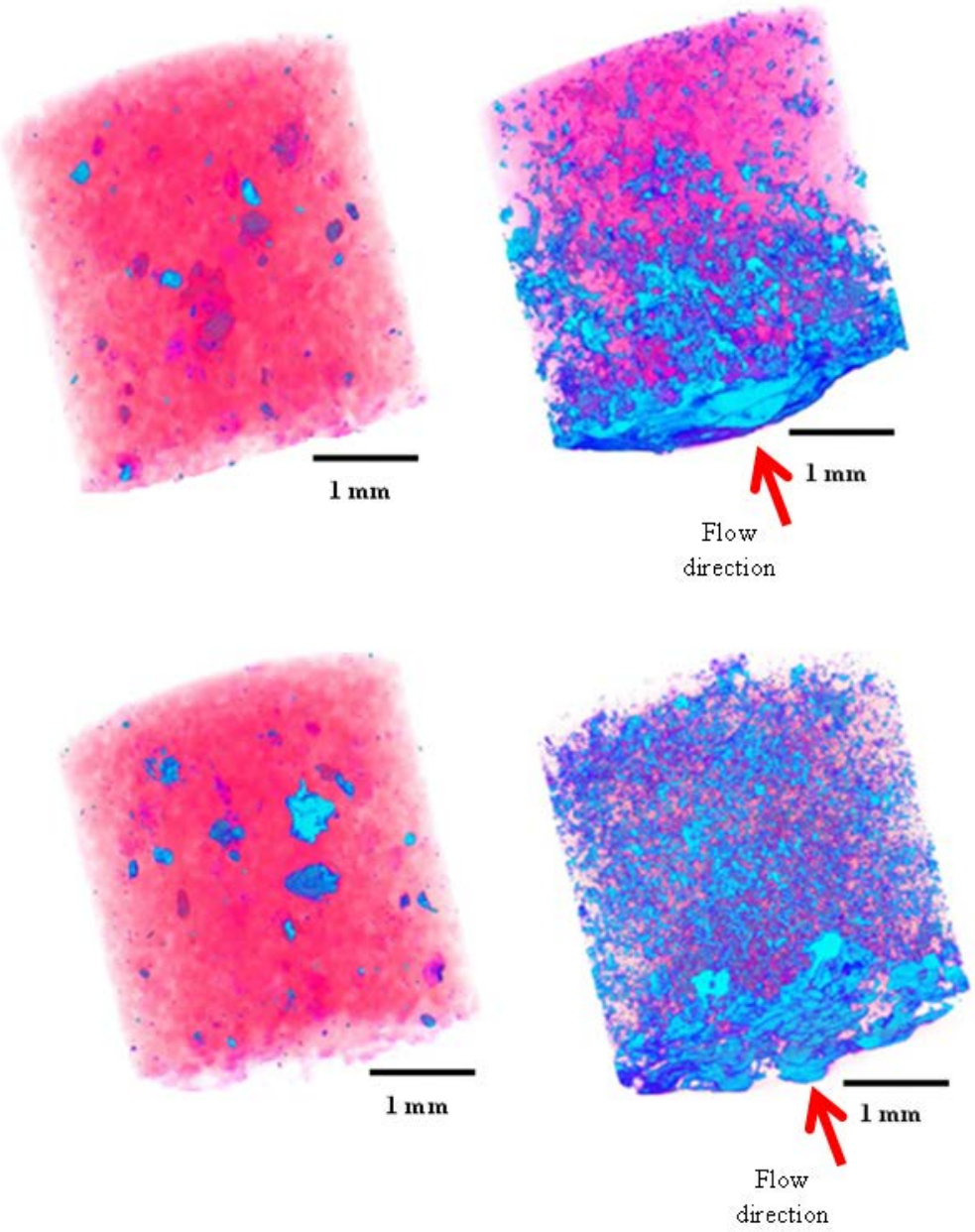

Figure 10. 3D μCT images (3.4 μm resolution) of the core plugs before and after barite injection; (a) is sample #1 and (c) is sample #2 before damage. (b) is sample #1 after damage (10 gm/L barite) and (d) is samp le #2 after damage (20 gm/L barite). The cylindrical volumes shown are 3.4mm in diameter and 3.4 mm in length (= 30.86mm^3). In the images (a) and (c) rutile (component of original rock, see XRD analysis above) is blue and sandstone (quartz) is pink. In the images (b) and (d) the deposited barite is also blue.

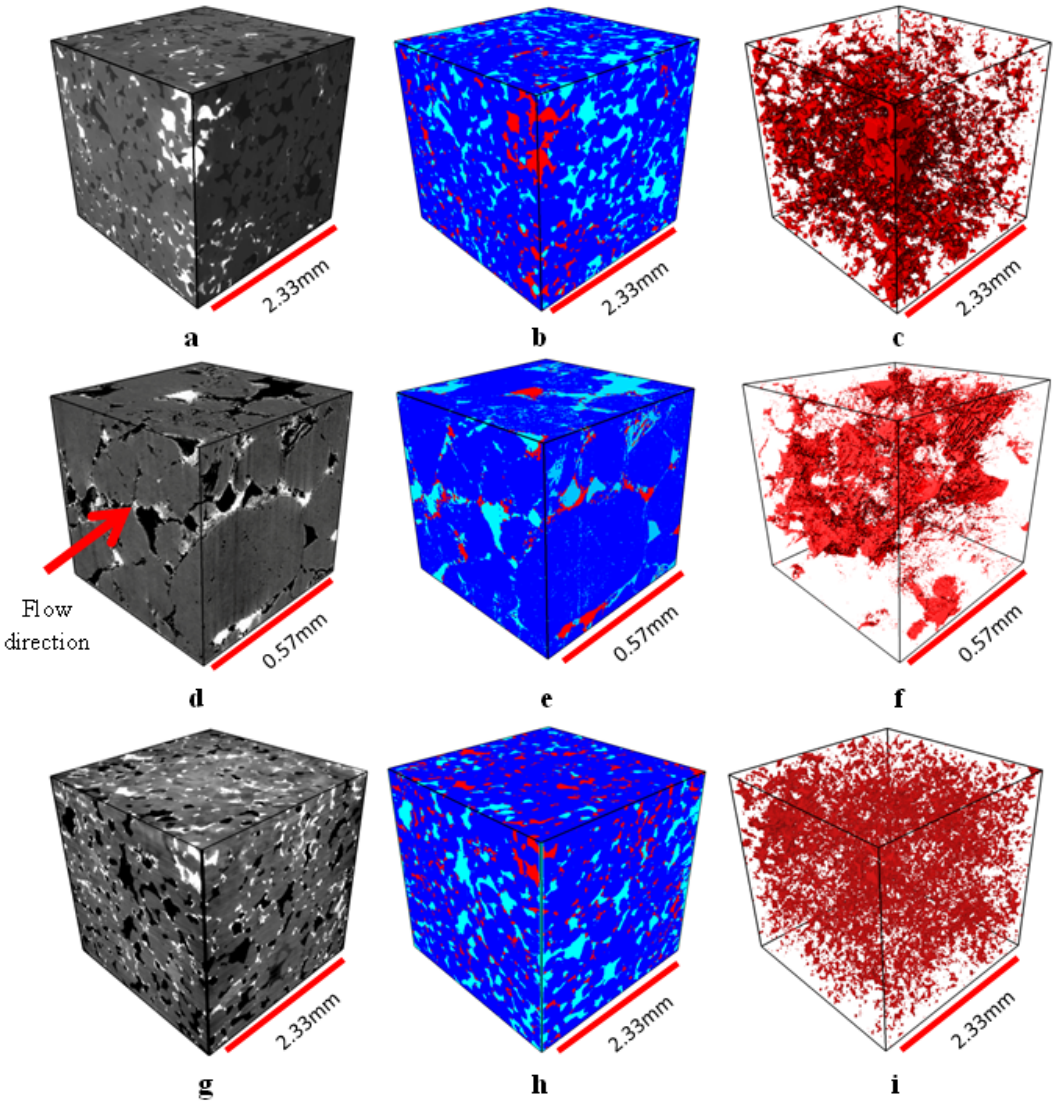

Figure 11. 3D µCT images of Bentheimer sandstone after formation damage caused by injection of barite suspension. (a) raw image for sample #1 (10g barite/L) at 3.4 µm resolution, a cubic volume (12.65mm^3) is shown, (b) segmented image (a), (c) segmented image for barite (shown in red) only, (d) raw image for sample #1 at a resolution of 0.89 µm, a cubic volume (0.185 mm^3) is shown, (e) segmented image (d), (f) segmented image for barite only, (g) raw image for sample #2 (20g barite/L) at 3.4 µm resolution, a cubic volume (12.65mm^3) is shown, (h) segmented image (g), (i) segmented image for barite only at 3.4 µm resolution. In the raw images barite is white, open pore space is black and sandstone is grey; in the segmented images rock is dark blue, barite red and open pore space is light blue.

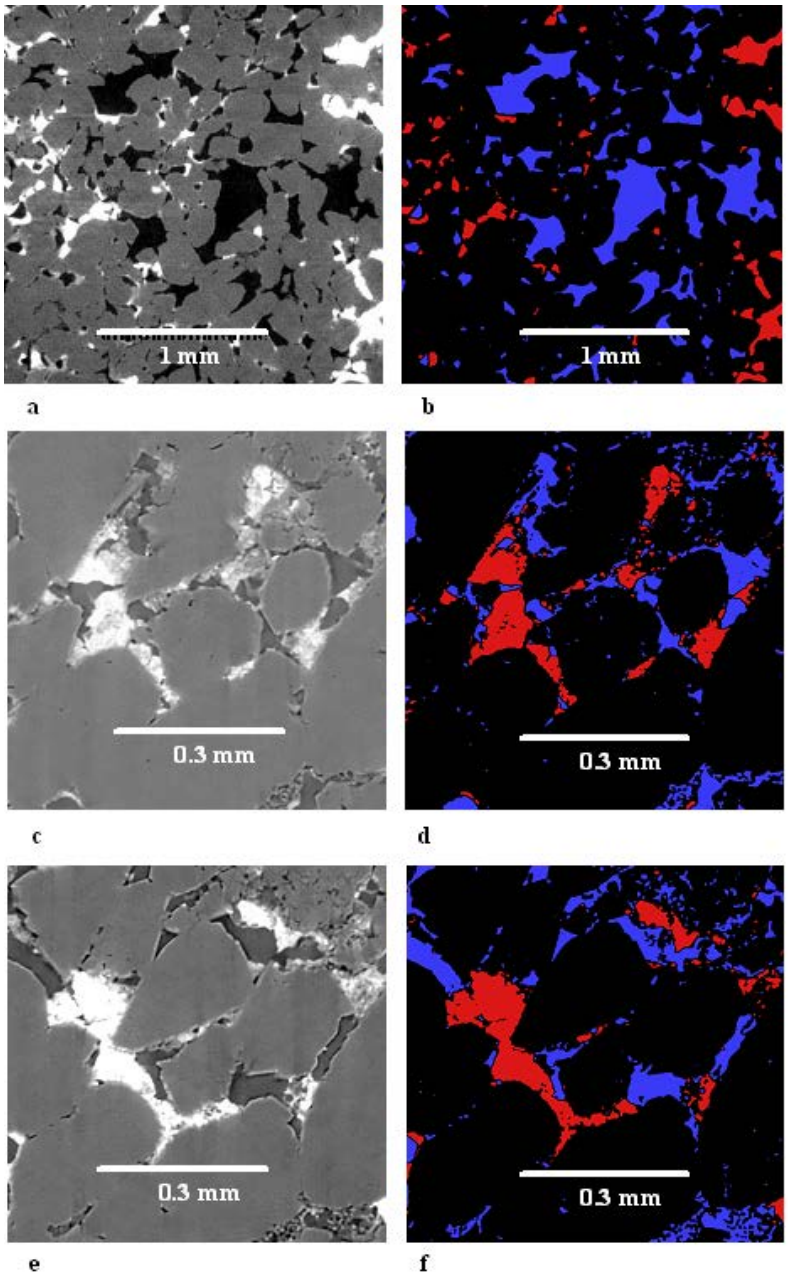

Figure 12. 2D slices through the rock and pore space: (a) damaged Bentheimer sandstone (sample #2) after injection of particle suspension (20 g/L barite), pores are black/dark grey, sandstone is light grey and barite is white, (b) segmented image, sandstone is black, pore space is blue and barite red at resolutions of 3.4 µm. (c and e) damaged Bentheimer sandstone (sample #1) after injection of particle suspension (10 g/L barite), pores are dark grey, sandstone is light grey and barite is white, (d and f) segmented images, sandstone is black, pore space is blue and barite red. These images (c-f) show an area of 0.67mm x 0.67mm (= 0.45mm^2) at resolutions of 0.89 µm.

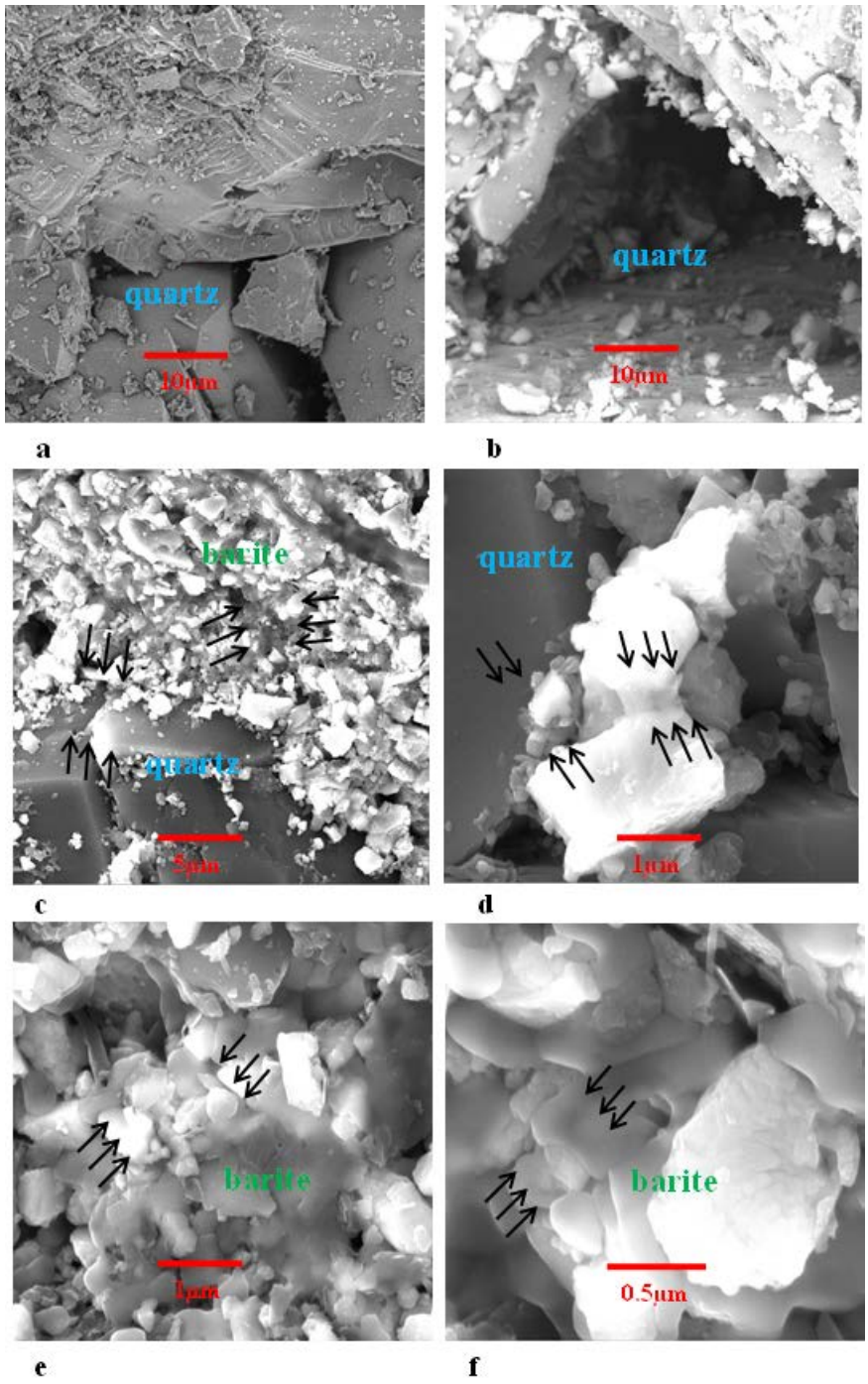

Figure 13. SEM images of Bentheimer # sample 1 before and after damage (10 g/L barite): (a) and (b) show the undamaged plug, only quartz crystals can be seen, (c) and (d) show the sample after damage, adhesion between quartz (grey) and barite (white) can be seen, (e) and (f) show the adhesion between barite particles in the damaged plug. The black arrows point towards barite-quartz and barite-barite interfaces.

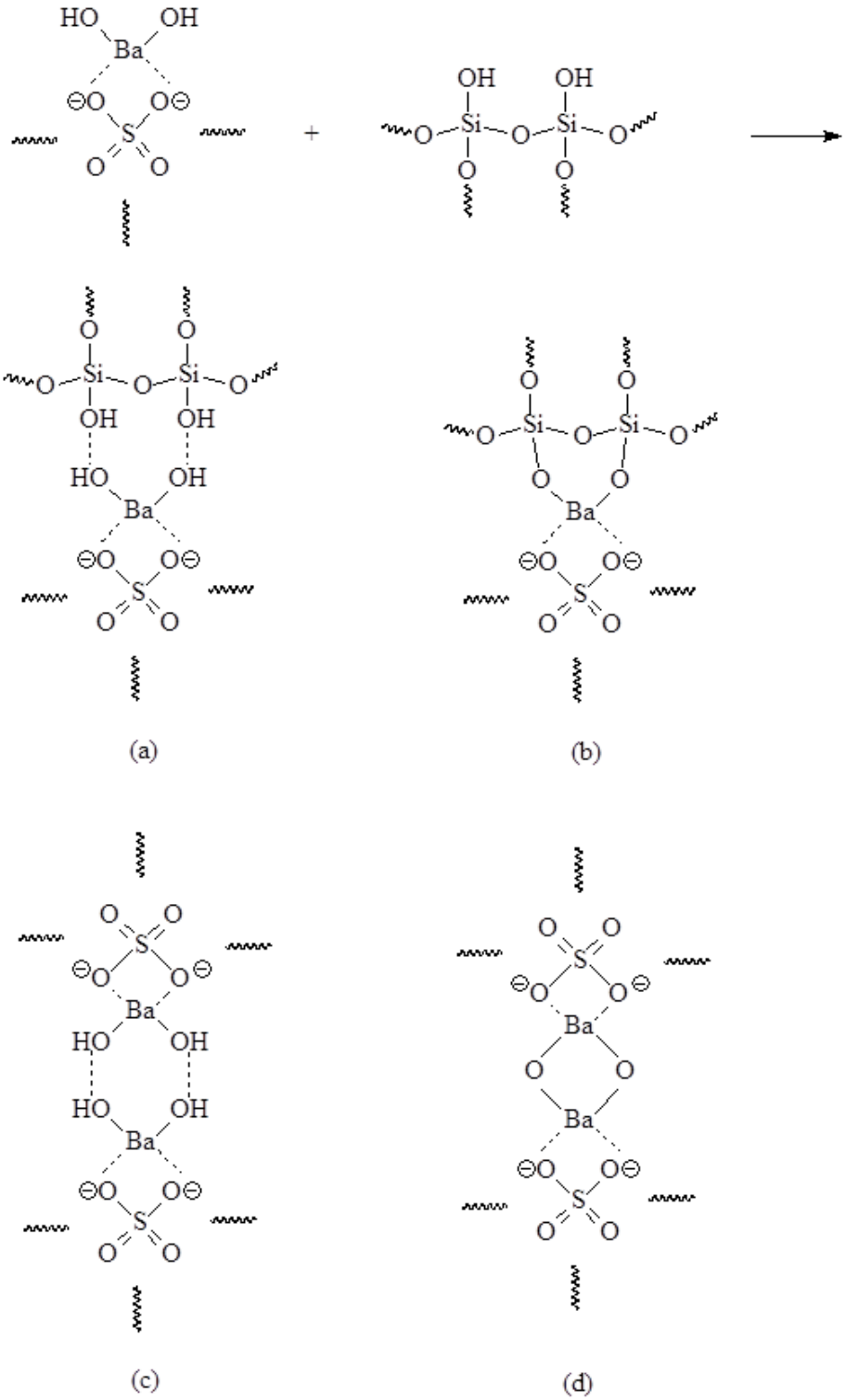

Figure 14. Barite-barite and quartz-barite surface interactions: the hydroxyl groups attract each other by Debye and Keesom forces or form hydrogen bridges (a) and (c), or a condensation reaction follows where Ba-O-Ba or Si-O-Ba bonds are formed and water is released (b) and (d). These scenarios would trigger tight barite packing and strong adhesion to the sandstone surface.

4. Conclusions

We observed formation damage caused by fines injection into sandstone plugs *in-situ* by μCT and NMR measurements. As expected higher fines concentrations led to greater reduction in porosity and permeability, consistent with the measured production curves and literature data [Krilov et al., 1991; Asghari et al., 1995; Nguyen and Civan, 2005; and Tran et al., 2009]. The *in-situ* experiments showed that the amount of fines trapped rapidly decreased with core depth, which confirms earlier measurements [Nguyen and Civan, 2005; Tran et al., 2010]; in addition, mainly larger pores were filled with the fines, which was reflected in the shift of the pore size distributions to smaller sizes, this confirms earlier suggestions in the literature [Nguyen and Civan, 2005; Tran et al., 2010]. Furthermore, the high resolution μCT images in combination with SEM imaging allowed us to investigate the detailed mechanisms causing the above damage: the barite particles were first trapped in thin pore throats apparently due to the interplay between mechanical and intermolecular forces. Once the throats were plugged, adjacent pore bodies were filled with the fines. Moreover, the barite particles were tightly packed – not loosely as previously suggested [Krilov et al., 1991; Asghari et al., 1995; Nguyen and Civan, 2005; Civan, 2007; and Tran et al., 2009], which we hypothesize is due to strong intermolecular forces between the barite particles. These conclusions enabled us to outline a new formation damage model, which we hypothesize will hold for strongly water-wet rock and strongly water-wet fines (and likely in an equivalent way for strongly oil-wet rock and oil-wet fines).

Acknowledgements

The authors thank the National Geosequestration Laboratory (NGL) for providing access to the μCT system VersaXRM-500 (Xradia Ltd). The National Geosequestration Laboratory is a collaboration between Curtin University, CSIRO, and the University of Western Australia established to conduct and deploy critical research and development to enable commercial-scale carbon storage options. Funding for this facility was provided by the Australian Federal Government.

References

Ahmed, T., and P. D., McKinney, 2005. Advanced Reservoir Engineering. Gulf Publishing Burlington, MA 01803, USA, 401pp.

Allen, S. G., Stephenson, P. C. L., and Strange, J. H.,1997. Morphology of porous media studied by nuclear magnetic resonance. The Journal of Chemical Physics, 106(18), 7802-7809pp. doi:http://dx.doi.org/10.1063/1.473780.

Asghari, K., Kharrat, R., and Vossoughi, S., 1995. Alteration of Permeability by Fine Particle Movement - A Water Injectivity Problem. SPE 29006, presented at the SPE international Symposium on Oilfield Chemistry held in San Antonio, TX, U.S.A., 14-17 February 1995.

Bennion, D. B., Bennion, D. W., Thomas, F. B., and Bietz, R. F., 1998. Injection Water Quality-A Key Factor to Successful Waterflooding. Petroleum Society of Canada Journal, 37 (6), 53-62pp.

Bennion, D. B., Thomas, F. B., Imer, D., Ma, T., and Schulmeister, B., 2011. Water Quality Considerations Resulting in the Impaired Injectivity of Water Injection and Disposal Wells. PETSOC-01-06-05, Journal of Canadian Petroleum Technology, 40(6), 54-61pp. doi: 10.2118/01-06-05.

Blunt, M. J., Bijeljic, B., Dong, H., Gharbi, O., Iglauer, S., Mostaghimi, P., and Pentland, C., 2013. Pore-scale imaging and modelling, Advances in Water Resources Journal, 51(0), 197-216pp. doi: http://dx.doi.org/10.1016/j.advwatres.2012.03.003.

Bradford, S. A., Torkzaban, S., and Simunek, J., 2011. Modeling colloid transport and retention in saturated porous media under unfavorable attachment conditions. Water Resources Research, 47(10), W10503. doi: 10.1029/2011WR010812.

Bowers, M. C., Ehrlich, R., Howard, J. J., and Kenyon, W. E., 1995. Determination of porosity types from NMR data and their relationship to porosity types derived from thin section. Journal of Petroleum Science and Engineering, 13(1), 1-14pp. doi: http://dx.doi.org/10.1016/0920-4105(94)00056-A

Buades, A., Coll, B., and Morel, J. M., 2005. A non-local algorithm for image denoising, presented at the Computer Vision and Pattern Recognition. Computer Society Conference (CVPR, IEEE), San Diego, CA, 20-25 June 2005.

Byrne, M. T., Patey, I. T. M., and Green, J. J., 2007. A New Tool for Exploration and Appraisal - Formation Damage Evaluation. SPE 107557-MS, presented at the European Formation Damage Conference, Scheveningen, The Netherlands, 30 May-1 June 2007.

Byrne, M. T., Spark, I. S. C., Patey, I. T. M., and Twynam, A. J., 2000. A Laboratory Drilling Mud Overbalance Formation Damage Study Utilising Cryogenic SEM Techniques. SPE 58738, presented at the SPE International Symposium on Formation Damage Control held in Lafayette, Louisiana, 23–24 February 2000.

Civan, F., 2007. Reservoir Formation Damage Fundamentals, Modeling, Assessment and Mitigation. Gulf Publishing Company, Houston, USA, Second Edition, 1114pp.

Dong, H., and Blunt, M. J., 2009. Pore-network extraction from micro-computerized-tomography images. Physical Review E, 80(3), 1-11pp. doi: 10.1103/PhysRevE.80.036307.

Ebrahimi, N., A., Jamshidi, S., Iglauer, S., and Boozarjomehry, R. B., 2013. Genetic algorithm-based pore network extraction from micro-computed tomography images. Chemical Engineering Science, 92(0), 157-166pp.

Elsaeh, A. E., and Ramdzani, I. A. B. A., 2014. Pore size and geometry of reservoir rocks used as key factor for drilling and completion fluid design of oil wells. European Scientific Journal, 10(10), 102-113pp.

Fenter, P., McBride, M. T., Srajer, G., Sturchio, N. C., and Bosbach, D., 2001. Structure of Barite (001)− and (210)−Water Interfaces. The Journal of Physical Chemistry, 105(34), 8112-8119pp. doi: 10.1021/jp0105600.

Fischer, S., Zemke, K., Liebscher, A., and Wandrey, M., 2011. Petrophysical and petrochemical effects of long-term CO_2 -exposure experiments on brine-saturated reservoir sandstone. Energy Procedia, 4(0), 4487-4494pp.

Fridjonsson, E.O, Hasan A.B., Fourie, A.B. and Johns M.L., 2013. Pore Structure in a Gold Mine Cemented Paste Backfill. Minerals Engineering Journal, 53, 144-151pp.

Green, J., Cameron, R., Patey, I., Nagassar, V., and Quine, M., 2013. Use of Micro-CT Scanning Visualisations to Improve Interpretation of Formation Damage Laboratory Tests Including a Case Study From the South Morecambe Field. SPE

165110, presented at the SPE European Formation Damage Conference, Noordwijk, The Netherlands,5-7 June 2013.

Gulati, M. S., and Maly, G. P., 1975. Thin-Section and Permeability Studies Call for Smaller Gravels in Gravel Packing. SPE 4773-PA, Journal of Petroleum Technology, 27(1), 107- 112pp. doi: 10.2118/4773-PA.

Hidajat, I., Rastogi, A., Singh, M., and Mohanty, K. K., 2002. Transport Properties of Porous Media Reconstructed from Thin-Sections. SPE 77270-PA, Society of Petroleum Engineers Journal, 7(1), 40-48pp. doi: 10.2118/77270-PA.

Iglauer, S., Favretto, S., Spinelli, G., Schena, G., and Blunt, M.J., 2010. X-ray tomography measurements of power-law cluster size distributions for the nonwetting phase in sandstones, Physical Review E, 82, 05631.

Israelachvili, J. N., 2011. Intermolecular and Surface Forces (Third Edition). Academic Press, London, 667pp.

Kandarpa, V., and Sparrow, J. T., 1981. A Useful Technique to Study Particle Invasion in Porous Media by Backscattered Electron Imaging. SPE 10134, presented at the SPE 56th Annual Fall Technical Conference and Exhibition, San Antonio, Texas, October 5-7, 1981.

Kleinberg, R. L., Kenyon, W.E., Mitra, P.P., 1994. Mechanism of NMR Relaxation of Fluids in Rock. Journal of Magnetic Resonance Series, 108, 206-214pp.

Krilov, Z., Steiner, I., Goricnik, B., Wojtanowicz, A. J., and Cabrajac, S., 1991. Quantitative Determination of Solids Invasion and Formation Damage Using CAT Scan and Barite Suspensions. SPE 23102, presented at the SPE Offshore Europe Conference, UK, Aberdeen, 3-6 September 1991.

Krueger, R. G., 1967. Effect of Pressure Drawdown on Clean-Up of Clay- or Silt-Blocked Sandstone. SPE-1605-PA, Society of Petroleum Engineers Journal, 19(3), 397-403pp. doi: 10.2118/1605-PA.

Liaw, H. K., Kulkarni, R., Chen, S., and Watson, A. T., 1996. Characterization of fluid distributions in porous media by NMR techniques. AIChE Journal, 42(2), 538-546pp.

Mahmoudi, H., Spahis, N., Goosen, M. F., Ghaffour, N., Drouiche, N., and Ouagued, A., 2010. Application of geothermal energy for heating and fresh water production in

a brackish water greenhouse desalination unit: A case study from Algeria. Renewable and Sustainable Energy Reviews, 14(1), 512-517pp.

McCaughan, J., Iglauer, S., and Bresme, F., 2013. Molecular Dynamics Simulation of Water/CO_2-quartz Interfacial Properties: Application to Subsurface Gas Injection. Energy Procedia Journal, 37(0), 5387-5402pp.

McDowell-Boyer, L. M., Hunt, J. R., and Sitar, N., 1986. Particle transport through porous media. Water Resources Research, 22(13), 1901-1921pp.

Nguyen, V., and Civan, F., 2005. Modeling particle migration and deposition in porous media by parallel pathways with exchange. Chapter 11, Handbook of Porous media, Second Edition, Vafai, K. (Ed), CRC Press, Taylor and Francis Group, Boca Raton, FL: 457-484.

Nowak, T. J., and Krueger, R. F., 1951. The Effect of Mud Filtrates and Mud Particles upon the Permeabilities of Cores. American Petroleum Institute (API-51-164), presented at Drilling and Production Practice Conference, New York, New York, 1 January 1951.

Okabe, H., Tsuchiya, Y., Pentland, C.H., Iglauer, S., and M.J. Blunt, 2013. Residual CO_2 saturation distributions in rock samples measured by X-ray CT. in: Advances in X-ray tomography, chapter 45, pp. 381-389 (ed. K Lui)

Otsu, N., 1979. A threshold selection method from gray-level histograms. IEEE Trans. Sys. Man. Cyber., 9(10), 62-66pp.

Rosenbrand, E., Kjøller, C., Riis, J. F., Kets, F., and Fabricius, I. L., 2015. Different effects of temperature and salinity on permeability reduction by fines migration in Berea sandstone. Geothermics, 53(0), 225-235pp.

Rosenbrand, E., Haugwitz, C., Jacobsen, P. S. M., Kjøller, C., and Fabricius, I. L., 2014. The effect of hot water injection on sandstone permeability. Geothermics, 50(0), 155-166pp. doi: http://dx.doi.org/10.1016/j.geothermics.2013.09.006.

Seright, R. S., Prodanovic, M., and Lindquist, W. B., 2006. X-Ray Computed Microtomography Studies of Fluid Partitioning in Drainage and Imbibition Before and After Gel Placement: Disproportionate Permeability Reduction. SPE-89393-PA, Society of Petroleum Engineers Jounral, 11(2), 159 - 170pp. doi: 10.2118/89393-PA.

Talabi, O., AlSayari, S., Iglauer, S., and Blunt, M. J., 2009. Pore-scale simulation of NMR response. Journal of Petroleum Science and Engineering, 67(3–4), 168-178pp. doi: http://dx.doi.org/10.1016/j.petrol.2009.05.013.

Tiab, D., and Donaldson, E. C., 2004. Petrophysics - Theory and Practice of Measuring Reservoir Rock and Fluid Transport Properties. Gulf Publishing Co., Elsevier, USA, Second edition, 889pp.

Tran, T. V., Civan, F., and Robb, I. D., 2009. Correlating Flowing Time and Condition For Perforation Plugging By Suspended Particles. SPE-120847-PA, Society of Petroleum Engineers Journal, 24(3), 398-403pp. doi: 10.2118/120847-PA.

Tran, T. V., Civan, F., and Robb, I. D., 2010. Effect of Permeability Impairment By Suspended Particles On Invasion Of Drilling Fluids. IADC/SPE 133724, presented at the IADC/SPE Asia Pacific Drilling Technology Conference and Exhibition, Vietnam, Ho Chi Minh, 1–3 November 2010.

Torkzaban, S., Bradford, S. A., and Walker, S. L., 2007. Resolving the Coupled Effects of Hydrodynamics and DLVO Forces on Colloid Attachment in Porous Media. Langmuir, 23(19), 9652-9660pp. doi: 10.1021/la700995e.

Wildenschild, D., and Sheppard, A. P., 2013. X-ray imaging and analysis techniques for quantifying pore-scale structure and processes in subsurface porous medium systems. Advances in Water Resources, 51(0), 217-246pp.

Zhuravlev, L. T., 2000. The surface chemistry of amorphous silica. Zhuravlev model. Colloids and Surfaces, A: Physicochemical and Engineering Aspects, 173(1–3), 1-38pp.

Receding and Advancing (CO_2+ Brine+ Quartz) Contact Angles as a Function of Pressure, Temperature, Surface Roughness, Salt Type and Salinity

Al-Yaseri, A.Z., Lebedev, M., Barifcani, A. and Iglauer, S., 2016. Receding and advancing (CO_2+ brine+ quartz) contact angles as a function of pressure, temperature, surface roughness, salt type and salinity. The Journal of Chemical Thermodynamics, 93, pp.416-423.

Receding and advancing CO_2-brine-quartz contact angles as a function of pressure, temperature, surface roughness, salt type and salinity

Ahmed Z. Al-Yaseri[1], Maxim Lebedev[2], Ahmed Barifcani[3], and Stefan Iglauer[1]
[1]Curtin University, Department of Petroleum Engineering, 26 Dick Perry Avenue, 6151 Kensington, Australia
[2]Curtin University, Department of Exploration Geophysics, 26 Dick Perry Avenue, 6151 Kensington, Australia
[3]Curtin University, Department of Chemical Engineering, 26 Dick Perry Avenue, 6151 Kensington, Australia

Abstract

The wetting characteristics of CO_2 in rock are of vital importance in carbon geo-storage as they determine fluid dynamics and storage capacities. However, the current literature data has a high uncertainty, which translates into uncertain predictions in terms of containment security and economic project feasibility. We thus measured contact angles for the CO_2/water/quartz system at relevant reservoir conditions, and analysed the effects of pressure (0.1–20 MPa), temperature (296-343K), surface roughness (56nm-1300nm), salt type (*NaCl*, $CaCl_2$, and $MgCl_2$) and brine salinities (0–35 wt%).

Water contact angles decreased with surface roughness, but increased with pressure, temperature, and brine salinity. Overall the contact angles were significantly increased at storage conditions (~50°) when compared to ambient conditions (always 0°). Consequently quartz is weakly water-wet (not completely water-wet) at storage conditions, and structural and residual trapping capacities are reduced accordingly.

Keywords

carbon geo-sequestration, contact angle, quartz, surface roughness, brine salinities, carbon dioxide, residual trapping, structural trapping

1. Introduction

In recent years CO_2 emission into the atmosphere has been recognized as a major cause for climate change [1]; these emissions are predicted to increase due to increased energy demand as global industrialization proceeds and generally the standard of living is targeted to increase (coupled with the fact that society heavily relies on fossil fuels, >80% [2]).

In this context, carbon geo storage (*CGS*) has been identified as a viable option to reduce CO_2 emissions [1,3]. *CGS* can be combined with hydrocarbon recovery schemes to enhance oil and gas recovery [1-4]. Specifically, in *CGS*, CO_2 is collected from large point-source emitters, compressed and injected deep underground into geological formations for storage [1]. The primary problem with *CGS* is that CO_2 has a lower density than formation brine and will flow upwards. However, four mechanisms prevent the CO_2 from leaking to the surface: a) structural trapping [5], b) residual trapping [6], c) dissolution trapping [7] and d) mineral trapping [8].

List of symbols

θ	contact angle
θ_a	advancing contact angles
θ_r	receding contact angles
θ_{rough}	contact angle measured on the rough surface
θ_{smooth}	contact angle measured on the smooth surface
θ_{arough}	advancing contact angle measured on the rough surface
θ_{rroughr}	receding contact angle measured on the rough surface
θ_{asmooth}	advancing contact angle measured on the smooth surface
θ_{rsmooth}	receding contact angle measured on the smooth surface
p	pressure
T	temperature
RMS	surface roughness
r	roughness ratio
s	salinity
r'	mean pore throat radius
h	CO_2 column height
$\Delta\rho$	density difference
γ	interfacial tensions
g	gravity

One parameter, which has received little attention, but has a dramatic impact on structural and residual trapping, is the CO_2-wettability of the rock [9]. Precisely, the published data has a large uncertainty even with the simplest systems: for instance water contact angles for CO_2/quartz varied between 0-95°, the main reasons being that receding and advancing angles were not distinguished and surface contamination led to artificially high contact angles [10]. It is thus necessary to constrain this parameter to a reasonable level to enable reliable reservoir flow predictions. Consequently we measured the contact angle (θ) on a quartz surface at reservoir conditions and analysed how pressure, temperature, surface roughness, brine salinity and salt types influence θ. In this text we present our results and discuss them in terms of the underlying reasons for the measured correlations and compare them with reliable literature results.

2. Experimental methodology

Four alpha-quartz crystals (*RMS* surface roughnesses were 56nm, 210nm, 560nm, and 1300 nm, respectively, Figure 1, measured with an Atomic Force Microscope, instrument model AFM DSE 95-200) were cleaned for at least 45min in an air plasma to remove surface contamination [11], following Iglauer et al.'s [10] and Sarmadivaleh et al.'s [12] procedure. This cleaning process is a crucial step to avoid significant systematic errors [10-14]. The cleaned samples were then placed inside a pressure chamber (Figure 2) at set temperatures (296, 323 and 343K). Subsequently CO_2 was injected into the chamber with a high precision syringe pump (ISCO 500D; pressure accuracy of 0.1% FS) and pressure was increased to a pre-set value (0.1, 5, 10, 15, 20 MPa). We note that the fluids were not thermodynamically equilibrated, however, earlier studies demonstrated that θ is not influenced by equilibration (contact angle decreased with time by 2^o/hr for the CO_2-water-quartz system [15]), if the θ measurement is rapid (<1 min), cp. Sarmadivaleh et al. [12], Al-Yaseri et al. [15]. In addition, un-equilibrated fluids are encountered at the leading edge of the CO_2 plume in the reservoir [16].

Once the target pressure had been reached, a droplet (average volume of a single drop was ~6μL±1 μL) of de-gassed (vacuumed for more than 10 hours) water or brine was dispensed onto the quartz surface through a needle (Figure 2). The tilting-plate technique was used for measuring the contact angle [17-19], because it

simultaneously measures advancing and receding contact angles under identical condition, which makes the comparison and analysis of the results more meaningful. Furthermore, the tilting plate method provides statistically more reliable data when compared with the sessile-drop technique [18]. For an experiment, the substrate was placed on a metal platform housed in the pressure cell, so that an inclination angle of α=12^{o} resulted, cp. Figure 3. Under these conditions the droplet slowly moved from the upper side of the substrate to the lower side driven by gravity.

The advancing water contact angle θ_a was measured at the advancing front of the droplet just before the droplet started to move, and the receding water contact angle θ_r was measured simultaneously at the trailing end of the droplet (Figure 3). The radius of the water droplet at the quartz interface was (≈ 1.7mm±0.2mm), which is smaller than the minimum capillary length (κ^{-1}=2.23mm); this implies that gravity had a negligible impact on θ [20,21].

Movies of the whole process were recorded with a high resolution video camera (Basler scA 640–70 fm, pixel size = 7.4 μm; frame rate = 71 fps; Fujinon CCTV lens: HF35HA-1B; 1:1.6/35 mm) and θ_a and θ_r were measured on images extracted from the movies (measurement uncertainty is ±3° based on replicate measurements), Figure 3. Finally, a range of brines with different salinities and salt (Table 1) types was investigated (3wt%, 6wt%, 10wt%, 20wt% and 35wt% *NaCl*, $CaCl_2$, and $MgCl_2$ in deionized (*DI*) water), as salinity can vary widely in subsurface reservoirs [22].

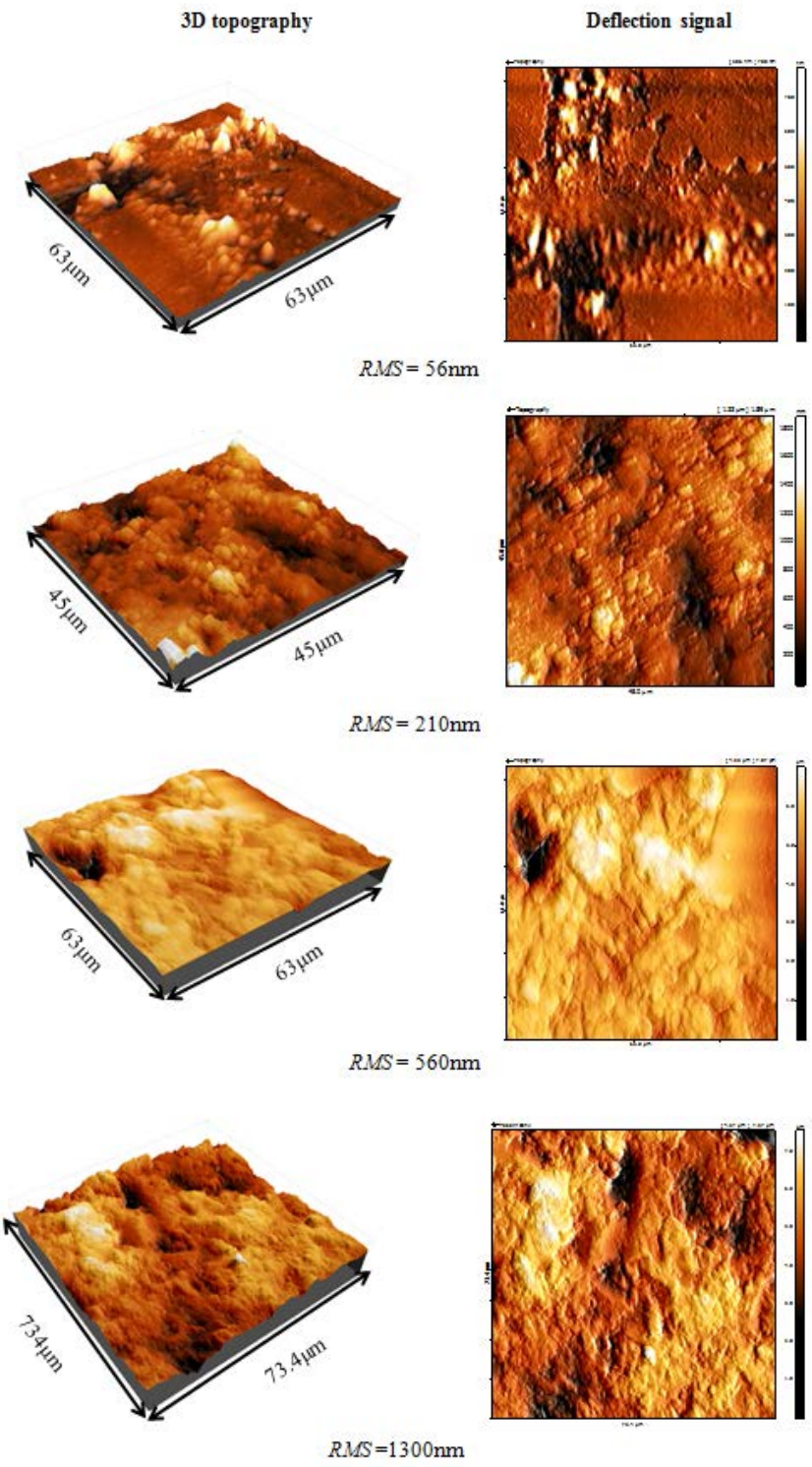

Figure 1. Atomic Force Microscopy images of the four quartz surfaces investigated; different heights are coloured differently (black is 0nm, white the highest value and ranges from 0.788µm for the smoothest surface (56nm *RMS* surface roughness) to 7.57µm for the roughest surface (1300nm *RMS* surface roughness).

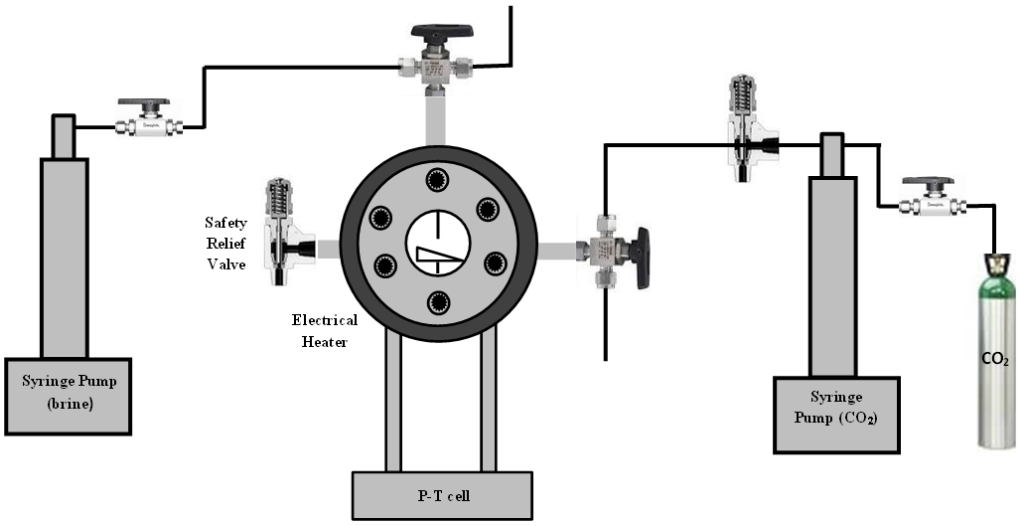

Figure 2. Schematic of the high temperature/high pressure contact angle measurement apparatus.

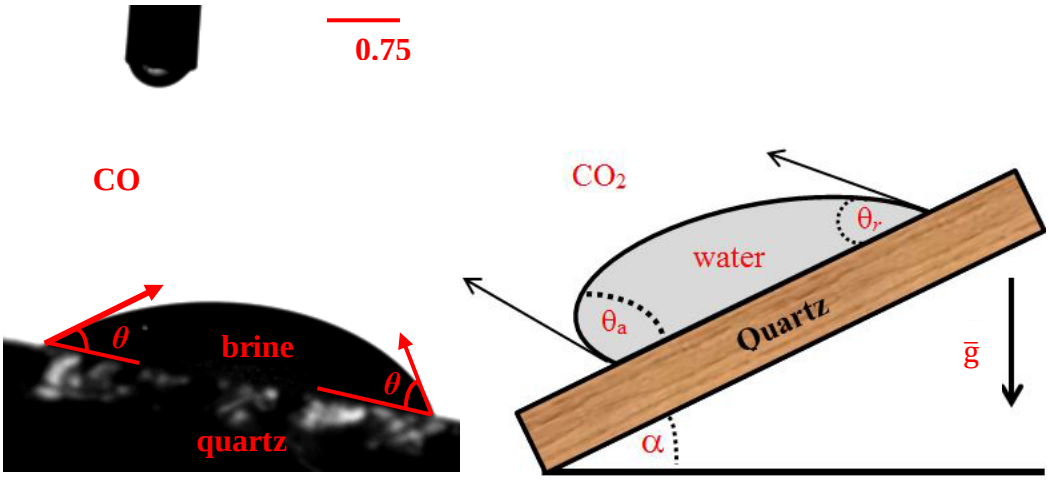

(a) (b)

Figure 3. (a) Optical image ofwater drop on quartz surface in CO_2 atmosphere with θ_a and θ_r indicated; (b) schematic of contact angle measurement using a tilted surface (redrawn from Extrand and Kumagi [19]).

Table 1. Provenance and mass fraction purity of chemicals used in this study.

Chemical name	Source of supply	State	Mass fraction purity
CO_2	BOC, Australia	gas	≥0.999
quartz	Ward's natural science, Canada	solid	≥0.9998 [23]
NaCl	Scharlab s.l., Spain	powder	≥0.995
$CaCl_2$	Scharlab s.l., Spain	powder	≥0.995
$MgCl_2$	Scharlab s.l., Spain	powder	≥0.995
DI water	David Gray's Deionized water	liquid	[a]Conductivity (0.02mS/cm)

[a]The Conductivity of DI water was measured with Multiparameter (HI 9823) at 294K.

3. Results and discussion

3.1 Influence of pressure on contact angles

θ was measured at various pressures (0.1, 5, 10, 15, and 20MPa) and temperatures (296, 323 and 343K) on one quartz surface (*RMS* surface roughness 560nm); advancing and receding contact angles at ambient conditions (296 K and 0.1 MPa CO_2 pressure) were 0^o as expected [10,24]. However, θ_a and θ_r both increased with pressure, up to θ_a=34^o and θ_r=13^o at 20MPa and 296K (Figures 4 and 5).The increase in θ_a and θ_r with increasing pressure was also observed for experiments conducted at 323K and 343K (Figures 4 and 5), which is consistent with most of the literature data [10,12,15,25-31], and molecular dynamics (MD) simulations [32-34]. Iglauer et al. [33] explained this behaviour by rapid increase in CO_2 density with pressure, which strengthens the intermolecular interactions between CO_2 and quartz, and thus leads to de-wetting of the surface.

3.2 Influence of temperature on contact angles

A clear increase in θ_a and θ_r was measured with increasing temperature. Specifically, when temperature increased from 296K to 343K at 5MPa pressure, θ_a increased by ~9^o and θ_r by ~9^o. This effect was even more pronounced at higher pressures (20 MPa): θ_a increased by ~17^o and θ_r by ~27^o, Figure 4, 5. This behaviour is consistent

with most literature results (Farokhpoor et al. [31] reported an increase of θ_a by ~12^o when temperature increased from 309K to 339K at 10MPa pressure; Saraji et al. [30] measured an increase in θ_a by ~15^o when temperature increased from 318K to 333K at 10MPa; and Sarmadivaleh et al. [12] observed an increase of θ_a by ~20^o at 20MPa when temperature increased from 296K to 343K); however, Saraji et al. [35] measured a slight decrease in θ_a when increasing the temperature from 323K to 373K at 27.57 MPa. The difference between these trends may be due to differences in salt concentration, salt type or surface roughness. Furthermore, the molecular dynamics (MD) simulations found that contact angles decrease with increasing temperature [33]; the discrepancy between the MD predictions and the measurements are probably due to the inadequate representation of the quartz surface chemistry (which is complex [36]) in the MD model, e.g. surface silanol groups exist [37] and significantly lower θ [34]; furthermore the silanol groups can dissociate, and this has not been implemented into the MD models yet.

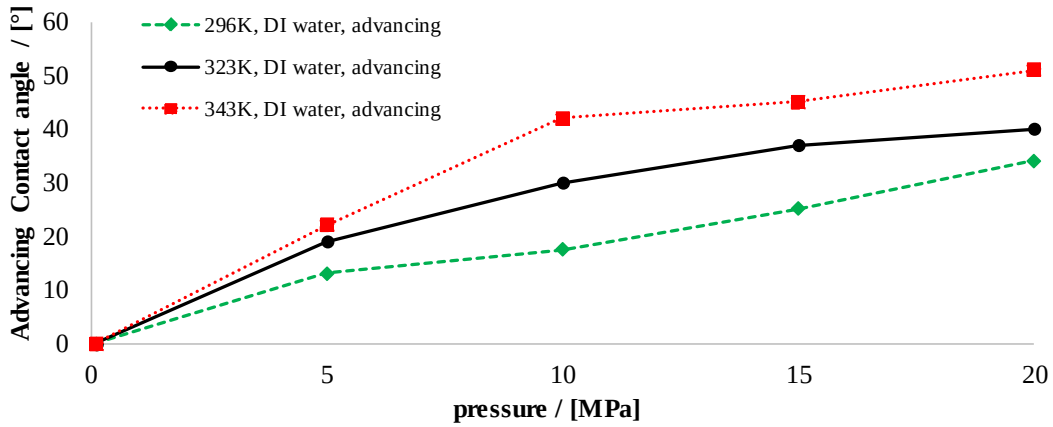

Figure 4. Advancing water contact angles for *CO_2/DI* water/quartz as a function of pressure and temperature, *RMS* = 560nm.

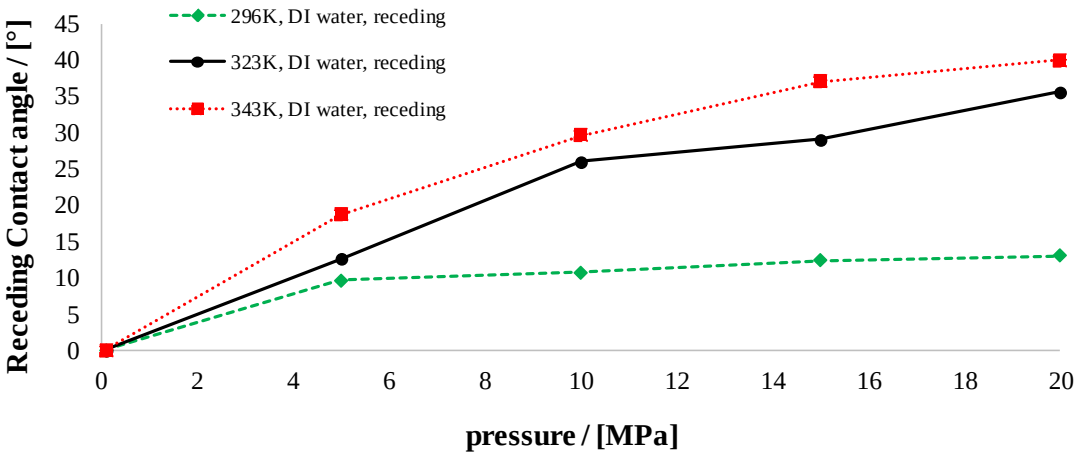

Figure 5. Receding water contact angles for CO_2/*DI* water/quartz as a function of pressure and temperature, *RMS* = 560nm.

3.3. Influence of salinity on contact angles

The effect of salinity on contact angle was investigated at 10MPa using the substrate with a 560nm *RMS* surface roughness at two different temperatures (323K and 343K). Salinity was varied over a large range: from 0 wt% to 35wt%, and several salts were tested (*NaCl*, $CaCl_2$, and $MgCl_2$), cp. Figures 6, 7.

θ_a increased by 14° and θ_r by 12° when salinity was increased from 0 to 35wt% *NaCl* at 323K, Figure 6. In case of divalent cations (i.e. Ca^{2+}, Mg^{2+}), θ_a and θ_r increased further (in total: θ_a by 19° and θ_r by 16° for $CaCl_2$; θ_a by 24° and θ_r by 22° for $MgCl_2$). This salinity effect was enhanced when the temperature rose from 323K to 343K, Figure 7 (θ_a increased by 26° and θ_r increased by 23° for *NaCl*; θ_a increased by 28° and θ_r increased by 28° for $CaCl_2$; and θ_a increased by 30° and θ_r increased by 27° for $MgCl_2$).Thus the increase in θ was more pronounced for divalent cations, and was strongest for Mg^{2+}.

In summary, saline brine resulted in higher contact angles when compared to *DI*-water, consistent with literature data [14,26,29,31,35,38-40]. The increase in θ changed with salt type and followed the ranking $MgCl_2 > CaCl_2 > NaCl$. We explain this effect as follows: the cations of the dissolved salt shield the electrical surface charge of quartz (the point of zero charge for quartz in water is *pH* = 3 [41,42]) thus reducing the effective (negative) surface charge. Consequently, the surface is less polar, which reduces the quartz-water attraction and de-wets the surface (= higher θ).

The ranking $Mg^{2+} > Ca^{2+} > Na^{+}$ in terms of the dewetting potential of quartz is probably due to the differences in cation charge-to-volume ratio, which is highest for Mg^{2+} and leads to more effective shielding [43], Table 2. These results are well supported by Kaya et al.'s [44] and Saraji et al.'s [45] studies where zeta potentials were measured for quartz. They reported that the zeta potential increased (from high negative to low negative values) when increasing the salt concentration or ion valency [45]. In an analogue way, higher electrolyte concentrations also lead to more effective shielding and stronger de-wetting.

Table 2. Cations charge-to-volume ratios.

cation	ionic radius[a] [pm]	ionic volume[b] [pm^3]	charge-to-volume ratio [C/pm^3]
Mg^{2+}	66	1204260	1.66 E-6
Ca^{2+}	99	4063612	4.92 E-7
Na^{+}	97	3822274	2.61 E-7

[a,b] calculated by Holleman et al. [46],([a,b]$= \frac{4}{3}\pi r^3$)

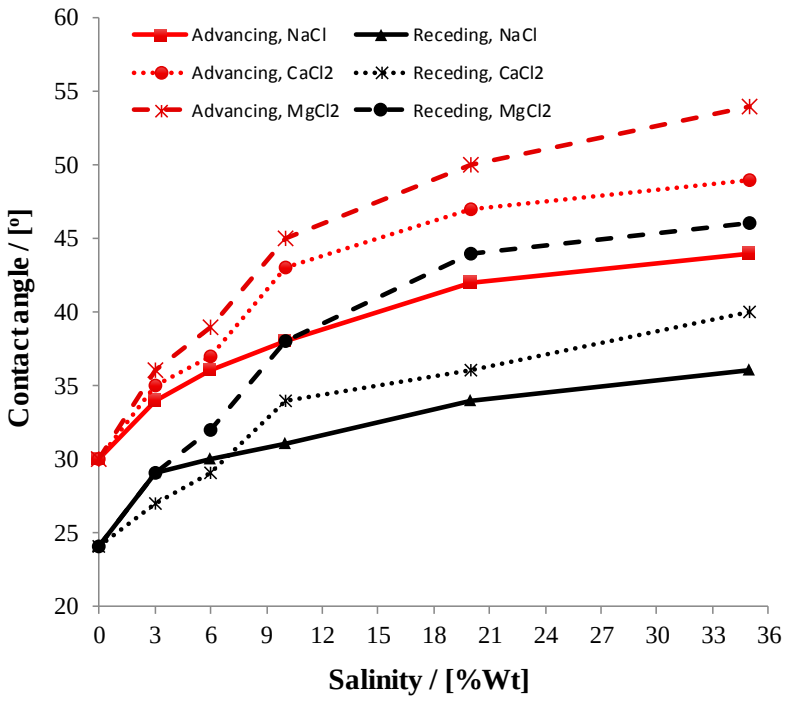

Figure 6. Effects of brine salinity (*NaCl*, $CaCl_2$, and $MgCl_2$) on advancing and receding contact angles at 323K, 10MPa, and 560nm surface roughness.

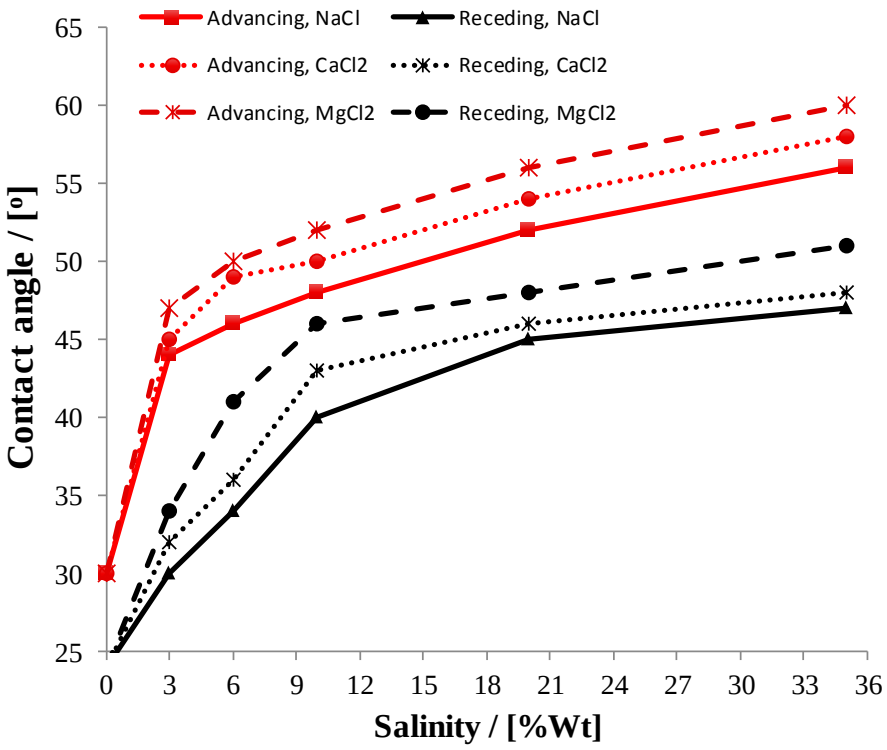

Figure 7. Effects of brine salinity (*NaCl*, $CaCl_2$, and $MgCl_2$) on advancing and receding contact angles at 343K, 10MPa, and 560nm surface roughness.

3.4 Influence of surface roughness on contact angles

The influence of surface roughness on CO_2–water advancing and receding contact angles was measured for one pressure (10MPa) and two different temperatures (296K and 323K) on four substrates with four different surface roughnesses (56nm, 210nm, 560nm, and 1300nm).

θ_a decreased by 6.5° and θ_r by 2° when surface roughness was increased from 56nm to 1300nm at 296K and 10MPa, Figure 8, consistent with literature data [40]. This effect was even more pronounced at higher temperature (323K): θ_a decreased by ~14° and θ_r by ~14°.

The effect of surface roughness on θ is known for a long time, and Wenzel [47] proposed equation (1) in 1936 to quantify the effect:

$$cos\ \theta_{rough} = r\ cos\ \theta_{smooth} \qquad (1)$$

where θ_{rough} is the contact angle measured on the rough surface ("apparent contact angle"), and θ_{smooth} is the conceptual contact angle on an imaginary ideal (= 100% mathematically flat) surface. r is the roughness ratio between the actual (measured) and projected (ideal) solid surface area; r is thus equal to one for an ideal surface, but greater than one for rough surfaces. In this work r was measured; Table 3; using an AFM-DSE 95-200 atomic force microscope: the actual length of the profile line (L_a) was divided by the projected length of the profile line (L_i) to obtain r, Figure 9. This was repeated twelve times for different profile lines and the arithmetic average for r was computed. The values obtained are consistent with roughness ratio data reported for glass [47]. Specifically surface roughness ratios between 1.002 and 1.04 were measured, with standard deviations ±0.0017, 0.0021, 0.007, and 0.0007 respectively.

The contact angle on a smooth (ideal) surface θ_{smooth} – this angle is also called Young's contact angle – is thus larger than the contact angle measured on a rough surface, θ_{rough}. Marmur [48] and Swain et al. [49] suggest that this effect is caused by liquid penetrating into the roughness grooves, cp. Figure 10. Moreover, Marmur [48] observed that if the droplet is larger than the roughness scale by two to three orders of magnitude, the Wenzel equation applies.

We computed θ_{smooth} with the Wenzel equation (1) and found that slightly higher contact angles are predicted for an ideal surface, similar to those expected from linear extrapolation (cp. Figure 8 and Tables 3-7).

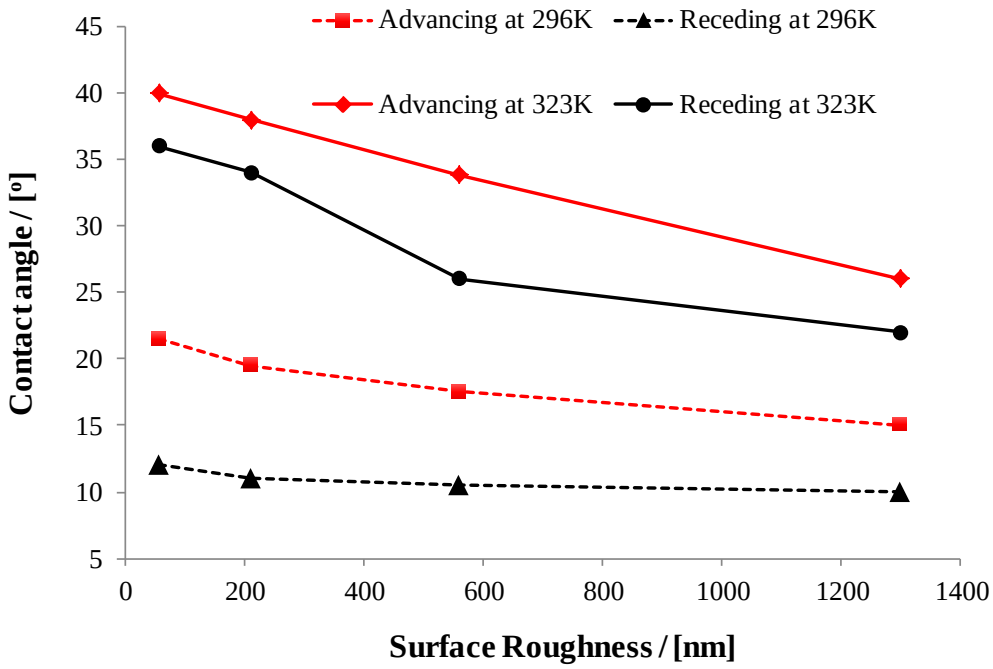

Figure 8. Effect of quartz' surface roughness (56nm, 210nm, 560nm, 1300nm) on advancing and receding *DI* water contact angles at different temperatures (296K, 343K) and pressure of 10MPa.

Table 3. θ_a and θ_r water contact angles on rough and smooth (ideal) surfaces at 10MPa for *DI* water (not saturated with CO_2).[a]

RMS [nm]	T [K]	θ_{arough} [°]	θ_{rrough} [°]	*r* [-]	$\theta_{asmooth}$[b] [°]	$\theta_{rsmooth}$[b] [°]
56	296	21.5	12	1.002	21.7	12.5
210	296	19.5	11	1.005	20.2	12.3
560	296	17.5	10.5	1.03	22.1	17.3
1300	296	15	10	1.04	21.7	18.7
56	323	40	36	1.002	40.1	36.1
210	323	38	34	1.005	38.3	34.4
560	323	33	26	1.03	35.4	29.2
1300	323	26	22	1.04	30.2	26.9

[a] Standard uncertainties *u* are *u*(T)=1K, *u*(*r*)=0.0028, *u*(θ) = 3°, *u*(p) =0.02MPa.

[b]Predicted with the Wenzel equation.

Table 4. θ_a and θ_r brine (not saturated with CO_2) contact angles on the substrate having a roughness ratio of 1.03 at 10MPa for *NaCl* brine.[a]

s [wt%]	T [K]	θ_{arough} [°]	θ_{rrough} [°]	$\theta_{asmooth}$[b] [°]	θ_{smooth}[b] [°]
3	323	34	29	36.4	31.9
6	323	36	30	38.2	32.8
10	323	38	31	40.1	33.7
20	323	42	34	43.8	36.4
35	323	44	36	45.7	38.2
3	343	44	30	45.7	32.8
6	343	46	34	47.6	36.4
10	343	48	40	49.5	42.0
20	343	52	45	53.3	46.6
35	343	56	47	57.1	48.5

[a]Standard uncertainties *u* are *u*(s) =0.001g, *u*(θ) = 3°, *u*(T)=1K, *u*(p) =0.02MPa, *u*(*r*)=0.0028.

[b] predicted by the Wenzel equation.

Table 5. θ_a and θ_r brine (not saturated with CO_2) contact angles on the substrate having a roughness ratio of 1.03 at 10MPa for $CaCl_2$ brine.[a]

s [wt%]	T [K]	θ_{arough} [°]	θ_{rrough} [°]	$\theta_{asmooth}$[b] [°]	$\theta_{rsmooth}$[b] [°]
3	323	35	27	37.3	30.1
6	323	37	29	39.2	31.9
10	323	43	34	44.8	36.4
20	323	47	36	48.5	38.2
35	323	49	40	50.4	42.0
3	343	45	32	46.6	34.6
6	343	49	36	50.4	38.2
10	343	50	43	51.4	44.8
20	343	54	46	55.2	47.6
35	343	58	48	59.0	49.5

[a] Standard uncertainties u are u(s) =0.001g, $u(\theta) = 3^o$, u(T)=1K, u(p) =0.02MPa, $u(r)$=0.0028.

[b] predicted by the Wenzel equation.

Table 6. θ_a and θ_r brine (not saturated with CO_2) contact angles on the substrate having a roughness ratio of 1.03 at 10MPa for $MgCl_2$ brine.[a]

s [wt%]	T [K]	θ_{arough} [°]	θ_{rrough} [°]	$\theta_{asmooth}$[b] [°]	$\theta_{rsmooth}$[b] [°]
3	323	36	29	38.2	31.9
6	323	39	32	41.0	34.6
10	323	45	38	46.6	40.1
20	323	50	44	51.4	45.7
35	323	54	46	55.2	47.6
3	343	47	34	48.5	36.4
6	343	50	41	51.4	42.9
10	343	52	46	53.3	47.6
20	343	56	48	57.1	49.5
35	343	60	51	61.0	52.3

[a]Standard uncertainties u are u(s) =0.001g, $u(\theta) = 3^o$, u(T)=1K, u(p) =0.02MPa, $u(r)$=0.0028.

[b] predicted by the Wenzel equation.

Table 7. θ_a and θ_r water contact angles for the substrate having a roughness ratio of 1.03 for DI water (not saturated with CO_2).[a]

p	T	θ_{arough}	θ_{rrough}	$\theta_{asmooth}$[b]	$\theta_{rsmooth}$[b]
[MPa]	[K]	[°]	[°]	[°]	[°]
5	296	13	9.5	18.9	16.8
10	296	17.5	11	22.2	17.6
15	296	25	12	28.4	18.3
20	296	34	13	36.4	18.9
5	323	19	12.5	23.4	18.6
10	323	30	24	32.8	27.5
15	323	37	27	39.2	30.1
20	323	40	33	42.0	35.5
5	343	22	18.5	25.8	23.0
10	343	42	29	43.8	31.9
15	343	45	37	46.6	39.2
20	343	51	40	52.3	42.0

[a]Standard uncertainties u are $u(\theta) = 3^o$, $u(P)$=0.02MPa, $u(T)$=1K, $u(r)$=0.0028.

[b] predicted by the Wenzel equation.

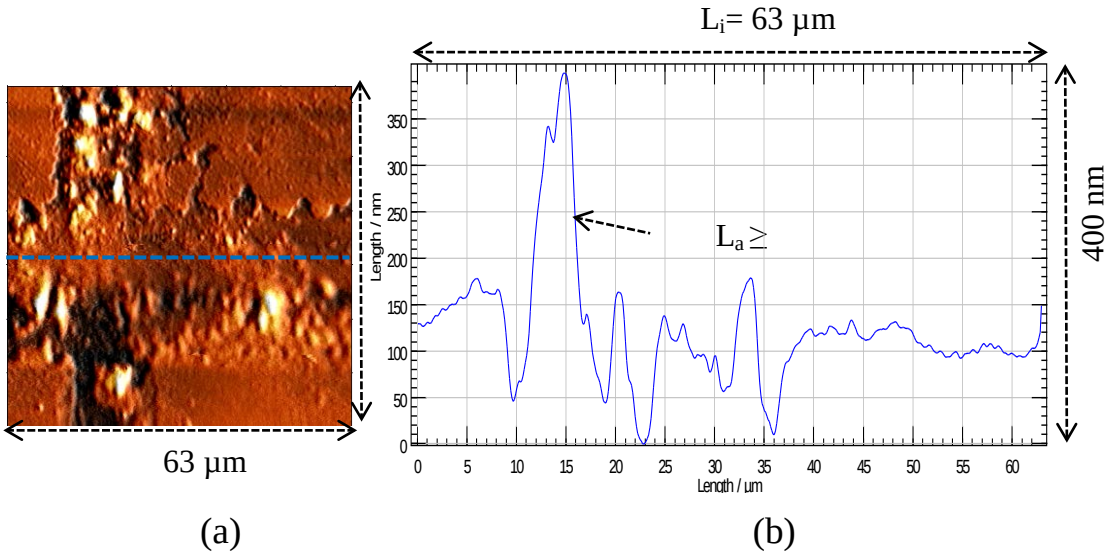

Figure 9. (a) Atomic Force Microscopy image of the 56nm quartz surface, (b) profile line for the blue dotted line shown in (a). L_i is the length of the image (63µm; → projected length of the profile line), and L_a is the actual length of the z profile line plotted against substrate length.

Theoretically the Wenzel equation should eliminate the roughness effect, and we expect that $\theta_{smooth,advancing}$ is identical for each temperature, pressure and salinity condition. This was indeed the case at 296K (and 10 MPa, DI water, Table 3), where a θ_{smooth} of ~21° is predicted, but the variation at 323K was large (30°-40° are predicted). The range predicted for $\theta_{smooth,receding}$ is also relatively large (12.5°-19° at 296K; and 27°-36° at 323K). Similar trends were observed for the other systems investigated (Tables 4-7). The Wenzel equation thus does not completely remove the surface roughness effect, although other factors, which were not investigated, may play a role (e.g. high line tension, energy dissipation, surface shape, adsorption/desorption, etc., cp. Butt et al. [50]), leading to the still existing but reduced uncertainty.

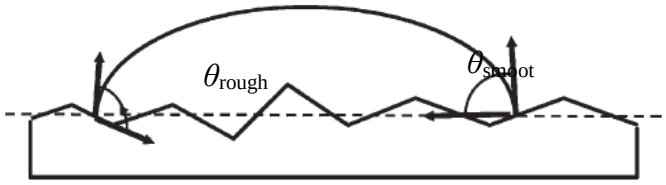

Figure 10. Definition of contact angles: θ_{smooth} is the Young's contact angle – the contact angle on an ideal surface, and θ_{rough} is the apparent or measured contact angle on the rough surface (redrawn from Marmur [48]).

4. Implications of measured data

We predict that a in a typical formation at ~1000m depth a maximum CO_2 column height h of ~952m can be permanently stored beneath a caprock (using a capillary force-buoyancy force balance, equation (2), [52], and θ_r =30°, 6wt%*NaCl*, 10MPa, 323K, $\Delta\rho$=686 kg/m^3, and γ = 37 mN/m from [53], r' = 0.015µm, from [54]; r' is the mean pore throat radius of shale). This height reduces to ~630m in hotter, more saline reservoirs (θ_r= 51°, 35wt% $MgCl_2$, 10MPa, 343K, $\Delta\rho$ =897 kg/m^3 and γ =44 mN/m from [53], r' =0.01µm, from [54]).

$$h = \frac{2\gamma cos\theta}{\Delta\rho g r'} \qquad (2)$$

5. Conclusions

The wettability of quartz with respect to CO_2 and water is of vital importance in CO_2 geo-storage as it strongly affects residual and structural trapping. Despite its importance, there is large uncertainty associated with the published data [10]. We thus report experimental brine-CO_2 advancing and receding contact angles on quartz surfaces; specifically, the impact of pressure, salinity, salt type, surface roughness and temperature conditions was studied.

A higher surface roughness resulted in lower advancing and receding contact angles, consistent with literature data [40]. θ_a and θ_r increased as pressure increased, which is consistent with most literature data [10,12,15,25-31]; furthermore, θ increased with increasing temperature, consistent with Saraji et al. [30], Farokhpoor et al. [31], and Sarmadivaleh et al. [12], but inconsistent with Saraji et al. [35] and molecular dynamics predictions [33]. This effect thus needs to be further analysed. Increasing salinity also significantly increased θ, consistent with literature data [26,28-29,31,35,38-40], while different salts resulted in different θ changes. We observed the ranking $Mg^{+2} > Ca^{+2} > Na^{+}$ in terms of dewetting potential, and we explain this effect by cation shielding of the electrical surface charge of quartz [43].

We conclude that quartz is weakly water-wet at typical storage conditions (high pressure, high salinity, elevated temperature). A significant increase in θ up to ~50° was measured at storage conditions (when compared to ambient conditions [10,24]). Residual and structural trapping are therefore expected to work, however, storage capacities are reduced accordingly [9,33,55].

Acknowledgements

The authors wish to acknowledge financial assistance provided through Australian National Low Emissions Coal Research and Development (ANLEC R&D). ANLEC R&D is supported by Australian Coal Association Low Emissions Technology Limited and the Australian Government through the Clean Energy Initiative.

References

[1] IPCC, Working Group III of the Intergovernmental Panel on Climate Change (2005)1-443.

[2] IEA, World Energy Outlook Special Report (2013) 1-126.

[3] P. Tomski, V. Kuuskraa, M. Moore, Atlantic Council (2013) 1-15.

[4] S. Iglauer, A. Paluszny, M.J. Blunt, Fuel 103(2013) 905-914.

[5] M. A. Hesse, F. M. Orr Jr., H. A. Tchelepi, J Fluid Mech (2008) 35-60.

[6] S. Iglauer, A. Paluszny, C. H. Pentland, and M. J. Blunt, Geophys. Res. Lett. 38 (2011) L21403.

[7] S. Iglauer, Mass Transfer (2011) 233-257.

[8] I. Gaus , Int. J. Greenh. Gas Control 4 (2010) 73-89.

[9] S. Iglauer, C. H. Pentland, and A. Busch, Water Resour. Res. (2015) WR015553.

[10] Iglauer, S., Hassan, A., Sarmadivaleh, M., Liu, K., and Pham, C., Int. J. Greenh. Gas Control 22 (2014) 325-328.

[11] J. C. Love, L. A. Estroff, J. K. Kriebel, R. G. Nuzzo, and G. M. Whitesides, Chem. Rev. 105 (2005) 1103-1170.

[12] M. Sarmadivaleh M., A. Z. Al-Yaseri, and S. Iglauer, J. Colloid Interface Sci. 441 (2015) 59-64.

[13] J. Mahadevan, Int. J. Greenh. Gas Control 7 (2012) 261-262.

[14] PK. Bikkina, Int. J. Greenh. Gas Control 7 (2012) 263-264.

[15] A. Z. Al-Yaseri, M. Sarmadivaleh, A. Saeedi, M. Lebedev, A. Barifcani, and S. Iglauer S., J. Pet. Sci. Eng. (2015) in press.

[16] C. H. Pentland, S. Iglauer, R. El-Maghraby, Y. Tsuchiya, H. Okabe, and M. Blunt, SPE Int. Conf. on CO2 Capture, Storage, and Utilization, NO, LA, USA (2010) 1-8.

[17] G. Macdougall, and C. Ockrent, Proc. Soc. Lond. 180 (1942) 152-174.

[18] l. M. Lander, M. Lisa, J. William, and A. Erwin, Langmuir 9 (1993) 2237-2239.

[19] Ch.W. Extrand, Y. Kumagi, J. Colloid Interface Sci. 170 (1995) 515–521.

[20] P.-G. DeGennes, F. Brochart-Wyart, and D. Quéré, Elsevier, Amsterdam (2004)1-291.

[21] J. Drelich, The J. Adhes. 63(1997) 31-51.

[22] D. D. McCoy, H. R. Jr. Warner, and T. E. Fisher, SPE J. 12 (1997) 37-44.

[23] A. Zdziennicka, K. Szymczyk and B. Jańczuk, J. Colloid Interface Sci. 340 (2009) 243-248.

[24] J. W. Grate, K.J. Dehoff, M.G. Warner, J.W. Pittman, C. Zhang, M. Oostrom, Langmuir 28 (2012) 7182-7188.

[25] A. Wesch, N. Dahmen, K. Ebert, and J. Schön, Chem. Ing. Tech. 69 (1997) 942-946.

[26] P. Chiquet, D. Broseta, S. Thibeau, Geofluids 7(2007) 112–122.

[27] Y. Sutjiadi-Sia, P. Jaeger, and R. Eggers, J. Supercrit. Fluids 46 (2008) 272-279.

[28] D. Broseta, N. Tonnet, and V. Shah, Geofluids 12 (2012) 280-294.

[29] J.W. Jung, J. Wan, Energy and Fuels 26 (2012) 6053–6059.

[30] S. Saraji, L. Goual, M. Piri, and H. Plancher, Langmuir 29 (2013) 6856-6866.

[31] R. Farokhpoor, B.J.A. Bjørkvik, E. Lindeberg, and O. Torsæter, Int. J. Greenh. Gas Control 12 (2013) 18-25.

[32] SY. Liu, XN.Yang, and Y. Qin, Chin. Sci. Bull. 55 (2010) 2252-2257.

[33] S. Iglauer, M. S. Mathew, F. Bresme, J. Colloid Interface Sci. 386 (2012) 405–414.

[34] J. McCaughan, S. Iglauer, and F. Bresme, Energy Procedia 37 (2013) 5387-

5402.

[35] Saraji S., Piri M., Goual L., Int. J. Greenh. Gas Control (2014) 147-155.

[36] E. F.Vansant, P. Van der Voort, K. C. Vrancken, Elsevier (1995) 1-381.

[37] L.T. Zhuravlev, Physicochem. Eng. Aspects 173(2000) 1-38.

[38] D. N. Espinoza, and J. C. Santamarina, Water Resour. Res. 46 (2010) W0753.

[39] S. Wang, I. M. Edwards, and A. F. Clarens, Environ. Sci. Technol. 47 (2013a) 234-24.

[40] S. Wang, Z. Tao, S. Persily, and A. F. Clarens, Environ. Sci. Technol. 47 (2013b) 11858-11865.

[41] K. Bourikas, J. Vakros, C. Kordulis, and A. Lycourghiotis J. Phys. Chem. 107 (2003) 9441-9451.

[42] Y. Wu, S. Iglauer, P. Shuler, Y. Tang, and W.A. Goddard III FRSC, Tenside Surf. Det. 48 (2011) 346-358.

[43] J. N. Israelachvili, Academic Press (2011)1-667.

[44] A. Kaya, and Y. Yukselen, Can. Geo. J. 42 (2005) 1280-1289.

[45] S. Saraji, L. Goual, and M. Piri, Physicochem. Eng. Aspects 434 (2013b) 260-267.

[46] A.F. Holleman, E. Wiberg, and N. Wiberg, ed. de Gruyter (1985) 1-1451.

[47] R. W. Wenzel, Ind. Eng. Chem. 28 (1936) 988-994.

[48] A. Marmur, Soft Matter 2 (2006) 12-17.

[49] P. S. Swain, R. Lipowsky, Langmuir 14 (1998) 6772-6780.

[50] H.-J. Butt, K. Graf, and Kappl M., Wiley-VCH, Weinheim (2006) 1-386.

[51] A. Georgiadis, M. Geoffrey, J.P. Martin, and B. Alexander, J. Chem. Eng. Data 55(2010) 4168–4175.

[52] L.P. Dake, Elsevier, Oxford (1978) 1-428.

[53] X. Li, E. Boek, G. C. Maitland, and J. P. M. Trusler, J. Chem. Eng. Data 57(2012) 1078-1088.

[54] A. A. Hinai, R. Rezaee, L. Esteban, and M. Labani, J. of Unco. Oil and Gas Resour. 8 (2014) 1-13.

[55] K. Chaudhary, M. Bayani, W. W. Wolfe, J. A. Maisano, R. A. Ketcham, and P. C. Bennett Geophys. Res. Lett. 40 (2013) 1-5.

5.5 CO_2 Wettability of Caprocks: Implications for Structural Storage Capacity and Containment Security

Iglauer, S., **Al-Yaseri, A.Z.**, Rezaee, R. and Lebedev, M., 2015. CO_2 wettability of caprocks: Implications for structural storage capacity and containment security. Geophysical Research Letters, 42(21), pp.9279-9284.

CO_2-wettability of caprocks: Implications for structural storage capacity and containment security

Stefan Iglauer, [1*] Ahmed Zarzor Al-Yaseri, [1] Reza Rezaee, [1] Maxim Lebedev [2]

[1] Department of Petroleum Engineering, Curtin University, 26 Dick Perry Avenue, 6151 Kensington, Australia

[2] Department of Exploration Geophysics, Curtin University, 26 Dick Perry Avenue, 6151 Kensington, Australia

Key points

Caprocks are intermediate-wet or weakly water-wet at typical storage conditions

CO_2-wettability increases with pressure and thus depth

Structural storage capacities are significantly lower than previously predicted

Abstract

Structural trapping, the most important CO_2 geo-storage mechanism during the first decades of a sequestration project [*IPCC*, 2005], hinges on the traditional assumption that the caprock is strongly water-wet [e.g. *Hesse et al.*, 2008]. However, this assumption has not yet been verified; and it is indeed not generally true as we demonstrate here. Instead, caprock can be weakly water-wet or intermediate-wet at typical storage conditions; and water-wettability decreases with increasing pressure or temperature. Consequently, a lower storage capacity can be inferred for structural trapping in such cases.

Keywords

CO_2 geo-sequestration, structural trapping, storage capacity, wettability

1. Introduction

Carbon Geo-Sequestration (CGS) has been identified as a feasible technology to reduce anthropogenic CO_2 emissions and thus mitigate global warming [*Lackner*, 2003; *IPCC*, 2005; *Orr*, 2009]. In CGS, CO_2 is captured from large point-source emitters (e.g. coal-fired power stations), purified, compressed and injected deep into the subsurface for storage. However, the CO_2 is buoyant as it has a lower density than the resident formation brine and thus flows upwards. The primary sequestration mechanism during the first few decades of a storage project is structural trapping, where a caprock acts as a seal barrier to the CO_2 flow [*Armitage et al.* 2013; *Wollenweber et al.*, 2010]. Caprock has a low permeability and associated with that small pores. Because of the small pore sizes (cp. equation 2 below) it is typically assumed that high capillary forces are created which prevent the CO_2 from entering the caprock [e.g. *Hesse et al.*, 2008]. However, a growing body of research papers suggests that pure minerals are not completely water-wet [*Chiquet et al.*, 2007; *Broseta et al.*, 2012; *Farokhpoor et al.*, 2013; *Saraji et al.*, 2013; *Iglauer et al.*, 2014; *Sarmadivaleh et al.*, 2015; *Al-Yaseri et al.*, 2015], and thus the capillary entry pressure for CO_2 can be dramatically reduced (and consequently also the structural trapping capacity).

However, despite these efforts, there is a serious lack of information in terms of real natural caprock, which is nevertheless most important. We thus tested several selected real caprock samples from a proposed storage site, and we demonstrate that the structural trapping capacity is significantly reduced at (high pressure) storage conditions.

2. Experimental Procedure

2.1 Caprock samples

In order to constrain the uncertainty associated with structural trapping capacity predictions to an acceptable level, we selected 8 caprock samples (Table 1) to experimentally evaluate their CO_2-wettability. These samples were retrieved from a proposed CO_2 storage site in New South Wales/Australia, and thoroughly

characterized (quantitative x-ray diffraction [XRD], total organic content [TOC], scanning electron microscopy-energy dispersive x-ray spectroscopy [SEM-EDS], thin section petrology, surface roughness, and mercury [Hg] intrusion measurements). Most samples consisted mainly of quartz (~50-60wt%), substantial amounts of clay (~20wt% illite and chlorite), significant amounts of feldspar and a few other minerals in low to medium concentrations, Table 1. An exception was sample 5, which had a high calcite content (47wt%) and sample 3, which contained high amounts of illite (33wt%). TOC ranged between 510-4400 mg/kg, typical for a deep saline aquifer. The SEM images show that clay (illite, illite-smectite, smectite or kaolinite) filled the pore space and thus covered the surface of the grains. This observation is consistent with the EDS analysis, which mainly detected clay. Thin sections were analysed for each sample at 40x and 100x magnification (Figure 1), and these results reflected the XRD and SEM-EDS measurements: the samples consisted mainly of quartz grains of varying size and angularity, with significant amounts of clays present. Several samples also contained calcite and dolomite intergranular cements. Quartz overgrowth and intergranular clay formation were the dominant diagenetic features.

Table 1. Geological and chemical properties of caprock samples tested

Sample	Depth (m)	TOC (mg/kg)	Chemical Composition[a] (wt %)		Contact Angle (deg)[b]	Capillary Threshold Pressure (MPa)[c]	CO_2 Column Height (m)[d]
1-Argillaceous siltstone	1979.00	510	Quartz	54	47	0.82	241.3
			Illite	17			
			Albite	11			
			Chlorite	9			
			K-feldspar (microcline)	7			
			Hematite	2			
2-Calcareous sandstone	1746.50	2600	Quartz	56	50	n/a	n/a
			Ankerite	12			
			Calcite	9			
			Illite	7			
			Albite	6			
			Chlorite	6			
			Anhydrite	4			
3-Shale	1547.00	810	Illite	33	49	0.40	116.6
			Quartz	31			
			Analcite	15			
			Albite	9			
			Chlorite	8			
			Hematite	4			
4-Siltstone	1506.00	2000	Quartz	46	44	1.35	392.8
			Analcite	20			
			Chlorite	12			
			Illite	12			
			Albite	9			
			K-feldspar (microcline)	1			
5-Calcareous siltstone	1426.50	4400	Calcite	47	68	3.58	1043.5
			Quartz	27			
			Albite	8			
			Ankerite	5			
			Illite	5			
			Analcite	3			
			Chlorite	3			
			K-feldspar (microcline)	2			
6-Silty, argillaceous very fine grained sandstone	1859.75	870	Quartz	64	48	0.25	74.5
			Albite	12			
			Chlorite	11			
			Illite	10			
			Hematite	2			
			Calcite	1			
7-Very fine grained clay bearing sandstone	1865.06	1100	Quartz	62	50	0.24	69.5
			Illite	10			
			Chlorite	10			
			Calcite	8			
			Albite	5			
			Anhydrite	4			
			Hematite	1			
8-Very fine grained clay bearing sandstone	1872	1600	Quartz	65	48	0.35	103.0
			Albite	13			
			Illite	10			
			Chlorite	10			
			Hematite	1			
			Calcite	1			

[a]Measured with a Bruker AXS XRD instrument.
[b]Water receding contact angle.
[c]Estimate for the conditions at 323 K and 15 MPa pore pressure using the *Boult et al.* [1997] method.
[d]Estimated from capillary threshold pressures using a capillary force-buoyancy force balance, equation (2).

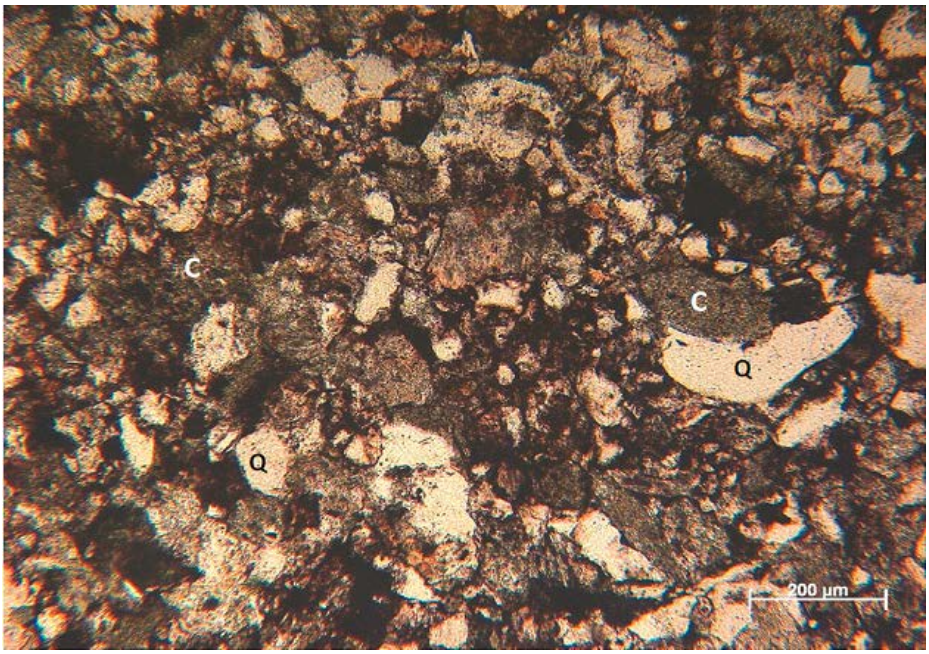

Figure 1. Selected thin section (clay = C and Q = quartz) image of caprock sample 6, 100x magnification.

2.2 Experimental tests

For the CO_2-wettability experiments, cuboid samples were cut with a high speed diamond blade (to ~ 0.5cm x 1cm x 1cm) and each sample was exposed to air plasma for 5min to remove surface contaminants (note that this cleaning step is vital as otherwise the measurements are highly biased; contaminants are essentially all organic molecules present in the laboratory air; although their concentrations are low they can significantly change the contact angles [*Love et al.*, 2005; *Iglauer et al.*, 2014]). Importantly, the caprocks contained large amounts (when compared to molecular layers on a crystal surface) of organic material (TOC ranged from 510-4400mg/kg, see above). During plasma cleaning, however, only the uppermost molecular layers of material are removed (Alam et al. 2014). As the caprock contained much more of the organic molecules, these naturally occurring organics were effectively not removed, and significantly higher contact angles (intermediate wetting) then for pure quartz crystals were measured, see below – thus the natural organic molecules in the caprock were preserved in the best possible way. Subsequently the advancing (θ_a) and receding (θ_r) water contact angles were measured using the tilted plate method [*Lander et al.*, 1993] at storage conditions

(15 MPa, 323K, [20wt% NaCl + 1wt% KCl = 4.15M ionic strength] brine). Note that prior to the measurements the surface topography of each sample was measured with an atomic force microscope (AFM, instrument model DSE 95-200), and the surface roughness was quantified as it can significantly influence θ and typically induces a difference between advancing and receding θ [*Marmur*, 2006] (Figure 2). The receding water contact angle θ_r corresponds to CO_2 entering the caprock and displacing brine and is thus most relevant to structural trapping capacity estimates (see equation 2 below). Root mean square (RMS) surface roughness ranged from 1100-1700nm, which is fairly rough when compared to pure mineral substrates, with the exception of sample 1, which was very smooth (28nm), similar to a geological single crystal mineral surface [*Sarmadivaleh et al.,* 2015]. The standard deviation of the measurements was determined as ±3° based on replicate measurements.

3. Results and Discussion

3.1. Contact Angles

All contact angles measured were quite similar, ~50°, except sample 5 had a higher contact angle (~70°). The hysteresis between θ_a and θ_r was small and insignificant despite significant surface roughness. We subsequently measured θ as a function of pressure at 343K for samples 3 and 7, Figure 3, as pressure and temperature are expected to vary with storage depth [*Dake*, 1978]. Both caprock samples showed a similar CO_2-wettability behaviour: θ increased dramatically with pressure and reached ~70° at 20 MPa. Such a trend has also been observed for clean silica surfaces [*Chiquet et al.*, 2007; *Jung and Wan*, 2012; *Saraji et al.*, 2013; *Iglauer et al.*, 2014; *Sarmadivaleh et al.*, 2015] and oil-wet surfaces [*Chi et al.*, 1988; *Dickson et al.*, 2006; *Li et al.*, 2007; *Yang et al.*, 2008]. Theoretical molecular dynamics predictions associate this effect with stronger CO_2-rock intermolecular interactions (which rise with pressure, [*Iglauer et al.*, 2012a]). An increase in temperature by 20K (from 323K to 343K) increased θ by ~15°, a significant increase. Although this is

consistent with what has been observed on quartz by some researchers [*Saraji et al.*, 2013; *Sarmadivaleh et al.*, 2015], it is inconsistent with *Wang et al.'s*, [2013] and *Farokhpoor et al.'s*, [2013] measurements where no temperature influence was observed, and with *Iglauer et al.'s*, [2012] molecular dynamics predictions (note that in the molecular dynamics work fully coordinated surfaces were investigated which are not fully representative of subsurface conditions). θ was significantly higher on the caprocks than on clean quartz [e.g. compare *Chiquet et al.*, 2007; *Farokhpoor et al.*, 2013; *Saraji et al.*, 2013; *Iglauer et al.*, 2014; *Sarmadivaleh et al.*, 2015] or calcite [*Farokhpoor et al.*, 2013], consistent with micro-computed tomography measurements (*Chaudhary et al.*, 2015); this is probably due to the presence of organic material in the caprock. This conclusion is based on the fact that high water contact angles were measured on oil-wet susbtrates (e.g. *Dickson et al.*, 2006, *Li et al.*, 2007, *Espinoza and Santamarina*, 2010); compare the summary provided by *Iglauer et al.* (2015). Hysteresis was small for sample 7, while a ~10° lower θ_r was measured for sample 3, which is probably due to its higher chemical heterogeneity as surface roughness of both samples were similar (1100nm versus 1300nm). The samples were thus weakly water-wet or intermediate-wet. This implies significantly lower structural trapping capacities [Iglauer et al., 2015].

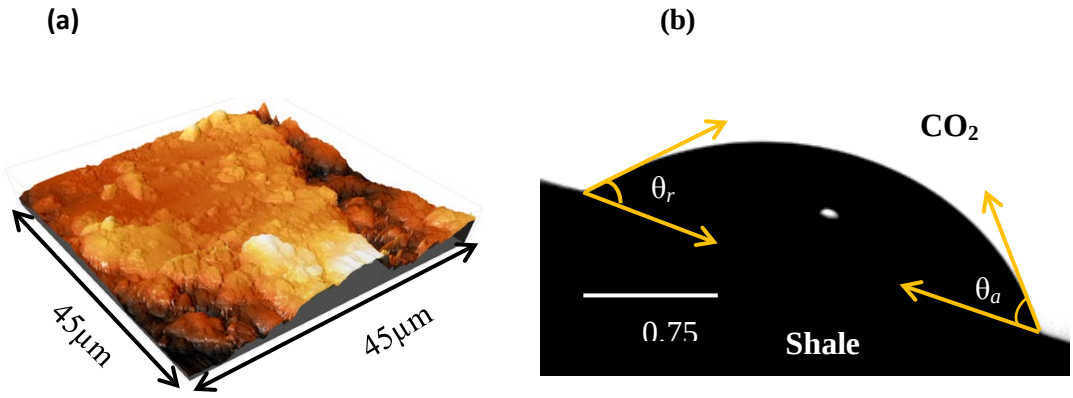

Figure 2. (a) Surface topography (measured with AFM, RMS surface roughness = 1100 nm, sample 7) and (b) brine drop on caprock sample with advancing (θ_a) and receding (θ_r) contact angles indicated.

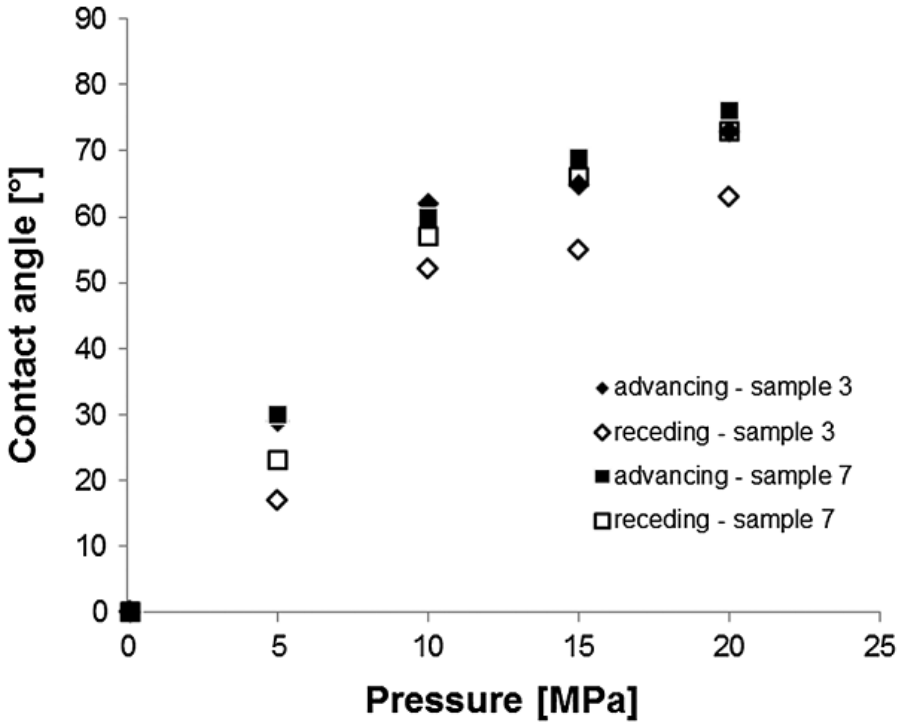

Figure 3. Advancing and receding water contact angles on caprock samples 3 and 7 as a function of pressure (measured at 343 K in (20 wt %NaCl + 1 wt % KCl) brine).

3.2 **CO_2 drainage behaviour**

CO_2 drainage curves (Figure 4) - which characterise how CO_2 displaces brine from the caprock - were obtained by scaling mercury intrusion data; equation 1:

$$P(CO_2) = \frac{P(Hg)\gamma(CO2)cos\theta(CO2)}{\gamma(Hg)cos\theta(Hg)} \quad (1),$$

where $P(CO_2)$ is the CO_2 (drainage or capillary) pressure, P(Hg) is the mercury intrusion pressure, $\gamma(CO_2)$ is the CO_2-brine interfacial tension (40 mN/m, taken from [*Li et al.*, 2012]), γ(Hg) is the mercury-air interfacial tension (480 mN/m), $\cos\theta(CO_2)$ is the CO_2-brine-rock contact angle (measured here, cp. Figure 3) and $\cos\theta$(Hg) is the mercury-air-rock contact angle (140°, [*Tiab and Donaldson*, 2004]).

From these capillary pressure curves the threshold pressures (p_t) – which correspond to the percolation threshold [*Thompson et al.*, 1987] – can be extracted. The threshold pressures extracted for the tested caprock samples varied substantially, between 0.2-3.6 MPa (Table 1), which is a significant variation, and which implies that a broad range of storage capacities can be expected (cp. equation 2 and Table 1). Please note that these are approximate estimates, as the extracted values depend on the method used to determine the threshold pressure (we used the method proposed by *Boult et al.* [1997], where a tangent through the drainage curve plateau is extrapolated to the pressure axis).

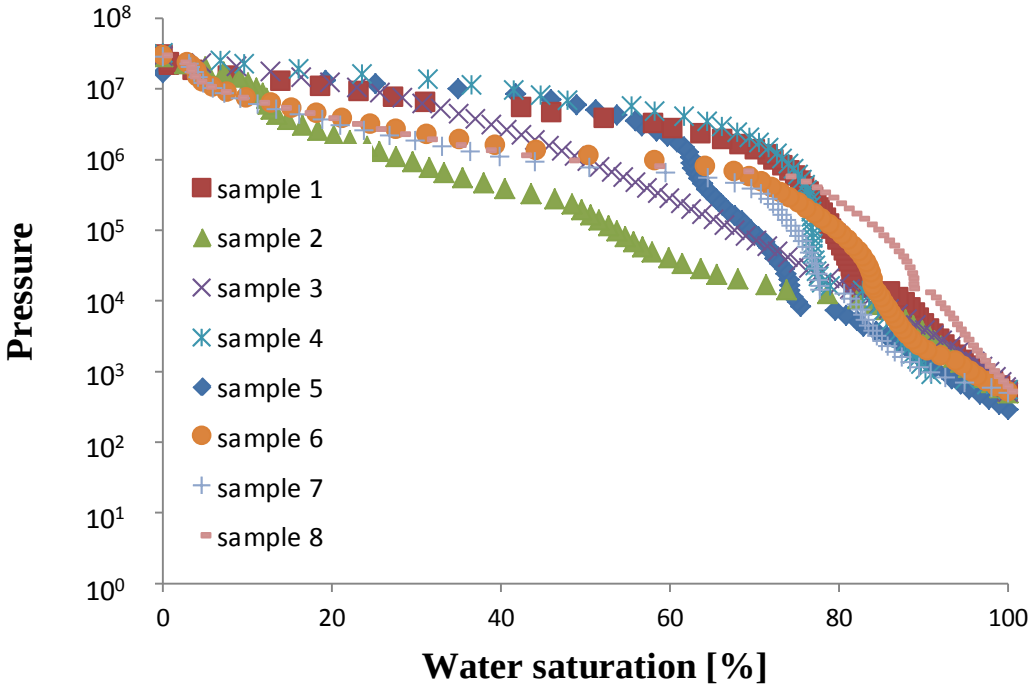

Figure 4. Supercritical CO2Primary Drainage Capillary Pressure Curves for the Caprock Samples Tested.

4. Conclusions and Implications

There is a serious lack of information regarding the CO_2-wettability of caprock despite its vital role for structural trapping capacity and containment security predictions. We thus measured CO_2-wettability of 8 real natural caprock samples extracted from a proposed storage site in NSW in Australia. Our results demonstrate that the traditional assumption that a caprock for a brine-CO_2 system is completely water-wet may not be true; instead, at reservoir conditions, the wettability of a caprock can reach up to 70°, implying a dramatically reduced sealing efficiency. Using the threshold pressures, equation 2 below (*Dake*, 1978; capillary force-buoyancy force equilibrium) and assuming $\Delta\rho$ = 350 kg/m^3 as a typical value for the fluid density difference [Iglauer et al., 2015], we were able to predict maximum CO_2 column heights, which varied substantially, between ~70-1000m. This implies that structural trapping is a feasible storage mechanism.

$$\boldsymbol{h = \frac{p_t}{\Delta\rho g} = \frac{2\gamma cos\theta}{\Delta\rho g r}} \qquad (2),$$

where h is the CO_2 column height which can be permanently immobilized beneath a caprock, p_t is the threshold pressure of the caprock, γ is the CO_2-brine interfacial tension, θ is the brine-CO_2-rock contact angle, $\Delta\rho$ is the CO_2-brine density difference, g is the gravitational constant, and r is the average pore throat radius of the caprock material. While equation 2 assumes a fully connected CO_2 ganglion spanning the length h as per Archimedes' principle, such connection, however, is difficult if not impossible to observe at the scale of tens to hundreds of meters. Hence we must base our prediction on the experimental data and the best theory available. In this context such large CO_2 clusters – which span essentially over the whole observed volume – have been measured with x-ray micro-computed tomography (e.g. *Iglauer et al.*, 2011, *Andrews et al.*, 2013; note: "large" here means several millimetres as this is the limit for micro-tomography). Invasion percolation theory then predicts a) a cluster size distribution, which follows a power law (as confirmed by many experiments: *Iglauer et al.*, 2010,2011,2012b,2013,2014b; *Georgiadis et al.*, 2013; *Andrews et al.*, 2014; *Geistlinger and Mohammadian*, 2015, etc.), which means that there are many small ganglia, and only very few large ganglia. But: 1. The large ganglia contribute most to the saturation, and 2. There are very large ganglia (although only very few of them) spanning through the whole volume, even if this volume is very large, and even for residual CO_2 clusters; and b) that the maximum CO_2 cluster volume S_{max} (= largest ganglion size) scales as:

$$S_{max} = S_{pores} n^D \qquad \text{(equation 3)},$$

where S_{pores} is the volume of a typical pore, n is the number of pores across the sample, and D is the fractal dimension (normally = 2.5), *Wilkinson and Willemsen* (1983), *Dias and Wilkinson* (1986), *Iglauer et al.* (2010).

In summary, importantly, structural trapping capacities are significantly reduced (when compared to completely water-wet caprock) by a factor of $\cos\theta = \cos(50°) \approx 0.64$ at ~1500m storage depth or $\cos(70°) \approx 0.34$ at ~2000m storage depth. These data need to be incorporated into reservoir simulators in order to obtain reliable predictions and to guarantee containment security.

Acknowledgements

The authors wish to acknowledge financial assistance provided through Australian National Low Emissions Coal Research and Development (ANLEC R&D; grant number 3-0911-0155). ANLEC R&D is supported by Australian Coal Association Low Emissions Technology Limited and the Australian Government through the Clean Energy Initiative.

The Iraqi Ministry of Higher Education and Scientific Research is thanked for providing financial support for Ahmed Zarzor Al-Yaseri. Furthermore we would like to thank the New South Wales Government's Division of Resources and Energy for providing the caprock samples and associated petrophysical data and analyses, and the National Measurements Institute of Australia for conducting the TOC measurements on the caprock samples.

References

Alam, A.U., Howlader, M.M.R., and M.J. Deen *(*2014), The effects of oxygen plasma and humidity on surface roughness, water contact angle and hardness of silicon, silicon dioxide and glass, *Journal of Micromechanics and Microengineering,* 24, 035010, doi:10.1088/0960-1317/24/3/035010.

M Andrew, B Bijeljic, MJ Blunt (2013), Pore-scale imaging of geological carbon dioxide storage under in situ conditions; *Geophysical Research Letters* 40 (15), 3915-3918.

Armitage, P.J., *D.R.* Faulkner, and R.H. Worden *(*2013), Caprock corrosion, *Nature Geoscience, 6, 79–80, doi:10.1038/ngeo1716.*

Boult, P.J., P.N. Theologou, and J. Foden (1997), Capillary seals within the Eromanga Basin, Australia: implications for exploration and production, in Seals, traps and the petroleum system, edited by R.C. Surdam, *AAPG Memoir*, 67, 143-167.

Broseta, D., Tonnet, N., Shah, V. (2012), Are rocks still water-wet in the presence of dense CO_2 or H_2S?, *Geofluids*, 12, 280-294.

Chaudhary, K., Guiltinan, E.J., Bayani Cardenas, M., Maisano, J.A., Ketcham, R.A., and P.C. Bennett (2015), Wettability measurement under high P-T conditions using x-ray imaging with application to the brine-supercritical CO_2 system, *Geochemistry, Geophysics, Geosystems,* in press.

Chi, S.-M., Morsi, B.I., Klinzing, G.E., and S.-H. Chiang (1988), Study of interfacial properties in the loiquid CO_2-water-coal system, *Energy & Fuels*, 2, 141-145.

Chiquet, P., Broseta, D. and S. Thibeau (2007), Wettability alteration of caprock minerals by carbon dioxide, *Geofluids*, 7, 112–122.

Dake, L.P. (1978), Fundamentals of Reservoir Engineering, *Elsevier, Amsterdam*.

Dias, M.M., and D. Wilkinson (1986), Percolation with trapping, *J. Phys. A: Math. Gen.*, 19, 3131-3146.

Dickson, J.L., Gupta, G., Horozov, T.S., Binks, B.P. and K.P. Johnston, K.P. (2006), Wetting Phenomena at the CO_2/Water/Glass Interface, *Langmuir*, 22(5), 2161-2170.

Espinoza, D.N., and J.C. Santamarina (2010), Water-CO_2-mineral systems: Interfacial tension, contact angle, and diffusion – Implications to CO_2 geological storage, *Water Resour* Res, 46, 7, W0753.

Farokhpoor, R., Bjørkvik, B.J.A., Lindeberg, E., and O. Torsæter (2013), Wettability behaviour of CO_2 at storage conditions, *International Journal of Greenhouse Gas Control*, 12, 18-25.

Geistlinger, H., Mohammadian, S. (2015), Capillary trapping mechanism in strongly water-wet systems: comparison between experiment and percolation theory, *Advances in Water Resources*, 79, 35-50.

Georgiadis, A., Berg, S., Makurat, A., Maitland, G, Ott, H. (2013), Pore-scale micro-computed tomography imaging: non-wetting-phase cluster-size distribution during drainage and imbibition, *Physical Review E*, 88, 033002.

Hesse, M.A., F.M. Orr, and H.A. Tchelepi (2008), Gravity currents with residual trapping, *Journal of Fluid Mechanics*, 611, 35-60, doi: 10.1017/S002211200800219X.

Iglauer, S., S. Favretto, G. Spinelli, G. Schena, and M. J. Blunt (2010), X-ray tomography measurements of power-law cluster size distributions for the nonwetting phase in sandstones, *Physical Review E*, 82, 056315.

Iglauer, S., A. Paluszny, C. H. Pentland, and M. J. Blunt (2011), Residual CO_2 imaged with X-ray micro-tomography, *Geophysical Research Letters*, 38, 21, L21403.

Iglauer, S., Mathew, M., and F. Bresme (2012a), Molecular dynamics computations of brine-CO_2 interfacial tensions and brine-CO_2-quartz contact angles and their effects on structural and residual trapping mechanisms in carbon geo-sequestration", *Journal of Colloid and Interface Science*, 386, 405-414.

Iglauer, S., M. A. Fernø, P. Shearing, and M. J. Blunt (2012b), Comparison of residual oil cluster size distribution, morphology and saturation in oil-wet and water-wet sandstone, *Journal of Colloid and Interface Science*, 375, 1, 187–192.

Iglauer, S., A. Paluszny, and M. Blunt (2013), Simultaneous oil recovery and residual gas storage: a pore-level analysis using in-situ x-ray micro-tomography. *Fuel.* 1, 1-11.

Iglauer, S., Hassan, A., Sarmadivaleh, M., Liu, K., and C. Pham (2014), Contamination of silica surfaces: impact on water-CO_2-quartz and glass contact angle measurements, *International Journal of Greenhouse Gas Control*, 22, 325-328.

Iglauer, S., Sarmadivaleh, M., Geng, C., and M. Lebedev (2014b), In-situ residual oil saturation and cluster size distribution in sandstones after surfactant and polymer flooding imaged with x-ray micro-computed tomography, IPTC 17312, International Petroleum Technology Conference, Doha, Qatar, 20-22 January.

Iglauer, S., C.H. Pentland, and A. Busch (2015), CO_2-wettability of seal and reservoir rocks and the implications for carbon geo-sequestration, *Water Resources Research*, 51, 1, 729-774, WR015553, doi: 10.1002/wrcr.21095.

Intergovernmental Panel on Climate Change (IPCC) (2005), *IPCC special report on carbon dioxide capture and storage*, prepared by Working Group III of the Intergovernmental Panel on Climate Change, Cambridge University Press.

Jung, J.-W., and J. Wan, J. (2012), Supercritical CO_2 and ionic strength effects on wettability of silica surfaces: equilibrium contact angle measurements, *Energy and Fuels*, 26, 6053-6059.

Lackner, K.S. (2003), Climate change. A guide to CO_2 sequestration, *Science*, 300, 1677-1678, doi:10.1126/science.1079033.

Lander, L.M., L.M. Siewierski, W.J. Brittain, and E.A. Vogler (1993), A systematic comparison of contact angle methods, *Langmuir*, 9, 2237-2239, doi:10.1021/la00032a055.

Li, Y., Pham, J.Q., Johnston, K.P., and P.F. Green (2007), Contact angle of water on polystyrene thin films: effects of CO_2 environment and film thickness, *Langmuir*, 23:9785-9793.

Li, X., E. Boek, G.C. Maitland, and J.P.M. Trusler (2012), Interfacial Tension of (Brines + CO_2): (0.864 NaCl + 0.136 KCl) at Temperatures between (298 and 448) K, Pressures between (2 and 50) MPa, and Total Molalities of (1 to 5) mol·kg-1, *Journal of Chemical & Engineering Data*, 57(4), 1078-1088, doi: 10.1021/je201062r.

Li, Y., Pham, J.Q., Johnston, K.P., and P.F. Green (2007), Contact angle of water on polystyrene thin films: effects of CO_2 environment and film thickness, *Langmuir*, 23:9785-9793.

Love, J.C., Estroff, L.A., Kriebel, J.K., Nuzzo, R.G., and G.M. Whitesides (2005), Self-assembled monolayers of thiolates on metals as a form of nanotechnology, *Chem. Rev*, 105, 1103-1169, 2005.

Orr, F.M. (2009), Onshore geologic storage of CO_2, *Science*, 325, 1656-1658, doi:10.1126/science.1175677.

Marmur, A. (2006), Soft contact: measurement and interpretation of contact angles, *Soft Matter*, 2, 12-17, doi: 10.1039/B514811C.

Saraji, S., Goual, L., Piri, M., and H. Plancher (2013), Wettability of supercritical carbon dioxide/water/quartz systems: simultaneous measurement of contact angle and interfacial tension at reservoir conditions, *Langmuir*, 29, 6856-6866.

Sarmadivaleh, M., A.Z. Al-Yaseri, and S. Iglauer (2015), Influence of temperature and pressure on quartz-water-CO_2 contact angle and CO_2-water interfacial tension, *Journal of Colloid and Interface Science*, 441, 59-64, doi:10.1016/j.jcis.2014.11.010.

Thompson, A.H., A.J. Katz, and R.A. Raschke (1987), Mercury injection in porous media: a resistance devil's staircase with percolation geometry, *Physcial Review Letters*, 58, 1, 29-32, doi.org/10.1103/PhysRevLett.58.29.

Tiab, D., and E.C. Donaldson (2004), *Petrophysics*, Elsevier, Amsterdam.

Wang, S., Tao, Z., Persily, S., and A.F. Clarens (2013), CO_2 adhesion on hydrated mineral Surfaces, *Environmental Science and Technology*, 47(20), 11858-11865.

Wilkinson, D., and J.F. Willemsen (1983), Invasion percolation: a new form of percolation theory, *J. Phys. A: Math. Gen.*, 16, 3365-3376.

Wollenweber, J., S. Alles, A. Busch, B.M. Krooss, H. Stanjek, and R. Littke (2010), Experimental investigation of the CO_2 sealing efficiency of caprocks, *International Journal of Greenhouse Gas Control*, 4, 231-241, doi:10.1016/j.ijggc.2010.01.003.

Yang, D., Gu, Y. and P. Tontiwachwuthikul (2008), Wettability Determination of the Reservoir Brine - Reservoir Rock System with Dissolution of CO_2 at High Pressures and Elevated Temperatures, *Energy & Fuels*, 22(1), 504-509.

5.6 **Dependence of Quartz Wettability on Fluid Density.**

Al-Yaseri, A.Z., Roshan, H., Lebedev, M., Barifcani, A. and Iglauer, S., 2016. Dependence of quartz wettability on fluid density. Geophysical Research Letters, 43(8), pp.3771-3776.

Dependence of quartz wettability on fluid density

Ahmed Zarzor Al-Yaseri,[1*] Hamid Roshan,[2] Maxim Lebedev,[3] Ahmed Barifcani,[4] Stefan Iglauer,[1]

[1] *Department of Petroleum Engineering, Curtin University, 26 Dick Perry Avenue, 6151 Kensington, Australia*

[2]*School of Petroleum Engineering, University of New South Wales, Kensington, Sydney, Australia*

[3] *Department of Exploration Geophysics, Curtin University, 26 Dick Perry Avenue, 6151 Kensington, Australia*

[4]*Department of Chemical Engineering, Curtin University, 26 Dick Perry Avenue, 6151 Kensington, Australia*

Key Points:

- Quartz wettability correlates with gas density
- Water wettability decreases with increasing gas density
- Wettability varies strongly with gas density (but not with gas type)

Abstract

Wettability is one of the most important parameters in multi-phase flow through porous rocks. However, experimental measurements or theoretical predictions are difficult and open to large uncertainty. In this work we demonstrate that gas densities (which are much simpler to determine than wettability and typically well known) correlate remarkably well with wettability. This insight can significantly improve wettability predictions and thus de-risk subsurface operations (e.g. CO_2 geo-storage or hydrocarbon recovery), and significantly enhance fundamental understanding of natural geological processes.

Keywords

Contact angle, CO_2 geo-sequestration, Structural trapping, Storage capacity, Wettability, Multi-phase flow

1. Introduction

Carbon geo-storage (CGS) has recently been explored as a technology to reduce anthropogenic greenhouse gas emissions and thus mitigate climate change [*IPCC* 2005*; Orr* 2009*; Lackner* 2013]. CGS containment security and storage efficiency rely on several storage mechanisms of which structural and residual trapping are the most important ones during the first several decades of a storage project [*IPCC* 2005, *Orr* 2009]. Both mechanisms depend on strong capillary forces, which are present in the pore network of the rock. The capillary forces counter balance the buoyancy forces exerted by the (lower density) CO_2, and they are determined by the contact angle (θ) between the rock, water and gas in the pore space as well as pore geometry [*Iglauer et al.,* 2015a]. Specifically, small water contact angles (<50°) lead to good structural [*Iglauer et al.,* 2015b] and residual trapping capacities [*Pentland et al.,* 2011*; Iglauer* 2011*; Andrew et al.,* 2013], while high contact angles (>90°) dramatically reduce structural [*Iglauer et al.,* 2015a,b] and residual trapping capacities [*Chaudhary et al.,* 2013*; Rahman et al.,* 2016]. However, there is a large uncertainty associated with such contact angle data reported in the literature [*Mahadevan* 2012*; Bikkina* 2012*; Iglauer et al.,* 2014*; Palamara et al.,* 2015] and such experiments are generally expensive and difficult to perform. Theoretical predictions – based on molecular dynamics computations – are also laden with uncertainty and the difficulty to mimic the solid surface in a representative way [*Liu et al.,* 2010*; Iglauer et al.,* 2012*; McCaughan et al.,* 2013; *Javanbakht et al.,* 2015; *Chen et al.,* 2015]. It is therefore highly desirable to well constrain θ to make reliable reservoir flow predictions, and related economic and safety risk assessments.

In this context, we demonstrate that the density of gas (ρ_g) in a brine/gas/quartz system correlates remarkably well with θ, and therefore ρ_g can be used to significantly simplify θ predictions. Implementation of such correlations in reservoir simulators will significantly improve CGS planning and de-risk projects.

2. Experimental Methodology

An alpha-quartz crystal was selected as it is the most common constituent mineral found in mudrocks and sandstone storage rocks [*Blatt and Schultz* 1976*; Hawkes et al.,* 2005*; Chiquet et al.,* 2007*; Qi et al.,* 2009*; Linstrom et al.,* 2011*; Grate et al.,*

2012*; Wang et al.*, 2012; *Broseta et al.*, 2012*; Al-Yaseri et al.*, 2015*; Sarmadivaleh et al.*, 2015*; Gallé* 2000*; Iglauer et al.*, 2015*a,b; Al-Yaseri et al.*, 2016]. The smooth sample (Root-Mean-Square surface roughness was 56nm [*Al-Yaseri et al.*, 2016]) was cleaned with acetone, and then exposed to air plasma for a period of 15 minutes to remove surface contaminants prior to each test [*Love et al.*, 2005, *Mahadevan* 2012*; Bikkina* 2012*; Iglauer et al.*, 2014]. Subsequently the substrate was placed in a high pressure cell and flooded with gas for a minimum period of 10 minutes. The gas pressure in the cell was then incrementally increased to pre-set values of (0.1, 5, 10, 15, 20 MPa) using a high precision syringe pump (ISCO pump model 500D), while the temperature was kept constant (343K). A droplet of brine (20wt% NaCl + 1wt% KCl in deionized water; de-gassed under vacuum for a period of 10 hours) was then dispensed onto the tilted substrate, so that advancing and receding water contact angles could be measured [*Lander et al.*, 1993], with a high performance video camera. Each experiment was repeated thrice, and therefore the average values of contact angle with associated error-bars are shown in the results. The density of the different gases (note: some of the components are supercritical at certain conditions, e.g. CO_2 above 304.8K and 7.39MPa, but for simplicity we call all volatile phases "gas" here; the purity of all gases used was ~ 99.9mol%) at different pressures was calculated using the real gas low (PV=ZnRT) [*Linstrom and Mallard* 2011]. Considering the fact that only quartz was tested (in presence of water), we limit our discussion to this material only; however, we hypothesize that similar trends could hold for other geological materials, this is further discussed below.

3. Results and Discussion

As abovementioned the contact angle is a key parameter required to predict subsurface flow processes [e.g. *Oren et al.*, 1998*; Blunt* 2001*; Valvatne et al.*, 2004]. The difficulty however lies in acquiring accurate data, and we present here a much simpler way to determine θ, namely through a correlation with the density of the gas phase. The contact angle of liquid (θ_l) can be related to the gas-solid (γ_{gs}), gas-liquid (γ_{gl}) and liquid-solid (γ_{ls}) interfacial tensions by Young's equation (*Young* 1805):

$$\cos\theta_l = \frac{(\gamma_{gs} - \gamma_{ls})}{\gamma_{gl}} \quad (1)$$

With the use of the sharp-kink approximation [*Dietrich and Napiorkowski 1991; Merath 2008*] and Young's equation (Eq. 1), the following macroscopic equation can be obtained [*Garcia et al.,* 2009; *Gatica et al.,* 2004; *Cheng et al.,* 1991]:

$$\cos\theta_l = \frac{I}{\gamma_{\mathrm{lg}}}\Delta\rho - 1 \quad (2)$$

Where $I = -\int_{z_{\min}}^{\infty} V(z)dz$, is the van der Waals potential integral (*I*) [*Garcia et al.,* 2009; *Gatica et al.,* 2004], and $\Delta\rho = \rho_g - \rho_{lf}$ (ρ_g is the gas density and ρ_{lf} is a function of the liquid and gas densities for a specific substrate), [*Merath 2008*]. Re-arranging equation 2 therefore yields:

$$\mathbf{cos\theta}_l = -\frac{I}{\gamma_{\mathrm{lg}}}\boldsymbol{\rho}_{\mathbf{g}} + \left(\frac{I}{\gamma_{\mathrm{lg}}}\rho_{lf} - 1\right) \quad (3)$$

Detailed discussion of equation 3 and how it has been derived is given in the supplementary information. In order to use equation 3, the measured advancing-receding water contact angles (Figure 1) were combined to obtain the Young's contact angle [*Chibowski and Terpilowski, 2008; Tadmor, 2004*]:

$$\theta_l = \arccos\left(\frac{r_A\cos\theta_A + r_R\cos\theta_R}{r_A + r_R}\right) \quad (4)$$

With

$$r_A = \left(\frac{\sin^3\theta_A}{2 - 3\cos\theta_A + \cos^3\theta_A}\right)^{1/3} \quad \text{and} \quad r_R = \left(\frac{\sin^3\theta_R}{2 - 3\cos\theta_R + \cos^3\theta_R}\right)^{1/3}$$

The measured advancing (θ_a) and receding (θ_r) water contact angles increased with pressure, but to different degrees based on the gas type (Figure 1), consistent with literature data [*Chiquet et al.,* 2007*; Espinoza et al.,* 2010; *Jung and Wang* 2012*; Saraji et al.,* 2013*; Iglauer et al.*, 2014, 2015b*; Al-Yaseri et al.,* 2016*; Sarmadivaleh et al.,* 2015],. The physico-chemical reason for this increase is the strengthening of

gas-quartz intermolecular interactions, which increase with increasing pressure [*Iglauer et al.,* 2012]. Note that the associated Wenzel contact angles were computed and used in Figure 1 to filter out the effect of surface roughness (*Al-Yaseri et al.* 2016 noticed that the effect of surface roughness is only minor).

The measurement (or estimation) of the van der Waals forces (term *I* in equation 3) is a significant challenge and typically requires substantial effort [*Cheng et al.,* 1991; *Gatica et al.,* 2004; *Garcia et al.,* 2009] and therefore we propose to use the concept presented in equation 3 and plot $\cos\theta_w$ vs ρ_g for the measured water-gas-quartz contact angles (Figure 2); note that the density of different gases are readily available in the literature (e.g. *Georgiadis et al*. 2010; *Linstrom and Mallard* 2011).

Remarkably, there is a linear relationship (equation 5, $R^2 \approx 0.98$) between $\cos\theta_w$ and ρ_g for a wide range of gases. This implies that the contact angle for such a system can be comfortably related to ρ_g:

$$\cos\theta_w = (-0.0012)\rho_g + 0.99 \qquad (5)$$

Where the slope of the line represents $-\frac{I}{\gamma_{lg}}$ (which remarkably stays constant with changes in pressure or gas type) and the intersection represents $(\frac{I}{\gamma_{lg}}\rho_{lf} - 1)$. It is however important to point out that this correlation holds only for quartz, a specific salinity (20wt% NaCl + 1wt% KCl = 4.48M ionic strength) and temperature (343K) as θ is also a function of salinity, temperature and the substrate itself [e.g. *Arif et al.* 2016*; Chiquet et al.,* 2007*; Broseta et al.,* 2012*; Al-Yaseri et al.,* 2016*; Sarmadivaleh et al.,* 2015*; cp. Iglauer et al.* 2015a]. Nevertheless this correlation can be extended to other salinity and temperature conditions, e.g. lower temperature as presented in Fig. 3.

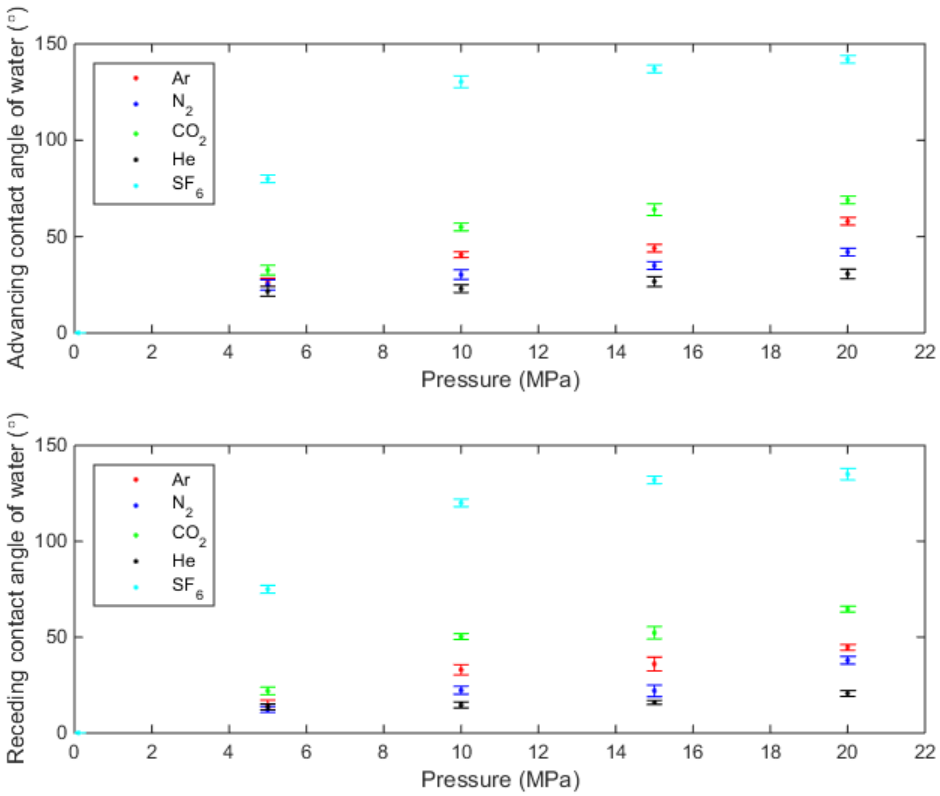

Figure 1. (top) Advancing and (bottom) receding water contact angles for SF_6, CO_2, N_2, Ar, and He/brine/quartz as a function of pressure at constant temperature (343 K and salinity, 4.48M ionic strength).

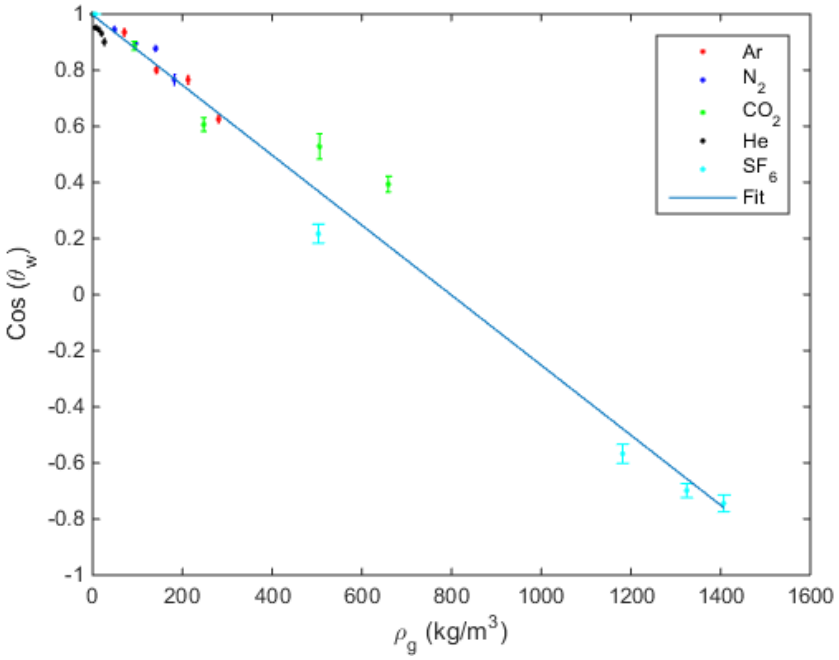

Figure 2. Cosine of the equilibrium water contact angles for SF_6,CO_2,N_2, Ar, and He/brine/quartz as a function of gas density at constant temperature (343 K) and salinity (4.48M ionic strength). The blue line is the fitted equation (5) (R^2= 0.98).

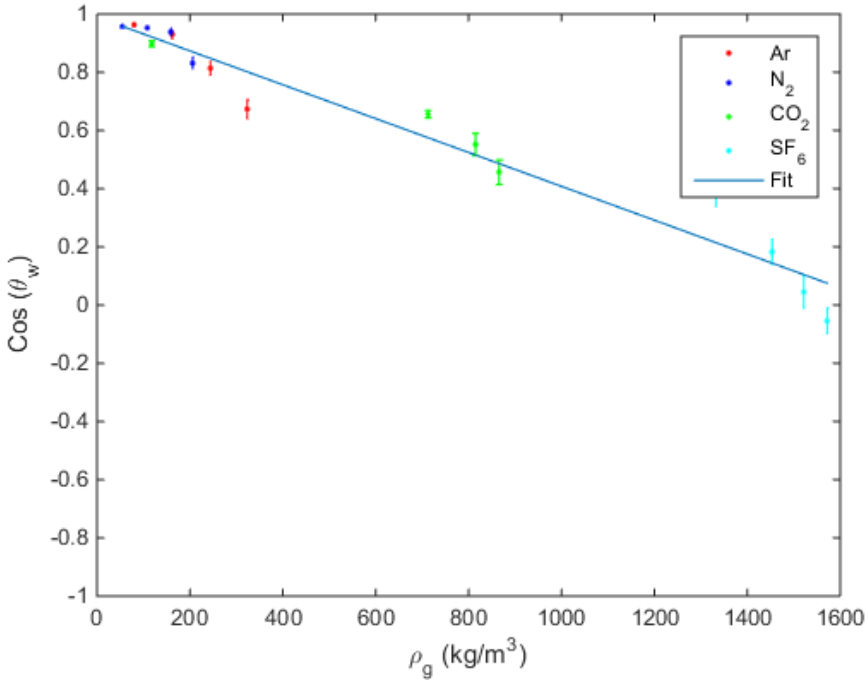

Figure 3. Cosine of the equilibrium water contact angles for SF_6,CO_2,N_2, Ar, and He/brine/quartz as a function ofgas density at constant temperature (308 K) and salinity (4.48M ionic strength). The blue line is the fitted equation (cosθ= (-0.0006)ρg + 0.99, R^2= 0.96).

4. **Conclusions and Implications**

We have shown that gas densities can be used to predict water contact angles on quartz for a specific temperature and brine composition, and thus rock wettability. Effectively the impact of pressure and gas type can be correlated by gas density, which represents a remarkable simplification of a complex phenomenon. Thus these findings enable a much more rapid and simplified determination of θ and associated with that more reliable pore-scale [*Valvatne et al.,* 2004] and reservoir scale [*Qi et al.,* 2009*; Iglauer et al.,* 2015a] predictions as gas densities can be swiftly and reliably calculated [*Linstrom and Mallard* 2011]. One word of caution is required; however, for each temperature, substrate and salinity a similar set of experiments need to be acquired to adjust the correlations (see above). Furthermore, we conclude that variability in rock wettability with depth can be expected as pressure and thus gas density increase with depth [*Hawkes et al.,* 2005*; Linstrom and Mallard* 2011].

References

Al-Yaseri, A., Lebedev, M., Barifcani, A., and Iglauer, S. (2016), Receding and advancing CO_2-brine-quartz contact angles as a function of pressure, temperature, surface roughness, salt type and salinity, *Journal of Chemical Thermodynamics*, 93, 416-423, doi:10.1016/j.jct.2015.07.031.

Al-Yaseri, A., Sarmadivaleh, M., Saeedi, A., Lebedev, M., Barifcani, A., and Iglauer, S. (2015), N_2+CO_2+NaCl brine interfacial tensions and contact angles on quartz at CO_2 storage site conditions in the Gippsland basin, Victoria/Australia, *Journal of Petroleum Science and Engineering*, 129(0), 58-62, doi:10.1016/j.petrol.2015.01.026.

Andrew, M., Bijeljic, B., Blunt, M.J. (2013), Pore-scale imaging of geological carbon dioxide storage under in situ conditions, *Geophysical Research Letters*, 40 (15), 3915-3918, doi: 10.1002/grl.50771.

Arif, M., Al-Yaseri, A. Z., Barifcani, A., Lebedev, M., and Iglauer, S. (2016), Impact of pressure and temperature on CO_2–brine–mica contact angles and CO_2–brine interfacial tension: Implications for carbon geo-sequestration, *Journal of colloid and interface science*, 462, 208-215, doi:10.1016/j.jcis.2015.09.076.

Bikkina, P.K. (2012), Reply to the comments on "Contact angle measurements of CO_2-water-quartz/calcite systems in the perspective of carbon sequestration", *International Journal of Greenhouse Gas Control*, 7(0), 263-264, doi: 10.1016/j.ijggc.2011.11.003.

Blatt, H., and Schultz, D.J. (1976), Size distribution of quartz in mudrocks, *Sedimentology*, 23, 857-866, DOI: 10.1111/j.1365-3091.1976.tb00113.x.

Blunt, M. J. (2001), Flow in porous media—pore-network models and multiphase flow, *Current opinion in colloid and interface science*, 6(3), 197-207.

Broseta, D., Tonnet, N., and Shah, V. (2012), Are rocks still water-wet in the presence of dense CO_2 or H2S?, *Geofluids*, 12(4), 280-294, doi: 10.1111/j.1468-8123.2012.00369.x.

Chaudhary, K., Bayani, C.M., Wolfe, W.W., Maisano, J.A., Ketcham, R.A., and Bennett, P.C. (2013), Pore-scale trapping of supercritical CO_2 and the role of grain wettability and shape, *Geophysical Research Letters*, 40, 1-5, doi: 10.1002/grl.50658.

Chen, C., Wan, J., Li, W., and Song, Y. (2015), Water contact angles on quartz surfaces under supercritical CO_2 sequestration conditions: Experimental and molecular dynamics simulation studies, *International Journal of Greenhouse Gas Control*, 42, 655-665, doi:10.1016/j.ijggc.2015.09.019.

Cheng, E., Cole, M. W., Saam, W. F., and Treiner, J. (1991), Helium prewetting and nonwetting on weak-binding substrates, *Physical Review Letters*, 67(8), 1007, DOI:http://dx.doi.org/10.1103/PhysRevLett.67.1007.

Chibowski, E., and K. Terpilowski (2008), Surface free energy of sulfur-Revisited: I. Yellow and orange samples solidified against glass surface, *Journal of Colloid and Interface Science*, 319(2), 505-513, doi:10.1016/j.jcis.2007.10.059.

Chiquet, P., Broseta, D., Thibeau, S. (2007), Wettability alteration of caprock minerals by carbon dioxide, *Geofluids*, 7, 112–122, doi: 10.1111/j.1468-8123.2007.00168.x.

Christian Merath (2008), Microscopic calculation of line tensions. *PhD thesis, Institute for Theoretical and Applied Physics, University of Stuttgart.*

Dake, L.P. (1978), Fundamentals of Reservoir Engineering. Developments in Petroleum Science, 8. *Elsevier, Amsterdam-London-New York-Tokyo*.

Dietrich, S., and Napiórkowski, M. (1991), Analytic results for wetting transitions in the presence of van der Waals tails, *Physical Review A*, 43(4), 1861, DOI:http://dx.doi.org/10.1103/PhysRevA.43.1861.

Espinoza, D.N. and Santamarina, J.C. (2010), Water-CO_2-mineral systems: Interfacial tension, contact angle, and diffusion—Implications to CO_2 geological storage, *Water Resources Research*, 46(7),1-10, DOI: 10.1029/2009WR008634.

Gallé C. (2000), Gas breakthrough pressure in compacted Fo–Ca clay and interfacial gas overpressure in waste disposal context, *Applied Clay Science*, 17: 85-97, doi:10.1016/S0169-1317(00)00007-7.

Gatica, S. M., Johnson, J. K., Zhao, X. C., and Cole, M. W. (2004), Wetting transition of water on graphite and other surfaces, *The Journal of Physical Chemistry* B, 108(31), 11704-11708, DOI: 10.1021/jp048509u.

Garcia, R., K. Osborne, and E. Subashi (2009), Validity of the "Sharp-Kink Approximation" for Water and Other Fluids, *The Journal of Physical Chemistry*, 113(23), 8199-8199, DOI: 10.1021/jp712181m.

Georgiadis, A., Maitland, G., Trusler, J. M., & Bismarck, A. (2010), Interfacial tension measurements of the (H2O+ CO2) system at elevated pressures and temperatures, *Journal of Chemical & Engineering Data*, 55(10), 4168-4175, DOI: 10.1021/je100198g.

Grate, J.W., Dehoff, K.J., Warner, M.G., Pittman, J.W., Zhang, C., Oostrom, M. (2012), Correlation of oil-water and air-water contact angles of diverse silanized surfaces and relationship to fluid interfacial tensions, *Langmuir*, 28, 7182-7188, doi**:** 10.1021/la204322k.

Hawkes, C.D., Mclellan, P.J., and Bachu, S. (2005), Geomechanical Factors Affecting Geological Storage of CO_2 in Depleted Oil and Gas Reservoirs, *Journal of Canadian Petroleum Technology*, 44 (10), 52-61, DOI: 10.2118/05-10-05.

Iglauer, S. (2011), Dissolution trapping of carbon dioxide in reservoir formation brine-a carbon storage mechanism, *INTECH Open Access Publisher*, doi: 10.5772/20206.

Iglauer, S., Mathew, M., and Bresme, F. (2012), Molecular dynamics computations of brine-CO_2 interfacial tensions and brine-CO_2-quartz contact angles and their effects on structural and residual trapping mechanisms in carbon geo-sequestration, *Journal of Colloid and Interface Science*, 386, 405-414.

Iglauer, S., Hassan, A., Sarmadivaleh, M., Liu, K., and Pham, C. (2014), Contamination of silica surfaces: impact on water-CO_2-quartz and glass contact angle measurements, *International Journal of Greenhouse Gas Control*, 22, 325-328, doi:10.1016/j.ijggc.2014.01.006.

Iglauer, S., Pentland, C. H., and Busch, A. (2015a), CO_2 wettability of seal and reservoir rocks and the implications for carbon geo-sequestration, *Water Resources Research*, 51(1), 729-774, doi: 10.1002/2014WR015553.

Iglauer, S., Al-Yaseri, A. Z., Rezaee, R., and Lebedev, M. (2015b), CO_2-wettability of caprocks: Implications for structural storage capacity and containment security, *Geophysical Research Letters*, 42, 1-6, doi: 10.1002/2015GL065787.

IPCC (2005), Carbon dioxide capture and storage, *Working Group III of the Intergovernmental Panel on Climate Change*, pp. 443.

Javanbakht, G., Sedghi, M., Welch, W., and Goual, L. (2015), Molecular Dynamics Simulations of CO_2/Water/Quartz Interfacial Properties: Impact of CO_2 Dissolution in Water, *Langmuir*, 31(21), 5812-5819, DOI: 10.1021/acs.langmuir.5b00445.

Jung, J.-W., and J. Wan, J. (2012), Supercritical CO_2 and ionic strength effects on wettability of silica surfaces: equilibrium contact angle measurements, *Energy and Fuels*, 26, 6053-6059, doi: 10.1021/ef300913t.

Kell, G. S., and E. Whalley (1975), Reanalysis of the density of liquid water in the range 0–150 °C and 0–1 kbar, *The Journal of Chemical Physics*, 62(9), 3496-3503, doi.org/10.1063/1.430986.

Lackner, K.S. (2003), Climate change. A guide to CO_2 sequestration, *Science*, 300, 1677-1678, doi: 10.1126/science.1079033.

Lander, L.M., Siewierski, L.M., Brittain, W.J., and Vogler, E.A. (1993), A systematic comparison of contact angle methods, *Langmuir*, 9(8), 2237-2239, doi: 10.1021/la00032a055.

Linstrom, P.J., and Mallard, W.G. (2011), The NIST Chemistry Web Book: A chemical data resource on the internet, *Journal of Chemical & Engineering Data*, 46(5), 1059-1063, doi: 10.1021/je000236i.

Liu, S., Yang, X., and Qin, Y. (2010), Molecular dynamics simulation of wetting behavior at CO_2/water/solid interfaces, *Chinese Science Bulletin*, 55(21), 2252-2257, doi: 10.1007/s11434-010-3287-0.

Love, J.C., Estroff, L.A., Kriebel, J.K., Nuzzo, R.G., and G.M.Whitesides (2005), Self-assembled monolayers of thiolates on metals as a form of nanotechnology, *Chemical Rev*iews, 105, 1103-1169, DOI: 10.1021/cr0300789.

Mahadevan, J. (2012), Comments on the paper titled "Contact angle measurements of CO_2-water-quartz/calcite systems in the perspective of carbon sequestration: a case of contamination?", *International Journal of Greenhouse Gas Control*, 7, 261-262, doi:10.1016/j.ijggc.2011.09.002.

McCaughan, J., Iglauer, S., and Bresme, F. (2013), Molecular dynamics simulation of water/CO_2-quartz interfacial properties: application to subsurface gas injection, *Energy Procedia*, 37, 5387-5402, doi:10.1016/j.egypro.2013.06.457.

Oren, P. E., Bakke, S., and Arntzen, O. J. (1998), Extending predictive capabilities to network models, *SPE Journal*, 3(04), 324-336, doi.org/10.2118/52052-PA.Orr, F. M. (2009), Onshore geologic storage of CO_2, *Science*. 325(5948), 1656-1658, doi: 10.1126/science.1175677.

Oyarzún, J. M. (2000), Pigment processing: physico-chemical principles, *Vincentz Network GmbH and Co KG*, PP.231.

Palamara, D.R., Neeman, T., Golab, A.N., Sheppard, A. (2015), A statistical analysis of the effects of pressure, temperature and salinity on contact angles in CO_2-brine-quartz systems, *International Journal of Greenhouse Gas Control*, 42, 516-524, doi:10.1016/j.ijggc.2015.09.007.

Pentland, C. H., El-Maghraby R., Iglauer S., and Blunt, M. J. (2011), Measurements of the capillary trapping of super-critical carbon dioxide in Berea sandstone, *Geophysical Research Letters*, 38, L06401, doi: 10.1029/2011GL046683.

Qi, R., Laforce, T.C., and Blunt, MJ. (2009), Design of carbon dioxide storage in aquifers, *International Journal of Greenhouse Gas Control*, 3: 195-205, doi:10.1016/j.ijggc.2008.08.004.

Rahman, T., Lebedev, M., Barifcani, A., and Iglauer, S. (2016), Residual trapping of supercritical CO_2 in oil-wet sandstone, *Journal of Colloid and Interface Sciene*, 469, 63-68, doi:10.1016/j.jcis.2016.02.020.

Saraji, S., Goual, L., Piri, M., and H. Plancher (2013), Wettability of supercritical carbon dioxide/water/quartz systems: simultaneous measurement of contact angle and interfacial tension at reservoir conditions, *Langmuir*, 29, 6856-6866, doi**:** 10.1021/la3050863.

Sarmadivaleh, M., Al-Yaseri, A.Z., and Iglauer, S. (2015), Influence of temperature and pressure on quartz–water–CO_2 contact angle and CO_2–water interfacial tension, *Journal of Colloid and Interface Sciene*, 441(0), 59-64.

Tadmor, R. (2004), Line Energy and the Relation between Advancing, Receding, and Young Contact Angles, *Langmuir*, 20(18), 7659-7664, doi: 10.1021/la049410h.

Valvatne, P.H., Blunt, M.J. (2004), Predictive pore-scale modelling of two-phase flow in mixed wet media, *Water Resource Research*, 40, W07406, DOI: 10.1029/2003WR002627.

Wang, S., Edwards, I.M. and Clarens, A.F. (2012), Wettability phenomena at the CO_2–brine–mineral interface: implications for geologic carbon sequestration, *Environmental Science and Technology*, 47(1), pp.234-241, DOI**:** 10.1021/es301297z.

Young, T. (1805), An Essay on the Cohesion of Fluids, *Philosophical Transactions of the Royal Society of London*, 95, 65-87.

Auxiliary Material: Dependence of quartz wettability on fluid density

Ahmed Zarzor Al-Yaseri,[1*] Hamid Roshan,[2] Maxim Lebedev,[3] Ahmed Barifcani,[4] Stefan Iglauer,[1]

[1] *Department of Petroleum Engineering, Curtin University, 26 Dick Perry Avenue, 6151 Kensington, Australia*

[2]*School of Petroleum Engineering, University of New South Wales, Kensington, Sydney, Australia*

[3] *Department of Exploration Geophysics, Curtin University, 26 Dick Perry Avenue, 6151 Kensington, Australia*

[4]*Department of Chemical Engineering, Curtin University, 26 Dick Perry Avenue, 6151 Kensington, Australia*

Content of this file

Derivation of the model

Introduction

This file includes auxiliary material for the above cited manuscript. The auxiliary material explains how the equation used to fit the experimental data (equation 3 in the script) was derived.

Derivation of the model

Young's equation (*Young* 1805) relates the contact angle of liquid (θ_l) to the gas-solid (γ_{gs}), gas-liquid (γ_{gl}) and liquid-solid (γ_{ls}) interfacial tensions:

$$\cos\theta_l = \frac{(\gamma_{gs} - \gamma_{ls})}{\gamma_{gl}} \qquad (1)$$

The main issue with estimating this macroscopic contact angle lies in the inability to measure the gas-solid and liquid-solid interfacial tensions [*Garcia et al.,* 2009; *Gatica et al.,* 2004]. The microscopic approach to estimate $(\gamma_{gs} - \gamma_{ls})$ has been already established in the field of physical science through integrating the van der Waals potentials at close proximity to the solid surface for a one-component fluid

system with its liquid and gas phases in equilibrium (for instance liquid water and water vapour) [*Cheng et al.*, 1991; *Garcia et al.*, 2009].

In such one-component fluid systems, the solid surface initiates a nucleation of a liquid film when approaching the saturated vapour pressure, e.g. if attractive interaction forces between the molecules and the surface are strong. Therefore the van der Waals integral takes into account the forces associated with both the vapour and liquid phases of the fluid. It should be noted that Young's equation (Eq. 1) in the one-component fluid system is thus valid when the saturated vapour pressure condition is reached.

The computation of the potential integral, however, is quite complex and therefore several approximations have been suggested to simplify the integral among which the 'sharp-kink approximation' has proved to be the simplest but yet efficient one [*Dietrich and Napiorkowski 1991*]. In this approximation, the solid-gas interface is approximated by a liquid-like film (with constant density) and further discontinuous change to constant bulk gas density [*Merath 2008*]. Obviously, this liquid-like film will have the same density as that of the bulk liquid phase in the one-component system when approaching saturated vapour pressure. Consequently it has been shown that $(\gamma_{gs} - \gamma_{ls})$ can be expressed as [*Garcia et al.*, 2009]:

$$\gamma_{ls} \approx \gamma_{gs} + \gamma_{lg} + \Delta\rho \int_{z_{min}}^{\infty} V(z)dz \qquad (2)$$

Where, V describes the net preference of the adsorbate molecule for wetting the substrate instead of forming a droplet (because of intermolecular forces), and $\Delta\rho = \rho_l - \rho_g$ (ρ is bulk density and subscripts l and g represent the liquid and gas (vapour) phases, respectively). Combination of equations 1 and 2 therefore yields [*Garcia et al.*, 2009; *Gatica et al.*, 2004]:

$$\cos\theta_l = \frac{I}{\gamma_{lg}}\Delta\rho - 1 \qquad (3)$$

Where, $I = -\int_{z_{min}}^{\infty} V(z)dz$. Equation 3 indicates that $\frac{I}{\gamma_{lg}}$ stays constant with change in $\Delta\rho$. While equation 3 is particularly useful for investigating contact angle changes

with density changes (due to pressure and/or temperature change), the equation was initially derived for one component systems.

As abovementioned, the gas density was equated to the bulk density of gas and the density of the liquid-like film of vapour (which condenses at atomic scale on the solid due to attractive intermolecular forces and grows with vapour pressure) was equated to the density of bulk liquid in the one component system [*Merath 2008*]. When extending this model to a two (or multi) component system, the gas density is equated to the bulk density of gas again, however, the density of the condensed liquid-like vapour film has to be adjusted as both liquid and gas molecules condense into this liquid-like film as two separate components for each specific substrate i.e. we write $\rho_{lf} = f(\rho_w, \rho_g^l)$. Such density is in fact a function of average density oscillations of condensed gas and liquid from the substrate to that of bulk and it is also indirectly related to substrate properties through *I*. The results of this study indicate that the sharp-kink approximation is still functioned in two-component system.

Re-arranging equation 3 with this argument ($\Delta\rho = \rho_{lf} - \rho_g$) therefore yields:

$$\mathbf{cos\theta}_l = -\frac{I}{\gamma_{\mathrm{lg}}}\boldsymbol{\rho}_{\mathbf{g}} + \left(\frac{I}{\gamma_{\mathrm{lg}}}\rho_{lf} - 1\right) \tag{4}$$

Remarkably, the equation explains that the contact angle of liquid (water here) has a linear relationship with the density of gas. In addition, fitting equation 4 to experimental data for different gases/brine/quartz systems shows only a small variation in slope and intersection. Therefore, when all gas densities are combined, the linear relationship still holds. Based on the above physical reasoning, it becomes clear that when the gas density approaches the water density or exceeds it (higher pressure or lower temperature), the influence of the gas density on the overall density of the liquid-like film increases and therefore a deviation from the linear relationship is observed. This is well-supported by our experimental data where a closer linear fit is seen for lower pressure and higher temperature (lower densities with respect to water density).

References

Cheng, E., Cole, M. W., Saam, W. F., and Treiner, J. (1991), Helium prewetting and nonwetting on weak-binding substrates, *Physical Review Letters*, 67(8), 1007, DOI:http://dx.doi.org/10.1103/PhysRevLett.67.1007.

Christian Merath (2008), Microscopic calculation of line tensions. *PhD thesis, Institute for Theoretical and Applied Physics, University of Stuttgart.*

Dietrich, S., and Napiórkowski, M. (1991), Analytic results for wetting transitions in the presence of van der Waals tails, *Physical Review A*, 43(4), 1861, DOI:http://dx.doi.org/10.1103/PhysRevA.43.1861.

Gatica, S. M., Johnson, J. K., Zhao, X. C., and Cole, M. W. (2004), Wetting transition of water on graphite and other surfaces, *The Journal of Physical Chemistry* B, 108(31), 11704-11708, DOI: 10.1021/jp048509u.

Garcia, R., K. Osborne, and E. Subashi (2009), Validity of the "Sharp-Kink Approximation" for Water and Other Fluids, *The Journal of Physical Chemistry*, 113(23), 8199-8199, DOI: 10.1021/jp712181m.

Young, T. (1805), An Essay on the Cohesion of Fluids, *Philosophical Transactions of the Royal Society of London*, 95, 65-87.

5.8 On Wettability of Shale Rocks.

Roshan, H., **Al-Yaseri, A.Z.**, Sarmadivaleh, M. and Iglauer, S., 2016. On wettability of shale rocks. Journal of Colloid and Interface Science, 475, pp.104-111.

On Wettability of Shale Rocks

H. Roshan[1*], A. Z. Al-Yaseri[2], M. Sarmadivaleh[2], S. Iglauer[2]

[1]School of Petroleum Engineering, University of New South Wales, Kensington, Sydney, Australia

[2]Department of Petroleum Engineering, Curtin University, 6151 Kensington, Western Australia

Abstract

The low recovery of hydraulic fracturing fluid in unconventional shale reservoirs has been in the centre of attention from both technical and environmental perspectives in the last decade. One explanation for the loss of hydraulic fracturing fluid is fluid uptake by the shale matrix; where capillarity is the dominant process controlling this uptake. Detailed understanding of the rock wettability is thus an essential step in analysis of loss of the hydraulic fracturing fluid in shale reservoirs, especially at reservoir conditions. We therefore performed a suit of contact angle measurements on a shale sample with oil and aqueous ionic solutions, and tested the influence of different ion types (NaCl, KCl, $MgCl_2$, $CaCl_2$), concentrations (0.1, 0.5 and 1 M), pressures (0.1, 10 and 20 MPa) and temperatures (35 and 70 °C). Furthermore, a physical model was developed based on the diffuse double layer theory to provide a framework for the observed experimental data.

Our results show that the water contact angle for bivalent ions is larger than for monovalent ions; and that the contact angle (of both oil and different aqueous ionic solutions) increases with increase in pressure and/or temperature; these increases are more pronounced at higher ionic concentrations. Finally, the developed model correctly predicted the influence of each tested variable on contact angle. Knowing contact angle and therefore wettability, the contribution of the capillary process in terms of water uptake into shale rocks and the possible impairment of hydrocarbon production due to such uptake can be quantified.

Keywords

contact angle, shale gas, oil shale, high pressure, elevated temperature, hydraulic fracturing

1. Introduction

With the decline of conventional oil and gas resources, gravitation towards unconventional resource development has increased significantly [1]. This is particularly true for oil and gas shales which have significantly contributed to the energy economy recently, in particular in the US [2]. Gas and oil shales typically have a very low permeability [3, 4], and production is therefore usually associated with hydraulic fracturing operations, which increases the reservoir permeability through activating pre-existing fractures and creating new fractures thereby enhancing connectivity [5]. However, one key technical-environmental issue associated with hydraulic fracturing is the very low recovery of hydraulic fracturing fluid; several hypotheses have been suggested to explain this disappearance of hydraulic fracturing fluids: hydration of clay minerals [6-8]; capillary forces [9-14]; creation of micro-fractures [3, 9, 15]; storage of the fluid within the fracture network [11, 16]; and osmotic flow [7, 17].

Water uptake is a complex function of these physico-chemical processes [7, 10, 14]. It is thus of vital importance to quantify the contribution of all processes in particular capillary forces [10, 18] with respect to water uptake. Therefore the contact angle between shale and the introduced fluids needs to be thoroughly investigated.

In this context, Fakcharoenphol et al. [17] showed that water-wet shale samples cannot significantly imbibe water of higher salinity than that of the in-situ pore water. In contrast, Xu and Dehghanpour [19] showed that organic-rich shale samples can absorb a considerable amount of water even when their surface is lipophilic. Moreover, Engelder et al. [16] investigated the wettability of organic shale samples and concluded that the samples are strongly oil-wet in the presence of air. They further mentioned that deionised (DI) water causes the highest contact angle on the sample surface and that highly saline solutions lead to the lowest contact angles, whereas other studies [7, 20] suggest that the (water) contact angle (θ) increases with salinity.

However, all above mentioned studies have been carried out under atmospheric conditions, although it is well known that pressure and temperature can have a dramatic impact on θ [21-28]. In addition, there is a lack of systematic measurements of contact angles for brines containing major exchangeable cations (Mg^{2+}, Ca^{2+}, K^{+}, Na^{+}) at different concentrations. We thus measured contact angles on a shale sample as a function of salinity and salt type at realistic reservoir conditions. Finally we proposed a physical model to qualitatively describe the physical processes responsible for variation in contact angle due to pressure, temperature, ion type and ionic concentration.

2. Experimental procedure

The shale sample was extracted from 1547 m depth of a nominated CO_2 storage site in New South Wales, Australia. The geological and chemical properties of this sample including X-ray diffraction (XRD), scanning electron microscopy (SEM), total organic carbon (TOC), and pore throat size distribution measurements using mercury intrusion were reported previously [28] and are therefore only briefly mentioned in this study. In the work presented here, an additional elemental analysis via X-ray fluorescence (instrument PW2400 XRF) was carried out to further deepen the understanding of the shale sample's chemical composition.

Due to the fact that higher gas solubility in the liquid phase makes the interpretation of contact angle data more complex, air (with low solubility in liquid phases: water and oil, especially with pressure) was chosen as the gas phase in this study. The shale sample was exposed to air plasma for 5 min to remove organic surface contaminations [29]. Subsequently the substrate was placed in a high pressure-high temperature cell (**Fig. 1**), and droplets of different ionic solutions or oil (n-decane) were dispensed onto the tilted substrate [30] at different pressures and temperatures. This process was videoed and advancing and receding contact angles were measured simultaneously following Al-Yaseri et al.'s [21] procedure.

A broad range of salt types (KCl, NaCl, $MgCl_2$ and $CaCl_2$ covering major exchangeable cations) and salinities (0.1, 0.5 and 1 M concentrations) were tested at 0.1, 10 and 20 MPa pressures at 70°C temperature. Additional measurements were conducted at 35 °C and 20 MPa to investigate the effect of temperature.

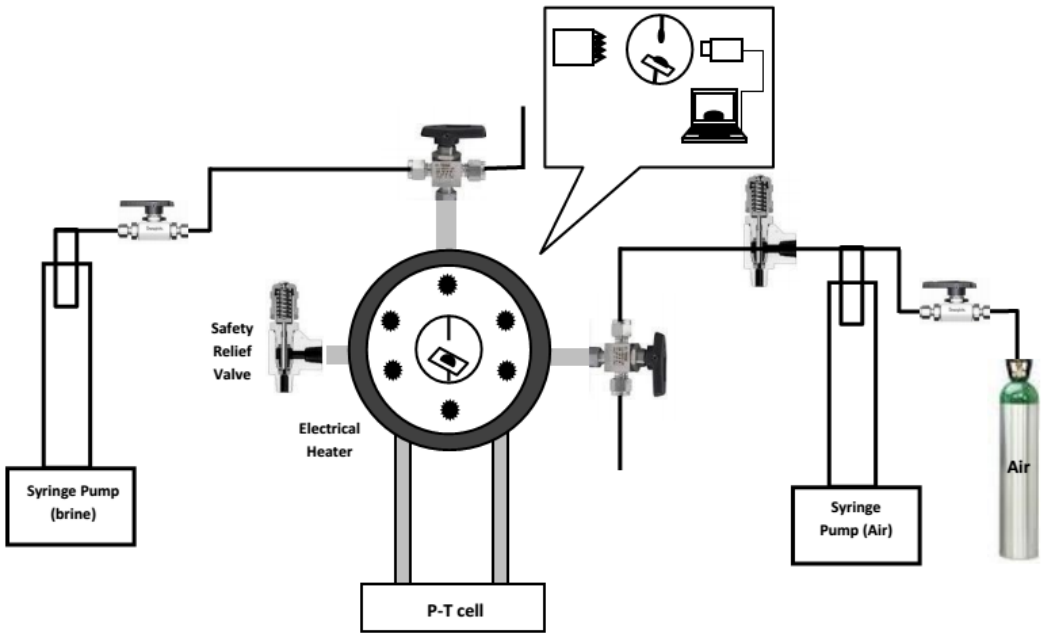

Fig. 1. Schematic of the high pressure-high temperature experimental apparatus used to conduct the contact angle measurements.

3. Model development

In order to describe the physical basis for variation of contact angle with pressure, temperature, ion type and ionic concentration on minerals carrying negative charges such as clays, we developed a constitutive equation. We begin with a formulation for contact angles on mineral surfaces without electric charges. This formulation is then extended to minerals with surface charges, assuming that the electrically charged mineral surface has a constant electric potential, and that this electric potential reduces exponentially towards the bulk solution. The zone where the electrical potential of the charged surface is active is the so-called diffuse double layer and its thickness is given by the Debye length [31]. This thickness coupled with the chemistry of the charged surfaces will be the basis for our model development for contact angle of charge surfaces.

3.1 Mineral without surface charges

When a drop of a liquid, in the presence of another fluid (liquid or gas), is placed on a solid surface with no electric potential, the droplet spreads across the solid surface,

until the minimum free energy is reached [32]. This is related to the cohesion forces in the fluids and adhesion forces between the fluids and the solid surface. If contact angle hysteresis due to energy dissipation is neglected, and the free energy change due to an infinitesimal increase in base area of the droplet on the solid surface (surrounded by another fluid) is considered, the free energy of the system is written [32, 33]:

$$dF = \gamma_{\mathrm{lg}} \cos\theta dA - \gamma_{sg} dA + \gamma_{sl} dA \qquad (1)$$

Where γ is the interfacial tension or surface free energy, F is total free energy of the system, θ is contact angle of the droplet and dA is the infinitesimal surface area (s, g and l represent the solid, fluid (gas or liquid) and liquid phases). When the minimum energy is reached and equilibrium is established, Eq. 1 turns in a especial case, the Young's equation [33].

3.2 Mineral with electrically charged surfaces

We now use the concept of altering the contact angle by applying an electric field between a solid surface and an electrolyte [32, 34]. Recall that the electric field is created by negative electrical charges present on the surface of the mineral [35] and there is no external electric field. Thus the solid-liquid free energy in Eq. 1 can be extended:

$$dF = \gamma_{\mathrm{lg}} \cos\theta dA - \gamma_{sg} dA + (\gamma_{sl} dA - dW_C) \qquad (2)$$

Where dW_C is the work performed by the electric potential of the solid surface to re-arrange the positions of the cations and anions in the diffuse double layer in the presence of the electric field and therefore adjusts the γ_{sl}. By using the concept of a charged parallel-plate, dW_c can be related to the electrical energy stored in the system [32, 34]:

$$dW_C = \frac{1}{2} dC\psi_S^2 \qquad (3)$$

Where, ψ is the electric potential of the solid surface and C is the capacitance per unit area, defined as $dC = D\varepsilon_0 \frac{dA}{k}$ according to Gauss's law: D is the dielectric constant of the medium (solid surface and surrounding liquid), ε_0 is the permittivity of vacuum and k is the distance between the charged plates where the electric potential is active. By combining Gauss's law with Eqs. 2 and 3 we obtain:

$$dF = \gamma_{\mathrm{lg}} \cos\theta(\psi_S) dA - \gamma_{sg} dA + (\gamma_{sl} dA - \frac{1}{2} D\varepsilon_0 \frac{dA}{k} \psi_S^2) \quad (4)$$

In order to take into account the effect of liquid-surface interaction on the dielectric properties, the medium dielectric constant was employed in the formulation. There is no general equation to evaluate the dielectric constant of the medium but the experimental data for different rocks are often available in the literature [36]. Further, we write the contact angle of a neutral surface at equilibrium ($\cos\theta = (\gamma_{sg} - \gamma_{sl}) / \gamma_{\mathrm{lg}}$; [33]) as [37]:

$$\cos\theta = \frac{\gamma_{sg} - \gamma_{sl}}{\gamma_{\mathrm{lg}}} = -1 + \frac{\Delta\rho}{\gamma_{\mathrm{lg}}} I \quad (5)$$

where, $\Delta\rho = \rho_{lf} - \rho_g$: ρ_g is the density of gas phase and ρ_{lf} is a function of gas and liquid density of a subtrate [38] and $I = -\int_{z_{\min}}^{\infty} V(z) dz$ where V is the net preference of the adsorbate molecule for wetting the substrate instead of forming a droplet due to intermolecular forces [37] e.g. *I* has been related to density difference in the formulation. A detailed discussion on the extension of equation 5 from a one-component fluid system to two-component fluid systems was given by Al-Yaseri et al [38]. Considering an equilibrated system ($dF = 0$ where dA disappears: $\cos\theta(\psi_S) = \frac{\gamma_{sg} - \gamma_{sl}}{\gamma_{\mathrm{lg}}} + (\frac{1}{2} D\varepsilon_0 \frac{\psi_S^2}{k\gamma_{\mathrm{lg}}})$) and combining Eqs. 4 and 5, the contact angle for a charged surface is written:

$$\cos\theta(\psi) = (-1 + \frac{\Delta\rho}{\gamma_{\mathrm{lg}}} I) + \frac{D\varepsilon_0 \psi_S^2}{2k\gamma_{\mathrm{lg}}} \quad (6)$$

It is noted that $\psi_S (= \psi_{S_0})$ is the constant potential at the mineral surface and it is assumed that it is not influenced by thermodynamic variables. We now define the distance between charged plates k in Eq. 6 as the distance where the effect of surface potential of the charged mineral vanishes in the bulk solution (with negative sign as it is oriented away from the surface towards the bulk solution); i.e. the Debye length [31]:

$$k = \left(\frac{\varepsilon_0 D_f K_B T}{2e^2 z^2 n_{bulk} N_a} \right)^{1/2} \tag{7}$$

where, D_f is the dielectric constant of the solution, T is the temperature, z is the ionic valency, K_B is the Boltzmann constant (1.38×10^{-23} JK^{-1}), n_{bulk} is the ionic concentration of the solution (mol/m^3), N_a is the Avogadro constant (6.022×10^{23} mol^{-1}) and e is the electric charge (1.602×10^{-9} C). The ion valency (z), temperature (T) and ionic concentration of bulk solution (n_{bulk}) are straightforward parameters; however, the effect of thermodynamic variables on the fluid dielectric constant (D_f) is complex and still an open research area [18, 39]. Combining equations 6 and 7, the final equation takes the form:

$$\cos\theta = \frac{I\boldsymbol{\Delta\rho}}{\gamma_{\mathrm{lg}}} - \frac{\varepsilon_0 \psi_S^2 D}{2\boldsymbol{\gamma_{lg}}} \left(\frac{2e^2 \mathbf{n_{bulk}} \mathbf{z}^2 N_a}{\varepsilon_0 K_B \mathbf{D_f T}} \right)^{1/2} - 1 \tag{8}$$

Where the bold parameters are the ones most influenced by pressure, temperature, ion type and ion concentration.

The first term on the right-hand-side (RHS) of equation 8 ($\frac{\mathrm{I}\Delta\rho}{\gamma_{\mathrm{lg}}}$) is related to the interfacial tensions between solid-liquid, solid-gas and liquid-gas and the second term takes into account the contribution of the formation of a diffusive double layer in an aqueous solution within the solid-liquid region.

It is noteworthy that the fluid dielectric constant in equation 8 is much more affected by temperature and pressure than the dielectric constant of the porous medium [40]. Furthermore, the effect of thermodynamic variables on I in equation 8 is not yet

fully understood. It is also assumed that ion adsorption on the surface of clay minerals are most likely to occur [14].

It is now possible to describe the physical processes responsible for contact angle variation in shales by Eq. 8 which is discussed further below. It should also be noted that the sum of the first and second terms of Eq. 8's RHS can only vary from 0 to 2 as contact angle varies between 0 and 180 ° and therefore $\cos\theta$ varies between 1 to -1. In order to understand the impact of the first and second terms of equation 8 on the resulting contact angles, we have extracted some data from the literature (**Table 1**) mostly for shale and 1 M NaCl brine and have plotted the ratio of the first term per second term ($\left\{\frac{I\Delta\rho}{\gamma_{lg}}\right\} / \left\{\frac{\varepsilon_0\psi_S^2 D}{2\gamma_{lg}}\left(\frac{2e^2 n_{bulk} z^2 N_a}{\varepsilon_0 K_B D_f T}\right)^{1/2}\right\}$) vs a range of surface potentials in **Fig. 2**.

Table 1. Extracted data from the literature (references given in the table) to investigate the ratio of the first and second right hand side terms of equation 8.

Parameter	Magnitude	Unit
T	25	°C
D_f	70 [62]	-
K_B	1.38×10^{-23}	JK^{-1}
ε_0	6.95×10^{-10}	Fm^{-1}
N_a	6.022×10^{23}	mol^{-1}
z	1 (NaCl)	-
n_{bulk}	1	Mol/L
e	1.602×10^{-9}	C
D	9 [63]	-
γ_{lg}	62 [64]	mNm^{-1}
I/γ_{lg}	0.0012 [38]	$Kg^{-1}m^3$
$\Delta\rho$	1600 [38]	Kgm^{-3}

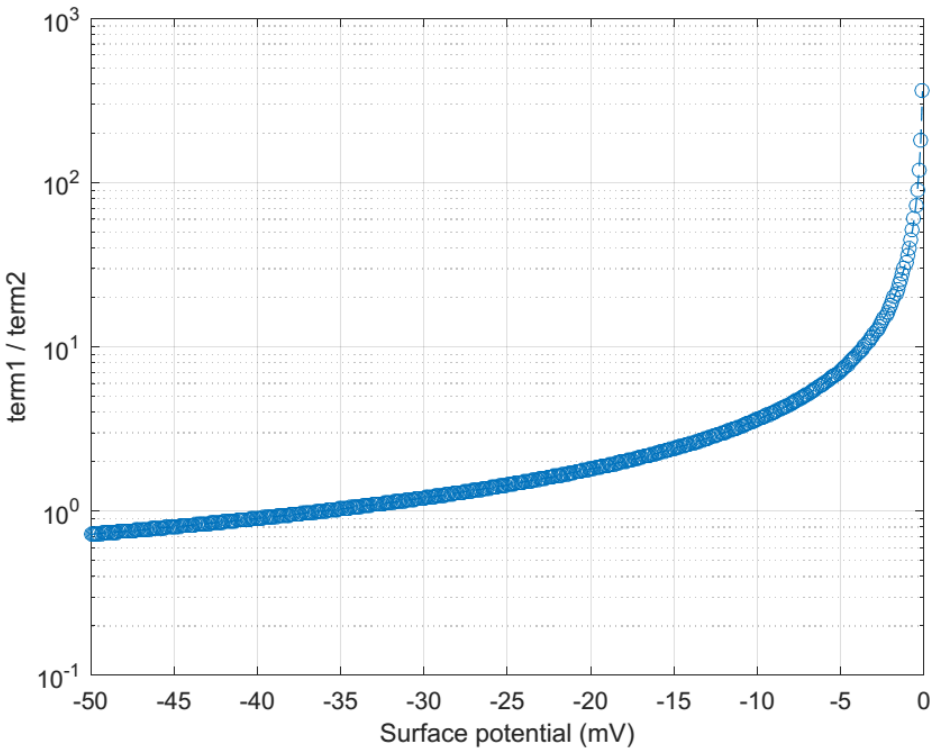

Fig. 2. Effect of surface potential on the ratio of the first and second right hand side terms of Eq.(8).

4. Results

4.1 Chemical-structural measurements

The total organic carbon of the sample was measured as 810 (mg/kg) and the chemical composition was measured as: 33 wt% illite, 31 wt% quartz, 15 wt% analcite, 9 wt% feldspar, 8 wt% albite and 4 wt% chlorite using XRD analysis. The major elemental oxides measured by XRF analysis (above 0.1 wt%) include 3.14 wt% Na_2O, 2.26 wt% MgO, 16.70 wt% Al_2O_3, 60.68 wt% SiO_2, 4.49 wt% K_2O, 0.22 wt% CaO, 0.77 wt% TiO_2 and 5.81 wt% Fe_2O_3. SEM micrographs of the shale sample are also presented in **Fig. 3;** they show the laminated nature of the sample's mineralization by clay minerals.

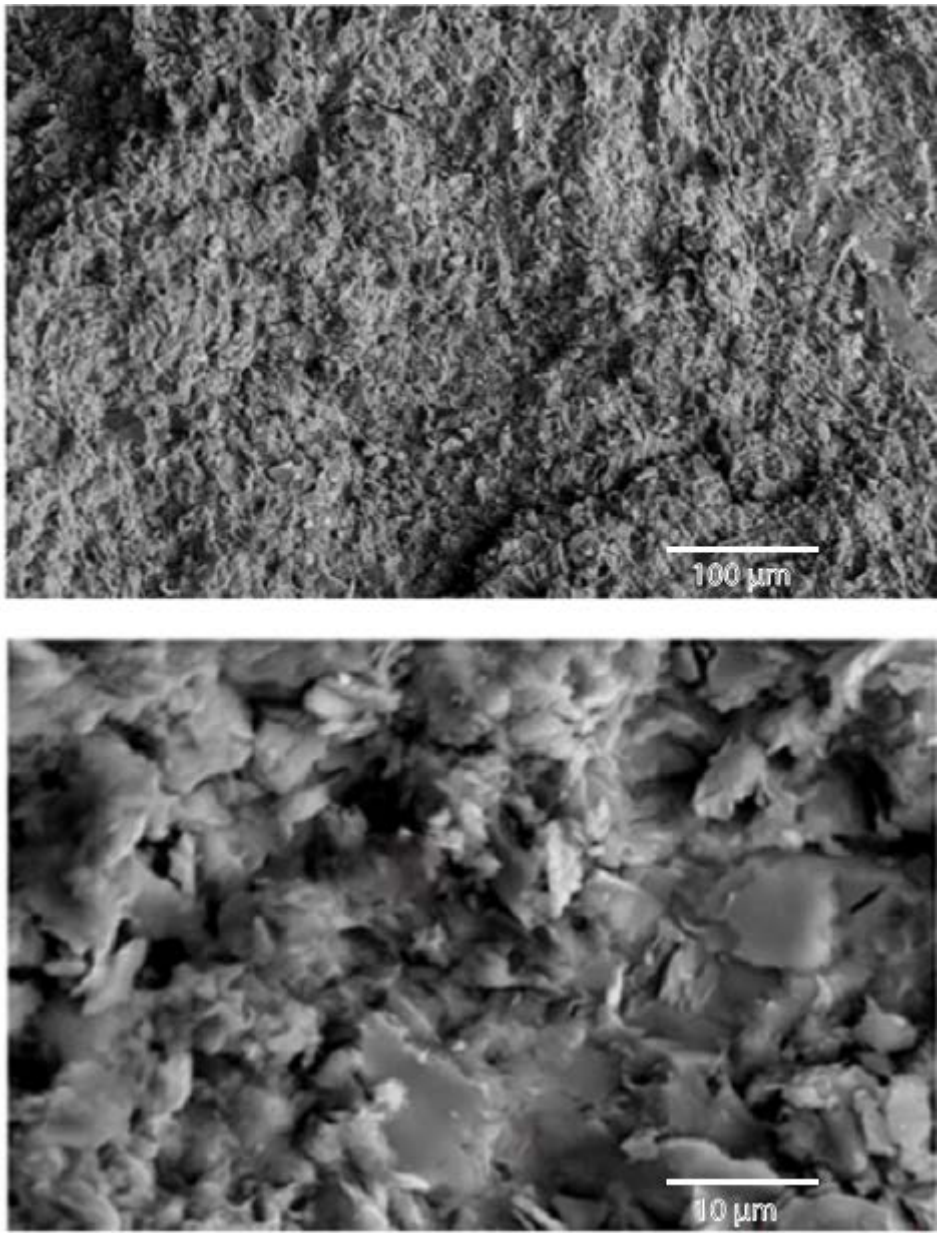

Fig. 3. SEM micrographs of the shale sample.

4.2 Contact angle measurements

All advancing and receding water contact angles measured are reported in **Tables 2** and **3**, respectively. The advancing and receding contact angles measured at 0.1 M salt (KCl, NaCl, $CaCl_2$ and $MgCl_2$) concentration at three different pressures (0.1, 10 and 20 MPa) and constant temperature (70 °C) are presented in **Fig. 4**. As expected the advancing contact angles were higher than the receding contact angles; and

generally contact angles increased with pressure, especially the advancing contact angles. For instance, a pressure increase from 0.1 to 20 MPa caused the advancing and receding contact angles to increase from 10° to 25° and 8° to 14° for 0.1 M KCl concentration, respectively. Furthermore, $MgCl_2$ brine consistently showed the highest contact angles followed by $CaCl_2$, NaCl and KCl; this was especially pronounced for the advancing contact angles. Moreover, both, advancing and receding contact angles consistently increased when the ion concentration increased (Figures **4-6**). This increase was stronger at higher pressures.

Table 2. Advancing water contact angle (˚) for all cases measured in this study.

	Pressure and Temperature			
	0.1 MPa	10 MPa	20 MPa	
Brine composition	70 °C	70 °C	70 °C	35 °C
0.1 M NaCl	17	21	28	26
0.5 M NaCl	18	25	31	28
1.0 M NaCl	30	34	48	31
0.1 M KCl	10	19	25	20
0.5 M KCl	17	22	29	23
1.0 M KCl	22	27	41	28
0.1 M $CaCl_2$	21	24	29	28
0.5 M $CaCl_2$	29	28	36	32
1.0 M $CaCl_2$	32	38	57	36
0.1 M $MgCl_2$	22	31	33	29
0.5 M $MgCl_2$	31	33	38	33
1.0 M $MgCl_2$	35	41	62	43
n-Decane*	6	14	18	12

*instead of brine n-decane was used.

A temperature increase from 35 °C to 70 °C led to a gradual increase in both advancing and receding contact angles for 0.1 and 0.5 M salt concentrations at 20 MPa pressure (**Fig. 7**). When salt concentration increased to 1M, an increase in temperature caused a sudden jump in contact angle, in contrast to the gradual increase seen at the relatively lower salt concentrations (0.1 and 0.5 M). For instance an increase in temperature from 35 °C to 70 °C caused the advancing contact angle of 0.1 M $MgCl_2$ brine to increase from 29 to 33°, whereas the advancing contact

angle changed from 43 to 62 ° at 1 M $MgCl_2$ concentration with the same temperature increment.

Table 3. Receding water contact angle (˚) for all cases measured in this study.

	Pressure and Temperature			
	0.1MPa	10Ma	20 MPa	
Brine composition	70 °C	70 °C	70 °C	35 °C
0.1 M NaCl	14	13	15	12
0.5 M NaCl	15	16	24	20
1.0 M NaCl	20	21	30	25
0.1 M KCl	8	12	14	10
0.5 M KCl	13	14	20	12
1.0 M KCl	15	16	28	17
0.1 M $CaCl_2$	15	10	18	16
0.5 M $CaCl_2$	18	13	26	21
1.0 M $CaCl_2$	20	20	42	25
0.1 M $MgCl_2$	17	16	23	20
0.5 M $MgCl_2$	20	19	26	21
1.0 M $MgCl_2$	24	22	51	37
n-Decane*	0	6	10	3

*instead of brine n-decane was used.

Fig. 8 presents the decane advancing and receding contact angles in air at different pressures (0.1, 10 and 20 MPa) and 70 °C. Both, advancing and receding contact angles increased with pressure. For instance, the advancing decane contact angle increased from 6 ° at 0.1 MPa pressure to 18 ° at 20 MPa pressure. Decreasing the temperature to 35 °C on the other hand caused the advancing and receding decane contact angles to slightly reduce (Tables 2 and 3). For example, the advancing decane contact angle decreased from 18 ° to 12 ° as temperature decreased from 70 °C to 35 °C at constant 20 MPa pressure (Tables 2 and 3). Generally, the decane-air contact angles were more affected by pressure than by temperature.

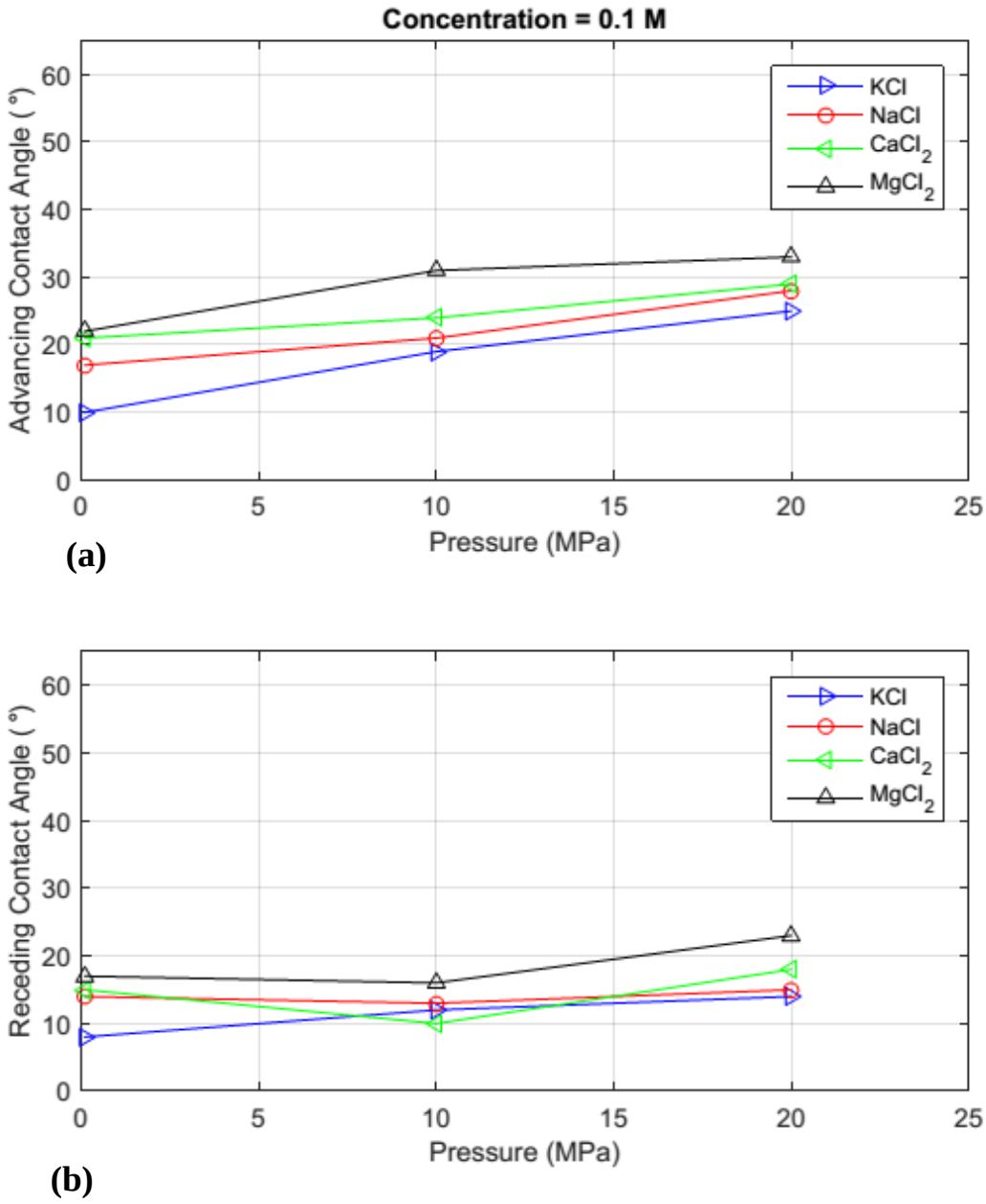

Fig. 4. (a) Advancing and (b) receding water contact angles measured at 0.1 M salt concentration (KCl, NaCl, $CaCl_2$ and $MgCl_2$) as a function of pressure and salt type at 70 °C.

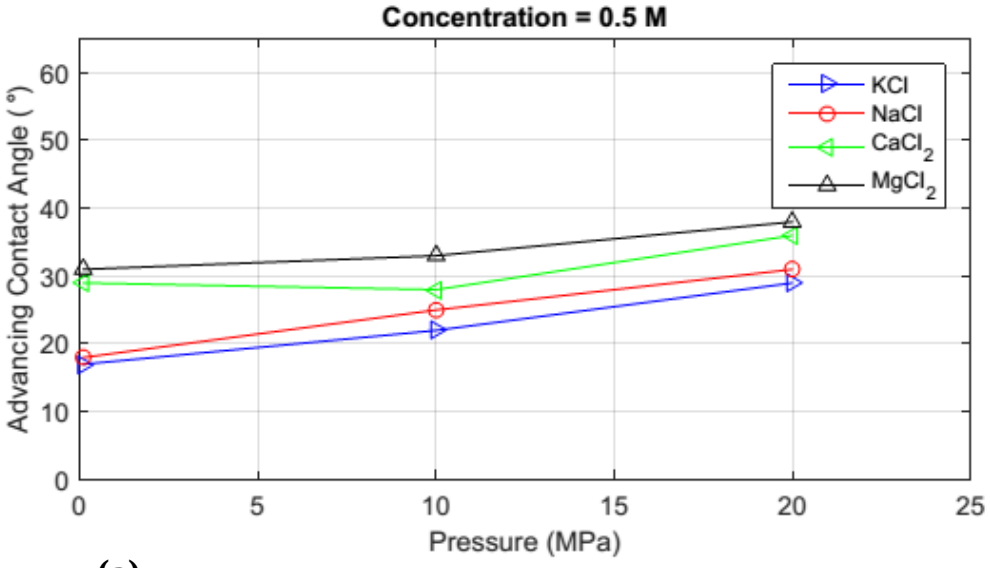

(a)

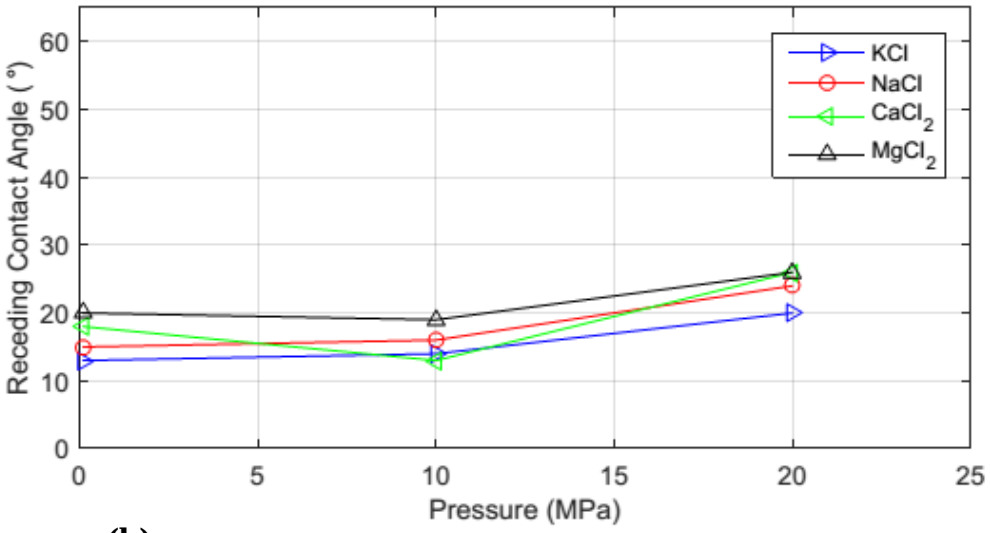

(b)

Fig. 5. (a) Advancing and (b) receding water contact angles measured at 0.5 M salt concentration (KCl, NaCl, $CaCl_2$ and $MgCl_2$) as a function of pressure and salt type at 70 °C.

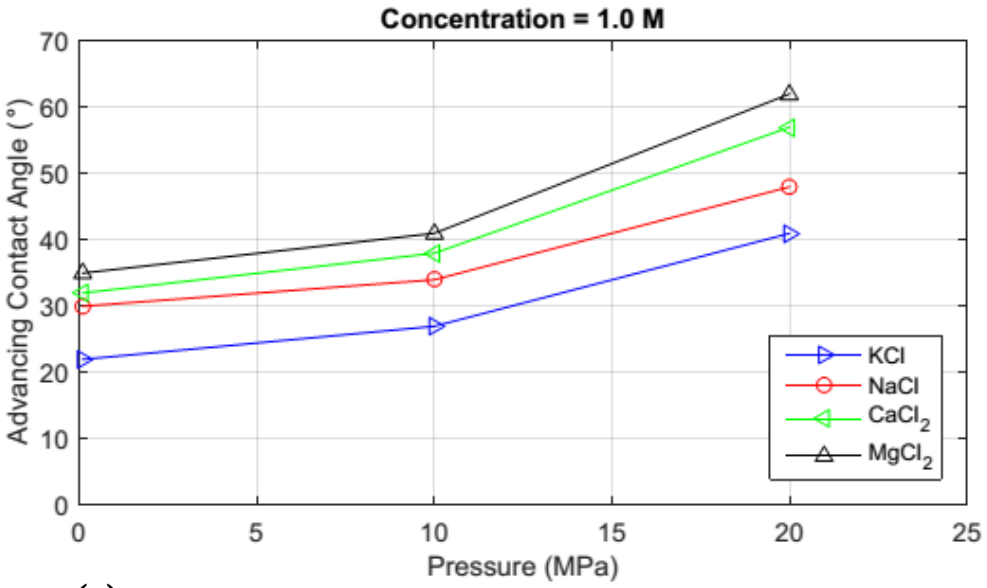

(a)

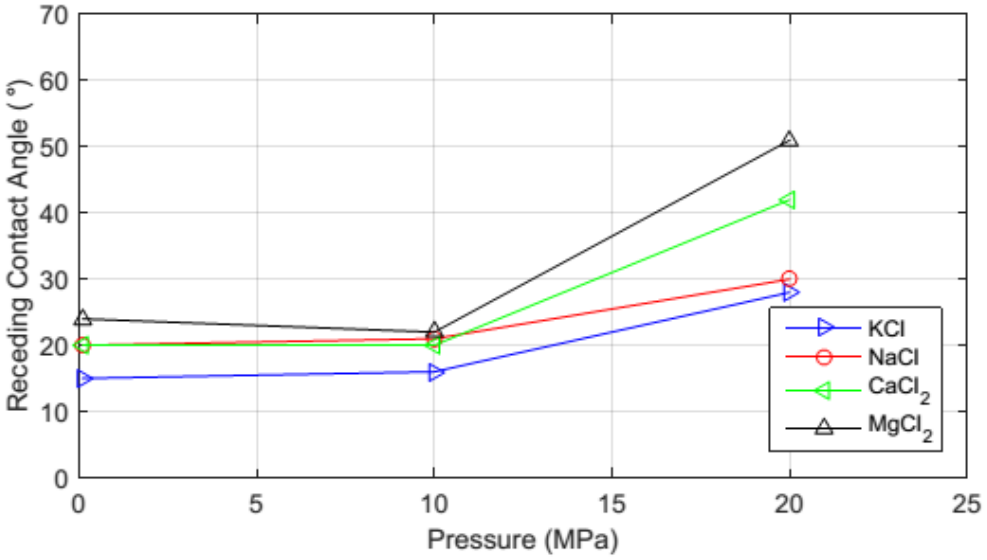

(b)

Fig. 6. (a) Advancing and (b) receding water contact angles measured at 1. M salt concentration (KCl, NaCl, $CaCl_2$ and $MgCl_2$) as a function of pressure and salt type at 70 °C.

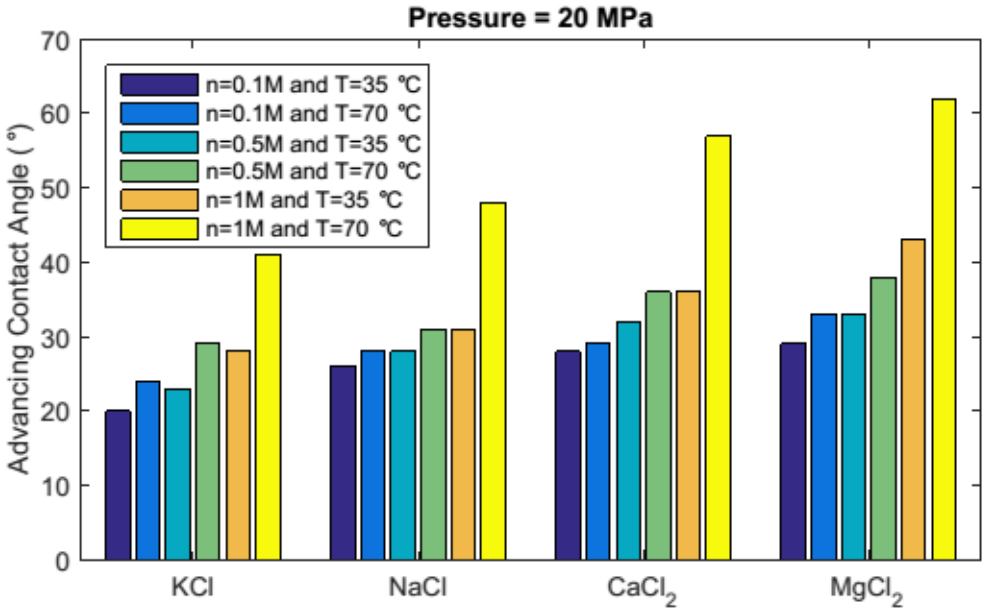

(a)

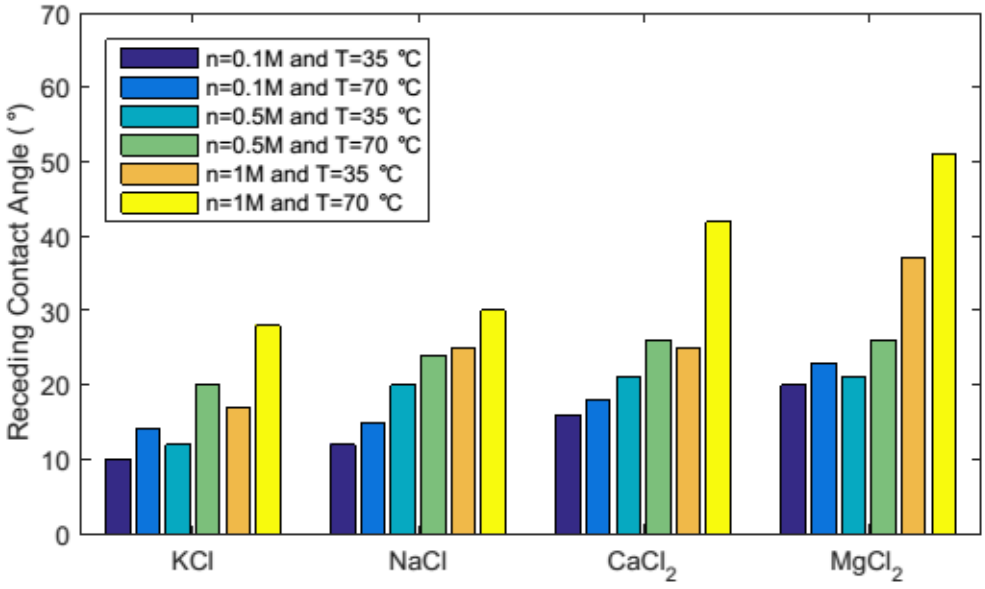

(b)

Fig. 7. (a) Advancing and (b) receding water contact angles measured at diffeionic concentrations (0.1, 0.5 and 1.0 M KCl, NaCl, $CaCl_2$ and $MgCl_2$ concentrations) at two temperatures (35°and 70°C) and 20 MPa pressure.

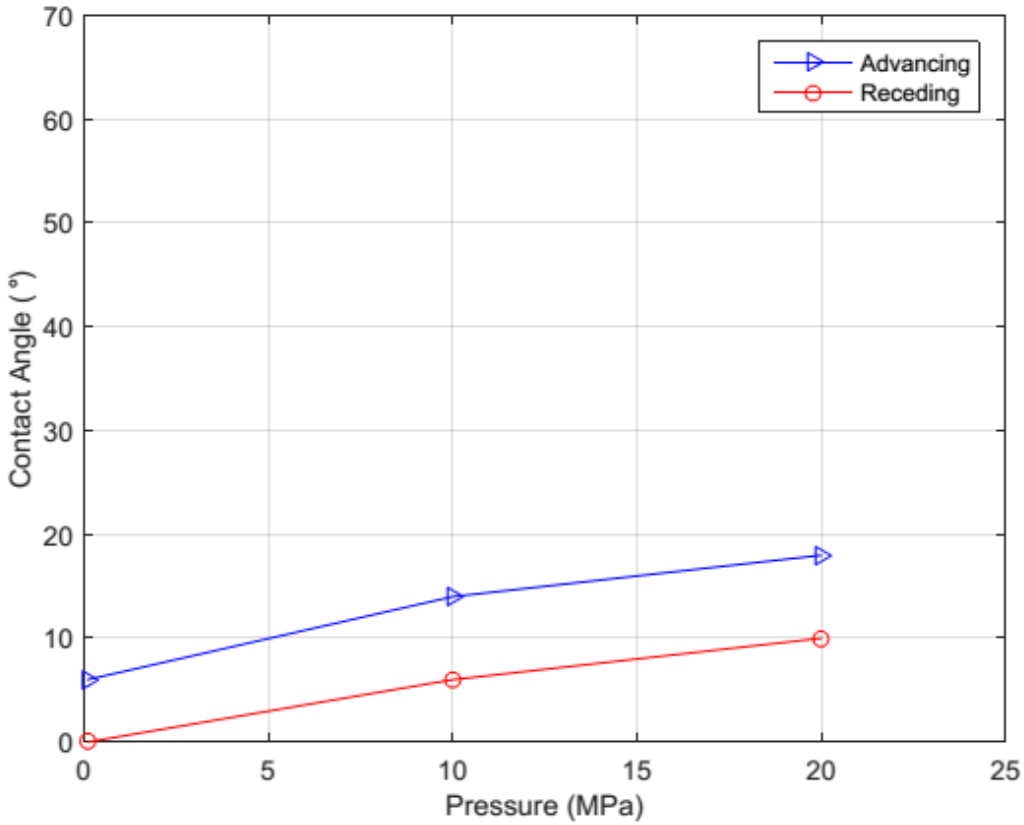

Fig. 8. n-Decane contact angles in air measured at different pressures (0.1, 10 and 20 MPa) at 70°C.

5. Discussion

Recall that in Fig. 2, it is seen that for the set of data used for the analysis, the contribution of the second term of the RHS of equation 8 on the contact angle (related to charged surfaces) increases with increase in the surface potential. At some surface potential (-12 mV here), the contribution of both terms (RHS of equation 8) to the contact angle are the same and as the surface potential reduces, the contribution of the charged surface term decreases dramatically. Based on the results obtained for the extracted data, when the surface charge falls below -7 mV, the second term of equation 8 can be comfortably neglected. Having above discussion in mind, the variations in contact angle with ion type, ionic concentration, pressure and temperature in the context of the proposed model (Eq. 8) are discussed below.

5.1 Effect of pressure on contact angle

Pressure has a profound effect on contact angle, both on charged and neutral surfaces. When examining Eq. 8, it is clear that several parameters are a function of pressure. For instance, the increase in pressure slightly affects the interfacial tension between the fluids [41] along with the dielectric constant of the liquid (D_f) [42]; however the main effect occurs through the change in the density difference induced by change in pressure [43]. Increasing pressure significantly reduces this density difference and causes the contact angle to increase [38] e.g ρ_{lf} variation with pressure is insignificant compared to ρ_g which considerably increases with pressure increase thus reducing $\Delta\rho(=\rho_{lf}-\rho_g)$. This is well-supported by our data and experimental literature data [22, 23, 28, 44-46] as well as molecular dynamics data [26, 47-49] reported previously.

5.2 Effect of temperature on contact angle

Temperature increased the contact angle for all cases (Figure 6), consistent with most literature data [22, 50-52]; however, there are other works [45, 53, 54] which show that the contact angle decreases with temperature.

Theoretically, based on Eq. 8, the contact angle is a function of temperature through several parameters among which the dielectric constant of the solution (D_f), the interfacial tension (γ_{lg}) between the fluids, the density difference between the phases ($\Delta\rho$) and temperature (*T*) itself are the main parameters. The effect of temperature on D_f [42] is relatively insignificant compared to its effect on the density difference, interfacial tension between fluids [55] and temperature by itself.

While the contact angle decreases with temperature itself and due to decrease in γ_{lg} with temperature, it increases due to decrease in density difference by temperature increase. The gas density slightly decreases with temperature increase (for the temperature range investigated herein) and if ρ_{lf} is assumed constant, the density difference ($\Delta\rho=\rho_{lf}-\rho_g$) increases with increase in pressure. However ρ_{lf} decreases significantly with temperature increment [38] e.g. ρ_{lf} is a function of gas

and liquid densities as well as substrate forces at microscale. This in turn leads to decrease in density difference by temperature increase leading to an increase in contact angle.

In the cases investigated in this study the contact angle increased with temperature which shows that the effect of temperature on ρ_{lf} over compensated the effect of temperature on γ_{lg} and temperature itself and thus caused the contact angle to increase. A further change in contact angle can take place by microscopic change in the van der Waals potential by temperature changes; however, this effect is neglected herein as such microscopic interactions are not yet fully understood.

5.3 Effect of ion concentration on contact angle

The contact angle consistently increased with increasing ionic concentration. This effect is primarily caused by two main parameters (equation 8): the ionic concentration (n) itself and D_f. D_f decreases with increasing n. Thus both effects result in a contact angle increase with increasing *n*, consistent with literature data [45, 50, 51, 53, 56].

5.4 Effect of ion type on contact angle

Our results (Figures 4-6) show that $MgCl_2$ produced the highest contact angles followed by $CaCl_2$, NaCl and KCl at any pressure, temperature and ionic concentration, consistent with literature data [21, 45, 56-58]. This is also consistent with the theory (equation 8), which predicts that an increase in ion valency increases the contact angle.

If the same valency is considered, for instance Na^+ and K^+, the variation in contact angle can be attributed to a change in solution dielectric constant (D_f), (Eq. 8). D_f of NaCl is lower than D_f of KCl e.g. D_f of 1M NaCl is 63 while D_f of 1M KCl is 70 [18]. A lower D_f consequently increases the contact angle (equation 8) as seen from Figs 4-6. However, the contact angle also depends on in-situ ionic concentration as well as ion adsorption on the mineral surfaces and the subsequent ion exchange. The bivalent ions (Ca^{2+} and Mg^{2+}) for instance can be strongly

adsorbed on clay surfaces (part of the shale) and reduce the surface potential [31]. This can in turn increase the contact angle although the effect of such interactions on contact angle are not yet fully understood.

5.5 Decane-air system: effect of pressure and temperature on contact angle

When oil (n-decane) is used as the liquid phase, the contact angle is not significantly influenced by the surface potential of the mineral (when compared to aqueous solutions), and therefore Young's equation is assumed valid. Consequently the parameters mostly affected by pressure and temperature variation are oil-air interfacial tension and air-oil density difference and therefore less variation in contact angles is expected. The pressure increase significantly reduces the density difference between the phases, which leads to an increase in contact angle. Furthermore, the effect of pressure on contact angle is stronger than the effect of temperature due to the fact that density difference is more sensitive to pressure changes than temperature [59] which is also supported by the results of this study (Tables 2 and 3).

6. Conclusions

The capillary process has been proposed as one of the main mechanisms involved in water uptake into shale reservoirs [12] and we have therefore conducted a suite of contact angle measurements on a shale sample with oil and aqueous solutions with different ion types and concentrations, pressures and temperatures to evaluate the wettability of shale at reservoir conditions. We systematically measured advancing and receding water contact angles on shale in air. The effect of different salt types (NaCl, KCl, $MgCl_2$, $CaCl_2$) and salt concentrations (0.1, 0.5 and 1 M), pressures (range 0.1, 10 and 20 MPa) and temperatures (35 °C and 70 °C) were examined. Furthermore, the contact angles of decane on shale in air were also measured as a function of temperature and pressure and compared with the water contact angles.

Generally, the water contact angles for solutions with higher ionic strength were higher: addition of $CaCl_2$ or $MgCl_2$ led to higher contact angles than addition of NaCl or KCl (same 0.1, 0.5 and 1 M concentrations), and increasing salt

concentration led to an increase in contact angle (from 17 to 30 ° for NaCl solution when moving from 0.1 to 1 M for instance); consistent with literature data [51, 53, 56, 60]. Moreover, oil and water contact angles both increased with pressure and/or temperature increase; this increase was more pronounced at higher ionic concentration. For instance an increase in pressure from 0.1 MPa to 20 MPa at constant temperature of 70 °C increased the contact angle of 1M $CaCl_2$ solution from 32 to 57 ° while a decrease in temperature from 70 °C to 35 °C reduced the contact angle from 57 to 36 °.

Finally, a physical model based on the diffuse double layer theory was developed to provide a theoretical framework for the observed behaviour of the systems analysed. The model correctly predicted the influence of the different variables (ion type, ionic concentration, temperature and pressure) and can be used to describe the physical phenomena behind the results obtained in a qualitative framework. A quantitative analysis can also be performed with the proposed model to predict the contact angle if all parameters needed are available. Knowing contact angle and therefore wettability, the contribution of the capillary process in terms of water uptake into shale rocks can be quantified, which in turn addresses the technical issue of gas production impairment by water uptake, as well as the environmental issue of disappearance of hydraulic fracturing fluid e.g. for instance an oil-wet shale can become water-wet when moving from atmospheric to reservoir conditions. Furthermore, increased contact angles are also relevant for CO2 geo-storage as they reduce structural storage capacities [28, 61].

References

[1] B.E. Law, J.B. Curtis, Introduction to unconventional petroleum systems, AAPG Bulletin, 86 (2002) 1851-1852.

[2] U.S.E.I.A. EIA, World Shale Resource Assessments, 2015.

[3] H. Roshan, M. Sarmadivaleh, S. Iglauer, Shale fracture surface area measured by tracking exchangeable cations, Journal of Petroleum Science and Engineering, 138 (2016) 97-103.

[4] O. Arogundade, M. Sohrabi, A Review of Recent Developments and Challenges in Shale Gas Recovery, SPE Saudi Arabia Section Technical Symposium and Exhibition, Society of Petroleum Engineers, Al-Khobar, Saudi Arabia, 2012.

[5] A.B. Yost, W.K. Overbey, Jr., Production and Stimulation Analysis of Multiple Hydraulic Fracturing of a 2,000-ft Horizontal Well, SPE Gas Technology Symposium, Society of Petroleum Engineers, Dallas, Texas, 1989.

[6] K. Makhanov, A. Habibi, H. Dehghanpour, E. Kuru, Liquid uptake of gas shales: A workflow to estimate water loss during shut-in periods after fracturing operations, Journal of Unconventional Oil and Gas Resources, 7 (2014) 22-32.

[7] H. Roshan, S. Ehsani, C.E. Marjo, M.S. Andersen, R.I. Acworth, Mechanisms of water adsorption into partially saturated fractured shales: An experimental study, Fuel, 159 (2015) 628-637.

[8] M. Binazadeh, M. Xu, A. Zolfaghari, H. Dehghanpour, Effect of Electrostatic Interactions on Water Uptake of Gas Shales: The Interplay of Solution Ionic Strength and Electrostatic Double Layer, Energy & Fuels, DOI 10.1021/acs.energyfuels.5b02990(2016).

[9] H. Dehghanpour, Q. Lan, Y. Saeed, H. Fei, Z. Qi, Spontaneous Imbibition of Brine and Oil in Gas Shales: Effect of Water Adsorption and Resulting Microfractures, Energy & Fuels, 27 (2013) 3039-3049.

[10] H. Dehghanpour, H.A. Zubair, A. Chhabra, A. Ullah, Liquid Intake of Organic Shales, Energy & Fuels, 26 (2012) 5750-5758.

[11] L. Yang, H. Ge, X. Shi, Y. Cheng, K. Zhang, H. Chen, Y. Shen, J. Zhang, X. Qu, The effect of microstructure and rock mineralogy on water imbibition characteristics in tight reservoirs, Journal of Natural Gas Science and Engineering, DOI http://dx.doi.org/10.1016/j.jngse.2016.01.002.

[12] B. Roychaudhuri, T.T. Tsotsis, K. Jessen, An experimental investigation of spontaneous imbibition in gas shales, Journal of Petroleum Science and Engineering, 111 (2013) 87-97.

[13] S. Takahashi, A.R. Kovscek, Spontaneous countercurrent imbibition and forced displacement characteristics of low-permeability, siliceous shale rocks, Journal of Petroleum Science and Engineering, 71 (2010) 47-55.

[14] H. Roshan, M.S. Andersen, H. Rutlidge, C.E. Marjo, R.I. Acworth, Investigation of the kinetics of water uptake into partially saturated shales, Water Resources Research, DOI 10.1002/2015WR017786(2016) n/a-n/a.

[15] E. Ghanbari, H. Dehghanpour, Impact of rock fabric on water imbibition and salt diffusion in gas shales, International Journal of Coal Geology, 138 (2015) 55-67.
[16] T. Engelder, L.M. Cathles, L.T. Bryndzia, The fate of residual treatment water in gas shale, Journal of Unconventional Oil and Gas Resources, 7 (2014) 33-48.

[17] P. Fakcharoenphol, B. Kurtoglu, H. Kazemi, S. Charoenwongsa, Y.-S. Wu, The Effect of Osmotic Pressure on Improve Oil Recovery from Fractured Shale Formations, SPE Unconventional Resources Conference, Society of Petroleum Engineers, Woodlands, Texas, 2014.

[18] A. Levy, D. Andelman, H. Orland, Dielectric Constant of Ionic Solutions: A Field-Theory Approach, Physical Review Letters, 108 (2012) 227801.

[19] M. Xu, H. Dehghanpour, Advances in Understanding Wettability of Gas Shales, Energy & Fuels, 28 (2014) 4362–4375.

[20] V. Mirchi, S. Saraji, L. Goual, M. Piri, Dynamic Interfacial Tensions and Contact Angles of Surfactant-in-Brine/Oil/Shale Systems: Implications to Enhanced Oil Recovery in Shale Oil Reservoirs, SPE Improved Oil Recovery Symposium, Society of Petroleum Engineers, Tulsa, Oklahoma, USA, 2014.

[21] A. Al-Yaseri, M. Sarmadivaleh, A. Saeedi, M. Lebedev, A. Barifcani, S. Iglauer, N2+CO2+NaCl brine interfacial tensions and contact angles on quartz at CO2 storage site conditions in the Gippsland basin, Victoria/Australia, Journal of Petroleum Science and Engineering, 129 (2015) 58-62.

[22] M. Sarmadivaleh, A.Z. Al-Yaseri, S. Iglauer, Influence of temperature and pressure on quartz–water–CO2 contact angle and CO2–water interfacial tension, Journal of Colloid and Interface Science, 441 (2015) 59-64.

[23] J.L. Dickson, G. Gupta, T.S. Horozov, B.P. Binks, K.P. Johnston, Wetting Phenomena at the CO2/Water/Glass Interface, Langmuir, 22 (2006) 2161-2170.

[24] D. Broseta, N. Tonnet, V. Shah, Are rocks still water-wet in the presence of dense CO2 or H2S?, Geofluids, 12 (2012) 280-294.

[25] P. Chiquet, D. Broseta, S. Thibeau, Wettability alteration of caprock minerals by carbon dioxide, Geofluids, 7 (2007) 112-122.

[26] J.-W. Jung, J. Wan, Supercritical CO2 and Ionic Strength Effects on Wettability of Silica Surfaces: Equilibrium Contact Angle Measurements, Energy & Fuels, 26 (2012) 6053-6059.

[27] N. Shojai Kaveh, K.H. Wolf, S.N. Ashrafizadeh, E.S.J. Rudolph, Effect of coal petrology and pressure on wetting properties of wet coal for CO2 and flue gas storage, International Journal of Greenhouse Gas Control, 11, Supplement (2012) S91-S101.

[28] S. Iglauer, A.Z. Al-Yaseri, R. Rezaee, M. Lebedev, CO2 wettability of caprocks: Implications for structural storage capacity and containment security, Geophysical Research Letters, DOI 10.1002/2015GL065787(2015) n/a-n/a.

[29] S. Iglauer, A. Salamah, M. Sarmadivaleh, K. Liu, C. Phan, Contamination of silica surfaces: Impact on water–CO2–quartz and glass contact angle measurements, International Journal of Greenhouse Gas Control, 22 (2014) 325-328.

[30] L.M. Lander, L.M. Siewierski, W.J. Brittain, E.A. Vogler, A systematic comparison of contact angle methods, Langmuir, 9 (1993) 2237-2239.

[31] J.K. Mitchell, K. Soga, Fundamentals of Soil Behavior, third ed., WILEY2005.

[32] H.J.J. Verheijen, M.W.J. Prins, Reversible Electrowetting and Trapping of Charge: Model and Experiments, Langmuir, 15 (1999) 6616-6620.

[33] S. Berry, J. Kedzierski, B. Abedian, Low voltage electrowetting using thin fluoroploymer films, Journal of Colloid and Interface Science, 303 (2006) 517-524.

[34] F.M. Francisca, D. Fratta, H.F. Wang, Electrowetting on mineral and rock surfaces, Geophysical Research Letters, 35 (2008) n/a-n/a.

[35] H. Roshan, M. Aghighi, Analysis of Pore Pressure Distribution in Shale Formations under Hydraulic, Chemical, Thermal and Electrical Interactions, Transport in Porous Media, DOI 10.1007/s11242-011-9891-x(2011) 1-21.

[36] A. Martinez, A. Byrnes, Modeling Dielectric-constant values of Geologic Materials: An Aid to Ground-Penetrating Radar Data Collection and Interpretation, Current Research in Earth Sciences, 247 (2002).

[37] R. Garcia, K. Osborne, E. Subashi, Validity of the “Sharp-Kink Approximation” for Water and Other Fluids, The Journal of Physical Chemistry B, 112 (2008) 8114-8119.

[38] A.Z. Al-Yaseri, H. Roshan, M. Lebedev, A. Barifcani, S. Iglauer, Dependence of quartz wettability on fluid density, Geophysical Research Letters, DOI 10.1002/2016GL068278(2016).

[39] J. Möller, Martin A. Schroer, M. Erlkamp, S. Grobelny, M. Paulus, S. Tiemeyer, Florian J. Wirkert, M. Tolan, R. Winter, The Effect of Ionic Strength, Temperature, and Pressure on the Interaction Potential of Dense Protein Solutions: From Nonlinear Pressure Response to Protein Crystallization, Biophysical Journal, 102 (2012) 2641-2648.

[40] M.S. Seyfried, L.E. Grant, Temperature Effects on Soil Dielectric Properties Measured at 50 MHz, Vadose Zone Journal, 6 (2007) 759-765.

[41] O.S. Hjelmeland, L.E. Larrondo, Experimental Investigation of the Effects of Temperature, Pressure, and Crude Oil Composition on Interfacial Properties, SPE Reservoir Eng, 1 (1986).

[42] W.B. Floriano, M.A.C. Nascimento, Dielectric constant and density of water as a function of pressure at constant temperature, Brazilian Journal of Physics, 34 (2004) 38-41.

[43] A. Georgiadis, G. Maitland, J.P.M. Trusler, A. Bismarck, Interfacial Tension Measurements of the (H2O + CO2) System at Elevated Pressures and Temperatures, Journal of Chemical & Engineering Data, 55 (2010) 4168-4175.

[44] S. Saraji, L. Goual, M. Piri, H. Plancher, Wettability of Supercritical Carbon Dioxide/Water/Quartz Systems: Simultaneous Measurement of Contact Angle and Interfacial Tension at Reservoir Conditions, Langmuir, 29 (2013) 6856-6866.

[45] M. Arif, A.Z. Al-Yaseri, A. Barifcani, M. Lebedev, S. Iglauer, Impact of pressure and temperature on CO2–brine–mica contact angles and CO2–brine interfacial tension: Implications for carbon geo-sequestration, Journal of Colloid and Interface Science, 462 (2016) 208-215.

[46] A. Ameri, N.S. Kaveh, E.S.J. Rudolph, K.H. Wolf, R. Farajzadeh, J. Bruining, Investigation on Interfacial Interactions among Crude Oil–Brine–Sandstone Rock–CO2 by Contact Angle Measurements, Energy & Fuels, 27 (2013) 1015-1025.

[47] J. McCaughan, S. Iglauer, F. Bresme, Molecular Dynamics Simulation of Water/CO2-quartz Interfacial Properties: Application to Subsurface Gas Injection, Energy Procedia, 37 (2013) 5387-5402.

[48] S. Iglauer, M.S. Mathew, F. Bresme, Molecular dynamics computations of brine–CO2 interfacial tensions and brine–CO2–quartz contact angles and their effects on structural and residual trapping mechanisms in carbon geo-sequestration, Journal of Colloid and Interface Science, 386 (2012) 405-414.

[49] M. Sedghi, M. Piri, L. Goual, Molecular dynamics of wetting layer formation and forced water invasion in angular nanopores with mixed wettability, The Journal of Chemical Physics, 141 (2014) 194703.

[50] A.Z. Al-Yaseri, M. Lebedev, A. Barifcani, S. Iglauer, Receding and advancing (CO2 + brine + quartz) contact angles as a function of pressure, temperature, surface roughness, salt type and salinity, The Journal of Chemical Thermodynamics, in press (2015).

[51] R. Farokhpoor, B.J.A. Bjørkvik, E. Lindeberg, O. Torsæter, Wettability behaviour of CO2 at storage conditions, International Journal of Greenhouse Gas Control, 12 (2013) 18-25.

[52] D. Yang, Y. Gu, P. Tontiwachwuthikul, Wettability Determination of the Crude Oil−Reservoir Brine−Reservoir Rock System with Dissolution of CO 2 at High Pressures and Elevated Temperatures, Energy & Fuels, 22 (2008) 2362-2371.

[53] S. Saraji, M. Piri, L. Goual, The effects of SO2 contamination, brine salinity, pressure, and temperature on dynamic contact angles and interfacial tension of supercritical CO2/brine/quartz systems, International Journal of Greenhouse Gas Control, 28 (2014) 147-155.

[54] M. de Ruijter, P. Kölsch, M. Voué, J. De Coninck, J.P. Rabe, Effect of temperature on the dynamic contact angle, Colloids and Surfaces A: Physicochemical and Engineering Aspects, 144 (1998) 235-243.

[55] C. Jho, D. Nealon, S. Shogbola, A.D. King, Effect of pressure on the surface tension of water: Adsorption of hydrocarbon gases and carbon dioxide on water at temperatures between 0 and 50°C, Journal of Colloid and Interface Science, 65 (1978) 141-154.

[56] F. Mugele, I. Siretanu, N. Kumar, B. Bera, L. Wang, R. de Ruiter, A. Maestro, M. Duits, D. van den Ende, I. Collins, Insights From Ion Adsorption and Contact-Angle Alteration at Mineral Surfaces for Low-Salinity Waterflooding, SPE, DOI 10.2118/169143-PA(2016).

[57] S. Saraji, L. Goual, M. Piri, Dynamic adsorption of asphaltenes on quartz and calcite packs in the presence of brine films, Colloids and Surfaces A: Physicochemical and Engineering Aspects, 434 (2013) 260-267.

[58] F. Mugele, B. Bera, A. Cavalli, I. Siretanu, A. Maestro, M. Duits, M. Cohen-Stuart, D. van den Ende, I. Stocker, I. Collins, Ion adsorption-induced wetting transition in oil-water-mineral systems, Scientific Reports, 5 (2015) 10519.

[59] R. Battino, T.R. Rettich, T. Tominaga, The Solubility of Nitrogen and Air in Liquids, Journal of Physical and Chemical Reference Data, 13 (1984) 563-600.

[60] A.Z. Al-Yaseri, M. Lebedev, A. Barifcani, S. Iglauer, Receding and advancing (CO2 + brine + quartz) contact angles as a function of pressure, temperature, surface roughness, salt type and salinity, The Journal of Chemical Thermodynamics, 93 (2016) 416-423.

[61] S. Iglauer, C.H. Pentland, A. Busch, CO2 wettability of seal and reservoir rocks and the implications for carbon geo-sequestration, Water Resources Research, 51 (2015) 729-774.

[62] N. Gavish, K. Promislow, Dependence of the dielectric constant of electrolyte solutions on ionic concentration, Chemical Physics, arXiv:1208.5169 [physics.chem-ph] (2012) 1-5.

[63] J.J. Sweeney, J.J. Roberts, P.E. Harben, Study of Dielectric Properties of Dry and Saturated Green River Oil Shale, Energy & Fuels, 21 (2007) 2769-2777.
[64] N.L. Jarvis, M.A. Scheiman, Surface potentials of aqueous electrolyte solutions, The Journal of Physical Chemistry, 72 (1968) 74-78.

5.9 Impact of Fines and Rock Wettability on Reservoir Formation Damage

Al-Yaseri, A.Z., Hani A., Lebedev, Barifcani, A. and Iglauer, S., 2016. Impact of fines and rock wettability on Reservoir formation damage. Journal of Geophysical Prospecting, 64, pp 860-874.

Impact of fines and rock wettability on Reservoir formation damage

Ahmed Al-Yaseri[1*], Hani Al-Mukainah[1], Maxim Lebedev[2], Ahmed Barifcani[3], and Stefan Iglauer[1]

[1]Curtin University, Department of Petroleum Engineering, 26 Dick Perry Avenue, 6151 Kensington, Australia

[2]Curtin University, Department of Exploration Geophysics, 26 Dick Perry Avenue, 6151 Kensington, Australia

[3]Curtin University, Department of Chemical Engineering, 26 Dick Perry Avenue, 6151 Kensington, Australia

Abstract

Pore throat plugging of porous rock by fine particles causes formation damage, and thus has attracted attention in various areas such as petroleum engineering, hydrology and geothermal energy production. Despite significant efforts, the detailed pore-scale mechanisms leading to formation damage and the associated permeability reduction are not well understood. We thus investigated plugging mechanisms and characteristics with a combination of *ex-situ* (coreflooding measurements, SEM imaging) and *in-situ* (NMR, μCT) methods, with a particular focus on the effect of wettability.

The corefloods indicated that permeability drops rapidly when fines are injected; mechanistically thin pore throats are plugged first, followed by filling of adjacent pore bodies with the fine material (as evidenced by the NMR and μCT experiments, which can measure the pore size distribution evolution with fines injection). Furthermore, it is clear that wettability plays a major role: if fines and rock wettability is identical, plugging is significantly accelerated; wettability also controls the 3D distribution of the fines in the pore space. Furthermore we note that the deposited fines were tightly packed, apparently due to strong adhesion forces.

Keywords

Formation damage, fines migration, wettability, Bentheimer, micro-computed tomography, plugging

1. Introduction

Fines migration and plugging of pores and pore throats by solid particles can be caused by drilling, completion, cementing, perforation, workover, stimulation, and injection of water and chemicals for enhanced oil recovery, with the potential consequence of significant reduction in rock permeability (Civan 2007; Kalfayan 2008). Such plugging may also result from proppant crushing at high fracture closure pressure during hydraulic fracturing (Kalfayan, 2008). Furthermore, fines are mobilized if the critical flow velocity (i.e. the critical value of viscous forces) for a particular rock is reached and particles detach from the matrix (Civan 2007). Krueger (1988), Economides and Nolte (1987), and Amaerule *et al.* (1988) indicated that migration of formation fines is the major factor for permeability damage, and it is well established that the induced permeability impairment strongly depends on particle and pore space geometry (e.g. Muecke 1979; Civan 2007; Al-Yaseri *et al.* 2015).

Generally, this damage is a problem in a variety of fields, ranging from water production (McDowell-Boyer *et al.* 1986; Torkzaban *et al.* 2007; Bradford *et al.* 2011), geothermal energy efficiency (Mahmoudi *et al.* 2010; Rosenbrand *et al.* 2014, 2015), hydrocarbon recovery (Ahmed and McKinney 2005; Iglauer *et al.* 2010) to carbon geo-storage (Iglauer *et al.* 2014).

Another factor influencing fines migration is wettability; in two-phase flow experiments Muecke (1979) found that calcium carbonate particles (2 to 15 μm size) migrated faster through quartz sand packs if the phase that wets them is moving. Sarkar and Sharma (1990) investigated fines migration in single phase and two phase flow through Berea sandstone, and they found that formation damage was significantly lower in two-phase flow (permeability ratio reduced from 1 to 0.04 compared with a reduction from 1 to 0.0016 in single phase flow). However, there is a lack of analysis in terms of how combinations of rock-fines wettability affect formation damage, and particularly *in-situ* experiments. Considering that wettability of petroleum reservoirs can vary widely (Cuiec 1984, Buckley *et al.* 1997, Buckley and Monsterleet 1998), and that wettability at the wellbore can be altered by drilling, completion and flooding fluids (Culec 1984; Sharma and Wunderlich 1987; Kalfayan 2008) this factor requires further attention.

We thus investigated formation damage mechanisms for various wettability combinations (water-wet rock/water-wet fines; water-wet rock/oil-wet fines; oil-wet rock/water-wet fines; oil-wet rock/oil-wet fines) with a range of experimental techniques, including high resolution micro-computed tomography (µCT) imaging, nuclear magnetic resonance (NMR) measurements, standard core flooding, and scanning electron microscopy (SEM) methods.

2. Experimental Methodology

2.1 Materials

Four homogeneous cylindrical Bentheimer sandstone plugs were drilled from the same block; these sister plugs had the same brine permeability (1.7 Darcy) and porosity (23%), Table 1. The composition of the Bentheimer sandstone was measured via XRD (Kaolinite 0.7 wt%, Quartz 99 wt%, Rutile 0.3 wt%; Al-Yaseri *et al.* 2015); the sandstone was thus quite clean and consisted mainly of quartz.

Fine Barite particles with a size distribution of 0.3-45µm which peaked at 26µm (measured with a Mastersizer Malvern Hydro 2000S, Figure 1) were used as a representative for the fines in the subsurface (Krilov *et al.* 1991; Tran *et al.* 2010). These Barite particles were suspended in brine (5wt% NaCl + 1 wt% KCl in deionized water) by continuous agitation with a magnetic stirrer. The rheological properties of this suspension were measured with an Anton Paar RheolabQC viscometer (Figures 2 and 3); the suspension was shear thickening as expected (Robertson and Stiff 1976).

Two of the Bentheimer plugs were left in the original state (i.e. strongly water-wet), but the remaining two plugs were aged in Triethoxy(octyl)silane (Grate *et al.* 2012) for one month at ambient conditions and then left to dry at room temperature for a week. Advancing (115^o) and receding (95^o) water contact angles were measured on the rock at ambient conditions (in air) using the tilted plate method (Al-Yaseri *et al.* 2016), this clearly indicated that the Bentheimer plugs turned oil-wet (Dake 1978).This process rendered the sandstone surface oil-wet by silylation (Hendraningrat and Torsæter 2014). Several Barite particle batches were also

rendered oil-wet using the same aging method (note: virgin Barite is water-wet, Fenter *et al.* 2001).

Table 1 Bentheimer sandstone properties**,** all samples have the same brine permeability (1.7 Darcy) and porosity (23%).

Plug no.	Absolute Permeability [Darcy]	Core length [cm]	Core Diameter [cm]	Bentheimer wettability	Barite wettability
1	1.7	1.7	0.5	Water-wet	Water-wet
2	1.7	1.3	0.5	Oil-wet	Oil-wet
3	1.7	1.4	0.5	Water-wet	Oil-wet
4	1.7	1.7	0.5	Oil-wet	Water-wet

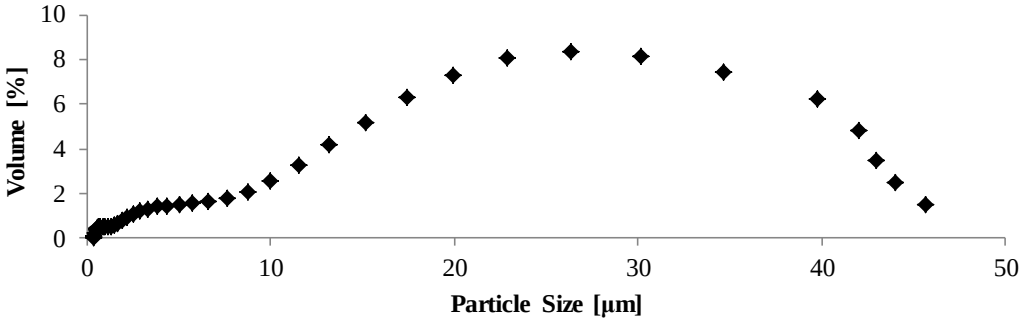

Figure 1. Particle size distribution of Barite powder used in the experiments.

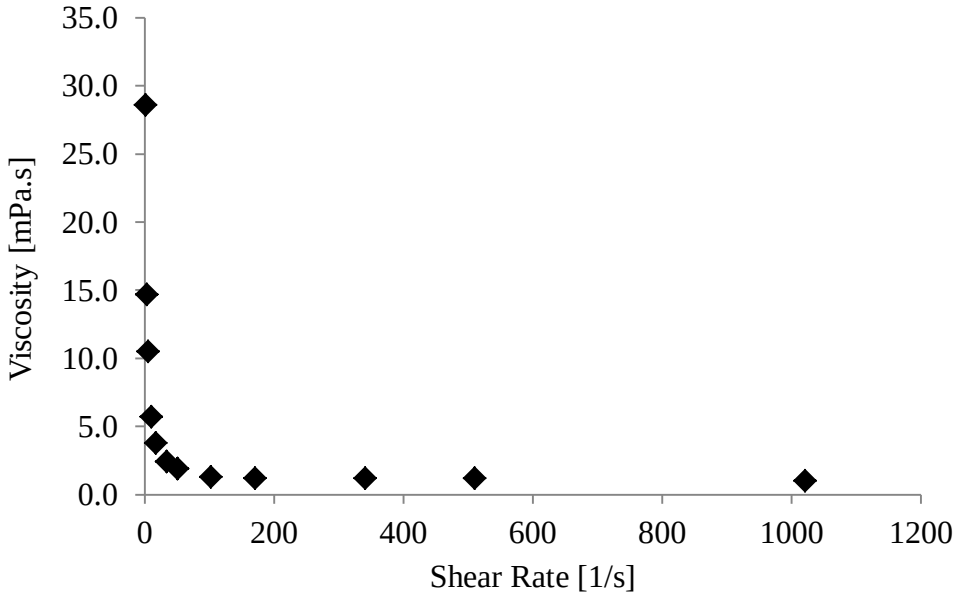

Figure 2 Viscosity of 10 g/L Barite suspension in brine as a function of shear rate at ambient conditions.

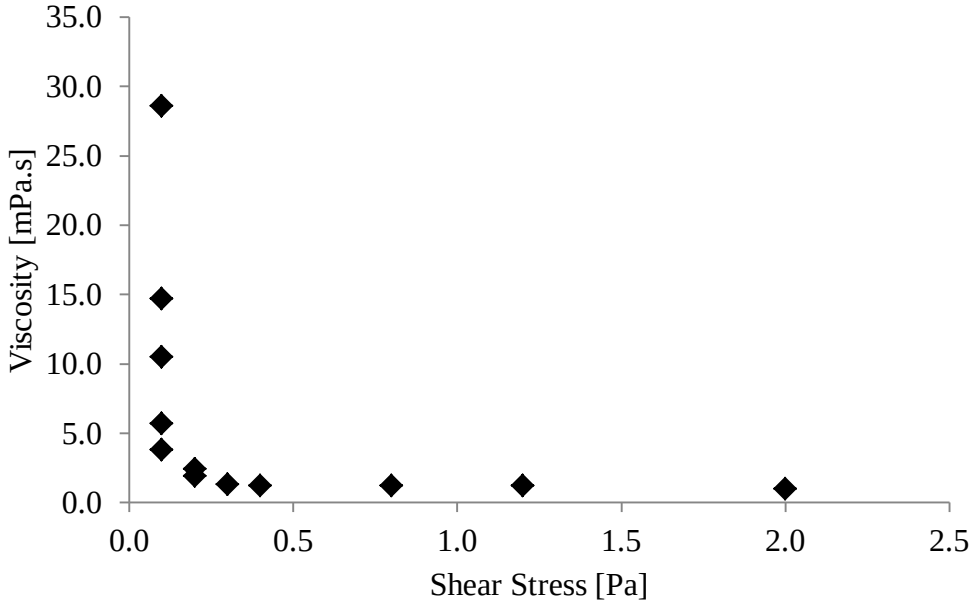

Figure 3 Viscosity of 10 g/L Barite suspension in brine as a function of shear stress at ambient conditions.

All plugs were imaged with a μCT scanner (Xradia Versa XRM-500T) at a constant high resolution of $(3.4\mu m)^3$, and NMR T_2 response curves were measured for each sample with a 20 MHz Bruker Minispec (1H resonance) instrument; these curves correlate with the pore size distribution in the core (Talabi *et al.* 2009; Fridjonsson *et al.* 2013). Subsequently these samples were sealed with a PTFE heat shrink sleeve at 653K for ~20min, vacuumed for 40 minutes and saturated with brine (note: oil-wet plugs were aged in silane after heating/flow cell construction). Afterwards the plugs were flooded with the brine suspension (10 g/L Barite concentration) at a constant Darcy flow rate (0.0127 m/s) using a peristaltic pump (Masterflex model 7518-10). The pressure drop across the plug was continuously measured, and the dynamic brine permeability was calculated with Darcy's law, Figure 4. In addition, the accumulative weight of produced fluid was measured as a function of time using a balance (Phoenix, BTA/BTB series, accuracy = 0.001g), Figure 5. Note that all experiments were performed at ambient conditions, i.e. 130000 Pa (±20000Pa) pressure and (296K ±1K) temperature. Suspension injection was stopped when the permeability was reduced by ~90%, and the plugs were again scanned by μCT and NMR.

Petrophysical properties (porosity, pore volumes, and pore size distributions) for each plug before and after damage were measured on the μCT images; the μCT images were filtered with a 3D non-local means filter (Buades 2005) and segmented with a watershed algorithm (Schlüter et al. 2014) prior to analysis. Moreover, SEM images were acquired for the plugs before and after damage: interior sections of the plugs were cut out, dried and gold-spray-coated. The microstructure was then observed at different magnifications with a MIRA3 FESEM-TESCAN instrument. Note that μCT images in combination with SEM imaging can provide detailed information in terms of where fines migrated, and how they interact with the rock (Al-Yaseri *et al.* 2015).

3. Results and discussion

The results show that permeability (k) continuously and smoothly decreased with time (t) during fines suspension injection following power law correlations (Figure 4,

Table 2) $k=3.214t^{-0.441}$, Pearson coefficient R^2=0.88, (sample#1); $k=3t^{-0.499}$, R^2=0.95 (Sample#2), $k=4.39t^{-0.412}$, R^2=0.99 (Sample#3), $k=2.4t^{-0.385}$, R^2=0.98 (Sample#4), which is approximately consistent with literatures data (Nguyen and Civan, 2005; Tran *et al.* 2009; Tran *et al.* 2010; Al-Yaseri *et al.* 2015). It is interesting to note that the power-law exponent was always around -0.40 (± 0.045). Furthermore, permeabilities of Bentheimer plugs (sample#1 and sample#2), which had the same wettability as the injected Barite particles were significantly more damaged than the plugs (sample#3 and sample#4), where fine-rock wettability did not match.

Moreover, Figure 5 shows the plugging time, which is the point where the production curve slope changes (Tran *et al.* 2009; Tran *et al.* 2010). Plugging times were shorter for systems with the same wettability (2700s and 2600s), and longer for systems with different wettability (4000s and 3600s), cp. Table 2 for details. These production data are consistent with the permeability measurements, see above.

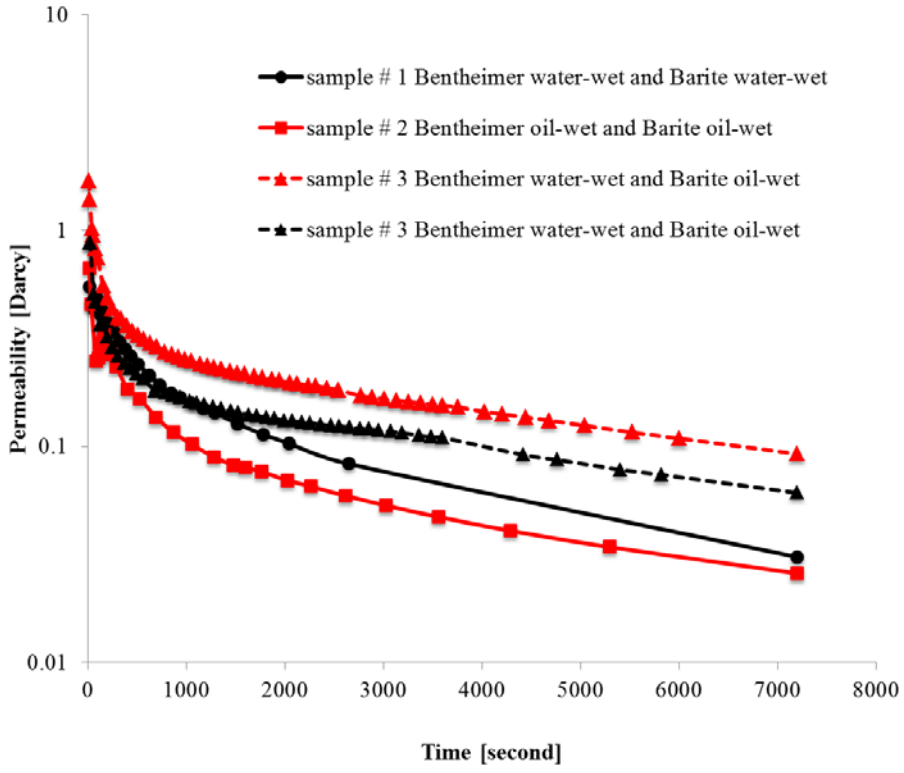

Figure 4 Dynamic permeability as a function of time for different rock-fine wettability conditions.

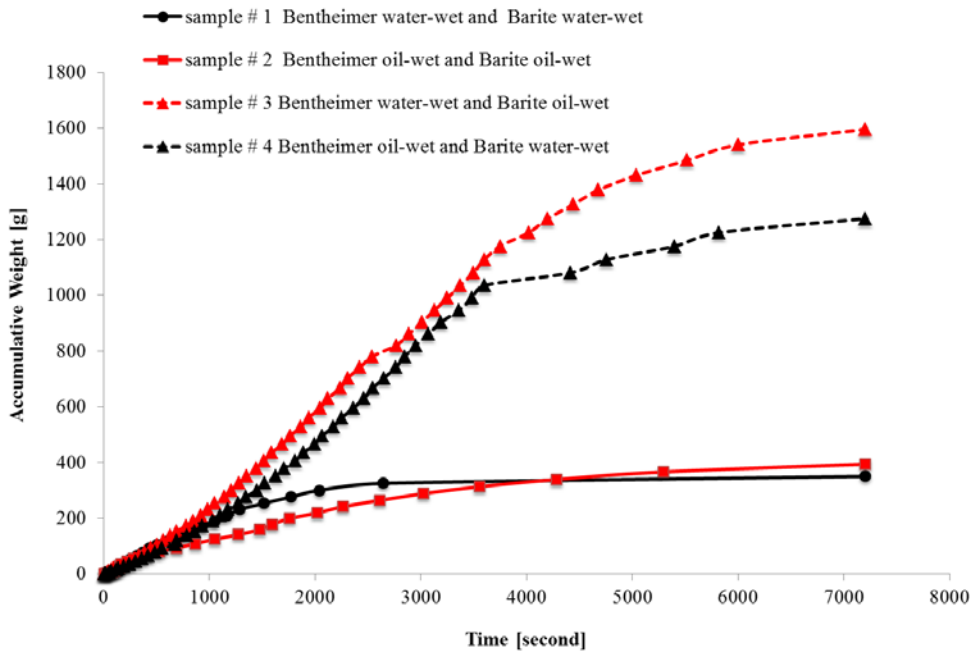

Figure 5 Accumulative weight of produced fluid as a function of time for different rock-fine wettability conditions.

Table 2 Plugging time for different rock-fine wettability conditions and associated statistics.

Sample No.	Wettability condition	Plugging time [sec]	Power law	Power law exponent
1	Bentheimer water-wet and Barite water-wet	2700	$k=3.214t^{-0.441}$	-0.441
2	Bentheimer oil-wet and Barite oil-wet	2600	$k=3t^{-0.499}$	-0.499
3	Bentheimer water-wet and Barite oil-wet	4000	$k=4.39t^{-0.412}$	-0.412
4	Bentheimer oil-wet and Barite water-wet	3600	$k=2.4t^{-0.385}$	-0.385

The NMR T_2 response curves for sample#1 (Bentheimer and Barite were water-wet) and sample#4 (Oil-wet Bentheimer and water-wet Barite) before and after damage are shown in Figures 6 and 7 respectively. These data show that the integral of the NMR T_2 signal (which corresponds to the amount of water in the pore space, and

thus porosity (Allen *et al.* 1997) shrunk significantly after fines injection, Table 3. Furthermore, the porosity of water-wet rock/water-wet fines (sample#1) was more reduced (by~ 35%) when compared with the oil-wet Bentheimer plug/water-wet Barite system (sample#4) (reduction by~22%), Table 3.

The samples (sample 1 and 2) before and after damage showed three different main pore sizes, the largest volume fraction was the largest pore size. The fines filled mainly the largest pores (shrinking of the largest peak at high T2 times), and generally reduced porosity. Although in both wettability cases the pore sizes were reduced, this was more pronounced in the water-wet/water-wet case. Here this effect was so strong that the main pore size strongly decreased, to an extend that the frequency of the medium sized pores actually increased (slightly).

Moreover, the clear reduction in the average NMR T_2 response time (which decreased from 0.66s before damage to 0.45s after damage for sample #1 (Bentheimer and Barite were water-wet), and from 0.66s to 0.55s for sample #4 (oil-wet Bentheimer and water-wet Barite)) indicate shrinking pore sizes (Talabi *et al.* 2009; Al-Yaseri *et al.* 2015).

The μCT images show that the undamaged Bentheimer plugs had pore sizes ranging from ~1-100μm (Figures 8-11). Fines deposition changed these size distributions towards smaller pore sizes. This shift was particularly significant if fine particle and core plug wettability was the same (samples 1 and 2). with Figures 8 and 9. Figures 8-11 also show that the count number of pore diameters <50μm after damage increased, particularly the count number of the smallest pores (<10μm); this increase was strong (same wettability) or moderate (different wettability). This implies that larger pores are split into smaller pores, and this result is consistent with the NMR (see above), and SEM measurements (see below), and literature data (Civan 2007; Tran *et al.* 2009; Tran *et al.* 2010; Al-Yaseri *et al.* 2015).

Table 3 Bentheimer sandstone porosities before and after fines injection.

Sample No.	Wettability condition	Damage state	Porosity measured by µCT [-]	Porosity measured by NMR [-]
1	Bentheimer water-wet and Barite water-wet	before damage	0.23	0.23*
		after damage	0.15	0.131
2	Bentheimer oil-wet and Barite oil-wet	before damage	0.23	0.23*
		after damage	0.14	0.131
3	Bentheimer water-wet and Barite oil-wet	before damage	0.23	0.23*
		after damage	0.17	0.182
4	Bentheimer oil-wet and Barite water-wet	before damage	0.23	0.23*
		after damage	0.18	0.182

*The initial porosity was set to the µCT porosity.

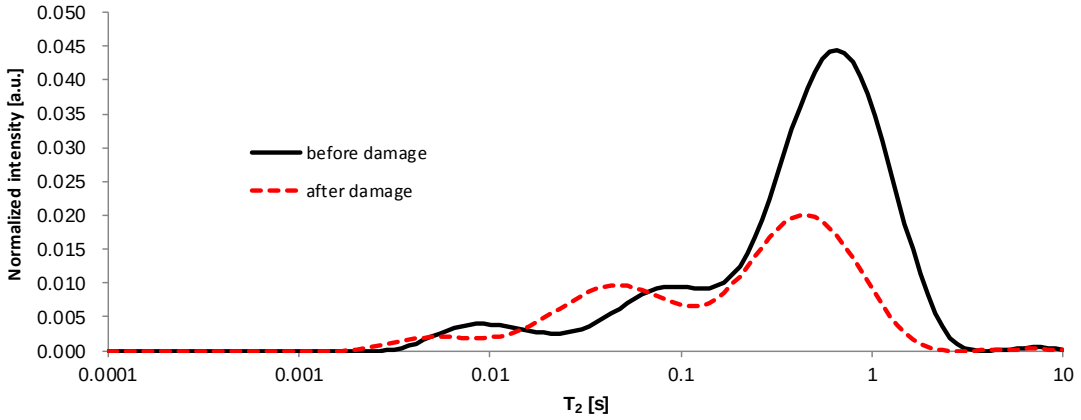

Figure 6 NMR T_2 response curves for sample #1 (water-wet Bentheimer and water-wet Barite) before and after fines suspension injection. Porosity was reduced from 23% to 15%.

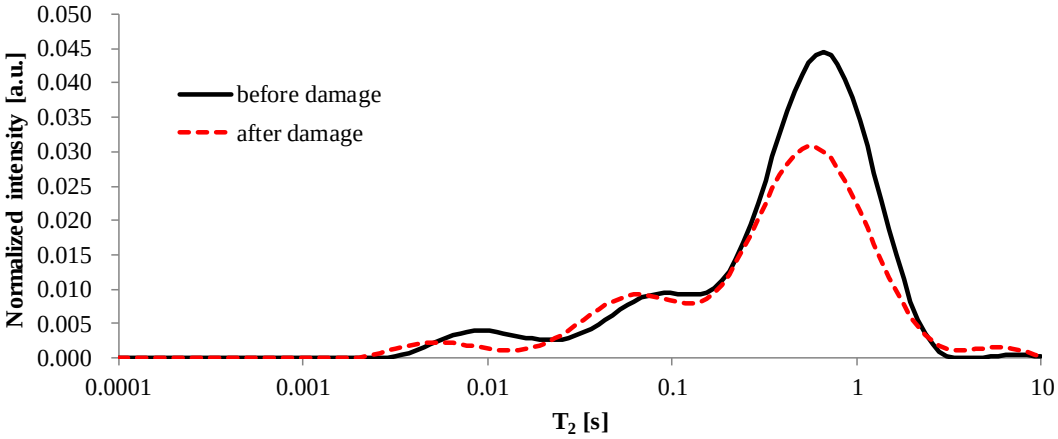

Figure 7 NMR T_2 response curves for sample #4 (oil-wet Bentheimer and water-wet Barite) before and after fines suspension injection. Porosity was reduced from 23% to 18%.

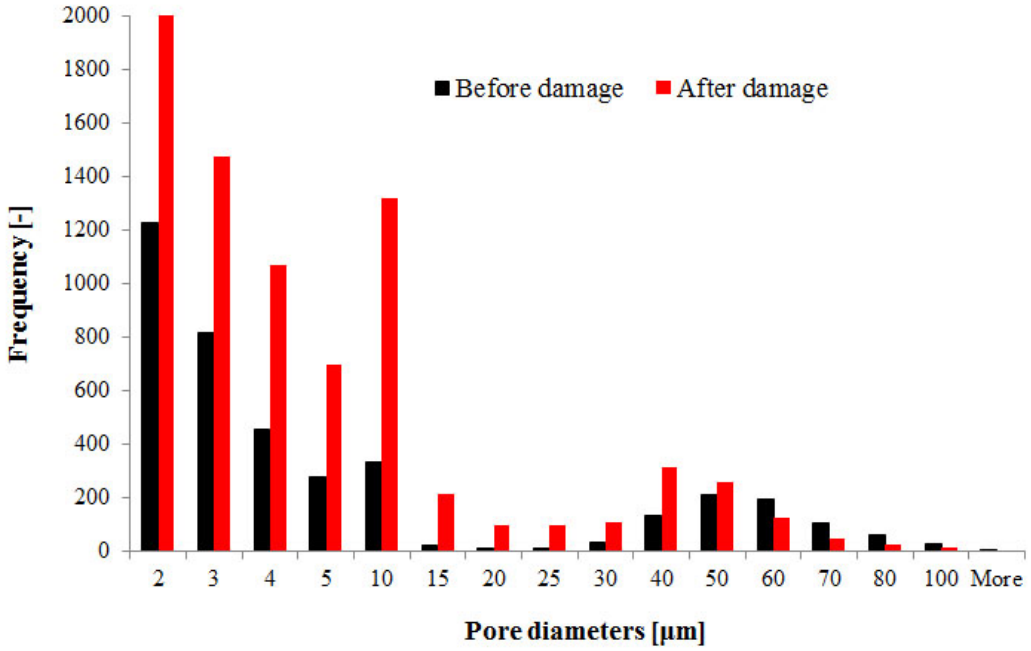

Figure 8 Pore diameter distribution of sample#1 (Bentheimer and Barite were water-wet) before and after damage caused by fines injection (10 g/L Barite, measured with µCT).

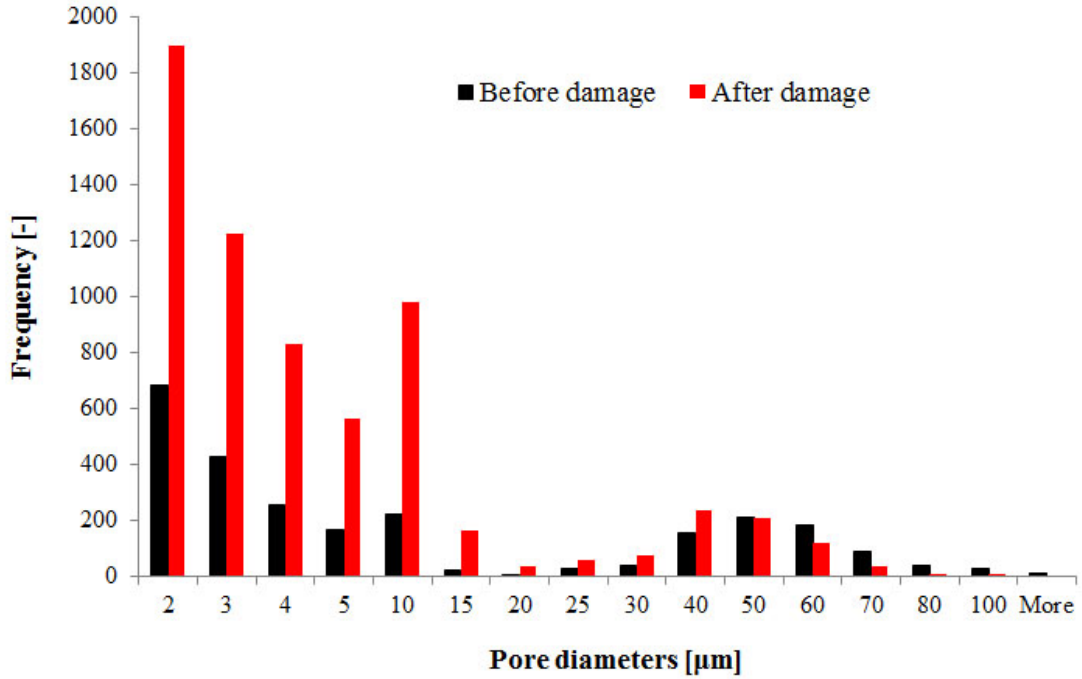

Figure 9 Pore diameter distribution of sample#2 (Bentheimer and Barite were oil-wet) before and after damage caused by fines injection (10 g/L Barite, measured with µCT).

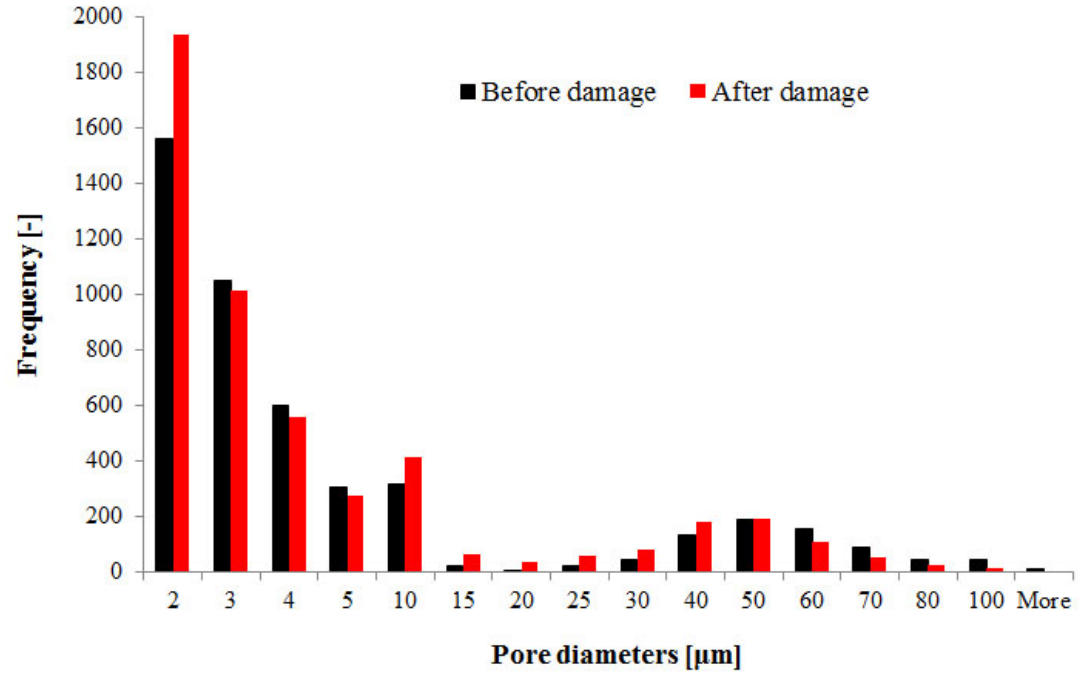

Figure 10 Pore diameter distribution of sample#3 (Bentheimer water-wet and Barite oil-wet) before and after damage caused by fines injection (10 g/L Barite, measured with µCT).

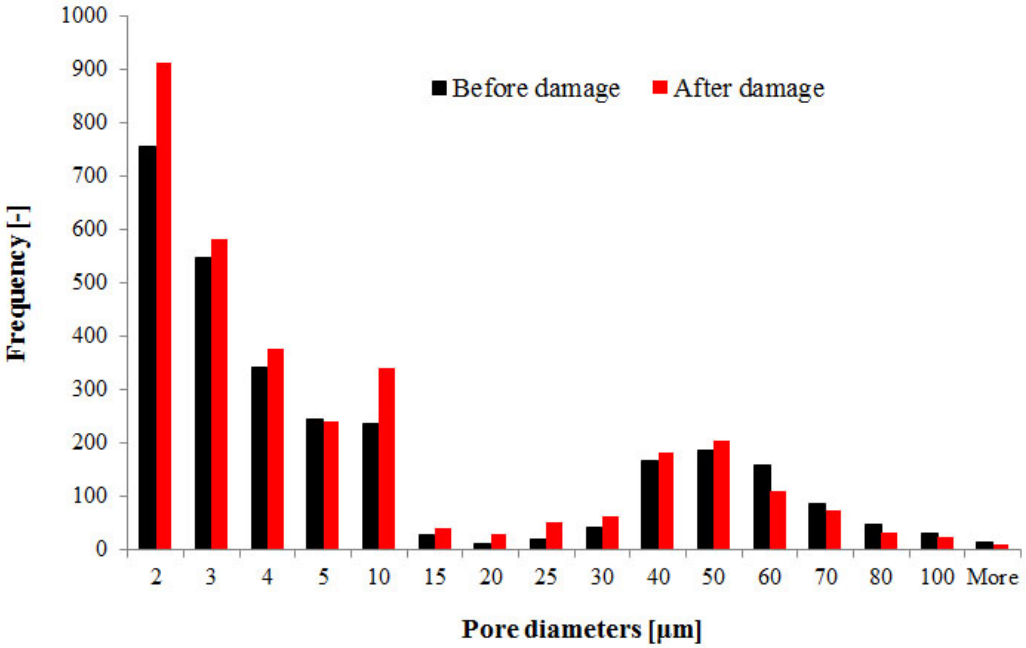

Figure 11 Pore diameter distribution of sample#4 (Bentheimer oil-wet and Barite water-wet) before and after damage caused by fines injection (10 g/L Barite, measured with µCT).

The amount of fines deposited as a function of plug length was also measured on the µCT images, Figures 12-15. The higher porosity reduction was observed when the wettability of Bentheimer plug and Barite particles were the same (from ~23% to ~15% for sample 1 and from ~23% to ~14% for sample 2), Figures 12 and 13. Furthermore, porosity was reduced gradually with core length; see Figures 12-15 and Table 3.

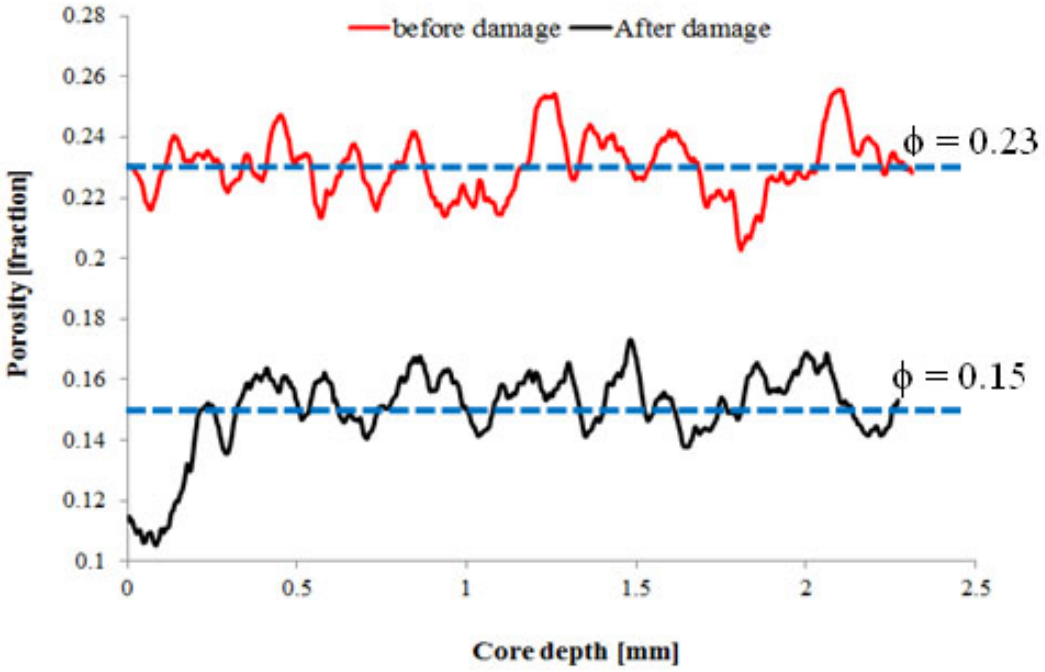

Figure 12 Porosity versus core depth before (red) and after (black) damage for sample#1 (Bentheimer and Barite were water-wet).

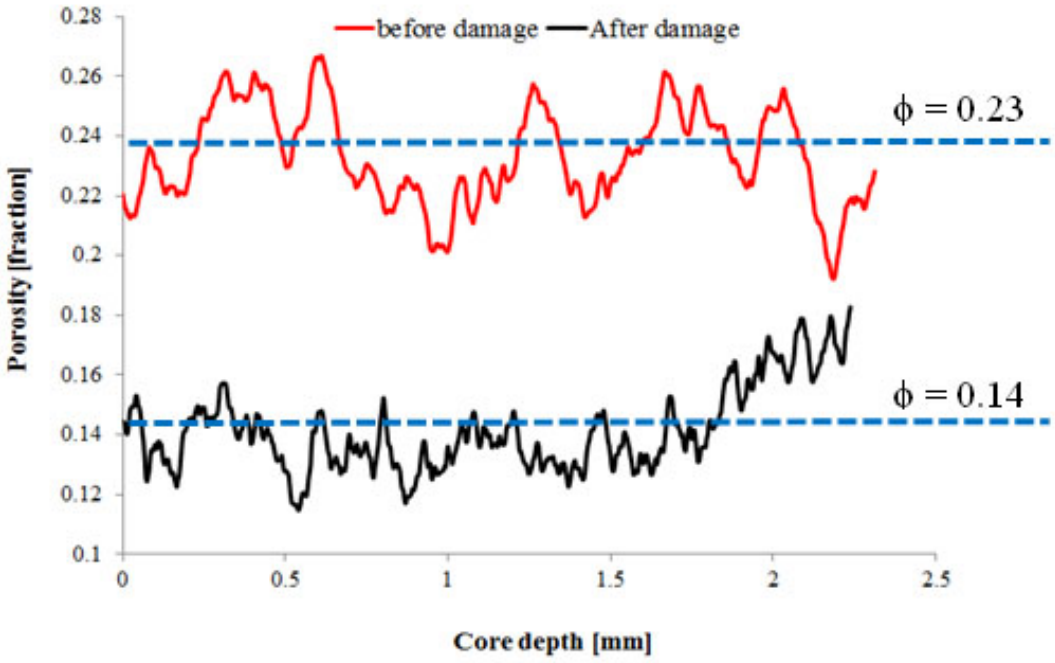

Figure 13 Porosity versus core depth before (red) and after (black) damage for sample#2 (Bentheimer and Barite were oil-wet).

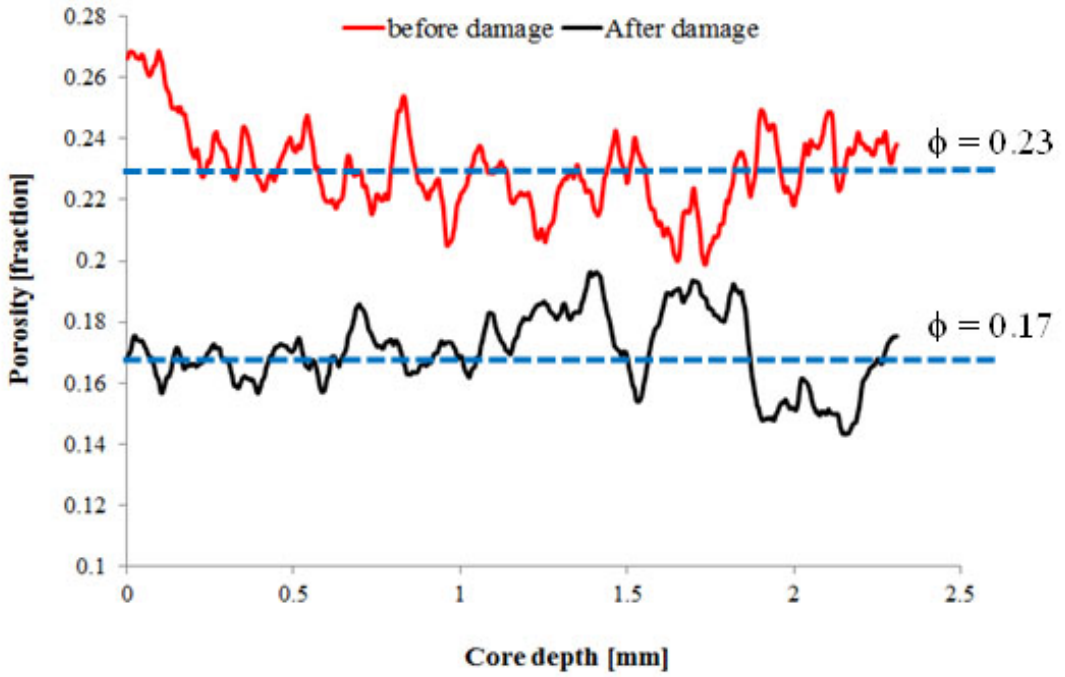

Figure 14 Porosity versus core depth before (red) and after (black) damage for sample#3 (Bentheimer water-wet and Barite oil-wet).

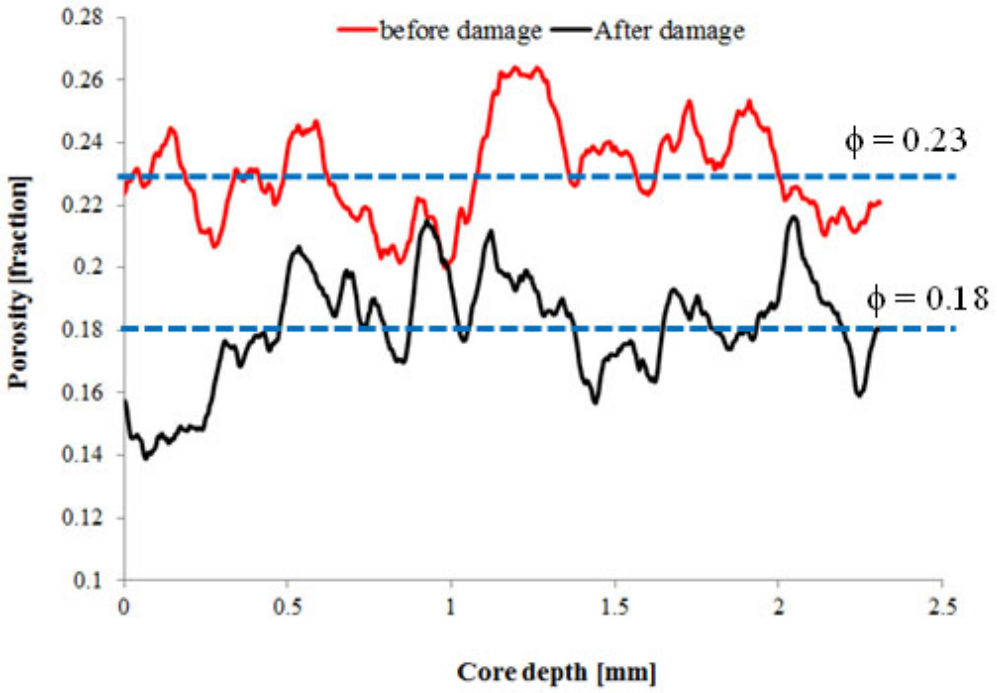

Figure 15 Porosity versus core depth before (red) and after (black) damage for sample#4 (Bentheimer oil-wet and Barite water-wet).

Furthermore the precise 3D spatial location of the deposited Barite particles can be measured on the μCT images, cp. Figures 16. The 3D-μCT images again indicated that if the core plug and fine particles have the same wettability (samples 1 and 2), they were more damaged (Figure 16a -16f); compare with samples 3 and 4, Figures 16g-16i, where core plug and fine wettability was different). Al-Yaseri *et al.* (2015) explained the pore-scale plugging mechanism with fine particles penetrating into the pore space until a thin pore throat is reached and plugged, followed by subsequent filling of larger adjacent pore bodies. Figure 16 (c, f, i and l) show the deposited fine particles in the pores space after plugging; it is clear from Figure 16c and 16f that more fines deposited and agglomerated when the core plug and fine particles had the same wettability (samples 1 and 2); when the wettabilies were different a more homogeneous fines distribution was observed. These observations were well supported by the high resolution 2D-μCT image slices (Figure 17): the water-wet or oil-wet Barite particles adhered to the water-wet or oil-wet quartz surface; also the Barite particles were significantly more agglomerated and distributed more heterogeneously if fines-rock wettability was the same (Figure 17).

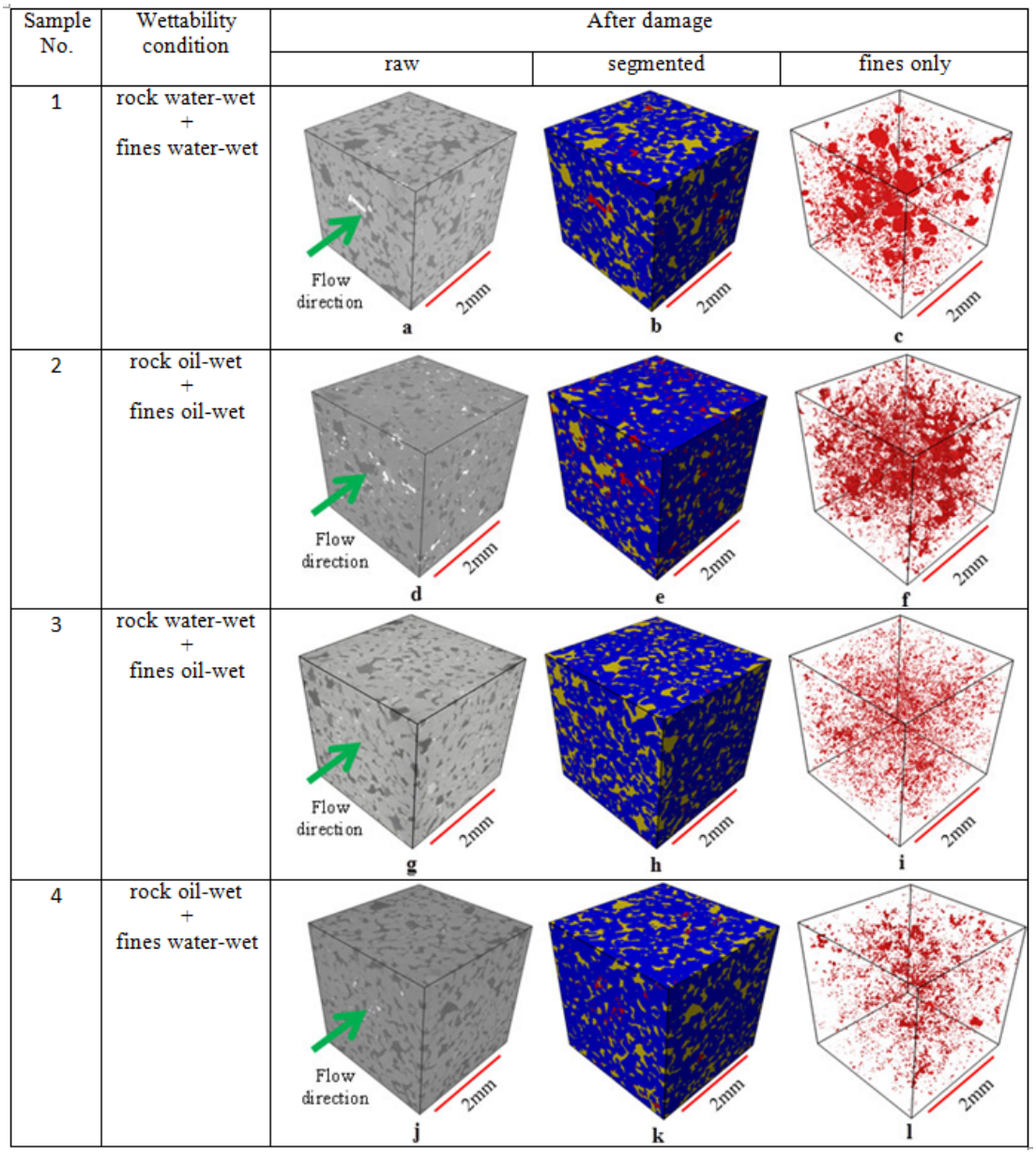

Figure 16 3D μCT images of Bentheimer sandstone after formation damage caused by injection of Barite suspension. (a,d,g,j) raw images for samples 1,2,3, and 4, respectively, at $(3.4\mu m)^3$ resolution, a cubic volume ($12.65mm^3$) is shown; (b,e,h,k) segmented images; (c,f,i,l) segmented images showing Barite (red) only. In the raw images Barite is white, open pore space is black and sandstone is grey; in the segmented images rock is dark blue, Barite red and open pore space is yellow.

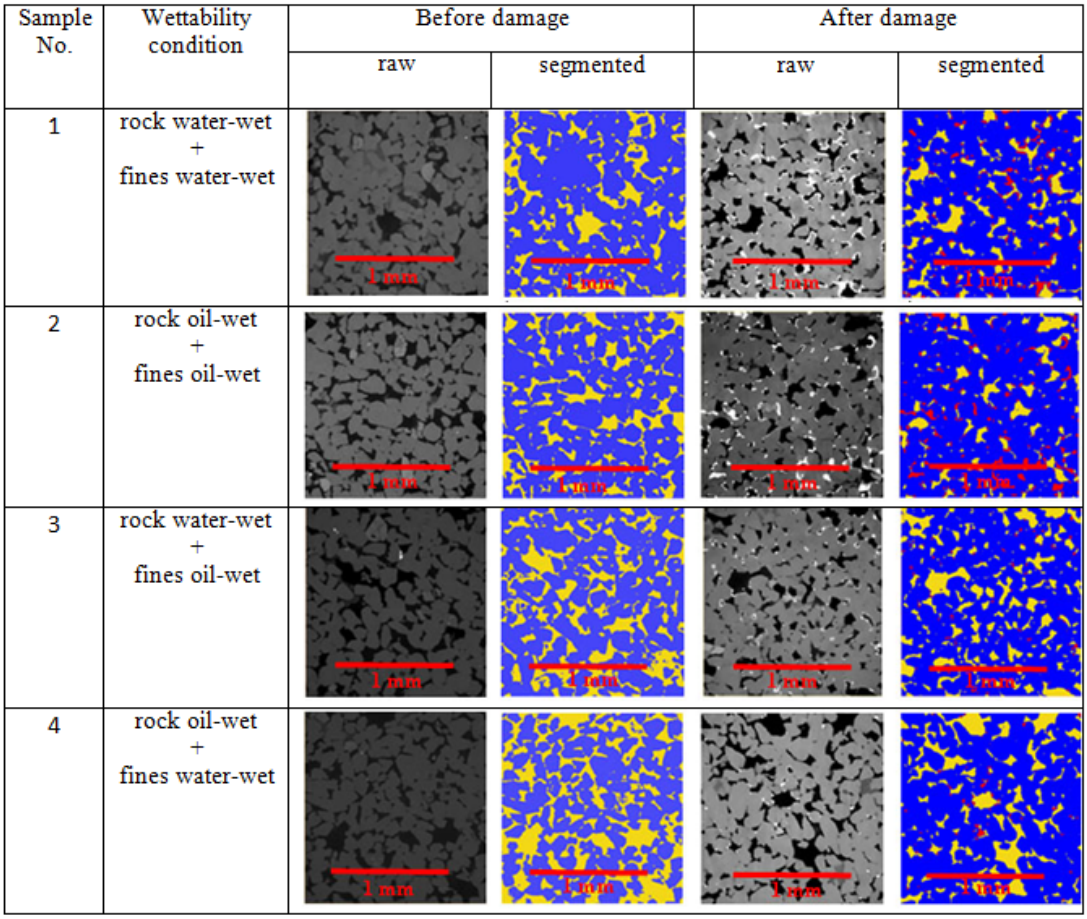

Figure 17 2D slices through the rock and pore space before and after damage (injection of 10 g/L Barite suspension): In the raw images, pores are black/dark grey, sandstone is light grey and Barite is white; in the segmented images sandstone is blue, pore space is yellow and Barite red. Resolution is $(3.4\mu m)^3$ for all images.

The high resolution 2D-SEM images clearly show that the Barite particles strongly adhered to the quartz surface (Figure 18), independent of the wettability condition. This indicates that strong adhesion forces between Barite-Barite particles (Figure 18e and 18f) and Barite-quartz were acting (Israelachvili 2011; Torkzaban et al. 2007). The adhesion forces between Barite-Barite particles or Barite and quartz surface lead to build-up of solid particle agglomerations inside the pores space which can significantly reduce permeability (Tiab and Donaldson 2004, Civan 2007).

Several cases can be distinguished:

Water-wet particles on water-wet rock surface

As discussed earlier (Al-Yaseri *et al.* 2015), silanol groups on the water-wet quartz surface (Zhuravlev 2000; McCaughan *et al.* 2013) strongly attract the hydroxyl groups on the water-wet Barite surface (Fenter *et al.* 2001). This results in strong Debye and Keesom forces, and probably hydrogen bonding (Hirasaki 1991, Israelachvili 2011).

Combined wettability conditions

In case of oil-wet particles – water-wet rock and oil-wet rock and water-wet fines, London and Debye forces create the cohesive forces between surfaces of different wettability. More importantly, some parts of the oil-wet surfaces were not covered by alkyl groups (advancing water contact angle was ~115°, see above), and were thus partially water-wet. For these water-wet surface patches the same forces act as in the water-wet/water-wet case, leading to strong adhesion.

Oil-wet particles and oil-wet rock surfaces

The largest contribution to the adhesion will again be contributed by the unaltered (i.e. water-wet) surfaces, although their relative contribution is smaller than for the above cases. Furthermore the overall adhesion force should be weaker as only London forces act between the (now larger) oil-wet surfaces.

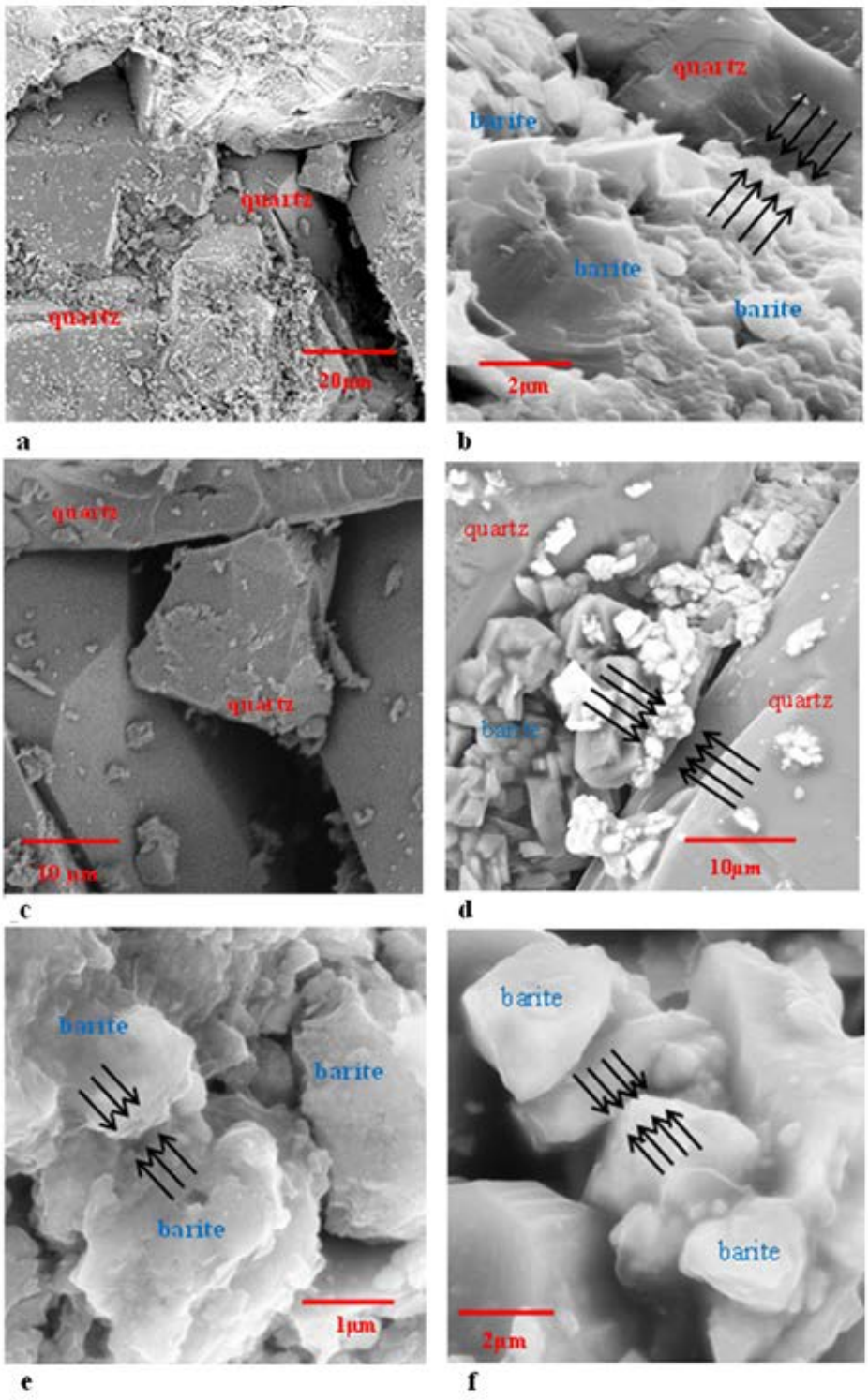

Figure 18 SEM images of damaged and undamaged water-wet Bentheimer: sample 1 (a) before and (b) after damage (10 g/L water-wet Barite suspension injection); sample 3 (c) before and (d) after damage (10 g/L oil-wet Barite suspension injection). Adhesion between Barite-Barite particles and Barite-quartz surfaces can be seen (b,d,e,f).

Conclusions

Permeability reduction due to pore plugging is a serious problem in many subsurface engineering fields, including petroleum engineering, hydrology or geothermal energy production. The detailed plugging mechanisms are, however, not well understood.

We thus investigated these mechanisms at the micrometre pore scale with *in-situ* (NMR, μCT), and ex-situ (coreflooding and SEM) techniques, and discuss their consequences for pore structure and permeability. The focus of the study was on wettability effects, which have received little attention so far.

We found that porosity and permeability were more reduced if the rock (quartz) surface and the fine (Barite) particles had the same wettability. Initially thin pore throats were plugged, followed by filling of large adjacent pore bodies. As a result, fines filled mainly larger pores and split these into smaller pores (as evidenced by μCT and NMR scanning). Furthermore, when the rock surface and particles had different wettabilities, fine particles migrated deeper into the plug, spread more homogeneously in the pore space, and generally caused less damage.

We note that Barite particles were tightly packed and strongly adhered to the quartz surface as reported earlier which apparently was caused by strong intermolecular forces between the Barite-Barite and Barite-quartz surfaces. We conclude that stimulating a damaged reservoir could be more difficult than expected. However, fine particles, which can travel deeper into the formation (and this happens if rock-fine wettability is different, see above), can be an advantage for hydraulic fracturing and drilling processes.

Acknowledgements

The authors thank the National Geosequestration Laboratory (NGL) for providing access to the μCT system VersaXRM-500 (Xradia Ltd). The National Geosequestration Laboratory is a collaboration between Curtin University, CSIRO, and the University of Western Australia established to conduct and deploy critical research and development to enable commercial-scale carbon storage options. Funding for this facility was provided by the Australian Federal Government.

References

Ahmed T. and P.D. McKinney 2005. Advanced Reservoir Engineering. *Gulf Publishing Burlington*, MA 01803, USA, 1-401.

Al-Yaseri A., Maxim M., Vogt S.J., Johns M. L., Barifcani A., and Iglauer S. 2015. Pore-scale analysis of formation damage in Bentheimer sandstone with *in-situ* NMR and micro-computed tomography experiments. *Journal of Petroleum Science and Engineering* 129, 48-57.

AL-Yaseri A.Z., Lebedev M., Barifcani A., and Iglauer S. 2016.Receding and advancing (CO2 + brine + quartz) contact angles as a function of pressure, temperature, surface roughness, salt type and salinity. *The Journal of Chemical Thermodynamics.*93, 416-423.

Allen S. G., Stephenson P.C.L., and Strange, J.H., 1997. Morphology of porous media studied by nuclear magnetic resonance. *The Journal of Chemical Physics* 106, (18), 7802-7809.

Amaerule J.O., Kersey D.G., Norman D.K., and Shannon P.M., 1988. Advances In Formation Damage Assessment And Control Strategies. *Petroleum Society of Canada* 65.1-65.37.

Bradford S.A., Torkzaban S., and Simunek J. 2011. Modeling colloid transport and retention in saturated porous media under unfavorable attachment conditions. *Water Resources Research* 47, (10), W10503.

Buades A., Coll B., and Morel J.M. 2005. A non-local algorithm for image denoising, presented at the Computer Vision and Pattern Recognition. Computer Society Conference (CVPR, IEEE), San Diego, CA, 20-25 June 2005.

Buckley J.S., Liu Y., Xie X., and Morrow N. 1997. Asphaltenes and crude oil wetting-The effect of oil composition. *SPE J.*, 2, 107–119.

Buckley J. S., Liu Y., and Monsterleet S. 1998. Mechanisms of wetting alteration by crude oils. *SPE J.*, 54–61.

Civan F. 2007. Reservoir Formation Damage Fundamentals, Modeling, Assessment and Mitigation. *Gulf Publishing Company*, Houston, USA, Second Edition, 1114pp.

Cuiec L. 1984. Rock/crude-oil interactions and wettability: an attempt to understand their interrelations. Annual Technical Conference and Exhibition of the SPE, Houston, Texas, 16-19 September 1984.

Dake, L.P. 1978. Fundamentals of Reservoir Engineering. Developments in Petroleum Science, 8. Elsevier, Amsterdam-London-New York-Tokyo.

Donaldson E., Alam, W. 2008. Wettability. *Gulf Publishing Company*, 229pp.

Economides M.J., and Nolte K.G. 1987. Reservoir stimulation. *Houston, TX: Schlumberger Educational Services*.

Fenter P., McBride M.T., Srajer G., Sturchio N.C., and Bosbach D. 2001. Structure of Barite (001)− and (210)−Water Interfaces. *The Journal of Physical Chemistry* 105, (34), 8112-8119.

Fridjonsson E.O, Hasan A.B., Fourie A.B., and Johns M.L. 2013. Pore Structure in a Gold Mine Cemented Paste Backfill. *Minerals Engineering Journal* 53, 144-151.

Grate J. W., Dehoff K. J., Warner M. G., Pittman J. W., Wietsma T. W., Zhang C., and Oostrom M. 2012. Correlation of Oil–Water and Air–Water Contact Angles of Diverse Silanized Surfaces and Relationship to Fluid Interfacial Tensions. *Langmuir* 28, (18), 7182-7188.

Hendraningrat L. and Torsæter O. 2014. Effects of the Initial Rock Wettability on Silica-Based Nanofluid-Enhanced Oil Recovery Processes at Reservoir Temperatures. *Energy & Fuels* 28, (10) 6228-6241.

Hirasaki G.J. 1991. Wettability: fundamentals and surface forces. *SPE Formation Evaluation* 6, (02), 217-226.

Iglauer S., Favretto S., Spinelli G., Schena G., and Blunt M.J. 2010. X-ray tomography measurements of power-law cluster size distributions for the nonwetting phase in sandstones. *Physical Review E* 82, 05631.

Iglauer S., Sarmadivaleh M., Al-Yaseri A., and Lebedev M. 2014. Permeability evolution in sandstone due to injection of CO_2-saturated brine or supercritical CO_2 at reservoir conditions. *Energy Procedia* 63: 3051-3059.

Israelachvili J. N. 2011. Intermolecular and Surface Forces (Third Edition). *Academic Press*, London, 667pp.

Kalfayan, L. 2008. Production enhancement with acid stimulation. *Pennwell Books*, 270 pages.

Krilov Z., Steiner I., Goricnik B., Wojtanowicz A.J., Cabrajac S. 1991. Quantitative determination of solids invasion and formation damage using CAT scan and barite suspensions. In: SPE 23102, Presented at the SPE Offshore Europe Conference, UK, Aberdeen, 3-6 September 1991.

Krueger R.F. 1988. An overview of formation damage and well productivity in oilfield operations: An update. SPE California Regional Meeting, Long Beach, California 23-25 March, 1988.

Mahmoudi H., Spahis N., Goosen M.F., Ghaffour N., Drouiche N., and Ouagued A. 2010. Application of geothermal energy for heating and fresh water production in a brackish water greenhouse desalination unit: A case study from Algeria. *Renewable and Sustainable Energy Reviews* 14, (1), 512-517.

McCaughan J., Iglauer S., and Bresme F. 2013. Molecular Dynamics Simulation of Water/CO_2-quartz Interfacial Properties: Application to Subsurface Gas Injection. *Energy Procedia* 37, (0), 5387-5402.

McDowell-Boyer L.M., Hunt J.R., and Sitar N. 1986. Particle transport through porous media. *Water Resources Research* 22, (13), 1901-1921.

Muecke T.W. 1979. Formation fines and factors controlling their movement in porous media. *Journal of Petroleum Technology* 31,144-150.

Nguyen V., and Civan F. 2005. Modeling particle migration and deposition in porous media by parallel pathways with exchange. Chapter 11, Handbook of Porous media, Second Edition, Vafai, K. (Ed), CRC Press, Taylor and Francis Group, Boca Raton, FL: 457-484.

Otsu N. 1979. A threshold selection method from gray-level histograms. *IEEE Trans. Sys. Man. Cyber.* 9, (10), 62-66.

Patel A.D., and Growcock F.B., 1999. Reversible invert emulsion drilling fluids: Controlling wettability and minimizing formation damage. SPE European Formation Damage Conference, The Hague, the Netherlands, 31 May–1 June 1999.

Robertson RE. and Stiff HA JR. 1976. An Improved Mathematical Model for Relating Shear Stress to Shear Rate in Drilling Fluids and Cement Slurries. *Society of Petroleum Engineers Journal* 16,(01), 31-36.

Rosenbrand E., Kjøller C., Riis J. F. Kets F., and Fabricius I. L. 2015. Different effects of temperature and salinity on permeability reduction by fines migration in Berea sandstone. *Geothermics* 53, (0), 225-235.

Rosenbrand E., Haugwitz C., Jacobsen P.S.M., Kjøller C., and Fabricius I.L. 2014. The effect of hot water injection on sandstone permeability. *Geothermics* 50, (0), 155-166.

Sarkar A.K., and Sharma M.M. 1990. Fines migration in two-phase flow. *Journal of Petroleum Technology*, 42, (05), 646-652.

Schlüter S., Sheppard A., Brown K., and Wildenschild D. 2014. Image processing of multiphase images obtained via X-ray microtomography: A review. *Water Resources Research* 50(4), 3615-3639.

Sharma M.M., and Wunderlich R.W. 1987. The alteration of rock properties due to interactions with drilling-fluid components. *Journal of Petroleum Science and Engineering* 1, (2), 127-143.

Talabi O., AlSayari S., Iglauer S., and Blunt M. J. 2009. Pore-scale simulation of NMR response. *Journal of Petroleum Science and Engineering* 67, (3–4), 168-178.

Tiab D., and Donaldson E.C. 2004. Petrophysics - Theory and Practice of Measuring Reservoir Rock and Fluid Transport Properties. *Gulf Publishing Co., Elsevier*, USA, Second edition, 889pp.

Tran T.V., Civan F., and Robb I.D. 2009. Correlating Flowing Time and Condition For Perforation Plugging By Suspended Particles. *Society of Petroleum Engineers Journal* 24, (3), 398-403.

Tran T.V., Civan F., and Robb I.D. 2010. Effect of Permeability Impairment By Suspended Particles On Invasion Of Drilling Fluids. IADC/SPE 133724, presented at the IADC/SPE Asia Pacific Drilling Technology Conference and Exhibition, Ho Chi Minh, Vietnam, 1–3 November 2010.

Torkzaban S., Bradford S.A., and Walker S.L. 2007. Resolving the Coupled Effects of Hydrodynamics and DLVO Forces on Colloid Attachment in Porous Media. *Langmuir* 23, (19), 9652-9660.

Zhuravlev L.T. 2000. The surface chemistry of amorphous silica. Zhuravlev model. *Colloids and Surfaces, A: Physicochemical and Engineering Aspects* 173, (1–3), 1-38.

Hendraningrat L. and Torsæter O. 2014. Effects of the Initial Rock Wettability on Silica-Based Nanofluid-Enhanced Oil Recovery Processes at Reservoir Temperatures. *Energy & Fuels* 28, (10) 6228-6241.

6 Appendix 1: Statement of Contributions of Others

6.1 **Appendix 1.1: Statement of Contributions of Others for**

Roshan H., **Al-Yaseri, A.Z.**, Sarmadivaleh M., and Iglauer S., 2016. On Wettability of Shale Rocks. Journal of colloid and interface science, 475, pp. 104-111.

Statement of Contribution of Others for “On Wettability of Shale Rocks”

11 April 2016

To Whom It May Concern

I, Mr Ahmed Al-Yaseri, contributed by samples preparation, measurement and all analysis of contact angle data to the paper publication entitled

Roshan H., **Al-Yaseri, A.Z.**, Sarmadivaleh M., and Iglauer S., 2016. On Wettability of Shale Rocks. Journal of colloid and interface science, 475, pp. 104-111.

Undertaken with Ahmed Yaseri

(Signature of Co-author 1)

Ahmed Yaseri

(Signature of First author)

Hamid Roshan

Statement of Contribution of Others for “On Wettability of Shale Rocks”

11 April 2016

To Whom It May Concern

I, Dr. Sarmadivaleh M., contributed by specialist technical advice and manuscript editing to the paper/publication entitled

Roshan H., **Al-Yaseri, A.Z.**, Sarmadivaleh M., and Iglauer S., 2016. On Wettability of Shale Rocks. Journal of colloid and interface science, 475, pp. 104-111.

Undertaken with Ahmed Yaseri

(Signature of Co-author 2)

Sarmadivaleh M.

(Signature of First author)

Hamid Roshan

Statement of Contribution of Others for “On Wettability of Shale Rocks”

11 April 2016

To Whom It May Concern

I, Dr. Sarmadivaleh M., contributed by specialist technical advice and manuscript editing to the paper/publication entitled

Roshan H., **Al-Yaseri, A.Z.**, Sarmadivaleh M., and Iglauer S., 2016. On Wettability of Shale Rocks. Journal of colloid and interface science, 475, pp. 104-111.

Undertaken with Ahmed Yaseri

(Signature of Co-author 2)

Sarmadivaleh M.

(Signature of Co-author 1)

Ahmed Yaseri

Statement of Contribution of Others for “On Wettability of Shale Rocks”

11 April 2016

To Whom It May Concern

I, Prof Stefan Iglauer, contributed by specialist technical advice and manuscript editing to the paper/publication entitled

Roshan H., **Al-Yaseri, A.Z.**, Sarmadivaleh M., and Iglauer S., 2016. On Wettability of Shale Rocks. Journal of colloid and interface science, 475, pp. 104-111.

Undertaken with Ahmed Yaseri

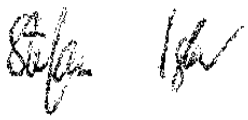

(Signature of Co-author 3)

Stefan Iglauer

(Signature of First author)

Hamid Roshan

Statement of Contribution of Others for “On Wettability of Shale Rocks”

11 April 2016

To Whom It May Concern

I, Prof Stefan Iglauer, contributed by specialist technical advice and manuscript editing to the paper/publication entitled

Roshan H., **Al-Yaseri, A.Z.**, Sarmadivaleh M., and Iglauer S., 2016. On Wettability of Shale Rocks. Journal of colloid and interface science, 475, pp. 104-111.

Undertaken with Ahmed Yaseri

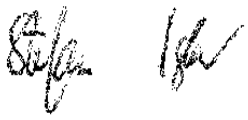

(Signature of Co-author 3)

Stefan Iglauer

(Signature of Co-author 1)

Ahmed Yaseri

6.2 **Appendix 1.2: Statement of Contributions of Others for**

Al-Yaseri, A.Z., Hamid Roshan, Maxim Lebedev, Barifcani Ahmed, and Stefan Iglauer, 2016. Dependence of quartz wettability on fluid density. Geophysical research letters.

Statement of Contribution of Others for “Dependence of quartz wettability on fluid density”

11 April 2016

To Whom It May Concern

I, Dr. Hamid Roshan, contributed by the derivation of the theoretical model and manuscript editing to the paper/publication entitled

Al-Yaseri, A.Z., Hamid Roshan, Maxim Lebedev, Barifcani Ahmed, and Stefan Iglauer, 2016.Dependence of quartz wettability on fluid density. Geophysical research letters

Undertaken with Ahmed Yaseri

(Signature of Co-author 1)

Hamid Roshan

(Signature of First author)

Ahmed Yaseri

Statement of Contribution of Others for “Dependence of quartz wettability on fluid density”

3 July 2017

To Whom It May Concern

I, Prof Lebedev M., contributed by Atomic force microscopy measurement and manuscript editing to the paper/publication entitled

Al-Yaseri, A.Z., Hamid Roshan, Maxim Lebedev, Barifcani Ahmed, and Stefan Iglauer, 2016.Dependence of quartz wettability on fluid density. Geophysical research letters

Undertaken with Ahmed Yaseri

(Signature of Co-author 2)

Lebedev M.

(Signature of First author)

Ahmed Yaseri

Statement of Contribution of Others for “Dependence of quartz wettability on fluid density”

11 April 2016

To Whom It May Concern

I, Prof Barifcani A., contributed by specialist technical advice and manuscript editing to the paper/publication entitled

Al-Yaseri, A.Z., Hamid Roshan, Maxim Lebedev, Barifcani Ahmed, and Stefan Iglauer, 2016. Dependence of quartz wettability on fluid density. Geophysical research letters

Undertaken with Ahmed Yaseri

(Signature of Co-author 3)

Barifcani A.

(Signature of First author)

Ahmed Yaseri

Statement of Contribution of Others for “Dependence of quartz wettability on fluid density”

11 April 2016

To Whom It May Concern

I, Prof Stefan Iglauer, contributed by specialist technical advice and manuscript editing to the paper/publication entitled

Al-Yaseri, A.Z., Hamid Roshan, Maxim Lebedev, Barifcani Ahmed, and Stefan Iglauer, 2016. Dependence of quartz wettability on fluid density. Geophysical research letters

Undertaken with Ahmed Yaseri

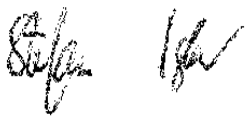

(Signature of Co-author 4)

Stefan Iglauer

(Signature of First author)

Ahmed Yaseri

6.3 APPENDIX 1.3: STATEMENT OF CONTRIBUTIONS OF OTHERS FOR

Al-Yaseri, A.Z., Hani A., Lebedev, Barifcani, A. and Iglauer, S., 2016. Impact of fines and rock wettability on Reservoir formation damage. Journal of Geophysical Prospecting, 64, pp. 860-874.

Statement of Contribution of Others for “Impact of fines and rock wettability on Reservoir formation damage”

3 July 2017

To Whom It May Concern

I, Prof Lebedev M., contributed by micro-computed tomography measurement and manuscript editing to the paper/publication entitled

Al-Yaseri, A.Z., Hani A., Lebedev, Barifcani, A. and Iglauer, S., 2016. Impact of fines and rock wettability on Reservoir formation damage. Journal of Geophysical Prospecting, 64, pp. 860-874.

Undertaken with Ahmed Yaseri

(Signature of Co-author 2)

Lebedev M.

(Signature of First author)

Ahmed Yaseri

Statement of Contribution of Others for “Impact of fines and rock wettability on Reservoir formation damage”

24 February 2016

To Whom It May Concern

I, Hani A., contributed by analysing of micro-computed tomography images using AVIZO software to the paper/publication entitled

Al-Yaseri, A.Z., Hani A., Lebedev, Barifcani, A. and Iglauer, S., 2016. Impact of fines and rock wettability on Reservoir formation damage. Journal of Geophysical Prospecting, 64, pp. 860-874.

Undertaken with Ahmed Yaseri

(Signature of Co-author 1)

Hani A.

(Signature of First author)

Ahmed Yaseri

Statement of Contribution of Others for “Impact of fines and rock wettability on Reservoir formation damage”

24 February 2016

To Whom It May Concern

I, Prof Barifcani A., contributed by specialist technical advice and manuscript editing to the paper/publication entitled

Al-Yaseri, A.Z., Hani A., Lebedev, Barifcani, A. and Iglauer, S., 2016. Impact of fines and rock wettability on Reservoir formation damage. Journal of Geophysical Prospecting, 64, pp. 860-874.

Undertaken with Ahmed Yaseri

(Signature of Co-author 3)

Barifcani A.

(Signature of First author)

Ahmed Yaseri

Statement of Contribution of Others for “Impact of fines and rock wettability on Reservoir formation damage”

24 February 2016

To Whom It May Concern

I, Prof Stefan Iglauer, contributed by specialist technical advice and manuscript editing to the paper/publication entitled

Al-Yaseri, A.Z., Hani A., Lebedev, Barifcani, A. and Iglauer, S., 2016. Impact of fines and rock wettability on Reservoir formation damage. Journal of Geophysical Prospecting, 64, pp. 860-874.

Undertaken with Ahmed Yaseri

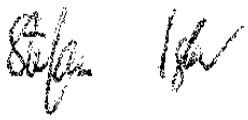

(Signature of Co-author 4)

Stefan Iglauer

(Signature of First author)

Ahmed Yaseri

6.4 **Appendix 1.4: Statement of Contributions of Others for**

Iglauer, S., Sarmadivaleh, M., Al-Yaseri, A. and Lebedev, M., 2014. Permeability evolution in sandstone due to injection of CO_2-saturated brine or supercritical CO_2 at reservoir conditions. Energy Procedia, 63, pp.3051-3059.

Statement of Contribution of Others for “Permeability evolution in sandstone due to injection of CO_2-saturated brine or supercritical CO_2 at reservoir conditions”

24 February 2016

To Whom It May Concern

I, Mr Ahmed Al-Yaseri, contributed by samples preparation, measurement and analysis of core flooding data to the paper publication entitled

Iglauer, S., Sarmadivaleh, M., **Al-Yaseri, A.** and Lebedev, M., 2014. Permeability evolution in sandstone due to injection of CO_2-saturated brine or supercritical CO_2 at reservoir conditions. Energy Procedia, 63, pp.3051-3059.

Undertaken with Ahmed Yaseri

(Signature of Co-author 2)

Ahmed Yaseri

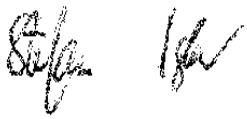

(Signature of first author)

Stefan Iglauer

Statement of Contribution of Others for “Permeability evolution in sandstone due to injection of CO_2-saturated brine or supercritical CO_2 at reservoir conditions”

24 February 2016

To Whom It May Concern

I, Dr. Sarmadivaleh M., contributed by samples preparation and measurement of core flooding data to the paper publication entitled

Iglauer, S., Sarmadivaleh, M., **Al-Yaseri, A.** and Lebedev, M., 2014. Permeability evolution in sandstone due to injection of CO_2-saturated brine or supercritical CO_2 at reservoir conditions. Energy Procedia, 63, pp.3051-3059.

Undertaken with Ahmed Yaseri

(Signature of Co-author 1)

Sarmadivaleh M.

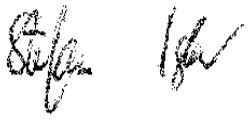

(Signature of first author)

Stefan Iglauer

Statement of Contribution of Others for "Permeability evolution in sandstone due to injection of CO_2-saturated brine or supercritical CO_2 at reservoir conditions"

24 February 2016

To Whom It May Concern

I, Dr Sarmadivaleh M., contributed by samples preparation and measurement of core flooding data to the paper publication entitled

Iglauer, S., Sarmadivaleh, M., **Al-Yaseri, A.** and Lebedev, M., 2014. Permeability evolution in sandstone due to injection of CO_2-saturated brine or supercritical CO_2 at reservoir conditions. Energy Procedia, 63, pp.3051-3059.

Undertaken with Ahmed Yaseri

(Signature of Co-author 2)

Ahmed Yaseri

(Signature of Co-author 1)

Sarmadivaleh M.

Statement of Contribution of Others for “Permeability evolution in sandstone due to injection of CO_2-saturated brine or supercritical CO_2 at reservoir conditions”

3 July 2017

To Whom It May Concern

I, Prof Lebedev M., contributed by specialist technical advice and manuscript editing to the paper/publication entitled

Iglauer, S., Sarmadivaleh, M., **Al-Yaseri, A.** and Lebedev, M., 2014. Permeability evolution in sandstone due to injection of CO_2-saturated brine or supercritical CO_2 at reservoir conditions. Energy Procedia, 63, pp.3051-3059.

Undertaken with Ahmed Yaseri

(Signature of Co-author 2)

Ahmed Yaseri

(Signature of Co-author 3)

Lebedev M.

Statement of Contribution of Others for “Permeability evolution in sandstone due to injection of CO_2-saturated brine or supercritical CO_2 at reservoir conditions”

3 July 2017

To Whom It May Concern

I, Prof Lebedev M., contributed by specialist technical advice and manuscript editing to the paper/publication entitled

Iglauer, S., Sarmadivaleh, M., **Al-Yaseri, A.** and Lebedev, M., 2014. Permeability evolution in sandstone due to injection of CO_2-saturated brine or supercritical CO_2 at reservoir conditions. Energy Procedia, 63, pp.3051-3059.

Undertaken with Ahmed Yaseri

(Signature of Co-author 3)

Lebedev M.

(Signature of first author)

Stefan Iglauer

6.5 **Appendix 1.5: Statement of Contributions of Others for**

Sarmadivaleh, M., **Al-Yaseri, A.Z.** and Iglauer, S., 2015. Influence of temperature and pressure on quartz–water–CO_2 contact angle and CO_2–water interfacial tension. Journal of colloid and interface science, 441, pp.59-64.

Statement of Contribution of Others for “Influence of temperature and pressure on quartz–water–CO_2 contact angle and CO_2–water interfacial tension”

24 February 2016

To Whom It May Concern

I, Mr Ahmed Al-Yaseri, contributed by samples preparation, measurement and all analysis of contact angle data to the paper publication entitled

Sarmadivaleh, M., **Al-Yaseri, A.Z.** and Iglauer, S., 2015. Influence of temperature and pressure on quartz–water–CO_2 contact angle and CO_2–water interfacial tension. Journal of colloid and interface science, 441, pp.59-64.

Undertaken with Ahmed Yaseri

(Signature of Co-author 1)

Ahmed Yaseri

(Signature of first author)

Sarmadivaleh M.

Statement of Contribution of Others for “Influence of temperature and pressure on quartz–water–CO_2 contact angle and CO_2–water interfacial tension”

24 February 2016

To Whom It May Concern

I, Prof Stefan Iglauer, contributed by specialist technical advice and manuscript editing to the paper/publication entitled

Sarmadivaleh, M., **Al-Yaseri, A.Z.** and Iglauer, S., 2015. Influence of temperature and pressure on quartz–water–CO_2 contact angle and CO_2–water interfacial tension. Journal of colloid and interface science, 441, pp.59-64.

Under taken with Ahmed Yaseri

(Signature of Co-author 1)

Ahmed Yaseri

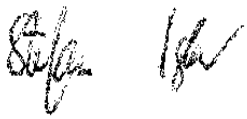

(Signature of Co-author 2)

Stefan Iglauer

Statement of Contribution of Others for “Influence of temperature and pressure on quartz–water–CO_2 contact angle and CO_2–water interfacial tension”

24 February 2016

To Whom It May Concern

I, Prof Stefan Iglauer, contributed by specialist technical advice and manuscript editing to the paper/publication entitled

Sarmadivaleh, M., **Al-Yaseri, A.Z.** and Iglauer, S., 2015. Influence of temperature and pressure on quartz–water–CO_2 contact angle and CO_2–water interfacial tension. Journal of colloid and interface science, 441, pp.59-64.

Undertaken with Ahmed Yaseri

(Signature of Co-author 2)

Stefan Iglauer

(Signature of first author)

Sarmadivaleh M.

6.6 APPENDIX 1.6: STATEMENT OF CONTRIBUTIONS OF OTHERS FOR

Iglauer, S., **Al-Yaseri, A.Z.**, Rezaee, R. and Lebedev, M., 2015. CO_2 wettability of caprocks: Implications for structural storage capacity and containment security. Geophysical Research Letters, 42(21), pp.9279-9284.

Statement of Contribution of Others for "CO_2 wettability of caprocks: Implications for structural storage capacity and containment security"

24 February 2016

To Whom It May Concern

I, Mr Ahmed Al-Yaseri, contributed by samples preparation, measurement and all analysis of contact angle data to the paper publication entitled

Iglauer, S., **Al-Yaseri, A.Z.**, Rezaee, R. and Lebedev, M., 2015. CO_2 wettability of caprocks: Implications for structural storage capacity and containment security. Geophysical Research Letters, 42(21), pp.9279-9284.

Undertaken with Ahmed Yaseri

(Signature of Co-author 1)

Ahmed Yaseri

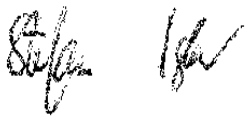

(Signature of first author)

Stefan Iglauer

Statement of Contribution of Others for "CO_2 wettability of caprocks: Implications for structural storage capacity and containment security"

24 February 2016

To Whom It May Concern

I, Prof Rezaee R., contributed by specialist technical advice and manuscript editing to the paper/publication entitled

Iglauer, S., **Al-Yaseri, A.Z.**, Rezaee, R. and Lebedev, M., 2015. CO_2 wettability of caprocks: Implications for structural storage capacity and containment security. Geophysical Research Letters, 42(21), pp.9279-9284.

Undertaken with Ahmed Yaseri

(Signature of Co-author 1)

Ahmed Yaseri

(Signature of Co-author 2)

Rezaee R.

Statement of Contribution of Others for "CO_2 wettability of caprocks: Implications for structural storage capacity and containment security"

24 February 2016

To Whom It May Concern

I, Prof Rezaee R., contributed by specialist technical advice and manuscript editing to the paper/publication entitled

Iglauer, S., **Al-Yaseri, A.Z.**, Rezaee, R. and Lebedev, M., 2015. CO_2 wettability of caprocks: Implications for structural storage capacity and containment security. Geophysical Research Letters, 42(21), pp.9279-9284.

Undertaken with Ahmed Yaseri

(Signature of Co-author 2)

Rezaee R.

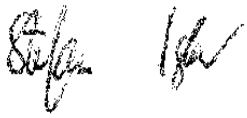

(Signature of first author)

Stefan Iglauer

6.7 **Appendix 1.7: Statement of Contributions of Others for**

Al-Yaseri, A.Z., Lebedev, M., Vogt, S.J., Johns, M.L., Barifcani, A. and Iglauer, S., 2015. Pore-scale analysis of formation damage in Bentheimer sandstone with in-situ NMR and micro-computed tomography experiments. Journal of Petroleum Science and Engineering, 129, pp.48-57.

Statement of Contribution of Others for “Pore-scale analysis of formation damage in Bentheimer sandstone with in-situ NMR and micro-computed tomography experiments”

24 February 2016

To Whom It May Concern

I, Prof Stefan Iglauer, contributed by specialist technical advice and manuscript editing to the paper/publication entitled

Al-Yaseri, A.Z., Lebedev, M., Vogt, S.J., Johns, M.L., Barifcani, A. and Iglauer, S., 2015. Pore-scale analysis of formation damage in Bentheimer sandstone with in-situ NMR and micro-computed tomography experiments. Journal of Petroleum Science and Engineering, 129, pp.48-57.

Undertaken with Ahmed Yaseri

(Signature of Co-author 5)

Stefan Iglauer

(Signature of First author)

Ahmed Yaseri

Statement of Contribution of Others for “Pore-scale analysis of formation damage in Bentheimer sandstone with in-situ NMR and micro-computed tomography experiments”

24 February 2016

To Whom It May Concern

I, Prof Barifcani A., contributed by specialist technical advice and manuscript editing to the paper/publication entitled

Al-Yaseri, A.Z., Lebedev, M., Vogt, S.J., Johns, M.L., Barifcani, A. and Iglauer, S., 2015. Pore-scale analysis of formation damage in Bentheimer sandstone with in-situ NMR and micro-computed tomography experiments. Journal of Petroleum Science and Engineering, 129, pp.48-57.

Undertaken with Ahmed Yaseri

(Signature of Co-author 4)

Barifcani A.

(Signature of First author)

Ahmed Yaseri

Statement of Contribution of Others for “Pore-scale analysis of formation damage in Bentheimer sandstone with in-situ NMR and micro-computed tomography experiments”

24 February 2016

To Whom It May Concern

I, Prof Johns M.L., contributed by specialist technical advice for NMR data and manuscript editing to the paper/publication entitled

Al-Yaseri, A.Z., Lebedev, M., Vogt, S.J., Johns, M.L., Barifcani, A. and Iglauer, S., 2015. Pore-scale analysis of formation damage in Bentheimer sandstone with in-situ NMR and micro-computed tomography experiments. Journal of Petroleum Science and Engineering, 129, pp.48-57.

Undertaken with Ahmed Yaseri

(Signature of Co-author 3)

Johns M.L.

(Signature of First author)

Ahmed Yaseri

Statement of Contribution of Others for “Pore-scale analysis of formation damage in Bentheimer sandstone with in-situ NMR and micro-computed tomography experiments”

24 February 2016

To Whom It May Concern

I, Dr. Vogt S.J., contributed by NMR measurement data and manuscript editing to the paper/publication entitled

Al-Yaseri, A.Z., Lebedev, M., Vogt, S.J., Johns, M.L., Barifcani, A. and Iglauer, S., 2015. Pore-scale analysis of formation damage in Bentheimer sandstone with in-situ NMR and micro-computed tomography experiments. Journal of Petroleum Science and Engineering, 129, pp.48-57.

Undertaken with Ahmed Yaseri

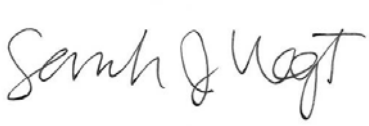

(Signature of Co-author 2)

Vogt S.J.

(Signature of First author)

Ahmed Yaseri

Statement of Contribution of Others for “Pore-scale analysis of formation damage in Bentheimer sandstone with in-situ NMR and micro-computed tomography experiments”

3 July 2017

To Whom It May Concern

I, Prof Lebedev M., contributed by micro-computed tomography measurement and manuscript editing to the paper/publication entitled

Al-Yaseri, A.Z., Lebedev, M., Vogt, S.J., Johns, M.L., Barifcani, A. and Iglauer, S., 2015. Pore-scale analysis of formation damage in Bentheimer sandstone with in-situ NMR and micro-computed tomography experiments. Journal of Petroleum Science and Engineering, 129, pp.48-57.

Undertaken with Ahmed Yaseri

(Signature of Co-author 1)

Lebedev M.

(Signature of First author)

Ahmed Yaseri

6.8 **Appendix 1.8: Statement of Contributions of Others for**

Al-Yaseri, A., Sarmadivaleh, M., Saeedi, A., Lebedev, M., Barifcani, A. and Iglauer, S., 2015. N_2+ CO_2+ NaCl brine interfacial tensions and contact angles on quartz at CO_2 storage site conditions in the Gippsland basin, Victoria/Australia. Journal of Petroleum Science and Engineering, 129, pp.58-62.

Statement of Contribution of Others for "N_2+ CO_2+ NaCl brine interfacial tensions and contact angles on quartz at CO_2 storage site conditions in the Gippsland basin, Victoria/Australia"

24 February 2016

To Whom It May Concern

I, Dr. Sarmadivaleh M., contributed by specialist technical advice and manuscript editing to the paper/publication entitled

Al-Yaseri, A., Sarmadivaleh, M., Saeedi, A., Lebedev, M., Barifcani, A. and Iglauer, S., 2015. N_2+ CO_2+ NaCl brine interfacial tensions and contact angles on quartz at CO_2 storage site conditions in the Gippsland basin, Victoria/Australia. Journal of Petroleum Science and Engineering, 129, pp.58-62.

Undertaken with Ahmed Yaseri

(Signature of Co-author 1)

Sarmadivaleh M.

(Signature of First author)

Ahmed Yaseri

Statement of Contribution of Others for "N_2+ CO_2+ NaCl brine interfacial tensions and contact angles on quartz at CO_2 storage site conditions in the Gippsland basin, Victoria/Australia"

24 February 2016

To Whom It May Concern

I, Dr. Saeedi Ali, contributed by specialist technical advice and manuscript editing to the paper/publication entitled

Al-Yaseri, A., Sarmadivaleh, M., Saeedi, A., Lebedev, M., Barifcani, A. and Iglauer, S., 2015. N_2+ CO_2+ NaCl brine interfacial tensions and contact angles on quartz at CO_2 storage site conditions in the Gippsland basin, Victoria/Australia. Journal of Petroleum Science and Engineering, 129, pp.58-62.

Undertaken with Ahmed Yaseri

(Signature of Co-author 2)

Saeedi Ali

(Signature of First author)

Ahmed Yaseri

Statement of Contribution of Others for "N_2+ CO_2+ NaCl brine interfacial tensions and contact angles on quartz at CO_2 storage site conditions in the Gippsland basin, Victoria/Australia"

3 July 2017

To Whom It May Concern

I, Prof Lebedev M., contributed by Atomic force microscopy measurement and manuscript editing to the paper/publication entitled

Al-Yaseri, A., Sarmadivaleh, M., Saeedi, A., Lebedev, M., Barifcani, A. and Iglauer, S., 2015. N_2+ CO_2+ NaCl brine interfacial tensions and contact angles on quartz at CO_2 storage site conditions in the Gippsland basin, Victoria/Australia. Journal of Petroleum Science and Engineering, 129, pp.58-62.

Undertaken with Ahmed Yaseri

(Signature of Co-author 3)

Lebedev M.

(Signature of First author)

Ahmed Yaseri

Statement of Contribution of Others for "N_2+ CO_2+ NaCl brine interfacial tensions and contact angles on quartz at CO_2 storage site conditions in the Gippsland basin, Victoria/Australia"

24 February 2016

To Whom It May Concern

I, Prof Barifcani A., contributed by specialist technical advice and manuscript editing to the paper/publication entitled

Al-Yaseri, A., Sarmadivaleh, M., Saeedi, A., Lebedev, M., Barifcani, A. and Iglauer, S., 2015. N_2+ CO_2+ NaCl brine interfacial tensions and contact angles on quartz at CO_2 storage site conditions in the Gippsland basin, Victoria/Australia. Journal of Petroleum Science and Engineering, 129, pp.58-62.

Undertaken with Ahmed Yaseri

(Signature of Co-author 4)

Barifcani A.

(Signature of First author)

Ahmed Yaseri

Statement of Contribution of Others for "N_2+ CO_2+ NaCl brine interfacial tensions and contact angles on quartz at CO_2 storage site conditions in the Gippsland basin, Victoria/Australia"

24 February 2016

To Whom It May Concern

I, Prof Stefan Iglauer, contributed by specialist technical advice and manuscript editing to the paper/publication entitled

Al-Yaseri, A., Sarmadivaleh, M., Saeedi, A., Lebedev, M., Barifcani, A. and Iglauer, S., 2015. N_2+ CO_2+ NaCl brine interfacial tensions and contact angles on quartz at CO_2 storage site conditions in the Gippsland basin, Victoria/Australia. Journal of Petroleum Science and Engineering, 129, pp.58-62.

Undertaken with Ahmed Yaseri

(Signature of Co-author 5)

Stefan Iglauer

(Signature of First author)

Ahmed Yaseri

6.9 **Appendix 1.9: Statement of Contributions of Others for**

Al-Yaseri, A.Z., Lebedev, M., Barifcani, A. and Iglauer, S., 2016. Receding and advancing (CO_2+ brine+ quartz) contact angles as a function of pressure, temperature, surface roughness, salt type and salinity. The Journal of Chemical Thermodynamics, 93, pp.416-423.

Statement of Contribution of Others for "Receding and advancing (CO_2+ brine+ quartz) contact angles as a function of pressure, temperature, surface roughness, salt type and salinity"

24 February 2016

To Whom It May Concern

I, Prof Stefan Iglauer, contributed by specialist technical advice and manuscript editing to the paper/publication entitled

Al-Yaseri, A.Z., Lebedev, M., Barifcani, A. and Iglauer, S., 2016. Receding and advancing (CO_2+ brine+ quartz) contact angles as a function of pressure, temperature, surface roughness, salt type and salinity. The Journal of Chemical Thermodynamics, 93, pp.416-423.

Undertaken with Ahmed Yaseri

(Signature of Co-author 3)

Stefan Iglauer

(Signature of First author)

Ahmed Yaseri

Statement of Contribution of Others for "Receding and advancing (CO_2+ brine+ quartz) contact angles as a function of pressure, temperature, surface roughness, salt type and salinity"

24 February 2016

To Whom It May Concern

I, Prof Barifcani A., contributed by specialist technical advice and manuscript editing to the paper/publication entitled

Al-Yaseri, A.Z., Lebedev, M., Barifcani, A. and Iglauer, S., 2016. Receding and advancing (CO_2+ brine+ quartz) contact angles as a function of pressure, temperature, surface roughness, salt type and salinity. The Journal of Chemical Thermodynamics, 93, pp.416-423.

Undertaken with Ahmed Yaseri

(Signature of Co-author 2)

Barifcani A.

(Signature of First author)

Ahmed Yaseri

Statement of Contribution of Others for "Receding and advancing (CO_2+ brine+ quartz) contact angles as a function of pressure, temperature, surface roughness, salt type and salinity"

3 July 2017

To Whom It May Concern

I, Prof Lebedev M., contributed by Atomic force microscopy measurement and manuscript editing to the paper/publication entitled

Al-Yaseri, A.Z., Lebedev, M., Barifcani, A. and Iglauer, S., 2016. Receding and advancing (CO_2+ brine+ quartz) contact angles as a function of pressure, temperature, surface roughness, salt type and salinity. The Journal of Chemical Thermodynamics, 93, pp.416-423.

Undertaken with Ahmed Yaseri

(Signature of Co-author 1)

Lebedev M.

(Signature of First author)

Ahmed Yaseri

7 Appendix 2: Copyright Forms

7.1 APPENDIX 2.1: ELSEVIER JOURNAL ARTICLES

Copyright information relating to:

Al-Yaseri, A., Sarmadivaleh, M., Saeedi, A., Lebedev, M., Barifcani, A. and Iglauer, S., 2015. N_2+ CO_2+ NaCl brine interfacial tensions and contact angles on quartz at CO_2 storage site conditions in the Gippsland basin, Victoria/Australia. Journal of Petroleum Science and Engineering, 129, pp.58-62.

Sarmadivaleh, M., **Al-Yaseri, A.Z.** and Iglauer, S., 2015. Influence of temperature and pressure on quartz–water–CO_2 contact angle and CO_2–water interfacial tension. Journal of colloid and interface science, 441, pp.59-64.

Al-Yaseri, A.Z., Lebedev, M., Barifcani, A. and Iglauer, S., 2016. Receding and advancing (CO_2+ brine+ quartz) contact angles as a function of pressure, temperature, surface roughness, salt type and salinity. The Journal of Chemical Thermodynamics, 93, pp.416-423.

Al-Yaseri, A.Z., Lebedev, M., Vogt, S.J., Johns, M.L., Barifcani, A. and Iglauer, S., 2015. Pore-scale analysis of formation damage in Bentheimer sandstone with in-situ NMR and micro-computed tomography experiments. Journal of Petroleum Science and Engineering, 129, pp.48-57.

Roshan, H., **Al-Yaseri, A.Z.**, Sarmadivaleh, M. and Iglauer, S., 2016.On wettability of shale rocks. Journal of Colloid and Interface Science, 475, pp.104-111.

Iglauer, S., Sarmadivaleh, M., **Al-Yaseri, A.** and Lebedev, M., 2014.Permeability evolution in sandstone due to injection of CO_2-saturated brine or supercritical CO_2 at reservoir conditions. Energy Procedia, 63, pp.3051-3059.

Al-Yaseri, A.Z., Roshan, H., Lebedev, M., Barifcani, A. and Iglauer, S., 2016. Dependence of quartz wettability on fluid density. Geophysical Research Letters, 43(8), pp.3771-3776.

Dear Ahmed Al-Yaseri

Thank you for your email.

Please note that as one of the authors of this article, you retain the right to include the journal article, in full or in part, in a thesis or dissertation. You do not require permission to do so.

For full details of your rights as a Journal Author, please visit:

http://www.elsevier.com/wps/find/authorsview.authors/copyright#whatrights

Your retained rights allow you to submit your article in electronic format and to post this Elsevier article online if it is embedded within your thesis. You are also permitted to post your Author Accepted Manuscript online; however posting of the final published article is prohibited.

Please refer to Elsevier's Posting Policy for further information:

http://www.elsevier.com/wps/find/authors.authors/postingpolicy

Feel free to contact me if you have any queries.

Regards,

Priya

Lakshmi Priya

Sr Copyrights Coordinator

Global Rights Department

ELSEVIER

JOHN WILEY AND SONS LICENSE
TERMS AND CONDITIONS

Jun 07, 2017

This Agreement between Ahmed Al ("You") and John Wiley and Sons ("John Wiley and Sons") consists of your license details and the terms and conditions provided by John Wiley and Sons and Copyright Clearance Center.

License Number	4123420664758
License date	Jun 06, 2017
Licensed Content Publisher	John Wiley and Sons
Licensed Content Publication	Geophysical Research Letters
Licensed Content Title	CO2 wettability of caprocks: Implications for structural storage capacity and containment security
Licensed Content Author	Stefan Iglauer,Ahmed Zarzor Al-Yaseri,Reza Rezaee,Maxim Lebedev
Licensed Content Date	Nov 6, 2015
Licensed Content Pages	6
Type of use	Dissertation/Thesis
Requestor type	Author of this Wiley article
Format	Print
Portion	Full article
Will you be translating?	No
Title of your thesis / dissertation	rock and co2 wettability
Expected completion date	Mar 2017
Expected size (number of pages)	200
Requestor Location	Ahmed Al-Yaseri 26 Dick Perry Ave Building 613, level 6 Kensington, 6151 Australia Attn: Ahmed Al-Yaseri
Publisher Tax ID	EU826007151
Customer VAT ID	AU61892663008
Billing Type	Invoice
Billing Address	Ahmed Al-Yaseri 26 Dick Perry Ave Building 613, level 6 Kensington, Australia 6151 Attn: Ahmed Al-Yaseri
Total	0.00 USD

JOHN WILEY AND SONS LICENSE
TERMS AND CONDITIONS

Jun 07, 2017

This Agreement between Ahmed Al ("You") and John Wiley and Sons ("John Wiley and Sons") consists of your license details and the terms and conditions provided by John Wiley and Sons and Copyright Clearance Center.

License Number	4123420297484
License date	Jun 06, 2017
Licensed Content Publisher	John Wiley and Sons
Licensed Content Publication	Geophysical Research Letters
Licensed Content Title	Dependence of quartz wettability on fluid density
Licensed Content Author	Ahmed Zarzor Al-Yaseri,Hamid Roshan,Maxim Lebedev,Ahmed Barifcani,Stefan Iglauer
Licensed Content Date	Apr 28, 2016
Licensed Content Pages	6
Type of use	Dissertation/Thesis
Requestor type	Author of this Wiley article
Format	Print
Portion	Full article
Will you be translating?	No
Title of your thesis / dissertation	CO2 wettability and implications for core flooding
Expected completion date	Mar 2017
Expected size (number of pages)	200
Requestor Location	Ahmed Al-Yaseri 26 Dick Perry Ave Building 613, level 6 Kensington, 6151 Australia Attn: Ahmed Al-Yaseri
Publisher Tax ID	EU826007151
Customer VAT ID	AU61892663008
Billing Type	Invoice
Billing Address	Ahmed Al-Yaseri 26 Dick Perry Ave Building 613, level 6 Kensington, Australia 6151 Attn: Ahmed Al-Yaseri
Total	0.00 USD

JOHN WILEY AND SONS LICENSE
TERMS AND CONDITIONS
Jun 07, 2017

This Agreement between Ahmed Al ("You") and John Wiley and Sons ("John Wiley and Sons") consists of your license details and the terms and conditions provided by John Wiley and Sons and Copyright Clearance Center.

License Number	4123950435406
License date	Jun 07, 2017
Licensed Content Publisher	John Wiley and Sons
Licensed Content Publication	Geophysical Prospecting
Licensed Content Title	Impact of fines and rock wettability on reservoir formation damage
Licensed Content Author	Ahmed Al-Yaseri,Hani Al Mukainah,Maxim Lebedev,Ahmed Barifcani,Stefan Iglauer
Licensed Content Date	Jun 28, 2016
Licensed Content Pages	15
Type of use	Dissertation/Thesis
Requestor type	Author of this Wiley article
Format	Print
Portion	Full article
Will you be translating?	No
Title of your thesis / dissertation	rock and co2 wettability
Expected completion date	Mar 2017
Expected size (number of pages)	200
Requestor Location	Ahmed Al-Yaseri 26 Dick Perry Ave Building 613, level 6 Kensington, 6151 Australia Attn: Ahmed Al-Yaseri
Publisher Tax ID	EU826007151
Customer VAT ID	AU61892663008
Billing Type	Invoice
Billing Address	Ahmed Al-Yaseri 26 Dick Perry Ave Building 613, level 6 Kensington, Australia 6151 Attn: Ahmed Al-Yaseri
Total	0.00 USD

“Every reasonable effort has been made to acknowledge the owners of copyright material. I would be pleased to hear from any copyright owner who has been omitted or incorrectly acknowledged”

Yaseri, Ahmed Zarzor Hussien

Signature

15/10/ 2017